QUALITY CONTROL UNDER STRESS: UBIQUILIN 2 BRIDGES PROTEIN AND RNA HOMEOSTASIS AT STRESS GRANULES IN ALS/FTD PATHOLOGY

by
Elizabeth J. Alexander

A dissertation submitted to Johns Hopkins University in conformity with the requirements for the degree of Doctor of Philosophy

Baltimore, Maryland
January 2019

Abstract

Both protein and RNA quality control are critical for cell survival during stress and are disrupted in the neurodegenerative diseases amyotrophic lateral sclerosis (ALS) and frontotemporal dementia (FTD). ALS is the most common adult onset motor neuron disease, while FTD is the second most common type of dementia for individuals under 65. Both are characterized by the accumulation of proteins in intracellular inclusions and are thought to be part of a continuous clinical spectrum, but their causes are largely unknown. Stress granules (SGs), a type of RNA granule, have recently emerged as potential seed sites for patient protein inclusions that incorporate both protein quality control (PQC) factors and RNA binding proteins (RBPs). SGs transiently sequester stalled translation initiation complexes and apoptosis signaling molecules in response to stress. These dynamic particles form via a liquid-liquid phase separation mediated by oligomerization of the low complexity prion-like domains in RBPs bound to RNA in a process tuned by RNA length and structure. Stable interactions between these proteins in SGs leads to the formation of protein aggregates. The PQC factors that regulate the dynamic incorporation of RBPs into SGs to prevent aggregate formation remain largely unknown.

In 2011, missense mutations in the ubiquitin-like protein ubiquilin 2 (UBQLN2) were found to cause ALS with FTD in rare X-linked cases. In an effort to characterize UBQLN2's normal cellular functions, I performed a proteomic screen for UBQLN2 interactors and found an enrichment of RBPs including SG components under non-stress conditions. Using an unconventional staining technique, I confirmed that UBQLN2 localizes to SGs under a variety of stress conditions and found that this association is transient. In the time period that UBQLN2 localizes to SGs, it also suppresses large SG formation suggesting that it modulates incorporation of SG components.

To characterize UBQLN2's regulatory role in SG formation, I focused on its interaction with the RBP fused in sarcoma (FUS). FUS was not only the most enriched RBP among the UBQLN2 interactors, but also is genetically and pathologically linked to ALS/FTD. In a single molecule Förster resonance energy transfer (FRET) assay, UBQLN2 increased the dynamics of FUS-RNA interaction, increasing the fluidity of FUS-RNA complex formation. This effect translated to a decrease in FUS partitioning

into liquid droplets *in vitro* and suppression of FUS-GFP recruitment into SGs in cells suggesting that UBQLN2 slows FUS recruitment into SGs by increasing the dynamics of its interaction with RNA. ALS/FTD-linked mutations in UBQLN2 partially impaired UBQLN2's ability to increase the dynamics of FUS-RNA interaction and suppress SG formation, indicating a partial loss of UBQLN2 function. These results reveal a previously unrecognized role for UBQLN2 in regulating the early stages of liquid-liquid phase separation of RBPs in SG formation by affecting the dynamics of RNA-protein interaction. Because SGs potentially seed toxic ALS/FTD patient inclusions, these findings have implications for understanding ALS/FTD pathogenesis and designing new treatments for these diseases.

Thesis advisor: Dr. Jiou Wang
Thesis readers: Dr. Jiou Wang, Dr. Michael J. Matunis, Dr. Susan Michaelis, Dr. Marie Hardwick
Alternate thesis readers: Dr. Anthony Leung, Dr. Mark Kohr

Acknowledgements

My thesis project has been a long and winding journey from worm genetics, to cell-based autophagy assays, to DNA damage repair assays and finally stress granule studies, but it has been enjoyable thanks to the support of many friends, family and colleagues. I am truly grateful to Dr. Jiou Wang and the BMB department for their support and the opportunity to pursue these studies at Johns Hopkins. Hopkins is a place where there seem to be an endless number of opportunities to exchange knowledge and form new collaborations. I will miss the School of Public Health's spirit of inclusion where in a single day I will receive an invitation to attend an African Public Health network symposium, STD journal club, and biostatistics help session. This has truly been a great place to spend the past seven years.

Were it not for the time and generosity of many professors, staff, postdocs and students, my thesis project would not have been possible. First, I would like to thank Dr. Jiou Wang for taking me into the lab as his first PhD student and helping me to always try for something slightly out of reach. I greatly appreciate his optimism, idealism and drive to achieve great things and am grateful to him for his patience with the development of the ubiquilin 2 project. I would like to thank all of the past and present Wang lab members and many BMB students who so unselfishly offered their time and technical advice during my PhD, especially Dr. Goran Periz, a master at building new genetic tools who taught me everything I know about molecular cloning, Dr. Yen-ching Wu who taught me the meaning of good "controls", Dr. Aaron Haeusler with Peter Steinwald who helped me to purify the UBQLN2 protein, and Dr. Janet Ugolino, who has been a friend and colleague always willing to help me troubleshoot and without whom I would not have remained sane while writing this thesis. Also, a special thanks to two collaborators, Dr. Raja Sekhar who put up with my persistent requests to process mass spec samples in the Pandey lab and Dr. Jaya Sarkar in Sua Myong's lab who did the initial single molecule FRET experiments with purified FUS, UBQLN2, and RNA to show that UBQLN2 increases FUS-bound RNA dynamics.

I also greatly appreciate the help and guidance from many of the BMB faculty members, especially Dr. Mike Matunis who always seems to find the time to provide thoughtful advice, Dr. Val Culotta who has given me feedback on my project since the beginning in joint lab meetings and whom I greatly admire, and Dr. Fengyi Wan who always manages to give me some encouraging words. Many thanks also to my thesis committee members Dr. Susan Michaelis, Dr. Anthony Leung, and Dr. Marie Hardwick for their advice and support through the years.

Also, thanks to the students and postdocs in BMB never too busy to stop to chat. To the guys of the Leung Lab, Lyle, Aravinth, and Mohsen, for the many fun discussions about stress, RNA granules and science in general. To my BMB classmates Nicole, Chynna, Fengrong and Xin for many fun nights out to celebrate our milestones in the PhD program together. To my late-night companions Marina and Ho-yon for keeping me company. And to a few of my senior classmates Katherine Reiter, Jolyn Gisselberg, Eric Wier and Casey Daniels who have offered help and advice over the years.

I probably would not have come to JHSPH had it not been for the support of my undergraduate advisor at Indiana University, Dr. Lingling Chen, my supervisor at the University of Wisconsin, Dr. Susan West, my manager at Nektar Therapeutics Shaoyong Ni, and Dr. Carmen Scholz, at the University of Alabama, Huntsville who supported my effort to return to graduate school in biochemistry after many years of working in industry as an analytical chemist. I am also grateful to Ms. Sharon Warner who convinced me to write another essay to the admissions committee about my commitment to a five-year PhD program and supported me during my first years at Hopkins. Many thanks to the BMB staff who kept the department running smoothly, especially Ms. Shannon Gaston who helped me in innumerable ways in preparing for my thesis defense.

Lastly, thanks to my family. First, to my Mom and Dad, Jean and Rich Alexander for always being there to listen and sacrificing so many mornings, noons and nights for my many years in school. To my Mom who gave me the tools to be a confident, assertive woman and my Dad who taught me to negotiate in life. They have always been there when no one else would be. I could not be luckier. To

my sister Sarah for always reminding me what is important in life and for being one of the dancers rather than one of the skeptics. And to my husband Chris who has been my champion and friend from preparing late night dinners to putting up with the inevitable 30-minute lab job turning into 3 hours, who has spent hours upon hours in rush hour Beltway traffic to pick up our daughter from daycare so that I could spend a few more hours working every night and never complains. And last but not least, to my daughter Sophie who always reminds me to be stronger, faster and more prompt for whom I hope to be the best Mom-scientist possible.

Table of Contents

List of Tables

List of Figures

Abbreviations and Nomenclature

°C	degrees Celsius
μg	microgram
μL	microliter
μm	micrometer
μM	micromolar
τ	dwell time
AA	amino acid
AAA	ATPases associated with diverse cellular activities
ALS	Amyotrophic lateral sclerosis
ATP	adenosine triphosphate
β-actin	beta-actin
BAG	bcl-2 associated anthogen
BSA	bovine serum albumin
cDNA	complementary deoxyribonucleic acid
CCT	chaperonin containing t-complex polypeptide (TriC)
CMV	cytomegalovirus
CNS	central nervous system
CO_2	carbon dioxide
CHAPSO	3-([3-Cholamidopropyl]dimethylammonio)-2-hydroxy-1-propanesulfonate. Zwitterionic detergent
Ct	carboxy-terminal end of protein
DAPI	4',6-diamidino-2-phenylindole (Nuclear chromatin stain)
DMEM	Dulbecco's modified eagle's medium
DNA	deoxyribonucleic acid
DSK2	duplication suppressor of Kar1 2 (yeast Ubiquilin)
DUB	deubiquitinating enzyme
EBSS	Earle's balanced salt solution
EDTA	ethylenediaminetetraacetic acid
EH	epsin homology domain
eIF2α	eukaryotic initiation factor 2 alpha
EMEM	Eagle's minimum essential media
ERAD	endoplasmic reticulum-associated degradation

fALS	familial (inherited) ALS
FBS	fetal bovine serum
FDR	false discover rate
FLP	flippase
FRAP	fluorescence recovery after photobleaching
FRET	Förster resonance energy transfer
FPLC	fast protein liquid chromatography
FRT	short flippase recognition target site
FTD	frontotemporal dementia (also FTLD), historically called Pick's disease
FTLD	frontotemporal lobar dementia (also FTD)
FUS	fused in sarcoma RNA-binding protein/Translocated in liposarcoma protein
G3BP	Ras-GAP-SH3-binding protein
GAPDH	glyceraldehyde 3-phosphate dehydrogenase
GFP	green fluorescent protein
Gly	glycine
GST	glutathione S-transferase
GUS	β-glucuronidase (plant enzyme)
HECT E3	homologous to the E6AP carboxy-terminus, E3 Ubiquitin ligase
HEK293T	human embryonic kidney cells modified by the SV40 T-antigen
HeLa	breast cancer cells derived from the patient Henrietta Lacks
HEPES	2-[4-(2-hydroxyethyl)piperazin-1-yl]ethanesulfonic acid (buffer)
hnRNP	heterogenous nuclear ribonucleoprotein (subclass of RNA binding protein)
HOP	Hsp70, Hsp90 Organizing Protein, yeast ST11 homolog
HSP70	heat shock protein 70, ATP dependent molecular chaperone (holdase)
hrs	hours
ICC	immunocytochemistry
IDR	intrinsically disordered region
IF	immunofluorescence
IGEPAL	octylphenoxy poly(ethyleneoxy)ethanol. Nonionic, nondenaturing detergent.
IP	immunoprecipitation
Kd	dissociation constant
kDa	kilodalton

LC3B	MAP1LC3B microtubule-associated protein 1A/1B light chain, conjugated to autophagosomes through phosphatidyl ethanolamine; autophagosome marker
LLPS	liquid-liquid phase separation
nLC-MS/MS	nanoscale-liquid chromatography tandem mass spectrometry
Nt	amino-terminal end of protein
MBP	maltose binding protein
mg	milligram
min	minute
MIP	maximum image projection
mL	milliliter
mM	millimolar
mRNA	messenger ribonucleic acid
nLC-MS/MS	nano-liquid chromatography-tandem mass spectrometry
nm	nanometers
NT	nucleotide
OP-Puro	O-propargyl-puromycin
P-bodies	Processing bodies (for cytoplasmic mRNA)
PAGE	polyacrylamide gel electrophoresis
PABP1	poly(A) binding protein 1
PB1	A ubiquitin-like domain in p62
PBS	phosphate buffered saline
PNS	peripheral nervous system
PQC	protein quality control
PrD	prion-like domain
PuroR	puromycin resistance gene (N-acetyl transferase) from *Streptomyces alboniger*
PXX repeat	unique 12x proline-x-x repeat in UBQLN2 where ALS/FTD mutations map
RBP	RNA binding protein
RFP	red fluorescent protein
RING E3	really interesting new gene, E3 ubiquitin ligase type
RNA	ribonucleic acid
RNP	RNA-protein complexes
ROS	reactive oxygen species
S5a	proteasome hinge cap subunit (PSMD4)/Rpn10

sALS	sporadic ALS
SCF	Skp1-Cul1-F box protein, E3 ubiquitin ligase complex
SDS	sodium dodecyl sulfate
sec	seconds
SG	stress granule
shRNA	short hairpin ribonucleic acid
siRNA	short interfering ribonucleic acid
SILAC	stable isotope labelling with amino acids in cell culture
SNP	single nucleotide polymorphism
SOD1	superoxide dismutase 1
SQSTM1	sequestosome 1/p62
STCH	HSPA13. Stress-70 protein chaperone microsome-associated 60 kDa protein
STI1	stress inducible protein (HOP in humans) Hsp90, Hsp70 cochaperone
TDP-43	TAR DNA-binding protein 43
TetR	tetracycline resistance element (tetA) repressor from Transposon 10
TIA-1	T-cell restricted intracellular antigen-1/Nucleolysin TIA-1 isoform p40
TPP	thiamine pyrophosphate
TriC	CCT. TCP-1 ring complex. ATP dependent chaperonin.
Tris	Tris(hydroxymethyl)aminomethane (buffer)
TX-100	Triton X-100
Uba	ubiquitin associated domain
Ubl	ubiquitin-like domain
UIM	ubiquitin interacting motif
UBQLN1	ubiquilin 1/PLIC-1/DA41
UBQLN2	ubiquilin 2/PLIC-2/CHAP1/N4BP4
UBQLN3	ubiquilin 3/TUP-1
UBQLN4	ubiquilin 4/AU1P/UBIN/CIP75/C1orf6
UBQLNL	ubiquilin-like
UPS	ubiquitin-proteasome system
UTR	untranslated region
VCP	Valosin containing protein/p97
WT	wild type
ZnF	zinc finger domain

Chapter 1 Introduction

Cells intimately depend on protein and RNA quality control to survive during stress. Dysregulation of protein and RNA homeostasis in neurons is central to the pathogenesis of the progressive neurodegenerative diseases amyotrophic lateral sclerosis (ALS) and frontotemporal dementia (FTD). In this work I describe a previously unrecognized role for the ALS/FTD-linked ubiquitin-like protein Ubiquilin 2 (UBQLN2) in regulating the cellular response to stress in cytosolic RNA-protein compartments known as stress granules (SGs). Because mutations in the UBQLN2 gene cause ALS with FTD and SGs may serve as the seed sites for patient inclusions, this role is relevant to understanding and designing new treatments for these devastating neurodegenerative diseases. Here I have laid out background on ALS/FTD pathology, SGs, and Ubiquilins that forms the basis of this thesis work.

ALS/FTD symptoms and etiology

ALS and FTD are two devastating, neurodegenerative diseases for which there are few effective treatments. ALS, also known as Lou Gehrig's disease is the most common adult onset motor neuron disease occurring in 5 out of every 100,000 people in the United States, while FTD is the second most common type of dementia for people younger than 65 accounting for 5-15% of dementia cases (Mehta, 2018; Ratnavalli et al., 2002). ALS is characterized by skeletal muscle wasting stemming from degeneration of both upper and lower motor neurons. Upper motor neurons include motor neurons descending from the motor cortex to the brainstem and spinal cord, while lower motor neurons include bulbar and spinal motor neurons descending to skeletal muscles (Taylor et al., 2016). Loss of upper motor neurons leads to jerky reflexes, clumsiness, spasticity, and functional limitations, while loss of lower motor neurons initially leads to weakness, cramps and fasciculations in limbs (spinal onset) or problems with speech or swallowing (bulbar onset) that spreads (Taylor et al., 2016). The French physician Jean-Martin Charcot played a pivotal role in distinguishing the symptoms of ALS from related motor neuron diseases in the mid-19th century. While working as a medical intern in the "Hospital de la Salpêtrière" which he dubbed the "grand asylum of human misery" he systematically

recorded and paired patient symptoms with postmortem anatomy from among the nearly 3000 patients with neurologic disorders housed at the facility (Charcot and Joffroy, 1869; Katz et al., 2015; Kumar et al., 2011). Using these criteria, he laid out criteria to distinguish ALS, a progressive neuropathy, from similar motor neuropathies and myopathies, diseases of muscle alone, many of which are still in use today.

Only recently was it recognized that 50% of ALS patients also show signs of dementia with 15% of patients meeting the criteria for FTD, suggesting that these diseases are part of a continuous clinical spectrum (Van Langenhove et al., 2012). FTD, also called Pick's disease for the physician Arnold Pick who first described it in detail, is characterized by changes in personality, behavior and language ability associated with atrophy of regions of the frontal and temporal lobes, where pyramidal neurons are most affected. Memory, however, is usually spared until the end stages of the disease (Pick, 1892; Rademakers et al., 2012). In FTD, like ALS, symptoms vary but can be subdivided into three clinical variants: behavioral, and two types of language and cognition loss termed primary progressive aphasia and semantic aphasia respectively. Besides ALS, FTD has also been associated with Parkinson's disease (Rademakers et al., 2012). The heterogeneity of FTD symptoms like ALS have made the disease difficult to characterize but recent determinations of disease linked mutations and identifying pathology are bringing both ALS and FTD into focus.

The overlap of ALS and FTD symptoms suggests that pathology in more than one neuronal and/or glial cell type may contribute to the disease progression. Motor neurons, whose degeneration is associated with ALS, are highly asymmetric cells with long axons that extend up to 1 meter from the cell body to enervate skeletal muscles controlling voluntary movement. These axons are insulated by oligodendrocytes in the brain and spinal cord and Schwann cells in the peripheral nervous system. Dendritic architecture differs between upper and lower motor neurons, but they are highly excitable and respond to glutamate input. The first FDA approved drug for ALS, riluzole, actually targets glutamate uptake, although its efficacy in extending life is somewhat limited. Glia such as astrocytes and microglia also contribute to motor neuron survival (Robberecht and Philips, 2013; Taylor et al.,

2016). In contrast, pyramidal neurons associated with FTD are large multipolar neurons, but are restricted to the frontal and temporal lobes. Apical and basal dendrites as well as the axons are large and can be highly branched, while short dendritic spines are numerous and receive synaptic input. These basic morphological differences in the cell types affected by ALS and FTD in the brain suggests that a basic rather than specialized cellular pathology may contribute to ALS/FTD pathology.

ALS and FTD have also interestingly been genetically and pathologically linked to some of the same proteins involved in both protein and RNA homeostasis. An estimated 90-95% of ALS and 50-75% of FTD cases occur without any prior family history of the disease (sporadic) (sALS/sFTD), while the remaining cases can be traced within families (fALS/fFTD) (Robberecht and Philips, 2013). All ALS cases and the majority of FTD cases appear to be linked to a defect in protein clearance due to the hallmark accumulation of intracellular protein inclusions (called Pick bodies in pure FTD) in patient brain tissue. Missense mutations in the *SOD1* gene encoding the superoxide dismutase 1 enzyme resulting in SOD1 aggregate formation, were the first to be linked to ALS in 1993 and account for 10% of fALS (Rosen et al., 1993). Missense mutations in the microtubule associated protein tau (MAPT) were linked to FTD in 1998 and are also present in ubiquitinated FTD associated inclusions (Hutton et al., 1998). Interestingly, prior to this discovery, the tau protein was a known component of intracellular tangles found in Alzheimer's disease, but without any known pathology (Alzheimer, 1991; Rademakers et al., 2012). These discoveries made understanding protein clearance mechanism central to understanding ALS and FTD pathology.

However, recent discoveries suggest that defects in RNA homeostasis and protein trafficking also are central to ALS/FTD pathology. Since 1993, mutations in more than 30 other genes have been linked to ALS/FTD. Protein quality control factors include autophagic receptors SQSTM1/p62 and optineurin, VCP, and UBQLN2, the subject of this thesis, RNA homeostasis factors such as TAR-DNA binding protein, fused in sarcoma (FUS), Ewing sarcoma protein (EWS), TAT-binding protein associated factor 15 (TAF-15), hnRNPA1 and hnRNPA2/B1 and protein traffickers such as profilin 1 (PFN1), dynactin (DCTN1), and neurofilament heavy chain (NFH) have all been found to cause

ALS/FTD by pedigree analysis (Table 1-1). The recently identified repeat expansion in the C9orf72 gene linked to more than 60% of ALS/FTD cases, appears to cause both RNA toxicity and proteotoxicity, highlighting the dual role of protein and RNA homeostasis in ALS/FTD disease pathology. For example, the C9orf72 hexanucleotide repeat causes RNA toxicity through formation of a G-quadraplex structure that acts as an RNA binding protein sponge, and proteotoxicity through production of dipeptide repeats that interfere with protein degradation by both the proteasome (Gupta et al., 2017; Haeusler et al., 2014). Additionally, a decrease in C9orf72 protein levels associated with the repeat region may also interfere with degradation of proteins in the cell through autophagy (DeJesus-Hernandez et al., 2011; Ugolino et al., 2016). These dipeptide repeats also interfere with the dynamic exchange of RNA binding proteins (RBPs) into and out of the cytoplasmic RNA granules known as stress granules (SGs) (Lee et al., 2016; Zhang et al., 2018c). Notably, the RBPs FUS and TDP-43 are principle components of patient inclusions in both ALS and FTD, so much so that FTD cases have been subclassified as FTLD-TDP, FTLD-FUS, and FTLD-tau, FTLD-UPS based on the presence of TDP-43, FUS, tau and other ubiquitin-proteasome components respectively (Arai et al., 2006; Munoz et al., 2009; Neumann et al., 2006, 2009a, 2009b; Rademakers et al., 2012). However, how RBP protein solubility is maintained in the cell and RBP's function in ALS/FTD pathology is still unclear (Ling et al., 2013; Robberecht and Philips, 2013).

Protein and RNA homeostasis intersect in RNP granules

A prominent feature of the ALS/FTD associated RBPs is their propensity to form dynamic ribonucleoprotein particles (RNPs), mainly composed of RNAs and proteins. In these granules, protein-bound RNA's form membraneless condensates that concentrate RNA processing and regulatory factors by a process increasingly recognized as a liquid-liquid phase separation (Boeynaems et al., 2018) (Figure 1-1B). Like oil in water, RNP granules exhibit the dripping, wetting and fusing behavior of spherical phase-separated liquid droplets (Hyman et al., 2014; Lin et al., 2015; Molliex et al., 2015; Patel et al., 2015). In cells, RNPs show the spherical distribution and viscoelastic properties expected of a phase separated liquid (Boeynaems et al., 2018; Patel et al., 2015). These properties

translate to the formation of dynamic liquid particles in which components are rapidly exchangeable, are deformable, and fuse to form larger and larger droplets over time.

The properties of RNA and protein that drive RNP granule formation continue to be more precisely defined, but several factors distinguish them. First, long stretches of low complexity amino acid sequence that oligomerize and RNA recognition motifs have been shown to mediate RBP phase separation (Mittag and Parker, 2018; Wang et al., 2018). Low complexity regions are stretches of amino acids containing a limited number of amino acids. Many of these stretches are intrinsically disordered regions (IDRs) and are thus flexible and able to adopt a variety of different structural conformations. This heterogeneity facilitates weak multivalent interactions and more stable induced structural interactions depending on the amino acid residues represented. Low complexity regions containing concentrated hydrophobic or aromatic kinked segments (LARKS), degenerate repeats, short regions that adopt discrete structures known as short linear interaction motifs (SLiMs), alternating charge blocks, and glutamine-asparagine (QN-rich) prion-like domains have been identified to mediate RNP granule formation (Boeynaems et al., 2018; Mittag and Parker, 2018). Protein posttranslational modifications that alter the conformational flexibility and/or surface charge of RBPs such as serine/tyrosine phosphorylation, arginine methylation, ubiquitylation, sumoylation, O-GlcNAC glycosylation, and parylation, have all in some way been observed to alter partitioning of proteins into RNP granules (Altmeyer et al., 2015; Boeynaems et al., 2018; Higgins et al., 2015; Leung et al., 2011; Nott et al., 2015; Ohn et al., 2008; Shen et al., 2006; Tourrière et al., 2003). RNA itself has also been observed to phase separate and drive RBPs into granules (Jain and Vale, 2017; Mao et al., 2011; Treeck et al., 2018). When RNA and purified proteins are combined, RNA length and structure tune both the viscosity and dynamics of RBP phase separation (Elbaum-Garfinkle et al., 2015; Langdon et al., 2018; Zhang et al., 2015). Consistent with a role of multivalent protein interactions regulating RNP granule formation, local protein concentration regulated by nucleocytoplasmic transport and interaction with microtubule transport motors such as dynein and kinesin also drive RNP formation (Kwon et al., 2007; Loschi et al., 2009; Zhang et al., 2018a). Thus, in the emerging model of RNP formation, both

structured and unstructured RBP-RBP, RBP-cytoskeleton, RBP-RNA, RNA-RNA interactions regulate RNP granule formation.

In cells, RNP granule formation has been observed both in the nucleus and cytoplasm (Figure 1-1A, C). In the nucleus, RNP granules include nucleoli, sites of ribosomal assembly, Cajal bodies, sites of pre-mRNA splicing, nuclear speckles, interchromatin regions also enriched in pre-mRNA splicing factors, and promyelocytic leukemia (PML) bodies, sites of recruitment of SUMoylated proteins (Brangwynne et al., 2011; Spector, 2001) (Figure 1-1C). In the cytosol, these RNP granules include processing bodies (P-bodies), constitutively present sites of mRNA decapping and degradation, and stress induced granules known as stress granules that are the focus of this study (Figure 1-1A). Other RNP granules in specialized cell types that have been investigated include neuronal granules, which carry mRNA to local sites of translation near the synapse, P-body-like structures in the dendrites of neurons (Cougot et al., 2008; Krichevsky and Kosik, 2001) and two types of germline RNP granules in the oocytes of the round worm *Caenorhabditis elegans*: germline messenger RNP processing bodies (grPBs) present in cell cycle arrested oocytes and processing bodies in the differentiated oocyte (PBs) (Brangwynne et al., 2009; Hubstenberger et al., 2015). All of these granules concentrate RNA and RBPs to perform specific RNA processes and the condensation of RNA and RBPs is critical to their formation. However, this condensation process also provides the opportunity for the weak dynamic interactions that drive RNP formation to slip into low energy stable conformations (Figure 1-1B).

In vitro, studies have shown that prolonged residence of proteins in these phase separated droplets leads to a liquid-to-solid phase transition that may be a precursor to toxic inclusions seen in neurodegenerative diseases such as ALS/FTD (Figure 1-1B) (Kim et al., 2013; Lin et al., 2015; Mackenzie et al., 2017; Molliex et al., 2015; Murakami et al., 2015; Patel et al., 2015). Both LARKs and QN-rich PrDs have also been shown to adopt amyloid-like stacked β-sheet structures that are more solid-like, suggesting that RBP dynamics within RNP granules is critical to RBP solubility (Mackenzie et al., 2017; Mittag and Parker, 2018; Murray et al., 2017). How the dynamics of RNPs is explored in

this thesis where I have specifically focused on maintenance of stress granules (SG) whose components have also been found in ALS/FTD patient inclusions.

SGs as precursors to ALS/FTD patient inclusions

SGs are one type of RNP granule that transiently forms in the cytoplasm in response to stress. Stress induces sequestration of stalled translation initiation complexes including 40S ribosomes, RBPs, mRNA, and translation initiation factors along with apoptotic factors into these cytoplasmic granules (Anderson and Kedersha, 2009). The first evidence for SGs came from biochemical and electron microscopy studies on Peruvian tomato (*Lycopersicon peruvianum*) cells exposed to heat shock in which specific untranslated mRNAs were observed to associate with heat shock proteins in particles in the cytosol (Nover et al., 1983, 1989; Scharf et al., 1998). Fifteen years later Kedersha *et. al.* reported the recruitment of silenced mRNA and RBP T-cell restricted intracellular antigen-1 (TIA-1), TIA-1 related (TIAR) and polyA binding protein I (PABP 1) in response to heat, hypoosmolarity, ultraviolet light and sodium arsenite treatments in mammalian cells (Kedersha et al., 1999). This formation was triggered by, but not dependent on, phosphorylation of the translation initiation factor eIF2α at serine 51 (Kedersha et al., 1999). SG formation could also explain earlier observations that cells rapidly recover from heat stress in a process requiring no new RNA or protein synthesis (Kedersha et al., 1999; Lindquist, 1981; Panniers and Henshaw, 1984; Storti et al., 1980).

Further studies suggested that mRNA rather than ribosomes or protein signaling factors is critical for mediating SG formation. eIF2α phosphorylation by one of the stress responsive kinases: protein kinase R (PKR), PKR-like endoplasmic reticulum kinase (PERK) or pancreatic eIF2α kinase (PEK), general control nonderepressible 2 (GCN2), heme-regulated initiation factor 2α (HRI), and Z-DNA kinase inhibits formation of the ternary eIF2-GTP-$tRNA_i^{Met}$ responsible for inserting the first methionine charged tRNA into the start site on the ribosome induces SG formation. Notably, however, inhibitors that bypass eIF2α phosphorylation such as puromycin, which promotes dissolution of polyribosomes on mRNA by promoting prematurely terminated protein formation and hippuristanol or pateamine A, which inhibit RNA helicase activity of eIF4A also induce SG formation (Dang et al., 2006; Kedersha

et al., 2000; Mazroui et al., 2006; Mollet et al., 2008). A subset of stresses (sodium selenite, hydrogen peroxide, cleaved tRNAs) that promote translational stalling through hypophosphorylation of the 4EBP-cap binding protein also induce SG formation (Emara et al., 2010, 2012; Fujimura et al., 2012; Ivanov et al., 2011; Panas et al., 2016). In contrast, inhibitors that trap ribosomes on mRNA such as emetine or cycloheximide, inhibit SG formation (Kedersha et al., 2000). These observations suggest that ribosome-free mRNA and bound RBPs rather than stalled 48S preinitiation ribosomes are the substrates for SG formation (Panas et al., 2016; Protter and Parker, 2016).

Despite an understanding of the driving forces of SG formation, the function of SGs remains incompletely understood. 60S ribosomal subunits and incompletely transcribed transcripts appear to be normally excluded from SGs counter to the hypothesis that 48S particles might be selectively incorporated into SGs to translate a subset of transcripts (Kedersha et al., 1999; Seguin et al., 2014). SG's do appose Processing-bodies (P-bodies), sites of mRNA decapping and degradation and exchange mRNA and RBPs under some stress conditions, but do not affect the deadenylation of polyA-RNA that precedes mRNA degradation in P-bodies. Even if mRNA is trapped in polysomes deadenylation is inhibited under stress, suggesting that SGs do not directly regulate mRNA stability (Buchan and Parker, 2009). Inhibition of SG formation also does not interfere with translation inhibition, suggesting that there is not a positive feedback loop from SG formation to the integrated stress response kinases that inhibit translation (Anderson and Kedersha, 2008). SG formation does repress the translation of some housekeeping genes and enhance translation of some stress responsive transcripts. However, recent reports suggest that as low as 15% of mRNA may be transiently sequestered in stress granules at one time consistent with proteomic studies showing that specific SG components and mRNAs incorporated into SGs are stress and cell type specific (Markmiller et al., 2018a; Treeck et al., 2018). These reports suggest that SGs function to integrate specific mRNAs and proteins with specific stress signals. The function of this sequestration is not yet well understood.

Cells that form SGs under many conditions do however survive better than those in which SG formation is inhibited, suggesting that SG formation is an adaptive response (Eisinger-Mathason et al.,

2008; Kim et al., 2012; Kwon et al., 2007; McEwen et al., 2005). The mechanism of this adaptive response is also incompletely understood but sequestration of apoptotic and anti-apoptotic factors into SGs could explain the integration of apoptotic signaling with SG formation in the cellular stress response. For example, the receptor of activated protein C kinase 1 (RACK1) and TNFα-receptor associated factor 2 (TRAF2) are proapoptotic factors sequestered into stress granules whose association with proapoptotic factors mitogen activated MAP kinase, kinase, kinase 4 (MTK1) and transcription factor NF-κB is required for induction of apoptosis (Arimoto et al., 2008; Buchan and Parker, 2009; Kim et al., 2005). In contrast, the anti-apoptotic factors ribosomal S6 kinase (RSK2) and Fas-activated serine/threonine kinase (FAST) kinase are two rare near static components (with a recovery time following photobleaching in FRAP experiments greater than 10 min) of SGs that bind to the QN-rich region of TIA-1 that suppresses TIA-1's apoptotic activity (Buchan and Parker, 2009). These factors all "piggy-back" onto core assembly factors: RSK2 and FAST with TIA-1, RACK1 with 40S ribosomes, and TRAF2 with eIF4G to be incorporated into SGs (Buchan and Parker, 2009). By a similar mechanism, raptor a component of the mTORC1 complex that inhibits autophagy is sequestered by the SG component astrin, suppressing apoptosis in response to oxidative and metabolic stresses (Protter and Parker, 2016; Thedieck et al., 2013). By an as yet unknown mechanism, loss of core stress granule component eIF3 associated with enhanced production of reactive oxygen species and depletion of ATP may mediate the conversion of SGs from anti-apoptotic to pro-apoptotic in nature (Aulas et al., 2018; Fujimura et al., 2012). Thus, incorporation of signaling molecules into SGs through their association with core SG components integrates formation of SGs with specific cellular stress responses.

While SG formation may allow cells to adapt to stress, because they concentrate intrinsically disordered proteins, SGs may also serve as the seed sites for the intracellular inclusion formation associated with ALS/FTD (Aulas and Vande Velde, 2015; Li et al., 2013). Like other RNP granules, SGs contain stable "cores" visible by electron microscopy that can be isolated via subcellular fractionation and immunoprecipitation (Jain et al., 2016; Ohn et al., 2008; Souquere et al., 2009), but also a dynamic

responsive "shell" thought to be formed by the oligomerization of low complexity, prion-like domains (PrDs) in RBPs (Kroschwald et al., 2015; Lin et al., 2015; Mittag and Parker, 2018; Molliex et al., 2015; Patel et al., 2015). These shell proteins may adopt more solid-like states as stress is prolonged and as SGs recruit additional components. Importantly, an increasing number of ALS/FTD-associated proteins found in patient inclusions have also been found in SGs, including FUS, TDP-43, C9orf72 protein and its poly-dipeptide repeats, ataxin 2, hnRNPA2/B1, hnRNPA1, SOD1 and profilin 1 (Boeynaems et al., 2017; Bosco et al., 2010; Dewey et al., 2011; Figley et al., 2014; Gal et al., 2016; Kim et al., 2013; Liu-Yesucevitz et al., 2010; Nonhoff et al., 2007; Sama et al., 2013). ALS/FTD-linked mutations in RBPs FUS and hnRNPA1 that phase separate into SGs, accelerate the phase transition of these proteins from a dynamic liquid state to a solid fibril state (Kim et al., 2013; Mackenzie et al., 2017; Molliex et al., 2015; Patel et al., 2015). Importantly, core SG components TIA-1, eIF3A, PABP, and eIF4G have also been found in patient inclusions (Aulas and Vande Velde, 2015; Mackenzie et al., 2017). Additionally, PQC factors linked to ALS, such as the disaggregase VCP, play a role in both assembling and disassembling SGs and shuttling them to the autophagosome-lysosome system for degradation (Buchan et al., 2013; Seguin et al., 2014). These data suggest that development of ALS/FTD inclusions may be inherently linked to the process of SG formation.

Protein quality control at SGs

Due to the promiscuous nature of the interactions that drive SG formation, PQC factors may play an active role in maintaining SG fluidity. Consistent with this hypothesis, components of the two systems of protein clearance in the cell, autophagy and the ubiquitin-proteasome system, localize to and regulate SG composition. For example, mono-ubiquitin, unanchored ubiquitin chains and unconjugated LC3B, E3 ubiquitin ligases, deubiquitinases (DUBs), and the proteasome have all been shown at SGs (Buchan et al., 2013; Markmiller et al., 2018b; Mateju et al., 2017; Mazroui et al., 2007; Seguin et al., 2014; Turakhiya et al., 2018; Xie et al., 2018). ROQUIN (RING finger and CCCH-type zinc finger domain-containing protein 1), its mammalian paralogue MNAB (membrane-associated nucleic acid binding protein) and TRAF-2 (TNF receptor-associated factor 2) are all RING-type E3 ligases that localize to

SGs with the effect of altering stability of particular mRNAs (Athanasopoulos et al., 2010; Kim et al., 2005). The DUBs USP5 and USP13 were recently found to regulate SG disassembly (Xie et al., 2018), while in a function not requiring its catalytic activity the DUB USP10 was found to limit G3BP incorporation into SGs by competing with caprin 1 (Kedersha et al., 2016). While the coordinated role of both the ubiquitin-proteasome system and autophagy in SG disassembly is still unclear, components of both PQC clearance systems in the cell appear to be present.

Several PQC factors do function at SGs to prevent the aberrant incorporation of misfolded, ubiquitinated proteins which disturb SG dynamics into SGs. Ubiquitinated prematurely terminated ribosomal transcripts (termed defective ribosomal products or DRiPs) induced by puromycin treatment were found to disrupt RBP fluidity in SGs and promote conversion of liquid SG assemblies into solid assemblies (Ganassi et al., 2016; Mateju et al., 2017). The ATPase activity of a small heat shock protein HSPB8, HSP70 and its nucleotide exchange factor BAG3 in cooperation with VCP/p97 and its cofactors UFD1L and NPL4 were found to actively extract DRiPs from SGs and transfer them to the aggresome for degradation by autophagy (Buchan et al., 2013; Ganassi et al., 2016; Seguin et al., 2014) (Figure 1-1B). In a non-mutually exclusive mechanism, VCP (yeast cdc48) was also recently found to cooperate with the human ZFAND1 (AN1-type zinc finger protein 1) (yeast Cuz1) and the proteasome to clear SGs during recovery from stress (Turakhiya et al., 2018). The specific karyopherin β2 specifically known for its solubilizing effect on the FG repeats of the nuclear pore complex appear to directly solubilize solid-like RBPs such as FUS in SGs (Guo et al., 2018; Hofweber et al., 2018; Qamar et al., 2018; Yoshizawa et al., 2018) Jain et. al. (2016) also implicated the ATP-dependent chaperonins RuvB, MCM, and TriC in regulating SG formation but their mechanisms of action remain to be tested. These studies suggest that PQC factors clearly play a role in preventing and clearing aberrant SGs, but other PQC factors that directly mediate the formation and maintenance of RBP fluidity in SGs, the topic of this thesis, are unknown.

UBQLN2 is a PQC factor genetically and pathologically linked to ALS/FTD

In 2011, Deng et. al. identified single point mutation in the UBQLN2 gene that causes a rare X-linked form of ALS with dementia in a 5-generation family with 19 affected individuals without male-to-male transmission (Deng et al., 2011). This inherited mutation mapped to a proline in a unique 12x PXX repeat in the UBQLN2 protein c.1490C.A (p.P497H) (Figure 1-2). This mutation resulted in 90% penetrance by age 70 with an age of onset between 17 and 71 years. Four other proline mutations mapping to this repeat were later identified in four unrelated families in this cohort (P497S, P506T, P509S, P525S) (Figure 1-2). These sequence variants were not present in the SNP database or 928 age matched controls (Deng et al., 2011). In another 5-generation family, a P497L mutation resulted in an earlier age of onset of 10 years of age in males and between 20 and 30 years of age in females, suggesting that mutations in UBQLN2 can cause severe motor neuron degeneration (Fahed et al., 2014). Missense mutations in other residues within and outside the PXX region have since been identified in French/French-Canadian, Italian, German, Australian, New Zealander and Turkish cohorts in both inherited and sporadic cases of ALS/FTD (Daoud et al., 2012; Fahed et al., 2014; Gellera et al., 2012; Huang et al., 2017; Özoğuz et al., 2015; Scotter et al., 2017; Synofzik et al., 2012; Williams et al., 2012) (Figure 1-2). One mutation identified (A282V) resulted in a pure FTD phenotype, while another (T487I) resulted in a pure ALS phenotype (Synofzik et al., 2012; Williams et al., 2012) suggesting that gene mutations in UBQLN2 can result in heterogenous pathology in the clinical spectrum of ALS/FTD. These studies bolster evidence that mutations in UBQLN2 cause both sporadic and familial ALS/FTD.

Interestingly, UBQLN2 is also pathologically associated with ALS/FTD. Both wild type and mutant UBQLN2 have been found in sporadic and familial ALS/FTD ubiquitinated inclusions with and without UBQLN2 mutations present (Brettschneider et al., 2012; Deng et al., 2011). In patients with and without UBQLN2 mutations, UBQLN2 stained characteristic ALS-linked skein-like spinal cord inclusions also containing other ALS/FTD-linked PQC factors p62, optineurin and ubiquitin, and RBPs TDP-43 and FUS. In addition, in the hippocampi of other ALS patients with dementia and

FTD patients with ubiquitin-positive inclusions examined, wild type UBQLN2 was present in dentate granular cell inclusions that were positive for p62, ubiquitin and optineurin (Deng et al., 2011). There is also a correlation between UBQLN inclusions in the cerebellar granular region and hippocampi of ALS/FTD patients with a hexanucleotide repeat expansion in an intronic region of the *C9ORF72* gene, (Brettschneider et al., 2012). Distinct from the spinal cord neurons, UBQLN2 positive inclusions generally do not contain FUS and sometimes are negative for TDP-43. Mutant UBQLN2 P506T itself forms inclusions in the hippocampus in cases with dementia that may be unique to mutant UBQLN2 pathology (Deng et al., 2011). These observations indicate that while UBQLN2 positive inclusions are distinct in motor neuron and hippocampal cells, both wild type and mutant UBQLN2 are involved in ALS/FTD pathology associated with patient inclusion formation.

Aspects of UBQLN2 pathology seen in human ALS/FTD patients have also been recapitulated in mouse, rat and Drosophila models (Ceballos-Diaz et al., 2015; Gorrie et al., 2014; Hjerpe et al., 2016; Kim et al., 2018; Le et al., 2016; Wu et al., 2015). Several mutant UBQLN2 mouse models showed cognitive deficits along with hippocampal inclusions characteristic of FTD. Transgenic mice that expressed human UBQLN2 from the Y-chromosome under the endogenous UBQLN2 promoter showed delayed fear response and poor performance in a Morris water maze associated with the accumulation of ubiquitinated aggregates in the dendritic spines of hippocampal neurons (Gorrie et al., 2014). Mice transduced with an adeno-associated virus carrying UBQLN2 P497S and P506T via somatic brain transgenesis showed clasping and rotarod deficits at 3-4 months of age (Ceballos-Diaz et al., 2015). And a P520T (P506T equivalent in mice) CRISPR knock-in mouse also showed impairment in novel object recognition and placement. In these mouse models, impaired synaptic function and protein aggregates were evident without neuronal loss. A rat overexpressing mutant UBQLN2 P497H did show cognitive deficits and neuronal loss without any motor deficits (Wu et al., 2015). Only when the UBQLN2 mutant (P497S or P506T) was expressed under a Thy1.2 neuronal mouse promoter were motor deficits and neurodegeneration observed in addition to cognitive deficits. (Le et al., 2016). Independently, mutant UBQLN2 aggregation has also been studied in the Drosophila

compound eye (Kim et al., 2018). Despite the mix of symptoms of neurodegeneration, all of these models showed accumulation of UBQLN2 in ubiquitinated intracellular neuronal inclusions suggesting that a defect in protein clearance is associated with the disease pathology.

The dominant inheritance of *UBQLN2* gene mutations suggests that a gain of toxicity, dominant negative effect or haploinsufficiency contribute to the disease pathology. Given the heterogeneity of symptoms associated with ALS/FTD associated UBQLN2 mutations, one or more of these mechanisms may contribute to the disease. The fact that a UBQLN2 knockout rat failed to show any phenotype while a rat overexpressing UBQLN2 showed cognitive decline could indicate that a simple "loss of function" associated with haploinsufficiency is not relevant to the disease pathology. However, there have been several examples of knockout animals that failed to recapitulate the symptoms of the disease in which loss of function clearly contributed to the disease pathology. For example, both the alsin (ALS2) knockout mouse (Cai et al., 2005; Deng et al., 2007; Devon et al., 2006; Hadano et al., 2006; Yamanaka et al., 2006) reviewed in (Cai et al., 2008) and the PINK1 knockout mouse (Morais et al., 2009) failed to show disease specific pathology. However, the loss of function mechanisms clearly contributed to these forms of disease. The knock-in UBQLN2 mutant mouse model also failed to show a "gain of toxicity" or "dominant negative" effect on motor neuron function or survival (Hjerpe et al. 2016)). It is conceivable that both loss of UBQLN2's cytoprotective effect and toxicity of the mutant protein could together contribute to the disease mechanism. Further characterization of UBQLN2 function may be required for a more detailed mechanism of pathogenesis. These studies together implicate mutations in UBQLN2 as both a genetic cause of ALS/FTD and UBQLN2 as part of ALS/FTD pathology, but the mechanism(s) by which it causes pathogenesis are unclear.

UBQLN2 has a conserved, modular domain structure

UBQLN2 is a type II ubiquitin-like protein encoded by an intronless gene with a cryptic intron on the X-chromosome. It is 74% identical to its nearest human homolog UBQLN1 with 11 exons encoded on chromosome 1. Ubiquilins have a conserved amino-terminal ubiquitin-like domain (Ubl) that is

only 36% identical to ubiquitin but adopts a highly similar fold (Figure 1-3 A, B). Like ubiquitin's Leu^{8}, Ile^{44}, Val^{76} hydrophobic pocket, this Ubl contains an Ile^{75} and Val^{101} important for its interaction with ubiquitin-interacting motifs (UIMs) of the proteasome, E3 ubiquitin ligases, DUBs and the ESCRT machinery (Beal et al., 1996; Walters et al., 2002). While it lacks the C-terminal Gly-Gly required for E1 activating enzyme conjugation in the ubiquitin conjugation cascade, it does interact with its own carboxy-terminal ubiquitin-associated domain (Uba).

The Uba domain in Ubiquilins is a 40 amino acid, 3 helix bundle that binds ubiquitin (Figure 1-3A, B). This domain was the first bioinformatically predicted ubiquitin binding domain from an alignment of a number of ubiquitin binding protein sequences (Hofmann and Bucher, 1996; Hurley et al., 2006). The Uba domain in UBQLN2 and its closet human homolog UBQLN1 has one of the strongest affinities for ubiquitin without chain-type specificity (Kd 20 μM) (Raasi et al., 2005; Zhang et al., 2008). Repeats of this Uba domain were thus used in the first molecular traps for ubiquitin chains, termed tandem-repeated ubiquitin-binding entities (TUBES) (Gao et al., 2016; Hjerpe et al., 2009). The Kd of this Uba's interaction with its own Ubl domain is ten-fold lower than that of its interaction with ubiquitin, which affects the availability of these domains to interact with ubiquitin and UIM containing proteins (Itakura et al., 2016; Lowe et al., 2006; Nguyen et al., 2017).

Between the Ubl and Uba domains in UBQLN2 is a flexible linker region of 474 amino acids that encompasses 76% of UBQLN2's composition (Figure 1-2A, B). This region contains a set of conserved Sti1-like repeats that appear to have been replicated in the evolution of ubiquilins from yeast to higher eukaryotes (Kaye et al., 2000; Marín, 2014) (Figure 1-3A). Sti1/p60 in yeast and HIP in humans, binds to the ATPase domain of Hsp70 stabilizing the ADP bound state of Hsp70 and promoting Hsp70-Hsp90 complex formation (Höhfeld et al., 1995; Lässle et al., 1997). Consequently, the Sti1-like repeats in UBQLN2 are part of a minimum binding region in the ATPase domain of the Hsp70 Stch (HSPA13) (Kaye et al., 2000). Whether these Sti1-like repeats stabilize client protein bound to Hsp70 or Hsp90 remains to be determined (Hjerpe et al., 2016; Kaye et al., 2000). However, both we and others, found that UBQLN2, but not UBQLN1 or UBQLN4, immunoprecipitates HSP70,

suggesting that these repeats do not bind HSP70 in all contexts (Hjerpe et al., 2016; Alexander et al., 2018). The repeats have been implicated, however in UBQLN oligomerization and phase separation, a topic relevant to this study (Dao et al., 2018; Ford and Monteiro, 2006; Sharkey et al., 2018). Bioinformatics predict that the first set of Sti1-like repeats in yeast Dsk2/Dph2 was replicated during the evolution of higher eukaryotes. This second set of Sti1-like repeats that have been implicated in UBQLN oligomerization are specific to higher eukaryotes (Dao et al., 2018; Kaye et al., 2000; Marín, 2014). The presence of these Sti1 repeats also distinguishes UBQLN's from other Ubl-Uba type proteins such as hHR23A, B (yRad23), hDdi1, KPC2 (Kip1 ubiquitylation promoting complex), hNUB1 (NEDD8 ultimate buster 1), and p62 that also contain this Ubl-Uba domain architecture and associate with UIMs, but lack these repeats (Su and Lau, 2009).

Prior to the identification of the Sti1-like repeats in UBQLN2, the central low complexity region of UBQLN2 was defined by 18 NPXφ repeats in UBQLN 1/2/4 where X is any amino acid and φ is any hydrophobic amino acid (Mah et al., 2000; Wu et al., 2002) (Figure 1-2 B). Three of these repeats are NPF, a recognized epsin homology (EH) binding motif, although later studies found that the Ubl domain alone was sufficient to bind the UIMs of endocytic adaptors Eps15, HRS and HBP containing the epsin homology domain (Regan-Klapisz et al., 2005). The significance of these repeats thus still remains unclear.

The Ubl and Uba domains of UBQLN2 are highly conserved among Ubiquilin paralogs, whereas the linker region is more variable and may be the source of protein functional specificity. Humans contain at least four Ubiquilins UBQLN1, UBQLN2, UBQLN3, UBQLN4 (Marín, 2014). UBQLN1, 2, and 4 are ubiquitously expressed, while UBQLN3 is testes specific and appears to have lost some of the Sti1 repeats (Conklin et al., 2000; Kim et al., 2014; Yuan et al., 2015). Its closest homolog, which may also be testes specific, UBQLNL contains only a Ubl domain followed by regions of low complexity without any Sti1 repeats (Figure 1-3 C) (Yuan et al., 2015). UBQLN4 is most similar to yeast homolog Dsk2, while UBQLN2 appears to be duplicated from UBQLN1 and shows higher expression in the brain and spinal cord (Marín, 2014). UBQLN1, 2, and 4 can homo- and hetero-dimerize as will be

discussed further below (Ford and Monteiro, 2006; Lee et al., 2013a), but also appear to have distinct localizations and functions at the cellular level (Hjerpe et al., 2009; N'Diaye and Brown, 2003; N'Diaye et al., 2008).

Between the Sti1-like repeats are a number of other low complexity regions annotated by the simple modular architecture research tool (SMART) (Schultz et al., 1998). These low complexity regions contribute to the compositional bias in UBQLN2. Ser, Pro, Gln, Ala, Leu, Gly compose nearly 60% of UBQLN1/2/4 sequences, with the addition of Gln in yeast Dsk2 (ProtParam). This composition is in stark contrast to the low complexity regions in RBPs that mediate LLPS which includes Asn, Gln, Tyr and Gly. UBQLN1 and 2 for example have only 4 Tyr. This difference may in part explain the difference in phase separation behavior of Ubiquilins vs. RBPs previously observed (Dao et al., 2018).

Compositionally, ubiquilins have several other distinguishing features. First, UBQLN1/2 contain no cysteine residues, but have an overabundance of Met's (10%). Second, Lys residues are restricted to the Ubl domain. And third, there are a limited number of aromatic residues: Trp (1), Tyr (4), His (4), and Phe (17). UBQLN1/2/4 contain only one Trp in the distinctive sequence PLPPNPWAPPP in UBQLN2 located between the two sets of Sti1 repeats of unknown function. UBQLN2 in particular also contains a unique PXX repeat region to which the majority of ALS/FTD mutations map (Figure 1-2 A, B). This repeat has been compared to an SH3 binding domain, collagen, elastin, and the herpesvirus saimiri oncogene STP-C488 phosphoprotein, but the PXX repeat has no true sequence homologues (Dao et al., 2018; Kaye et al., 2000; Mah et al., 2000) and its function is still unclear. Currently there is no evidence that the prolines in these PXX repeats are hydroxylated as in collagen, however ALS/FTD linked mutations in this region do interfere with UBQLN2 function as a proteasome adaptor (Chang and Monteiro, 2015; Hjerpe et al., 2009; Sharkey et al., 2018).

Ubiquilins function as both chaperones and shuttles

The Ubiquilin Ubl-Uba domain structure suggests that these proteins may bridge ubiquitylated proteins with UIM containing proteins such as the proteasome, E3 ubiquitin ligases, DUBs and the ESCRT machinery (Heir et al., 2006; Kleijnen et al., 2000; Ko et al., 2004; Regan-Klapisz et al., 2005).

Consistent with this functional role at the proteasome, UBQLN1 and 2 interact with the proteasome cap subunits S5a (Rpn10) and ADMR1 (Rpn13 via both the Uba and Ubl domain (Chen et al., 2016; Walters et al., 2002). This interaction has been proposed to function in proteasome shuttling of ubiquitinated substrates, protection of proteasome substrates from deubiquitinases, a ubiquitin-chain length sensor for the proteasome, and more recently, a ubiquitin-proteasome vs. autophagy pathway selector (Fushman and Wilkinson, 2011; Hartmann-Petersen et al., 2003; Kleijnen et al., 2003; Ko et al., 2004; Lu et al., 2017).

This regulatory function can translate to either a stabilizing or destabilizing effect. For example, for p53 and IkBα which are ubiquitinated by the HECT-type E3 ligase UBE3A (E6AP) and the SCF-type E3 ubiquitin ligase F-box/WD repeat-containing protein 1A (βTRCP), UBQLN1/2 overexpression inhibited their degradation. UBQLN2 overexpression, however, did not inhibit degradation of ornithine decarboxylase (ODC) indicating that UBQLN2 did not interfere with the proteasome itself, but instead its substrates (Kleijnen et al., 2003). In contrast, UBQLN overexpression accelerated the degradation of misfolded endoplasmic reticulum (ER) substrates in ER associated degradation (ERAD) facilitated by an interaction with the molecular motor VCP and a Ubx protein (Erasin (UBXD8) and HERPUD1 for UBQLN1 and FAF2 for UBQLN2) (Lim et al., 2009; Su et al., 2010; Xia et al., 2014). In hepatitis C infected Huh7 hepatoma cells, UBQLN1 overexpression also accelerated the polyubiquitination and degradation of the hepatitis C virus RNA-dependent RNA polymerase (NS5B) (Gao et al., 2003).

The stabilization or destabilization of UBQLN substrates can in part be attributed to the domain of UBQLN protein required for the interaction, such that interaction with the Ubl or central domain of UBQLN proteins is stabilizing and interaction with the UBA domain is destabilizing (Kurlawala et al., 2017a). Recent evidence suggests that the low complexity flexible linker region of Ubiquilins may participate with the Uba domain in selecting substrates for proteasome degradation giving Ubiquilins a broad substrate specificity (Itakura et al., 2016). Consequently, UBQLN2 has been shown to mediate the degradation of substrates as diverse as misfolded ERAD substrates, mitochondrial precursor

proteins, and intermediate filament proteins (Gavriilidis et al., 2018; Itakura et al., 2016; Xia et al., 2014). So UBQLN2 clearly regulates degradation of ubiquitinated substrates but the mechanism of this action is unclear.

Ubiquilin function as a proteasome shuttle may be coupled to its function as a molecular chaperone. As noted above, previous reports have suggested that ubiquilins stabilize protein substrates in the ER and Golgi (Ayadi et al., 2012; Massey et al., 2005; Saliba et al., 2008). *In vitro*, UBQLN1 stabilized a temperature-sensitive citrate synthase mutant and promoted firefly luciferase refolding after thermal denaturation suggesting that this stabilizing effect is a molecular chaperone effect (Ayadi et al., 2012). UBQLN1 has also been shown to stabilize model nuclear encoded mitochondrial precursor proteins OMP25, TOM5, BAK and ATP5G via its Sti1-like linker region (Itakura et al., 2016). Notably, introduction of ubiquitinated OMP25 *in vitro* stabilized UBQLN1 interaction with OMP25 and promoted UBQLN1 binding to the proteasome and enhanced OMP25 degradation (Itakura et al., 2016). These data suggest that ubiquilins may have two interconvertible modes of action, one as a stabilizing molecular chaperone and the other as a proteasome shuttle. In the case of mitochondrial precursor proteins, UBQLN1 interconversion between a molecular chaperone and proteasome shuttle was induced by UBQLN1 Uba domain binding to ubiquitin. Given that the Uba domain has a ten-fold lower affinity for its own Ubl domain than ubiquitin, ubiquitin binding freed the Ubl domain to interact with the proteasome (Itakura et al., 2016; Lowe et al., 2006). This model in other systems is also supported by the observation that UBQLN2 binding to the molecular chaperone Hsp70 via its C-terminus (including the Uba domain) in the presence of thermally denatured luciferase promoted its binding to the proteasome (Hjerpe et al., 2016). Effectively, ubiquilins respond to substrate ubiquitination by changing conformation. It will be interesting if this conformational switching model applies to other cellular functions of ubiquilins.

In addition to its conformational state, the oligomerization states of ubiquilins may also contribute to their functional roles in the cell. Intermolecular interactions between Uba and Ubl domains may also be functionally important (Ford and Monteiro, 2006; Kang et al., 2007; Lee et al., 2013a; Lowe et al.,

2006). While UBQLN1, 2, and 4 may have distinct substrate specificities, homo- and hetero-dimerization of ubiquilins may expand this substrate specificity further (Ford and Monteiro, 2006). For example, UBQLN1 and 4 were found to form a heterodimer that acts as an autophagic receptor. In this role, UBQLN4 binds to the autophagosome membrane via an LC3B recognition domain while UBQLN1 binds to ubiquitinated substrate (Lee et al., 2013a). UBQLN2 has also recently been shown to form oligomers that phase separate in warm temperature, high salt conditions suggesting that they are mediated by interactions between hydrophobic regions of the low complexity and Sti1-like repeat regions (Dao et al., 2018). Based on studies in yeast, human ubiquilin oligomerization state might be critically important for determining the fate of bound protein substrate shuttling to the proteasome or autophagosome. Unlike human ubiquilins, the yeast ubiquilin Dsk2 lacks the second set of Sti1-like repeats found to mediate ubiquilin oligomerization (Kaye et al., 2000). In yeast, instead the ubiquitin receptor Cue2 oligomerizes. In an assay in which the half-life of a wild type or mutant protein prone to misfolding and degradation was measured, strains expressing oligomerization competent and incompetent ubiquitin receptors Cue2 and Dsk2 respectively differentially mediated protein degradation. Dsk2 mediated proteasomal degradation of soluble protein as a monomer, while Cue2 mediated autophagosomal degradation of insoluble aggregated protein as an oligomer (Lu et al., 2017). Whether this functional difference is conserved in higher eukaryotes remains to be tested, but is an intriguing possibility.

Levels of ubiquilins determine their cytoprotective vs. cytotoxic effect

The relative levels of ubiquilins to their substrates appears to determine their cytoprotective vs. cytotoxic effects. In healthy cells, overexpression of ubiquilin has been found to be cytotoxic at both cell and organismal levels. Overexpression of the yeast ubiquilin, duplication suppressor of a Kar1 defect (DSK2) interferes with the G2/M transition during mitosis eventually leading to yeast cell death (Biggins et al., 1996). Overexpression of the *Xenopus laevis* frog ubiquilin (XDRP1) in egg extracts inhibits cell cycle progression by interfering with degradation of cyclin A (Funakoshi et al., 1999). Overexpression of the fly *Drosophila melanogaster* ubiquilin (DSK2) causes morphological abnormalities

in late pupal stages and later death (Lipinszki et al., 2011). This toxicity is associated with DSK2 interference with proteasome degradation by saturating the proteasome ubiquitin receptors (Lipinszki et al., 2011). In all of these studies increasing the concentration of ubiquilin protein relative to the proteasome or its substrate was in some way toxic to cells by interfering with proteasomal degradation.

In contrast, increasing the concentration of ubiquilin in the presence of a toxic misfolded substrate is cytoprotective. For example, the yeast DSK2 protein was originally identified as a high copy number suppressor in cells with a *kar1* allele with a spindle pole body duplication defect (Vallen et al., 1994). Overexpression of ubiquilin in the presence of polyglutamine, polyalanine, amyloid beta, TDP-43 and Huntington fragments, lessened the burden of toxic aggregates that cells accumulated (Adegoke et al., 2017; Ayadi et al., 2012; Hanson et al., 2010; Lim et al., 2009; Safren et al., 2015; Wang and Monteiro, 2007a, 2007b). Ubiquilin depletion via transcript silencing sensitizes cells to nutrient starvation and heat stress, stressors which increase the burden of misfolded proteins that tend to aggregate (Hjerpe et al., 2009; Rothenberg et al., 2010). Natural aging also reportedly leads to a decline in UBQLN1 levels in the brain making cells more susceptible to amyloid beta and Huntingtin protein aggregation in Alzheimer's and Huntington's diseases respectively (Safren et al., 2015). The cytoprotective effect of increasing ubiquilin levels or cytotoxic effect of suppressing ubiquilin levels in all of these cases depends on the presence of an aggregation prone substrate. Consistent with these observations, stresses that increase the burden of misfolded proteins in the cell, such as sodium arsenite, hypoxia and ER stressors, lead to an increase in ubiquilin transcript levels (Esler et al., 2002; Heir et al., 2006; Ko et al., 2004; Tsukamoto et al., 2015), suggesting that the cell uses ubiquilin to buffer against aggregation in response to a higher burden of misfolded proteins.

Ubiquilins function in diverse cellular contexts

Like the ubiquitous protein tag, ubiquitin, ubiquilins function in a broad range of cellular contexts. The lack of ubiquilin specificity for a particular ubiquitin-chain linkage type (Raasi et al., 2005; Zhang et al., 2008) and flexible linker region may allow it to function in these many different contexts. Cell homeostasis is integrally dependent on regulated proteolysis, protein assembly, translocation and

assembly at the correct location in the cell. Ubiquilins not only function as a proteasome shuttles in the cytosol, but also at the ER, Golgi, plasma and mitochondrial membranes and in cell signaling, transcription and autophagy as discussed below.

Initially many of the substrates for UBQLN1, 2, and 4 were identified via yeast two-hybrid screens. UBQLN1, 2, and were originally identified as interactors for the proteasome, both HECT and RING type E3 ubiquitin ligases, presenilin, mTor, the Hsp70 Stch, the DAN tumor suppressor protein, the integrin associated receptor CD47, and the basic helix loop helix (bHLH) transcription factor achaete-scute homolog 1 (HASH1) (Kaye et al., 2000; Kleijnen et al., 2000; Mah et al., 2000; Ozaki et al., 1997; Persson et al., 2004; Wu et al., 2002). UBQLN4 which has a more nuclear distribution than UBQLN1 and 2, and is most similar to the yeast Dsk2 protein, was identified as an interactor for ataxin 1, connexin 43 and the ER targeting signal sequence of Hsp47 by this method (Davidson et al., 2000; Li et al., 2008; Matsuda et al., 2001). From these screens, several classes of interactors for UBQLN1, 2, and 4 emerged, placing ubiquilins in diverse contexts in the cell.

First, UBQLN1 and 2 appear to play an integral role in membrane protein biogenesis in the ER, Golgi, plasma membrane in the secretory pathway. Membrane protein interactors for UBQLN1 include presenilin, GABAA receptor, retinoic acid receptor, nicotinic acid receptor, the DAN tumor suppressor and the amyloid precursor protein (Bedford et al., 2001; Ficklin et al., 2005; Hiltunen et al., 2006; Massey et al., 2004; Ozaki et al., 1997; Zhu et al., 2010). UBQLN1 stabilizes the membrane insertion of GABAA receptors by stabilizing them in the ER (Saliba et al., 2008). UBQLN1 expression suppresses endoproteolysis of the amyloid precursor protein to the neurotoxic amyloid beta fragment 42 (Aβ42) by sequestering it in the Golgi (Ayadi et al., 2012). At the mitochondrial and ER membranes UBQLN1 and 4 appear to cooperate in targeting nascent tail anchored proteins respectively (Itakura et al., 2016; Suzuki and Kawahara, 2016). This stabilizing regulatory mechanism depends on the ability of ubiquilins to bring together ubiquitinated proteins and the proteasome at the membrane.

Less well studied functions of ubiquilins include UBQLN1's role in calcium homeostasis by regulating stability of the store operated calcium channel protein Orai1, and apoptosis by stabilizing the anti-apoptotic factor Bcl-b (Beverly et al., 2012; Lee et al., 2013b). A recent report cites the transcriptional role of Drosophila Dsk2 in development (Kessler et al., 2015). A role for ubiquilins in DNA repair has yet to be shown. Overall ubiquilins show functions in a diverse set of cellular processes suggesting their broad specificity. Note however, that majority of these studies have focused on UBQLN1 or 4 except for the specific characterization of UBQLN2's interaction with Hsp70 and its role in G-protein coupled receptor mediated endocytosis (Hjerpe et al., 2016; Kaye et al., 2000; N'Diaye and Brown, 2003). UBQLN2's specific substrates prior to this study have largely been uncharacterized.

Thesis summary/rationale

To investigate specific cellular functions of UBQLN2 associated with ALS/FTD in collaboration with Akhilesh Pandey's lab, I performed a proteomic screen for UBQLN2 interactors. Among those interactors, I found an enrichment of stress granule (SG) components. In Chapter 2, I show that UBQLN2 associates with SGs via its linker region and plays a negative regulatory role in SG formation in the cytosol. In Chapter 3, I focus on the interaction between UBQLN2 and the ALS/FTD linked RNA binding protein FUS. I show that UBQLN2 forms a complex with FUS and increases the dynamics of FUS-RNA interaction, increasing the fluidity of FUS-RNA complex formation. This effect translates to a decrease in the size of phase-separated FUS droplets *in vitro* and suppression of FUS phase separation into SGs in cells. ALS/FTD-linked mutations within the low complexity linker region of UBQLN2 partially impair UBQLN2's ability to increase the dynamics of FUS-RNA interaction and suppress SG formation. These data suggest that UBQLN2 plays a previously unrecognized role in regulating the early stages of SG formation by disrupting RBP-RNA interaction. In Appendix A, full lists of UBQLN1, UBQLN2 and UBQLN4 interactors and a brief comparison of their association with SGs is given. In Appendix B, extended methods and tools for studying UBQLNs cellular function are described. Together this data provides support for a previously unrecognized function of UBQLN2 in SG formation by modulating the dynamics of hnRNP-RNA interaction.

Because SGs potentially seed toxic ALS/FTD patient inclusions, these findings have implications for understanding ALS/FTD pathology and designing new treatments for these diseases.

FIGURES & TABLES

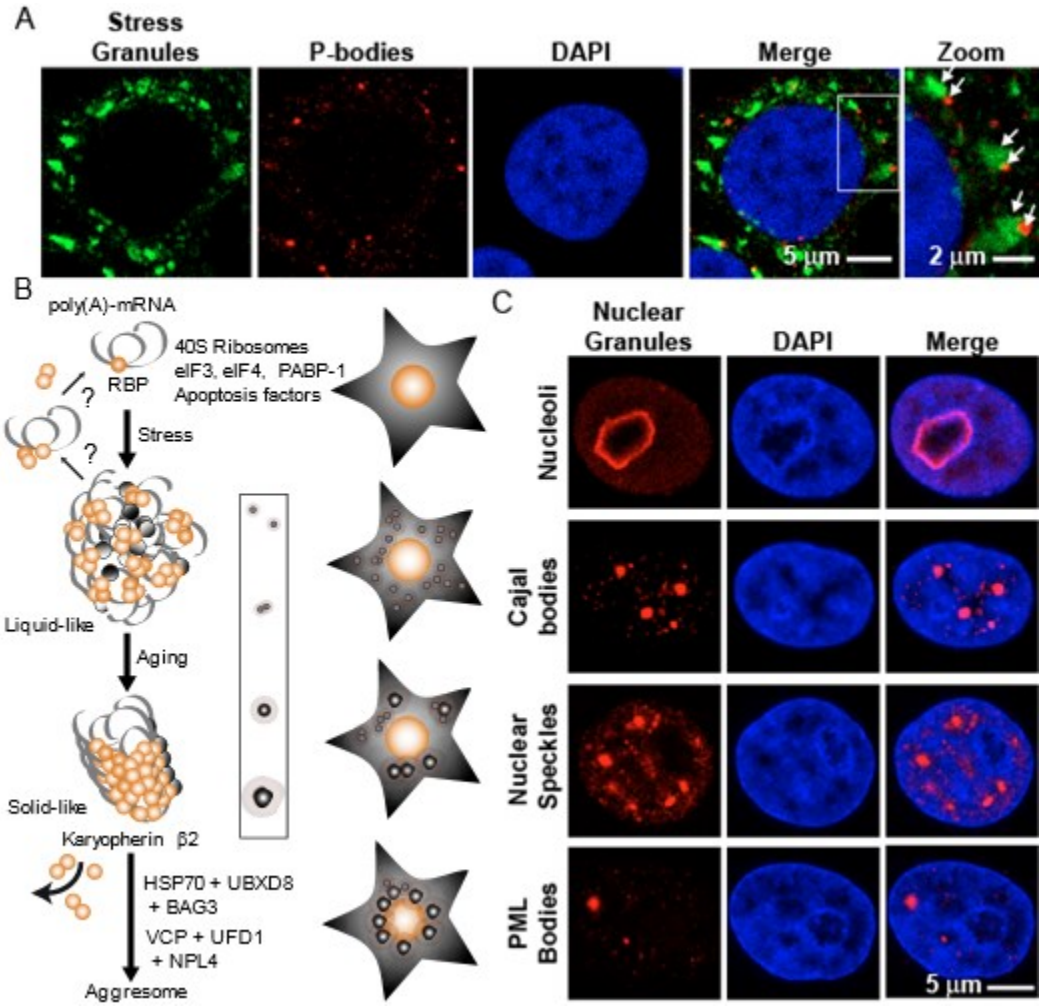

Figure 1-1 RNP granules and a model of SG granule formation

(A) Immunofluorescence (IF) images of cytoplasmic ribonucleoprotein (RNP) granules in HeLa cells after 30 min of heat stress (43.7°C). Mouse anti-G3BP [BD 611126] and goat anti-4E-T [Santa Cruz sc-13453 (N18)] mark SGs and P-bodies respectively. White arrows point to juxtaposed P-bodies (red) and SGs (green).

(B) Model of RNP liquid-liquid phase separation focusing on SG formation. (Left panel) Molecular level diagram (Right panel) Cellular level diagram. Stress induces a redistribution of RNA binding proteins (RBPs) and stalled poly(A)-mRNA from the nucleus to the cytoplasm where they oligomerize and phase separate into liquid-like granules. Prolonged

stress or aging leads to the conversion of these dynamic granules into static solid-like granules. These solid-like granules may be trafficked to perinuclear aggresomes and degraded by autophagy and potentially serve as the seed sites for toxic intracellular inclusions associated with neurodegenerative diseases such as ALS/FTD. Protein quality control factors VCP and HSP70 extract ubiquitinated misfolded proteins from SGs to the aggresome for degradation. Karyopherin β2 disassociates solid-like granules. (Center Box) SGs fuse like liquid droplets to form larger droplets. As liquid droplet components solidify, the droplets lose their spherical structure and grow in size. Ribbons in grey are RNA. Grey spheres are other SG components.

(C) IF images of some nuclear RNP granules in HeLa cells. Mouse anti-nucleophosmin [Abcam ab10530 (FC82291)], rabbit anti-coilin [Abcam ab11822], mouse anti-SC35 (phospho) [Abcam 11826], and rabbit anti-PML [Abcam ab200200 (EPR16768)] mark nucleoli, Cajal bodies, nuclear speckles and PML bodies respectively. These granules differ in composition, localization and morphologies, but are all thought to form via a liquid-liquid phase separation.

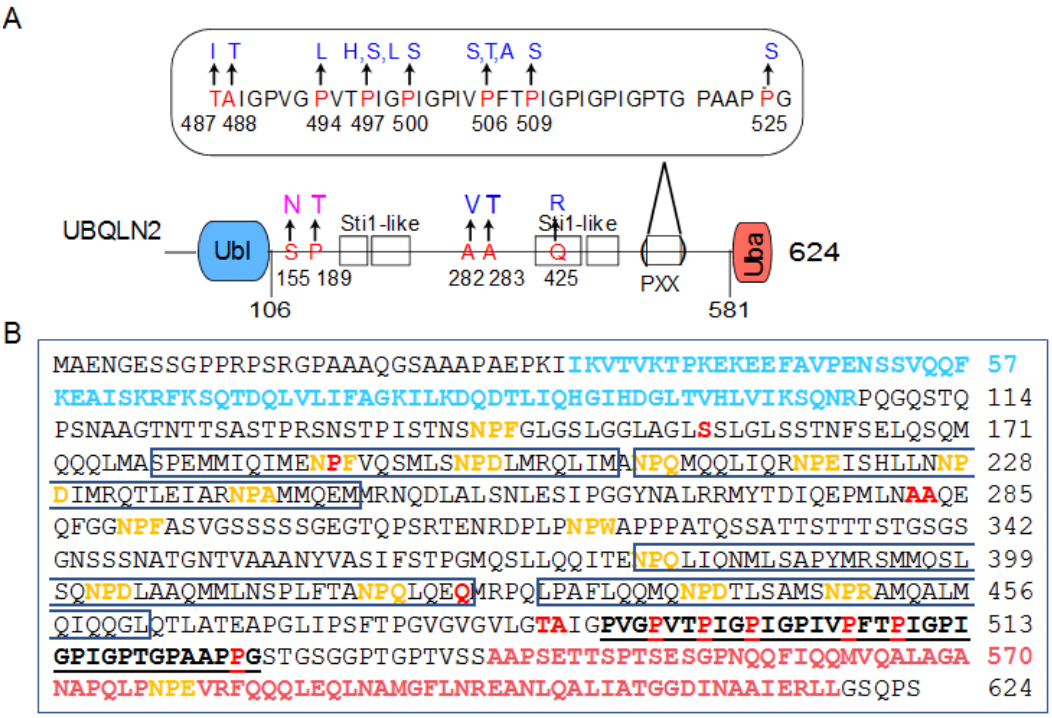

Figure 1-2 ALS/FTD linked mutations in UBQLN2 map to the Sti1-like linker region

(A) Domain map of UBQLN2 drawn to scale with amino acid residues affected by ALS/FTD-linked mutations highlighted in red. fALS mutations are shown in blue, while sALS mutations are shown in purple. The M392V mutation resulted in a pure FTD phenotype, while the T487I mutations resulted in a pure motor neuron phenotype, indicating that UBQLN2 mutations cause a spectrum of ALS/FTD pathology.

(B) ALS/FTD-linked mutations shown in the context of the UBQLN2 protein sequence (RefSeq NP_038472.2). The Ubl domain is in blue (33-107). The Uba domain (581-621) is in red. Boxes outline the predicted Sti1-like repeats (I 178-206, II 208-247, III 379-426, IV 430-462), and the PXX repeat (491-526) is underlined and shown in bold. Asparagine-proline (NP) repeats are highlighted in orange. Domains are shown were annotated by SMART (Schultz et al., 1998). Mutations in residues that cause ALS/FTD are highlighted in bright red as in (A).

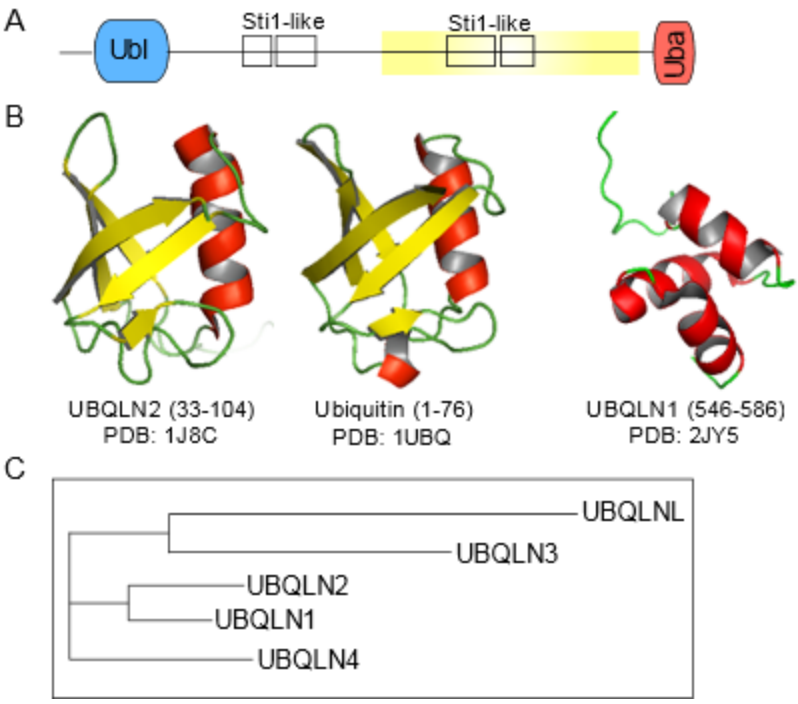

Figure 1-3 UBQLNs have a conserved modular domain structure

(A) Domain map of human ubiquilin structure drawn to scale. Ubl=ubiquitin-like domain Uba=ubiquitin-associated domain. Sti1=Sti1-like repeat. The orange box highlights the portion of ubiquilins believed to have been replicated from the first set of Sti1-like repeats in yeast Dsk2 during the evolution of higher eukaryotes.

(B) Ribbon drawings of the UBQLN2 Ubl domain, ubiquitin, and UBQLN1 Uba domain rendered in PyMOL (Shrödinger, LLC). UBQLN2 and ubiquitin have similar β-grasp folds. The Uba domain forms a three-helix bundle that binds ubiquitin.

(C) Tree map showing the evolutionary distance between human UBQLNs. UBQLN1 and 2 are 74% identical. UBQLN4 is most similar to Dsk2. UBQLN3 is testes specific and contains only 1 Sti1-like domain. UBQLNL contains a Ubl but its Sti1 repeats and Uba have been replaced by a low complexity region. UBQLNL may also be testes specific.

Table 1-1 ALS-linked genes

Protein qualty control factors

Gene	Protein	ALS	Inheritence	Citation
OPTN	Optineurin	ALS12	Dominant	Maruyama H, et al. (2010)
VCP (p97)	Valosin containing protein	ALS14	Dominant	Johnson JO, et al. (2010)
UBQLN2	Ubiquilin 2	ALS15	X-linked	Deng H-X, et al. (2011)
SQSTM1 (p62)	Sequestosome 1	ALS	Dominant	Fecto F, et al. (2011)
TBK1	Tank Binding Kinase 1	ALS	Dominant	Freischmidt A, et al. (2015) Cirulli ET, et al. (2015)
VAPB	Vesicle associated, membrane protein-associated protein B	ALS8	Dominant	Nishimura AL, et al. (2004)
CHMP2B	Charged multivesicular Body	ALS17	Dominant	Parkinson N, et al. (2006)
FIG4	Phosphatidylinositol 3,5-bisphosphate 5-phosphatase	ALS11	Dominant	Chow CY, et al. (2009)

RNA Binding Proteins

TARDBP	TAR DNA-binding protein 43	ALS10	Dominant	Sreedharan J, et al. (2008) Rutherford NJ, et al. (2008)
FUS	Fused in sarcoma	ALS6	Dominant	Kwiatkowski TJ, et al. (2009) Vance C, et al. (2009)
TAF15	TATA-binding protein associated factor 15	ALS	Unknown	Couthouis J, et al. (2011)
EWS	Ewing sarcoma breakpoint region 1	ALS	Unknown	Couthouis J, et al. (2012)
HNRNPA1	Heterogenous ribonucleoprotein A1	ALS20	Unknown	Kim HJ, et al. (2013)
HNRNPA2/B1	Heterogenous ribonucleoprotein A2/B1	ALS	Unknown	Kim HJ, et al. (2013)
MATR3	Matrin 3	ALS21	Dominant	Johnson JO, et al. (2014)
ANG	Angiogenin	ALS9	Dominant	Greenway MJ, et al. (2006)
SETX	Senataxin	ALS4	Dominant	Chen Y-Z, et al. (2004)

Expanded repeats

Gene	Protein	ALS	Inheritence	Citation
ATXN2	Ataxin 2		Dominant	Elden AC, et al. (2010)
C9orf72	Non-coding intronic repeat	ALS-FTD1	Dominant	DeJesus-Hernandez M, et al. (2011)

Trafficking Proteins

DCTN1	Dynactin	ALS	Dominant	Münch C, et al. (2004)
NFH	Neurofilament heavy chain		Dominant?	Figlewicz DA, et al. (1994)
PFN1	Profilin 1	ALS18	Dominant	Wu C-H, et al. (2012)
TUBA4A	Tubulin 4A			Smith BN, et al. (2014)

Neuron Excitotoxicity

DAO	D-amino-acid oxidase	ALS	Dominant	Mitchell J, et al. (2010)

Other

SOD1	Superoxide dismutase 1	ALS1	Dominant	Rosen DR, et al. (1993)
ALS2	Alsin	ALS2	Recessive	Yang Y, et al. (2001)

Newly identified genes

CHCHD10	coiled-coil-helix-coiled-coil-helix domain containing 10	ALS-FTD2		Bannwarth S, et al. (2014)
NEK1	Ser/Thr Protein Kinase NEK1	ALS		Kenna KP, et al. (2016)
C21ORF2	Chromosome 21 open reading frame 2	GWAS		van Rheenen W, et al. (2016)
MOBP	Myelin-associated oligodendrocyte basic protein	GWAS		
SCFD1	Sec1 family domain-containing protein 1	GWAS		

Key
Role in protein homeostasis
Involved in RNA homeostasis
Involved in cytoskeletal trafficking

Chapter 2 UBQLN2 associates with SGs and negatively regulates SG formation

INTRODUCTION

Both protein and RNA homeostasis have been both genetically and pathologically linked to cases of the neurodegenerative diseases amyotrophic lateral sclerosis (ALS) and frontotemporal dementia (FTD). However, a role for these molecular players in a common cellular pathway has not been well characterized (Robberecht and Philips, 2013; Taylor et al., 2016). In September of 2011, when I started my PhD rotation in the Wang lab, ubiquilin 2 (UBQLN2) was identified as one of the first bona fide protein quality control (PQC) factors to cause ALS with FTD in rare dominant X-linked cases of this disease (Deng et al., 2011). UBQLN2 is one of four conserved ubiquilins with an amino-terminal ubiquitin-like domain (Ubl) and carboxy-terminal ubiquitin-associated domain (Uba) separated by a long low complexity linker region. This modular domain structure suggests that ubiquilins can bridge ubiquitinated substrates and ubiquitin binding proteins, however, very few specific cellular roles for UBQLN2 except as a proteasome shuttle had been identified. ALS/FTD mutations in UBQLN2 did inhibit degradation of a model proteasome substrate, but its specific substrates had not been characterized (Deng et al., 2011).

Through a quantitative proteomic screen for UBQLN2 interactors in collaboration with the Pandey lab, I identified an enrichment of RNA binding proteins also found in stress granules (SGs). This enrichment coincided with emerging evidence suggests that SGs seed ALS/FTD patient inclusions (Li et al., 2013). SGs form by dynamically concentrating proteins with intrinsically disordered prion-like domains (PrDs) in a process recently recognized as a liquid-liquid phase separation. Prolonged stable incorporation of PrDs in SGs disrupts SG dynamics leading to large aberrant SG formation. These aberrant SGs misincorporate ubiquitinated proteins potentially serving as the seed sites of patient ALS/FTD inclusions (Kroschwald et al., 2015; Mateju et al., 2017). ALS/FTD-linked protein quality control factors such as VCP have been shown to mediate disassociation of ubiquitinated proteins from SGs, but PQC factors that mediate the process of SG formation have not been well characterized.

In this chapter, I present the first pieces of evidence that UBQLN2 suppresses large aberrant SG formation by modulating the dynamics of PrD protein incorporation into SGs. Using an unconventional stress granule staining technique, I found that under stress conditions, UBQLN2 is recruited to SGs and this association is transient. With a stable cell line that inducibly expresses UBQLN2 at near endogenous levels, I determined that this recruitment is mediated by a low complexity region within the linker of UBQLN2. Furthermore, I found that UBQLN2 overexpression suppresses SG formation, while UBQLN2 depletion enhances the rate at which SG size increases without affecting basal levels of core SG components TIA-1 or G3BP or stalled translation initiation complexes.

These results suggest that UBQLN2 physically interferes with the process of SG formation bridging protein and RNA homeostasis at SGs. UBQLN2 protein carrying ALS/FTD-linked mutations failed to suppress SG formation as well as the wild type UBQLN2. Given that aberrant SGs are thought to seed toxic ALS/FTD patient inclusions, these results support the conclusion that UBQLN2 plays a protective role at SGs and ALS/FTD-linked mutations lead to a loss of this function.

Note: The results presented here are given with minor modifications to fit the thesis format from the published manuscript: Alexander EJ, Niaki AG, Zhang T, Sarkar J, Liu Y, Nirogi RS, Pandey A, Myong S, and Wang J (2018) Ubiquilin 2 Modulates ALS/FTD-linked FUS-RNA Complex Dynamics and Stress Granule Formation. *PNAS* 115(49): E11485-E11494.

RESULTS

UBQLN2 associates with SG components

To identify specific cellular functions for the UBQLN2 protein, working with Raja Sekhar from Akhilesh Pandey's lab, I performed an unbiased quantitative proteomic screen for UBQLN2-interacting partners by stable isotope labelling with amino acids in cells (SILAC) coupled with liquid chromatography-tandem mass spectrometry (SILAC LC-MS/MS) (Ong et al., 2002). I first prepared

stable HEK293T cell lines with an integrated tetracycline-inducible FLAG-UBQLN2 construct and cultured them with $^{13}C_6{}^{15}N_4$ Arg and $^{13}C_6{}^{15}N_2$ Lys heavy isotope media until complete labelling was attained, which Raja assessed by mass spectrometry. I extracted proteins from cell lysate with CHAPSO lysis buffer, co-immunoprecipitated them with FLAG-UBQLN2 on anti-FLAG (M2) beads and eluted them with FLAG peptide. Identically processed lysate from $^{12}C_6{}^{14}N_4$ Arg and $^{12}C_6{}^{14}N_2$ Lys light-labelled HEK293T cells treated with doxycycline was used as a control. Raja and I pooled the eluants, separated them by SDS-PAGE, and trypsin digested the proteins and extracted the peptides for LC-MS/MS analysis, which Raja performed (Figure 2-1A, B).

From this proteomic analysis, we identified 180 putative interactors for UBQLN2 enriched over 1.5-fold, 13 of which were enriched more than 10-fold (Figure 2-1). These interactors could be subclassified by domain structure into four groups: molecular chaperones, AAA ATPases, RNA/DNA binding proteins, and transmembrane proteins (vesicle trafficking, ER/Golgi/lysosomal membrane, and mitochondrial membrane proteins) (Figure 2-1D). Included in this list were previously identified UBQLN2 interactors: Hsp70 molecular chaperones HSPA1A, HSPA8 and HSPA13/Stch, ERAD chaperones FAF2/UBXD8 and HERPUD1, AAA ATPases VCP, proteasome cap subunits, hnRNPU, hnRNPA3, and membrane proteins ESyt2 and INSR (Table A-1) (Gilpin et al., 2015; Hjerpe et al., 2016; Kaye et al., 2000; Kim et al., 2008; Kleijnen et al., 2000; Kurlawala et al., 2017b, 2017a; Xia et al., 2014). Western blot validation of some of the most enriched interactors confirmed our peptide search results from this proteomic analysis (Figure 2-2).

During the course of this analysis, I noticed that members of every group except the membrane proteins were also represented in the SG proteome (Jain et al., 2016; Markmiller et al., 2018a; Ohn et al., 2008; Youn et al., 2018). To identify functional classes of proteins in SGs that UBQLN2 binds, I mapped the connectivity of SG-associated UBQLN2 interactors via STRING network analysis (Szklarczyk et al., 2015). Four major classes of proteins emerged from this analysis: heterogenous ribonucleoproteins (hnRNPs) (I), molecular chaperones (II), translation factors (III), and RNA trafficking proteins (IV) (Figure 2-1E). The majority of ATP-dependent molecular chaperone

assemblies found in the G3BP-dependent SG proteome, including VCP/p97, MCM, RuvB, and TriC (Jain et al., 2016), were also identified as UBQLN2 interactors (Group II, IV). The karyopherins, A2 and B1, a class of proteins recently identified to solubilize hnRNP fibrils (Guo et al., 2018; Hofweber et al., 2018; Qamar et al., 2018; Yoshizawa et al., 2018) were present in Group IV. Notably however, a subclass of ALS-linked hnRNPs known as the FET family, including FUS, EWS, and TAF15 (Couthouis et al., 2011, 2012; Ticozzi et al., 2011), were also identified (group I). FUS among RNA binding proteins (RBPs) showed the highest peak intensity among the hnRNPs (Table 3-1). Overall the results of this proteomic analysis indicated that UBQLN2 associates with SG components in the absence of stress.

UBQLN2 localizes to SGs

To determine if UBQLN2 localizes to SGs with SG components, I examined cells by immunofluorescence staining with UBQLN2-specific antibodies (Figure B-1) to detect endogenous UBQLN2 protein under stress conditions. In response to acute sodium arsenite stress (0.5 mM, 30 min), endogenous UBQLN2 formed cytoplasmic puncta that colocalize with core SG components G3BP and TIA-1 in HeLa cells (Figure 2-3 A middle row; Figure 2-3 D second row). Depleting UBQLN2 with a specific shRNA (Figure B-1) eliminated the UBQLN2 signal in G3BP-containing SGs, confirming that the UBQLN2 signal in SGs is specific (Figure 2-3A bottom row, Figure 2-10, bottom row).

Visualization of UBQLN2 in SGs was enhanced by use of an unconventional SG staining technique. I found that simultaneously fixing and permeabilizing cells with paraformaldehyde and Triton X-100 effectively limited the background cytoplasmic signal revealing UBQLN2's underlying localization to SGs (Figure 2-4). UBQLN2 could also be detected in SGs by the conventional SG staining technique (Kedersha and Anderson, 2007), but its localization with SG marker TIA-1 is largely obscured by its strong cytoplasmic signal (Figure 2-4, third row). This method of simultaneously fixing and permeabilizing cells was particularly effective in HeLa cells where the cytoplasmic volume is more compressed than in other cell types such as U2OS cells. I am not aware of any previously published

reports in which this method systematically used to detect SG components, but a similar approach was used previously to wash away nucleoplasmic components to enhance the detection of substructures of the nucleus (Fey et al., 1986; Guzzo et al., 2012). Although this method does not allow calculation of the percentage of total protein in SGs, it does provide clear evidence of SG localization for proteins with strong cytoplasmic signals and did not appear to influence detection of core SG components G3BP or TIA-1 used in later experiments. Using this method, I was able to show that other predicted SG components, such as VCP, TriC, Hsp72, and Hsc70 (Jain et al., 2016), are in fact present in SGs (Figure 2-5). As negative controls, other functionally related Ubl/Uba proteins SQSTM1/p62 and/or BAG6 were not found to be components of SGs (Figure 2-6) (Mateju et al., 2017). Based on this finding, I believe this method may prove useful for examining the SG association of proteins with strong cytoplasmic signals.

Since some proteins localize to SGs only under specific conditions, I next tested if under other stress conditions UBQLN2 localizes to SGs. When treated with oxidative (CCCP, H_2O_2), heat, proteotoxic (MG132) and osmotic stressors (sorbitol, NaCl), UBQLN2 invariably localized to SGs (Figure 2-3D, Figure 2-7). Some SG components are also cell line-dependent (Anderson and Kedersha, 2009), so I then tested if UBQLN2 localizes to SGs in other cell lines, such as HEK293T (human embryonic kidney), U2OS (bone marrow), and SHSY-5Y (neuroblastoma) cells. In all tested cell lines, UBQLN2 localized to SGs (Figure 2-8). Based on these results, UBQLN2 appears to universally localize to SGs.

Notably, under all of the acute stress conditions tested initially, nearly all cells formed SGs containing UBQLN2, indicating that UBQLN2 is a SG component. However, SGs grow in size and change morphology and composition over time, so I then tested the types of granules with which UBQLN2 associates. After 30 min of heat stress, HeLa cells contained a variety of SG morphologies that I classified as i) diffuse ii) concentrated but not punctate iii) perinuclear punctate iv) large cytoplasmic puncta (Figure 2-3E). Interestingly, enrichment of UBQLN2 was mainly found in cytoplasmic punctate granules. UBQLN2 appeared to only weakly associate with perinuclear punctate SGs at 30 min. These cells were rounded and the cytoplasm was highly compressed. As stress was prolonged, this cell

morphology predominated and UBQLN2 visibility in SGs weakened (Figure 2-9). This loss of UBQLN2 in SGs corresponded with the relocalization of UBQLN2 to the nucleus as previously reported (Hjerpe et al., 2016). After this time point, cells begin to undergo apoptosis. This selective association of UBQLN2 with a subset of SGs, suggests that UBQLN2 localization is functionally linked to SG morphology and/or composition.

P-bodies, unlike SGs, are constitutively present in the cytosol and contain enzymes for RNA decapping and degradation. Some components of P-bodies are also present in SGs and vice versa (Anderson and Kedersha, 2009). I next tested if UBQLN2 could also localize to P-bodies. Staining for UBQLN2, however, did not overlap with P-bodies under nonstress conditions (Figure 2-10). Only in cases where the P-bodies were directly juxtaposed to SGs, did UBQLN2 show partial overlap with P-body marker 4E-T (Figure 2-10, second row). Thus, UBQLN2 localizes to SGs in response to stress, not P-bodies.

The Sti1 linker region is sufficient for UBQLN2 sequestration into SGs

To predict if annotated low complexity regions in UBQLN2 might be functionally relevant to its localization to SGs, I first performed bioinformatic analysis of this region. Between the Ubl and Uba domains in UBQLN2 is a 474 amino acid stretch that composes the Sti1-like linker region. This region contains several low complexity regions annotated by the SMART algorithm (Schultz et al., 1998). Analysis of the full-length protein via PLAAC (Prion-like Amino Acid Composition) software revealed that UBQLN2 contains two putative prion-like domains (PrD), a type of low complexity domain that can mediate protein self-association (March et al., 2016) within this linker (Figure 2-11A). The first region is located just downstream of the Ubl domain prior to the first set of Sti1-like repeats. The second region includes a second set of Sti1-like repeats specific to higher eukaryotes (Kaye et al., 2000). The second region is the same one recently found to be essential for UBQLN2 oligomerization (Dao et al., 2018). The liquid droplet theory of SG formation predicts that low complexity flexible regions in SG proteins can oligomerize to drive the phase separation of these proteins with RNA into granules. Based on this theory, I predicted that the Sti1-like linker would be sufficient to drive UBQLN2 into SGs.

To test if the Sti1-linker of UBQLN2 is sufficient to drive it into SGs, I constructed a new regulatable FLAG-UBQLN2 Flp-In HeLa cell line that would be ideal for imaging. This cell line inducibly expresses UBQLN2 at near endogenous levels when treated with a low level of tetracycline (1 μg/mL). The full-length FLAG-UBQLN2 but not FLAG-GFP colocalized with SG marker TIA-1 after 30 min of heat stress, indicating that the FLAG tag itself does not drive protein localization to SGs (

Figure 2-11B). The expression of FLAG-tagged Sti1-linker in the Flp-In system was relatively low, but it colocalized with SGs indicating that the linker region is sufficient for UBQLN2 localization to SGs.

UBQLN2 negatively regulates SG formation

Overexpression of core SG components that contain low complexity domains such as TIA-1, G3BP, FUS and TDP-43 alone can drive SG formation. To test if UBQLN2 alone could seed SG formation, I overexpressed FLAG-tagged UBQLN2 in transiently transfected HeLa cells (Figure 2-12C) and stained for SG marker TIA-1. In no case did overexpressing UBQLN2 drive SG formation (Figure 2-12A, second column, D). Instead, overexpressing UBQLN2 suppressed SG formation. The percentage of cells with large SGs was significantly decreased at all time points during heat stress in the presence of elevated levels of UBQLN2 (Figure 2-12D). ALS-linked mutants P497H or P506T partially interfered with UBQLN2's ability to suppress SG formation (Figure 2-12A, third and fourth column, D) despite being overexpressed at the same level as the wild type protein (Figure 2-12C).

Next, I asked if depleting endogenous UBQLN2 would enhance SG formation. 96 hrs after transfection with UBQLN2 specific shRNAs, HeLa cells were exposed to heat stress. The depletion of UBQLN2 resulted in a nearly twofold increase in the percentage of cells with large SGs beginning at 30 min (Figure 2-12B, F). As the percentage of cells with SGs increased to nearly 100% at 2 hrs, UBQLN2 levels no longer affected the percentage of cells with large SGs, indicating that SGs enlarge faster when UBQLN2 levels are decreased (Figure 2-12F). Even among the cells treated with UBQLN2 shRNA, those with higher levels of UBQLN2 expression showed a significantly lower level of large SGs (Figure 2-13), supporting this finding. This increase in the percentage of cells with large SGs corresponded with a significant increase in SG cross-sectional area and an increase in number of all

SGs per cell at time points prior to 2 hrs of heat stress (Figure 2-14). This change could not be adequately explained by increases in levels of core SG components G3BP or TIA-1 (Figure 2-15) or an increase in stalled ribosomes marked by eIF2α phosphorylation (Figure 2-16), suggesting that depletion of UBQLN2 led to a concentration of SG components in larger SGs rather than altered core SG component levels. Together, these data indicate that UBQLN2 negatively regulates SG growth during stress.

DISCUSSION

In this chapter, I provide the first evidence for a previously unrecognized role for the UBQLN2 protein in modulating SG formation. UBQLN2 interacting proteins identified by quantitative nLC-MS/MS analysis contained four groups of SG components: hnRNPs, molecular chaperones, translation factors, and RNA trafficking proteins. Under stress conditions, I verified that UBQLN2 localizes to SGs using an unconventional staining method and determined that the low complexity linker region alone of UBQLN2 was sufficient for this recruitment. UBQLN2 overexpression suppressed SG formation, while UBQLN2 depletion enhanced SG size indicating that UBQLN2 negatively regulates SG formation. Mutations in UBQLN2 impaired UBQLN2's negative regulatory function. These results expand on the known cellular roles of UBQLN2 and provide a potential direct link between protein and RNA homeostasis in normal stress responses and the pathogenesis of ALS/FTD.

The role of UBQLN2 as a negative regulator of SG formation represents a function for UBQLN2 independent of its previously established roles in mediating protein clearance. Instead of engaging with the proteasome or autophagy machinery via its Uba and Ubl domains, UBQLN2 associates with SG components through its Sti1-like region and influences the early stages of SG formation. Our quantitative proteomic analysis shows that UBQLN2 associates with SG components under homeostatic conditions, suggesting that these interactions exist prior to SG formation and UBQLN2 acts to regulate the exchange of these components into and out of SGs. Our time course analysis of SGs demonstrates that UBQLN2 is not a stable component of SGs but is present instead at the initial

phases of SG assembly, delaying SG initiation, resulting in negative regulation of SG size. Notably, UBQLN2 does not appear to regulate the levels of core SG components and inhibition of translation.

The function of UBQLN2 in decelerating the rate of expansion of individual SGs, potentially expands the mechanisms of SG regulation. By bioinformatic analysis of UBQLN2's amino acid composition, I discovered that UBQLN2 contains two putative prion-like domains in the long linker region between Ubl and Uba domains, and that this linker region is sufficient for UBQLN2s recruitment to SGs. However, unlike RBPs with low complexity PrDs TIA-1, TDP-43, and FUS and signaling protein G3BP, that seed SG formation (Gilks et al., 2004; Liu-Yesucevitz et al., 2010; Patel et al., 2015; Reineke et al., 2012; Tourrière et al., 2003), UBQLN2 inhibits SG formation. The ATP-dependent molecular chaperones Hsp70 and VCP that act as SG disaggregases are also incorporated in SGs (Buchan et al., 2013; Jain et al., 2016), but this association has not been associated with a PrDs in these proteins, as is true for UBQLN2. Consistent with the observation by us and others that UBQLN2 moves out of SGs during prolonged stress, UBQLN2 could also participate in extraction of misfolded RBPs or aggregates from SGs in cooperation with other ATP dependent chaperones. The loss of UBQLN2 mutant function in suppressing SG formation suggests UBQLN2 links PQC and RNA homeostasis in ALS pathology**.** This study opens the door to mechanistically understanding the negative regulatory role of the network of molecular chaperones in the early stages of SG formation and ALS/FTD pathogenesis that I explore further in Chapter 3.

METHODS

DNA vectors

pcDNA3.1 was modified to include a tetracycline operator (SacI-tetO-SacI), amino-terminal 3xFLAG tag (HindIII-3xFLAG-HindIII), attR1-CmR-ccdB-attR2 Gateway destination cassette (from pQXCP-DEST), and TetR-IRES-PuroR cassette (from Tet-pLKO-Puro). This CMV/TO-n3xFLAG-attR1-CmR-ccdB-attR2 DEST cassette was then introduced into pcDNA5-FRT by Gibson assembly and transformed into electrocompetent *ccdB* Survival T1 *E. coli* cells by electroporation. UBQLN2 wild

type, mutants, and fragments along with GUS and GFP were cloned into Entry vector pENTR221. pENTR221 was then used to introduce this cDNA into the modified pcDNA3.1 and pcDNA5-FRT DEST vectors by LR Gateway cloning (ThermoFisher, Waltham, MA).

All shRNAs were cloned into the BamHI/HindIII restriction sites in the p-RFP-C-RS vector from Origene, which was modified to remove RFP by *Mlu*I, *Bgl*II digestion followed by blunting and religation. The scramble control was also from Origene (TR30015). shRNA targeting sequences were as follows: gcactaccagagctaactcagatagtact (non-targeting), tgtatatgaccttaatctttgtgcagcct (UBQLN2-1), aaccacgagtcctacatcagaatctggac (UBQLN2-2), ctgaactacagagtcagatgcagcgacaa (UBQLN1-1), tacatcctctggtgaaggtagtcaacctt (UBQLN1-2), gctgctcagatgatggtgaatgtgccgct (UBQLN4-1) and ggcttcatcaatcgtgaggctaacctgca (UBQLN4-2).

Cell Culture

HeLa, U2OS, and HEK293T were cultured in DMEM with 10% FBS. SHSY-5Y cells (Sigma) were cultured in Ham's F12: EMEM (EBSS) (1:1) + 2mM Glutamine + 1% Non-Essential Amino Acids + 15% Fetal Bovine Serum at 37°C/5% CO_2 in standard tissue culture dishes. HEK293T clones with randomly integrated, linearized pcDNA3.1_CMV/TO_n3xFLAG-UBQLN2_TetR_IRES_Puro were selected, expanded, and subcloned under continuous 3 μg/mL puromycin treatment. UBQLN2 overexpression was induced with 1 μg/mL doxycycline for 24-72 hrs. Flp-In UBQLN2 fragment HeLa cells were generated by cotransfecting pcDNA5_FRT_nxFLAG-UBQLN2 fragments with pOG44 at a 9:1 molar ratio. Integrants were selected with 400 μg/mL Hygromycin B and 16 μg/mL Blasticidin and pooled. 1 μg/mL tetracycline was used to induce fragment expression for 24 hrs.

Transfection was performed with lipofectamine 2000 (Invitrogen) in Opti-MEM (Gibco) reduced serum media, halving the manufacturers recommended volumes and following the manufacturer's protocol. Opti-MEM was replaced with DMEM/10% FBS 5 hrs after transfection for HeLa cells, and 12 hrs after transfection for HEK293T cells.

For cell stress experiments the following treatments/reagent concentrations were used unless otherwise indicated in figure legends: 43.7°C, 0.5 mM $NaAsO_2$, 1 μM CCCP in Glucose-free DMEM, 0.4 M Sorbitol, 0.2 M NaCl, 2 mM H_2O_2.

Antibodies for Western blotting and Immunocytochemistry

Rabbit anti-UBQLN2 (Sigma HPA0006431) and mouse anti-UBQLN2 (Novus, NBP2) antibodies were used to specifically detect UBQLN2 via immunofluorescence and western blot (Appendix B). Goat anti-TIA-1 (Santa Cruz, C-20) and Mouse anti-G3BP (BD 611126) were used to detect SGs, and goat anti-4E-T (Santa Cruz, N-18) to detect P-bodies. Mouse and rabbit anti- DYKDDDDK (Sigma F3165 and CST) respectively were used to detect FLAG constructs by Western blot, whereas mouse anti-DYKDDDDK (Sigma F1804) was used for immunocytochemistry (ICC). Antibodies used to validate high SILAC hits include rabbit anti-ALDH3A2 (Genetex), mouse anti-HSP70 (Enzo ADI-SPA-822-D), mouse anti-ESYT2 (Sigma HPA002132), and mouse anti-LETM1 (Proteintech, 16024-1-AP). Rabbit anti-eIF2α-pSer51 (CST 9721) and mouse anti-eIF2α (Abcam ab119495) were used to track translation inhibition. Rabbit anti-SQSTM1 (CST D10E10), rabbit anti-BAG6 (gift, Yihong Ye), mouse anti-VCP (Novus NBP120), goat anti-TCP1 theta (Santa Cruz sc-13891), rat anti-Hsc70 (Enzo ADI-SPA-815-D), and mouse anti-Hsp72 (Enzo ADI-SPA-810-D) to check localization of other proteins to SG by immunofluorescence staining. Mouse anti-β-actin (Santa Cruz, C4) was used as a loading control for Western blots. Secondary antibodies Donkey anti-goat IgG-Alexa fluor 647 nm, Donkey anti-mouse IgG-Alexa flour 488 nm, and Donkey anti-rabbit IgG-Alexa fluor 555 nm (Invitrogen) were used for 3 color immunofluorescence staining. Cell nuclei were stained with DAPI (4',6-diamidino-2-phenylindole). Secondary antibodies Goat/Donkey anti-mouse IgG and anti-rabbit IgG-800CW and 680LT pair were used for two color Odyssey Western blots (Licor).

SDS-PAGE and Immunoblotting

Cell lysates were collected in 1% CHAPSO [3-([3-Cholamidopropyl]dimethylammonio)-2-hydroxy-1-propanesulfonate], 50 mM HEPES pH 7.9, 150 mM NaCl, 2 mM EDTA supplemented with 1x Protease Inhibitor Cocktail (Sigma P8340) and 0.2 mM Na_3VO_4 and sonicated using a Diagenode

Bioruptor 5 min (high setting, 30 sec pulse, 5 min) prior to spinning at 20,000 x g at 4°C. In our experience, ubiquilin protein separated well on an 8% isocratic Tris-Gly SDS-PAGE gel with 4% stacking gel at 65V or TGX Criterion 4-20% gradient gel at 85V (Bio-rad). Protein was transferred to 0.2 μm nitrocellulose membrane via Bio-rad Turboblot transfer (25V, 1.3 Amp, 12-15 min), the membrane was blocked with 5% Milk/TBS-T (20 mM Tris pH 7.6 ± 0.1, 150 mM NaCl, 0.1% Tween 20), and then incubated with primary antibody in 5% BSA, TBS-T, 0.03% Sodium Azide solution at 4°C overnight. Secondary antibodies Donkey anti-Mouse IgG-680LT or 800CW and Donkey anti-Rabbit IgG-680LT or 800CW (Licor Biosciences, Nebraska, USA) at 1:10,000-1:20,000 in milk were incubated 1-2 hrs at room temperature protected from light to detect primary antibody. An Odyssey scanner (Licor Biosciences, Nebraska, USA) equipped with 700 nm and 800 nm laser channels was used to image the blot.

Immunoprecipitation for SILAC LC-MS/MS analysis

Expression of FLAG-UBQLN2 in stable HEK293T cells was induced by treatment with 1 μg/mL doxycycline for 72 hrs. Equal numbers of cells were washed with phosphate buffered saline (1 mM Na_2HPO_4, 0.2 mM KH_2PO4, 0.27 mM KCl, 13.7 mM NaCl pH 7.4 ± 0.2) (PBS), pelleted and resuspended in lysis buffer (1% CHAPSO, 50 mM HEPES pH 7.9, 150 mM NaCl, 2 mM EDTA, 0.2 mM $NaVO_4$, 2x Protease Inhibitor Cocktail (Sigma P8340)). Cells were rocked in lysis buffer 30 min at 4°C, sonicated in 10 sec intervals, 3x on high power, and passed through a 25G needle 10x on ice, then spun at 20,000 x g, 10 min at 4°C to pellet insoluble debrís. Equal amounts of lysate were then loaded directly onto FLAG-M2 antibody coated agarose magnetic beads (Sigma M8823) and rocked overnight at 4°C. Beads were washed with wash buffer (lysis buffer without detergent), 5 min at room temperature 5x, and FLAG-UBQLN2 was eluted with 300 ng/μL FLAG peptide (Sigma F4799) in wash buffer 30 min at 4°C at 850 rpm 3x. Eluant was flash frozen in liquid N_2 for storage until analysis. The amount of target protein immunoprecipitated was checked against a BSA standard via Blue-Silver

staining of protein separated by Tris-Gly-SDS-PAGE or Silver staining using the Pierce Silver Stain kit (Cat. No. 24612).

SILAC LC-MS/MS Analysis

HEK293T stable cell lines were cultured for more than 6 generations in heavy ($^{13}C_6$,$^{15}N_4$ L-Arginine, $^{13}C_6$,$^{15}N_2$ L-Lysine) or light ($^{12}C_6$,$^{14}N_4$ L-Arginine, $^{12}C_6$,$^{14}N_2$ L-Lysine) SILAC DMEM supplemented with 10% Gibco Performance FBS, and Penicillin-Streptomycin Solution. Lysate was checked for labeling completion by mass spectrometry. Immunoprecipitate eluants were quickly thawed on ice, pooled, dialyzed, concentrated and separated via Tris-Gly SDS-PAGE. Proteins were visualized by silver staining or colloidal Coomassie. Individual bands were cut out and protein was digested in-gel with trypsin. Peptides were extracted, precipitated and separated via capillary electrophoresis through an Easy nLCII liquid chromatography system, then analyzed in an Orbitrap Elite mass spectrometer. Peptides were matched via the Proteome Discoverer 1.4 Suite against human Refseq 59 protein database applying a 1% peptide-spectrum-match and peptide-level false discovery rate. Proteins were groups by domain structure based on DAVID GO term analysis and manual annotation from the UniProt database and visualized using Revigo software.

STRING network analysis

Proteins that immunoprecipitated with both UBQLN2 (our study) and G3BP under sodium arsenite stress (Jain et al., 2016), as a representative of SGs, were identified using the vlookup function in Excel. Network analysis was performed using the publicly available STRING tool (Szklarczyk et al., 2015). All proteins from the UBQLN2 SILAC analysis with H/L ≥ 1.5 or no detected ratio with more than one peptide were included in the analysis. Proteins were clustered using an mcl clustering value of 3, and a "high confidence" network association level of 0.7. For completeness, I included hnRNPA1 as another SG protein that interacts with UBQLN2 as previously identified (Gilpin et al., 2015).

Immunofluorescence microscopy

Cells grown on glass coverslips were simultaneously fixed and permeabilized to visualize UBQLN2 in SGs (Figure 2-4, Table 2-1). Coverslips were washed with PBS prior to blocking with 5%

Donkey/Horse serum in 0.25% Triton X-100 for 1 hr at room temperature or overnight at 4°C. Primary antibody was incubated 3 hrs at room temperature or overnight at 4°C and secondary antibody was incubated 2 hrs at room temperature in the dark. DAPI was diluted to 1 μg/mL with secondary antibody to label cell nuclei. Primary and secondary antibodies were diluted in a 3% BSA, 0.25% Triton X-100 solution. Three washes for 5 min each were performed after primary and secondary antibody incubations at room temperature on an orbital shaker. Coverslips were mounted with Prolong Gold mounting media (Molecular Probes) and allowed to cure 24 hrs at room temperature in the dark prior to imaging on a Leica SP8 scanning confocal microscope. All solutions were buffered with PBS. Live cell images of FUS-GFP were taken on a Nikon fluorescent microscope.

Colocalization Analysis

Pearson's R correlation coefficient analysis was performed using the Colocalization threshold plugin, Costes method in Fiji. 50 cells chosen were chosen at random and outlined with the polygon tool for analysis. Data analysis was performed in GraphPad Prism.

Percentage of cells with SGs analysis

Cells were counted by DAPI stained nuclei by applying the Analyze Particle function in Image J to smoothed, automatically thresholded, MIPs of confocal z-stacks. The number of cells with SGs was manually counted using the Counter plugin in ImageJ and data was graphed and analyzed in GraphPad Prism.

SG size distribution analysis

To determine the SG size distribution in fixed cells, a maximum intensity projection (MIP) of each confocal image stack was created in Fiji to measure the cross-sectional area of SG particles. Images were automatically thresholded via the Renyi Entropy method and converted to binary images using the Threshold plugin in Fiji. Particles in the binary image were then analyzed and added to the ROI manager using the Analyze Particles Plugin with a minimum particle size of 4 pixels and no limits on circularity. ROI's were overlayed onto the original MIP and used to measure SG area. The fraction of cells with SG area >1 um^2 was calculated in GraphPad Prism. 4 fields were analyzed for each time

point. Significance was calculated using a two-way ANOVA with the Sidak's method of multiple comparisons.

Prion-like amino acid composition analysis (PLAAC)

Analysis of prion-like domains in UBQLN2 was performed using a hidden Markov model on the MIT resource (http://plaac.wi.mit.edu/Accessed September 6, 2017) (Alberti et al., 2009; Lancaster et al., 2014). A default core length of 60 amino acids and a relative weighting of background probabilities α of 50 (meaning 50% yeast, 50% human composition bias) was used for this analysis.

Statistical analysis

All statistical analysis for cell data was performed in GraphPad Prism 7. Column data was analyzed by a standard one-way ANOVA with Dunnett's method of correction for multiple paired comparisons. Grouped data was analyzed via a standard two-way ANOVA with Sidak's correction method for multiple comparisons.

Acknowledgements

Many thanks to Raja Sekhar Nirujogi and Min-Sik Kim from Dr. Akhilesh Pandey's at JHMI with whom I collaborated to perform the quantitative proteomics analysis of UBQLN2 interacting partners. Also, thanks to Kate Guzzo from Dr. Mike Matunis' lab for assisting me with my first cell staining experiments. Han-Xiang Deng provided the UBQLN2 P497H and P506T cDNA. Andrew Holland provided the HeLa Flp-In cell line, pOG44 and pcDNA5-FRT transfection plasmids. Yihong Ye provided the BAG6 antibody serum.

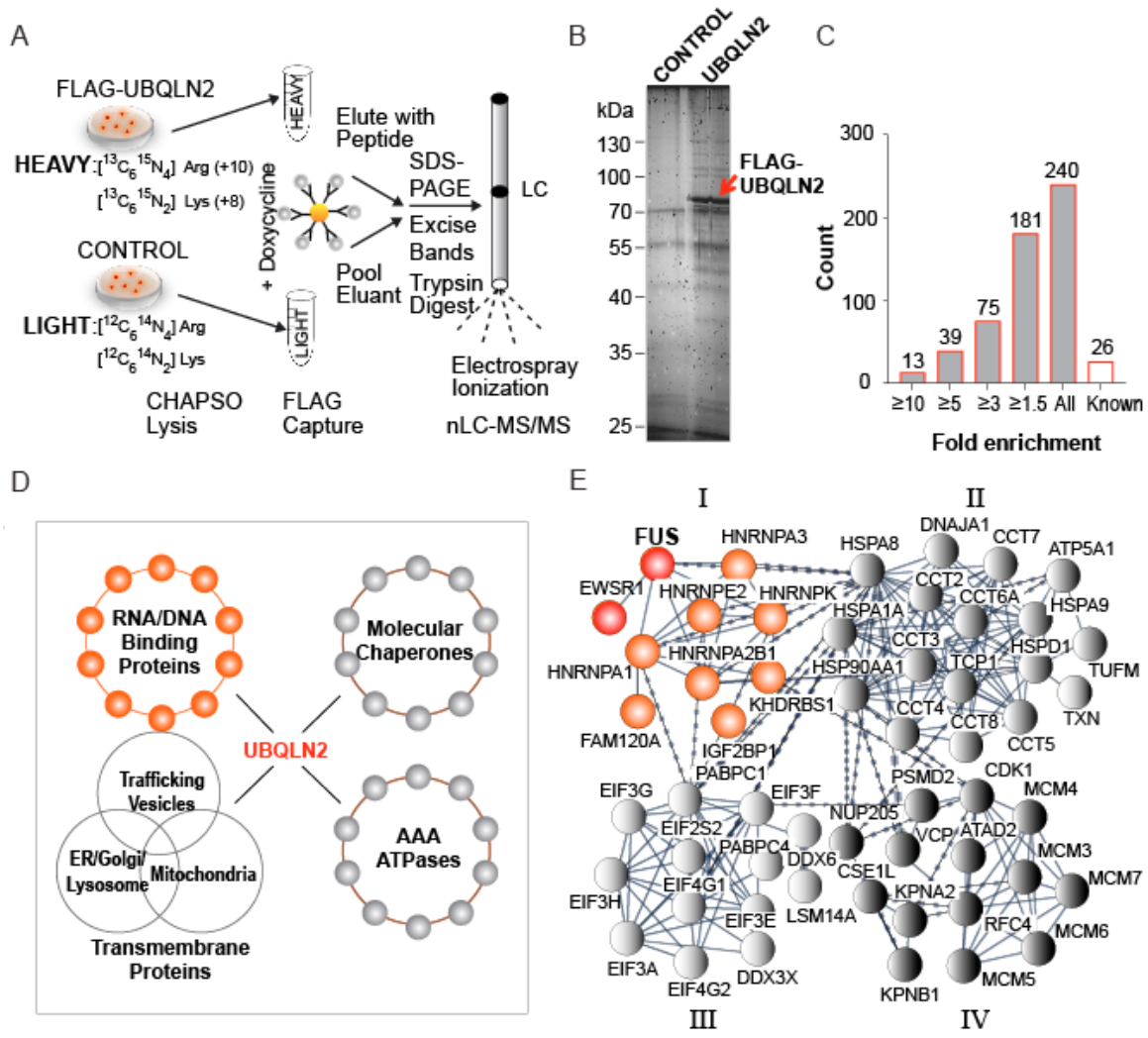

Figure 2-1 SG components immunoprecipitate with UBQLN2

(A) Schematic of SILAC coIP LC-MS/MS analysis. Heavy isotope labelled stable HEK293T cell lines that inducibly express amino-terminal FLAG-UBQLN2 were treated with doxycycline and lysed in buffer containing the detergent CHAPSO. Light isotope labelled HEK293T cells treated with doxycycline were used as a control. Lysates were incubated with FLAG M2-magnetic beads and eluted with FLAG peptide. Eluants were pooled in a 1:1 ratio and separated by SDS-PAGE. Bands were cut out and proteins were digested with trypsin. Peptides were then extracted,

separated via nano-scale liquid chromatography (nLC), and injected via electrospray ionization into an LTQ Orbitrap Elite mass spectrometer for analysis.

(B) Representative silver stained gel of UBQLN2 CHAPSO IP. The red arrow points to exogenously expressed FLAG-UBQLN2 protein.

(C) Cumulative frequency distribution of SILAC Heavy (UBQLN2)/Light (Control) (H/L) ratios from LC-MS/MS analysis of proteins that coimmunoprecipitate with FLAG-UBQLN2. 26 known interactors are shown in a separate category. A total of 240 putative novel interactors were identified, many of which cluster into complexes as shown in **(E)** for SG components.

(D) Classes of UBQLN2 interactors grouped by domain structure.

(E) STRING network of UBQLN2 interactors found in the G3BP-dependent SG Proteome (Jain et al., 2016). Dotted lines represent lower confidence connections, whereas solid lines represent higher confidence connections. Members represented in the four clusters include **I** hnRNPs, **II** molecular chaperones, **III** translation factors and **IV** RNA trafficking proteins. I focused further work on the class I hnRNP FUS.

A

Gene symbol	Protein name	SILAC Ratio	Peptides	Intensity
UBQLN2	Ubiquilin 2	33.3	73	159,943,535
UBQLN1	Ubiquilin 1	*	59	1,331,669,710
ALDH3A2	Fatty aldehyde dehydrogenase	32.0	40	275,359,967
HSPA1A	Heat shock 70 kDa protein 1A/1B	20.3	120	440,917,747
ESYT2	Extended synaptotagmin-2	21.4	17	25,724,668
LETM1	LETM1 and EF-hand domain-containing protein 1	10.7	3	14,751,288
FUS	RNA-binding protein FUS	1.6	3	21,808,551

B

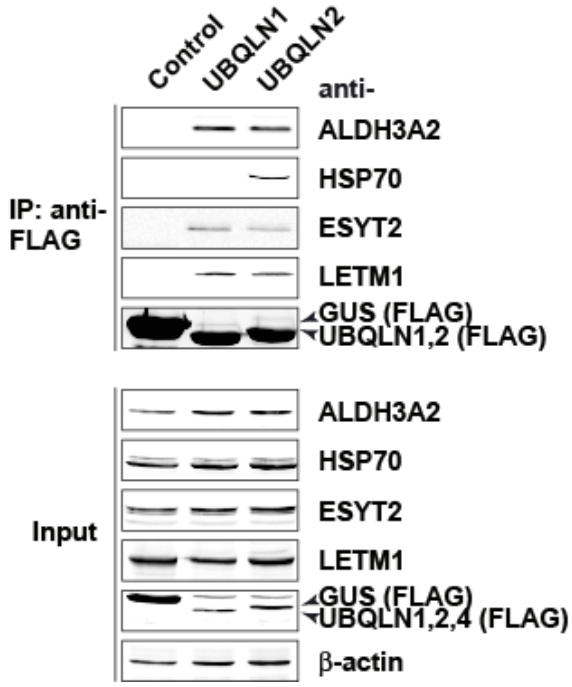

Figure 2-2 Western blot validation of SILAC nLC-MS/MS top results

(A) SILAC LC-MS/MS data for highly enriched UBQLN2 associated proteins. SILAC ratio is the HEAVY (UBQLN2 IP)/LIGHT (CONTROL IP) peptide average ratio. * indicates that a corresponding light peptide was not identified by peptide search software. Peptides are the number of Peptide-Spectrum-Matched Hits. Intensity is the integrated precursor ion peak density.

(B) Western blot of proteins coimmunoprecipitated with FLAG-UBQLN2 or its paralog UBQLN1 from HEK293T cell lysate. The Control is FLAG-GUS (β-glucuronidase derived from plants). Hsp70 was the only strong interactor that immunoprecipitated only with UBQLN2. Validation of the FUS-UBQLN2 interaction is shown in Figure 3-1.

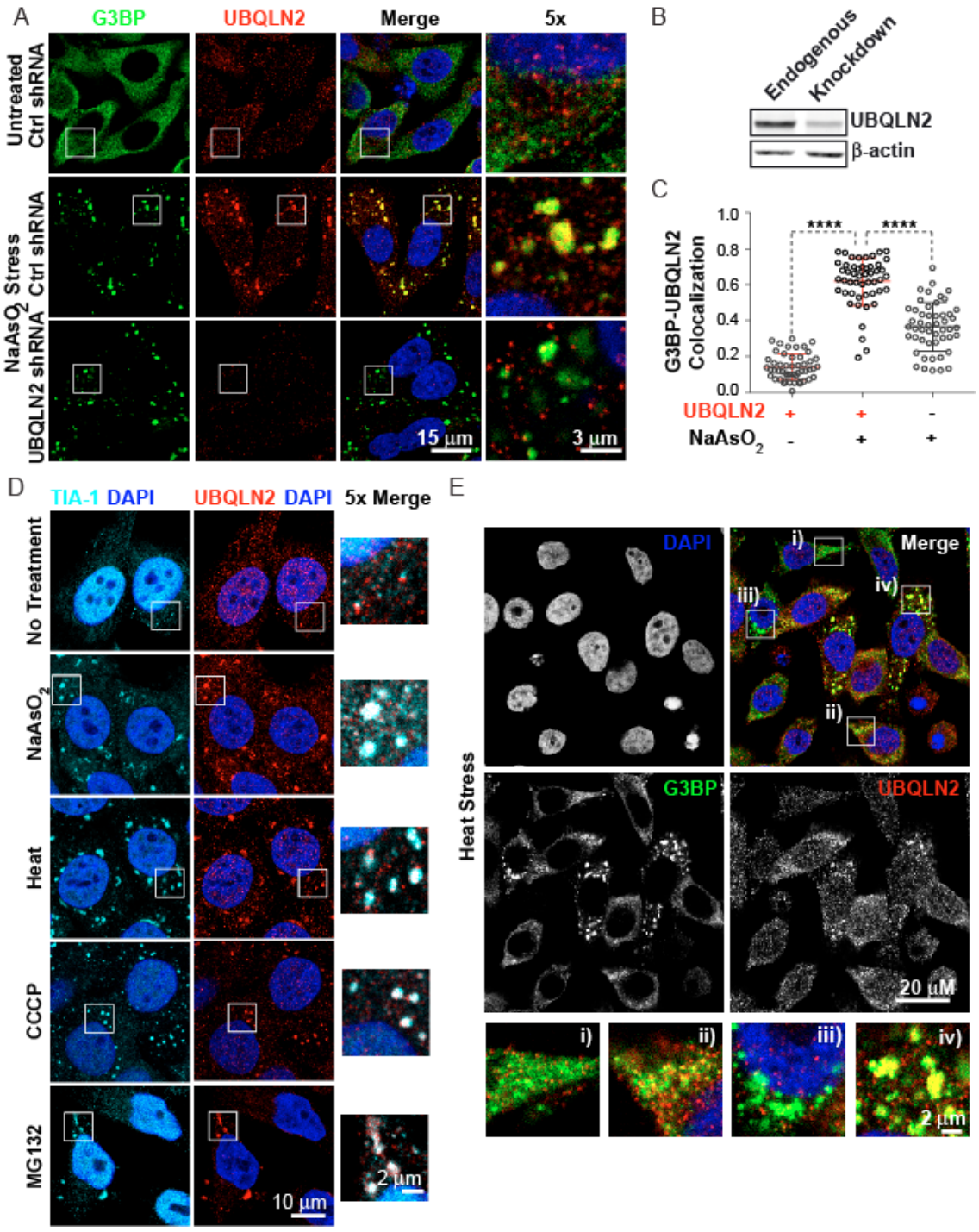

Figure 2-3 UBQLN2 localizes to SGs

(A) Immunofluorescence (IF) images of endogenous UBQLN2 at SG in response to sodium arsenite stress (30 min, 0.5 mM $NaAsO_2$) in HeLa cells. G3BP marks SG. Regions of UBQLN2-G3BP

overlap are yellow. Specific depletion of UBQLN2 eliminates the UBQLN2 signal and regions of overlap. Ctrl shRNA is a scrambled non-targeting shRNA.

(B) Western blot of average endogenous UBQLN2 protein level depletion 96 hrs post-shRNA transfection of the cells shown in (B). β-actin is a loading control.

(C) Scatter plot showing the Pearson's R coefficient of overlap for 50 individual cells chosen at random (dots) between the G3BP (green) and UBQLN2 (red) signal shown in (A). Error bars are 1 SD. **** $p<0.0001$ by Dunnett's multiple comparison test done with a one-way ANOVA. UBQLN2 (-) represents the partial shRNA depletion of UBQLN2 shown in (B). The UBQLN2 signal in SGs appears specific based on this analysis.

(D) IF images of UBQLN2 localization under different stress conditions. HeLa cells were fixed and permeabilized simultaneously as shown in (A). Stress conditions include: 0.5 hr 0.5 mM $NaAsO_2$, 1 hr 43.7°C Heat Stress, 1.5 hr 1 μM CCCP in Glucose free media, 1hr 10 μM MG132.

(E) IF images showing localization of UBQLN2 to SGs with differing morphologies and localization after 30 min of heat stress at 43.7°C. G3BP SG distribution is i) diffuse ii) concentrated but not punctate iii) perinuclear punctate iv) large cytoplasmic puncta.

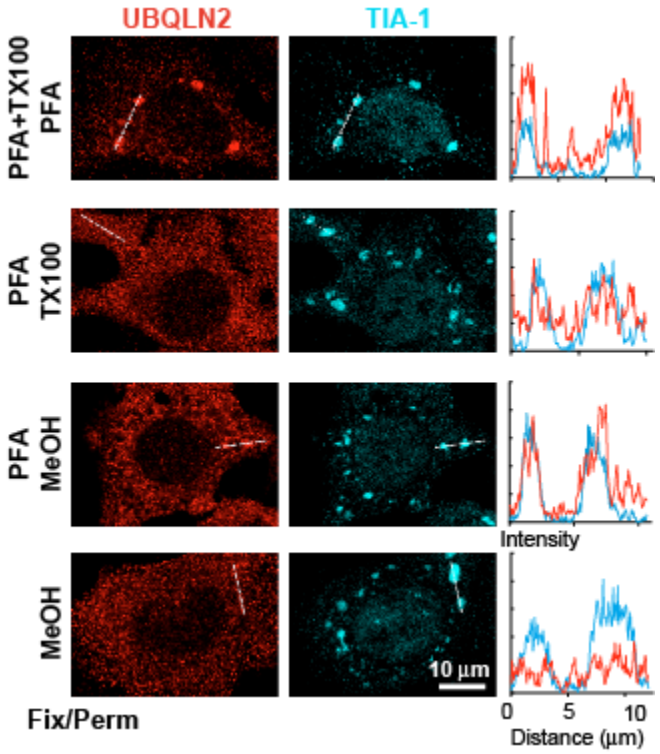

Figure 2-4 Visualization of endogenous UBQLN2 at SGs is enhanced by simultaneous fixation and permeabilization.

Immunofluorescence images of HeLa cells exposed to heat stress at 43.7°C for 45 min prior to fixation. See Methods section for details of individual fix/permeabilization protocols. Graphs to the right are line scans of fluorescence intensity. Intensity is the grey scale value. Distance is distance along the line. UBQLN2 colocalization with SG is visible under all fix/stain conditions except MeOH alone, but is most obvious with simultaneous fixation and permeabilization.

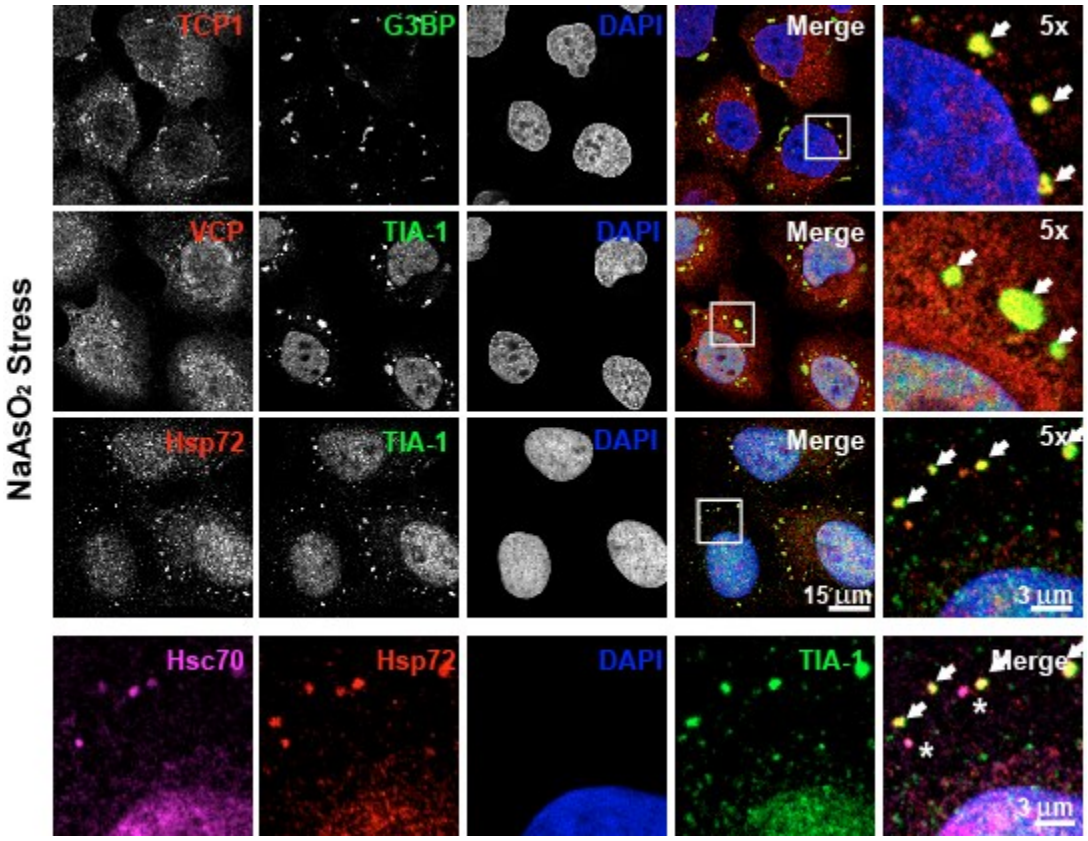

Figure 2-5 Other PQC factors visible in SGs with simultaneous fixation and permeabilization

Immunofluorescence images of other putative SG components in U2OS cells following 2 hrs 0.5 mM $NaAsO_2$ treatment. Cells were fixed and permeabilized simultaneously. TCP1 (TriC), VCP, and Hsp70 (Hsp72, Hsc70) were identified as putative SGs in the SG Proteome. White arrows point to regions of overlap. *Marks Hsc70 puncta that do not overlap with SG marker TIA-1. Either G3BP or TIA-1 was used as a SG marker depending on the species of the other antibody used for staining.

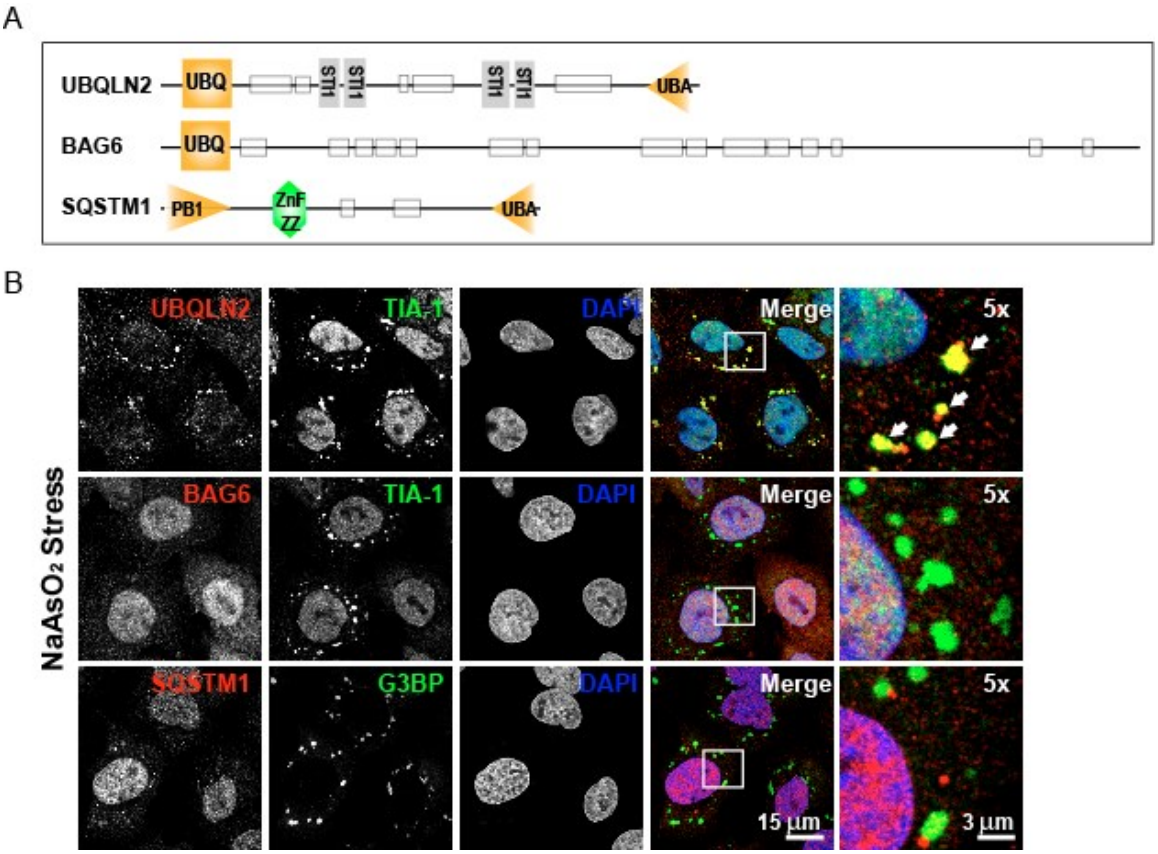

Figure 2-6. Related Ubl/Uba proteins like UBQLN2 not found in SGs

(A) Domain maps of UBQLN2, BAG6, and p62/SQSTM1 highlighting UBQ (ubiquitin-like) and UBA (ubiquitin-associated) domains in orange generated by SMART (Schultz et al., 1998). PB1 is another type of Ubiquitin-like domain. Low complexity regions are shown as grey rectangles. Only UBQLN2 contains the predicted STI1-like repeats in grey. The domains were drawn to scale.

(B) Immunofluorescence images of U2OS cells following 2 hrs 0.5 mM $NaAsO_2$ treatment after simultaneous fixation and permeabilization as described. White arrows point to regions of overlap. Either G3BP or TIA-1 was used as a SG marker depending on the species of the other antibody used. Both BAG6 and SQSTM1 are absent from SG, while UBQLN2 is present under the conditions tested.

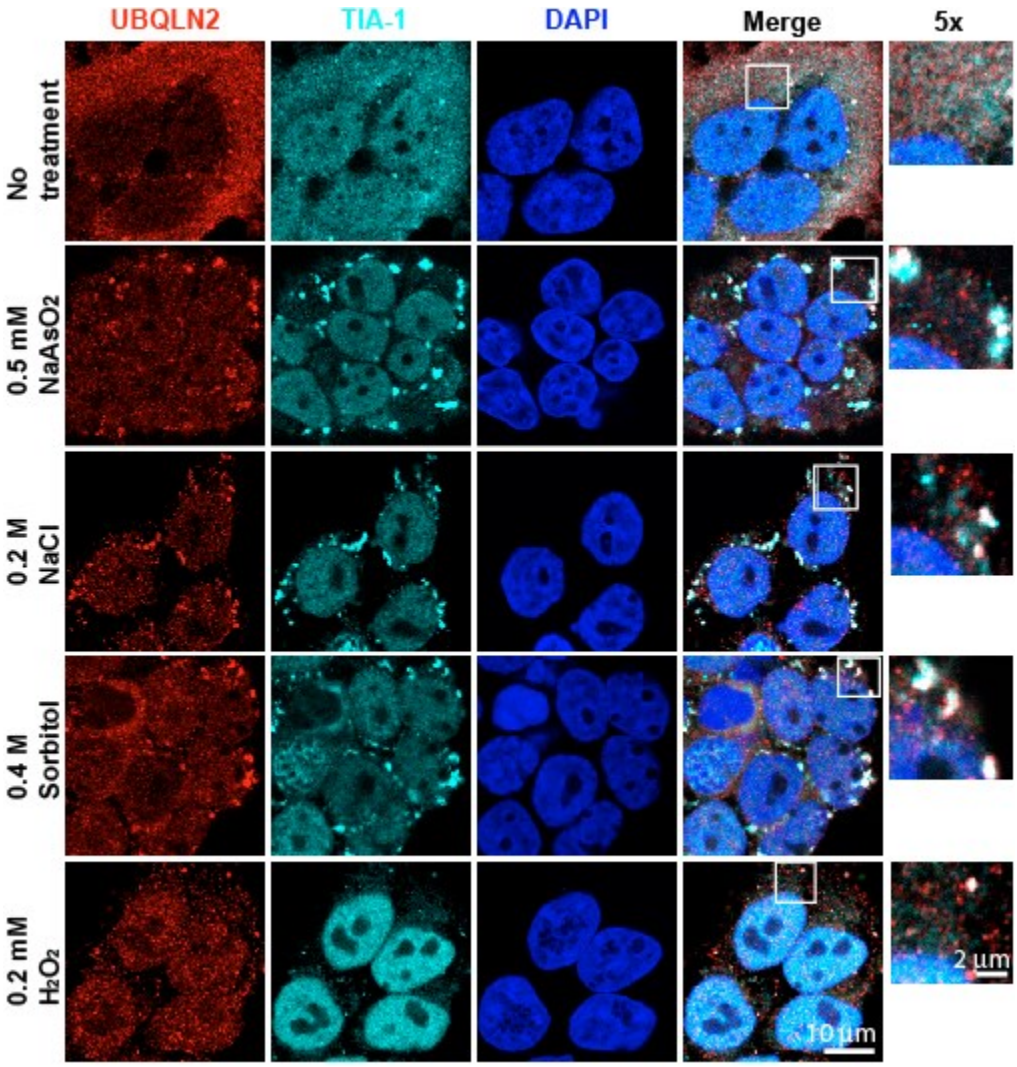

Figure 2-7 UBQLN2 localizes to SGs under many different stresses

Immunofluorescence images of fixed HEK293T cells. HEK293T cells were treated with the stressor indicated for 2 hrs prior to fixation. Concentrations of each stressor used were as follows: 0.5 mM $NaAsO_2$, 0.2 M NaCl, 0.4 M Sorbitol, 0.2 mM H_2O_2. Colocalization of UBQLN2 and SG marker TIA-1 is seen as white pixels. SG formed under the different stress conditions have different morphologies, but in all cases UBQLN2 is present in SG.

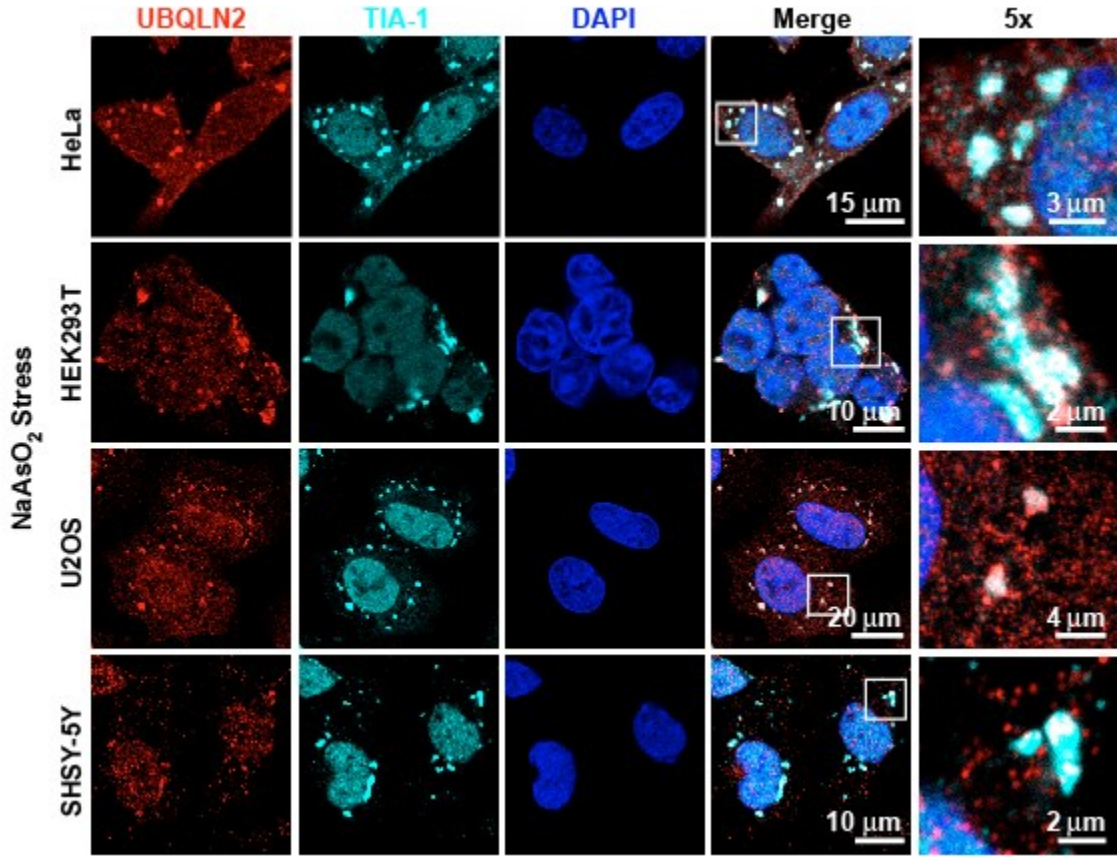

Figure 2-8 UBQLN2 localizes to SGs in different cell types

Immunofluorescence images of fixed cells. Cells were treated with 0.5 mM $NaAsO_2$ for 2 hrs prior to fixing and permeabilizing simultaneously. Overlap of UBQLN2 and the SG marker TIA-1 is shown as white pixels in the Merged image. In all of these cell types, UBQLN2 colocalizes with TIA-1 in SGs.

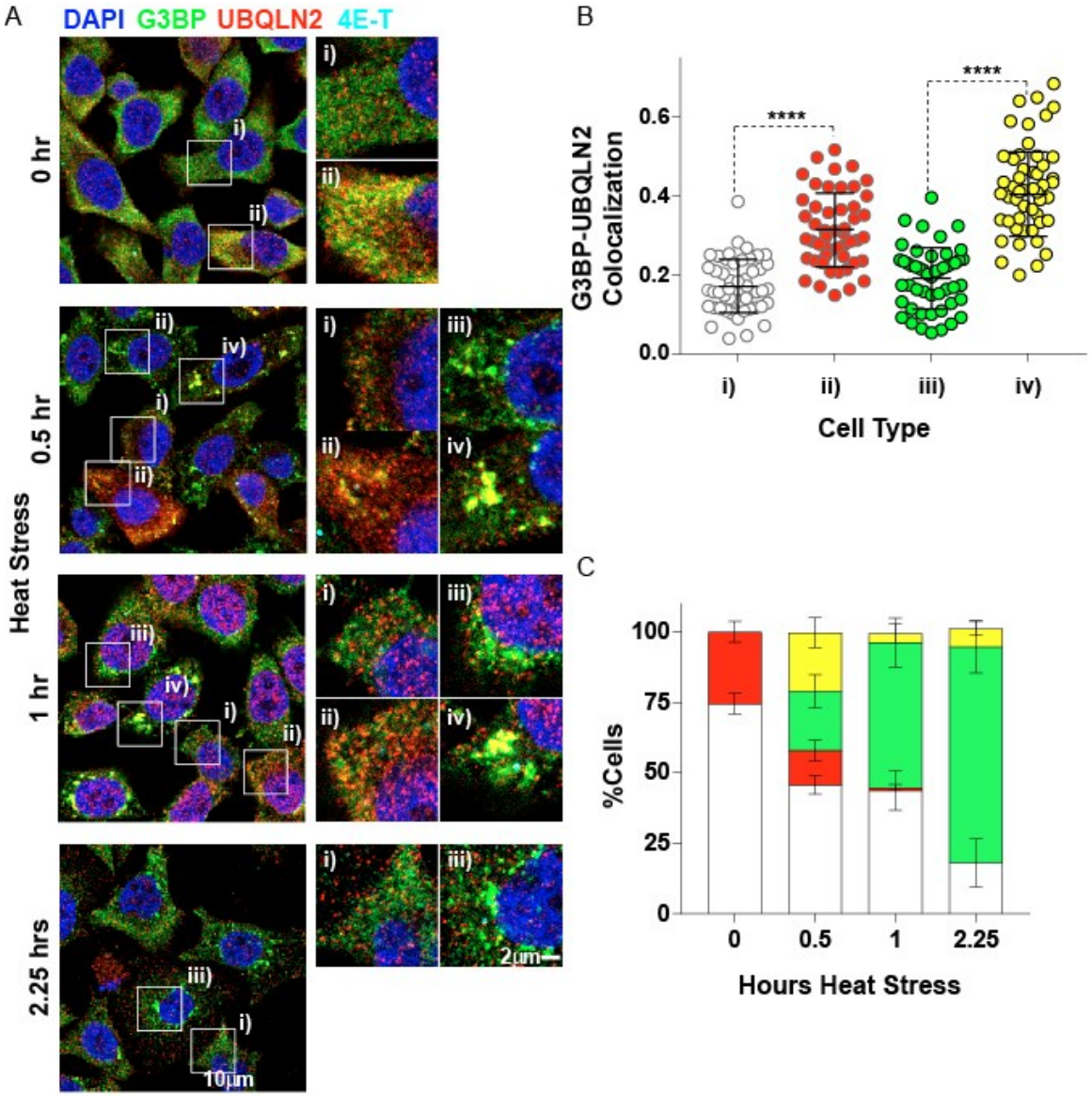

Figure 2-9 UBQLN2 localization to SGs changes over time

(A) Immunofluorescence (IF) images of HeLa cells exposed to acute heat stress (43.7°C) fixed at the time points shown. Overlap between UBQLN2 (red) and SG marker G3BP (green) is shown as yellow pixels. UBQLN2 colocalization with SGs changes as SG morphology and localization changes.

(B) Scatter plot showing the Pearson's R coefficient of overlap for G3BP (green) and UBQLN2 (red) for 50 individual cells with SGs (open circles) of each cell type after 30 min of heat stress at 43.7°C as in (A). Error bars are 1 SD from the mean. **** $p<0.0001$ by Tukey's multiple comparison test done with a one-way ANOVA $p<0.0001$.

(C) Bar graph showing the proportion of each cell type present in the cell population from four 246 μm^2 image fields during heat stress shown in (A). Error bars are 1 SD from the mean.

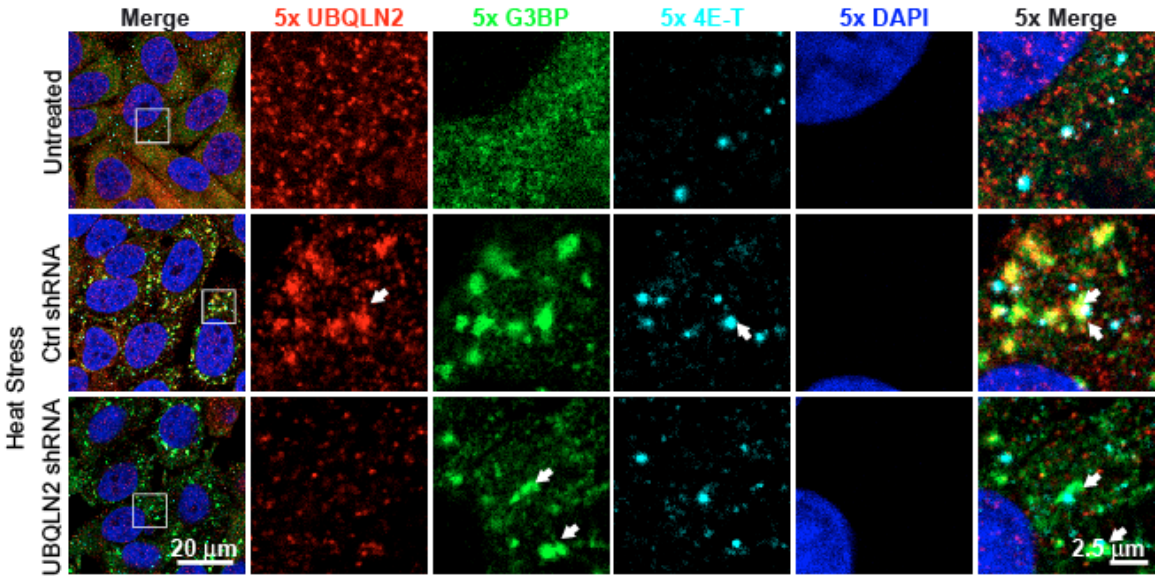

Figure 2-10 UBQLN2 is in SGs not P-bodies

Immunofluorescence images. Single channel images of the 5x magnified region are shown to the right of the full-scale image to the left. Cells were exposed to 30 min of heat stress at 43.7°C prior to simultaneously fixing and staining. G3BP marks SG and 4E-T marks P-bodies. White arrows mark juxtaposed SGs and P-bodies. UBQLN2 depletion in the bottom panel eliminates the UBQLN2 signal colocalizing with G3BP as in Fig. 1A. UBQLN2 only appears to colocalize with SGs when P-bodies are juxtaposed to SGs following stress.

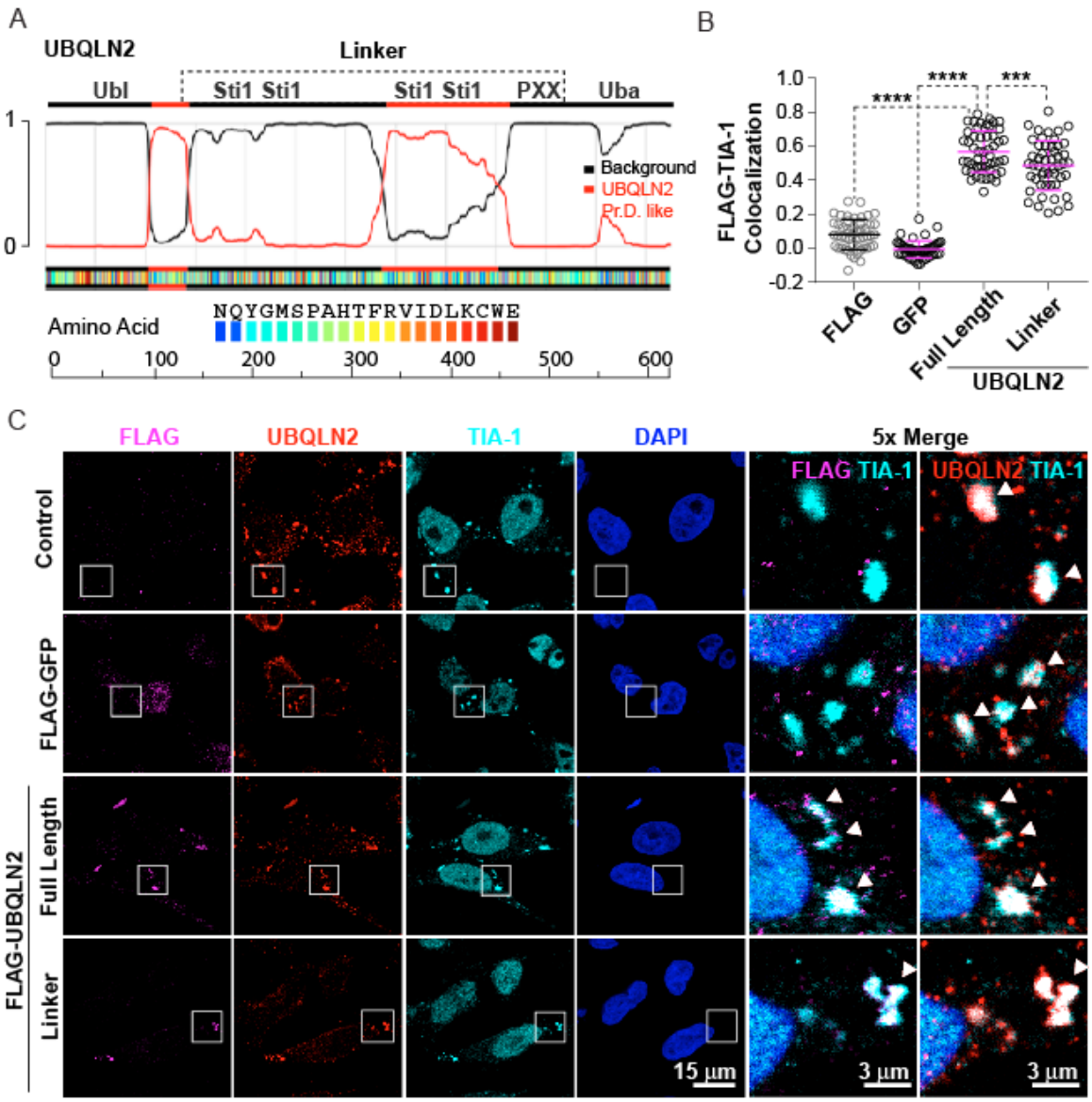

Figure 2-11 The Sti1-like linker alone is sufficient for UBQLN2 localization to SGs

(A) Prion-like domain (PrD) analysis of UBQLN2. The dotted line highlights the bounds of the linker region tested in (B). Identified PrD 1 is amino acids 105-143. PrD 2 is amino acids 338-460 of human UBQLN2.

(B) Scatter plots showing the Pearson's R coefficient of overlap between FLAG-tagged proteins (magenta) with SG marker TIA-1 for 50 individual cells (open circles) chosen at random. FLAG-tagged proteins were expressed from an integrated FRT site in HeLa Flp-In TRex cells and

exposed to 60 min of heat stress at 43.7°C. Error bars are 1 SD from the mean. **** $p<0.0001$, ***$p=0.0006$ by Dunnett's multiple comparison test.

(C) Representative immunofluorescence images of HeLa Flp-In TRex cells expressing FLAG-tagged proteins as quantitated in (B). The linker region alone drives UBQLN2 into SGs.

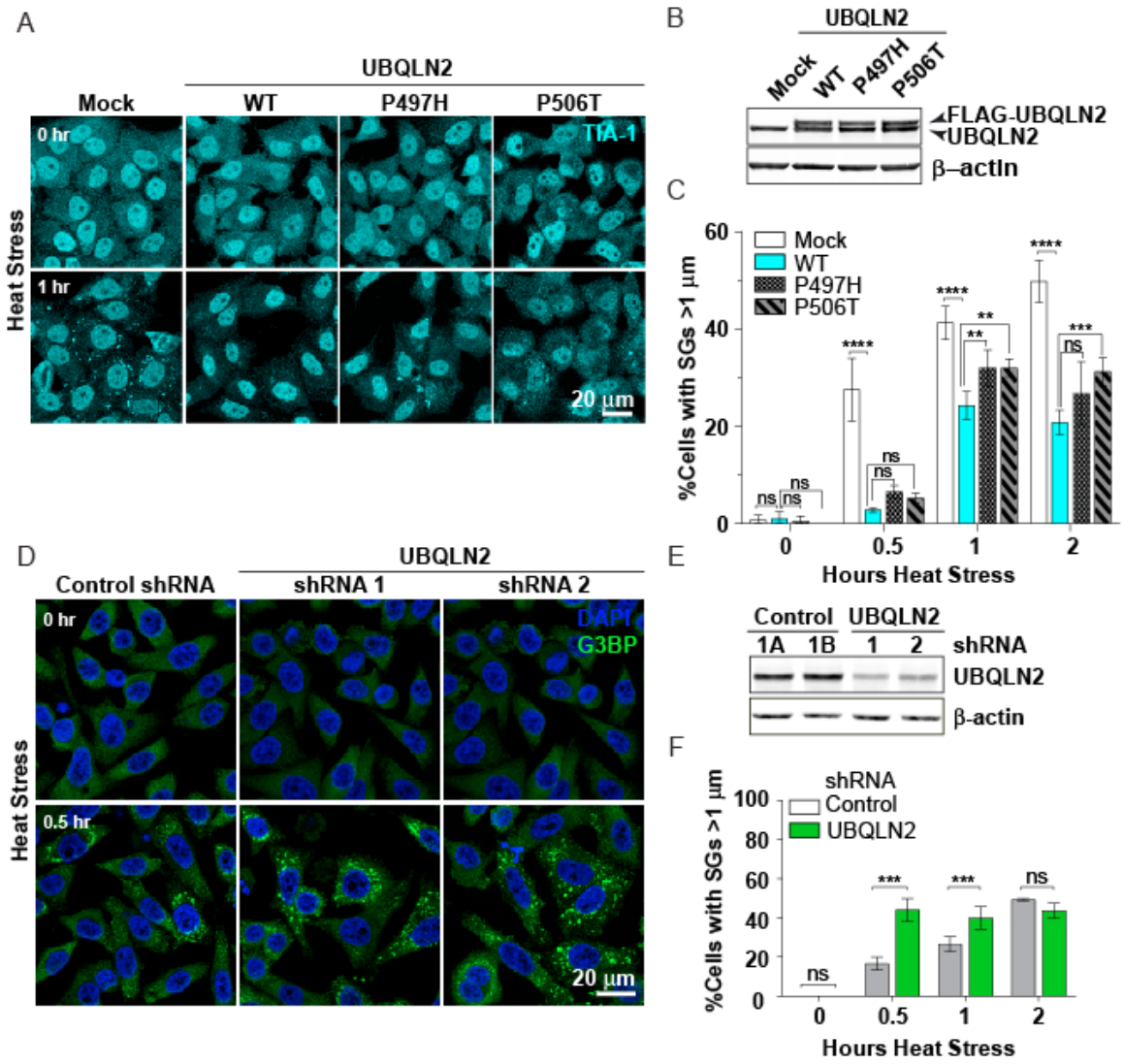

Figure 2-12 UBQLN2 levels negatively regulate SG assembly

(A) Immunofluorescence (IF) maximum intensity projections (MIPs) of SGs in Mock, FLAG-UBQLN2 wild type (WT), FLAG-UBQLN2 P497H, and FLAG-UBQLN2 P506T transfected HeLa cells fixed and stained before and after heat stress. TIA-1 was used as a SG marker. A Western blot showing the level of UBQLN2 WT and mutant overexpression is shown in **(B)**. β-actin is used as loading control.

(C) Quantitation of percentage of cells with SGs larger than 1 µm shown in (A).

(D) IF MIPs of SGs in control and UBQLN2 specific shRNA treated HeLa cells before and after heat stress. G3BP was used as a SG marker with DAPI marking nuclei of individual cells. A Western blot

showing the level of UBQLN2 depletion by the two UBQLN2 specific shRNAs is shown in **(E)**. Approximately double the number of UBQLN2 shRNA depleted cells show large cytoplasmic SGs after 30 min of heat stress.

(F) Quantitation of percentage of cells with SGs larger than 1 μm shown in (D).

****p<0.0001 ***p<0.001, **p<0.01, *p<0.05; P values are for Sidak's multiple comparison tests. A representative data set is shown. More than 400 cells from 4 fields of view were imaged and averaged at each time point. Error bars are SD. The experiments were repeated using both G3BP and TIA-1 markers. UBQLN2 appears to negatively regulate SG formation in all cases.

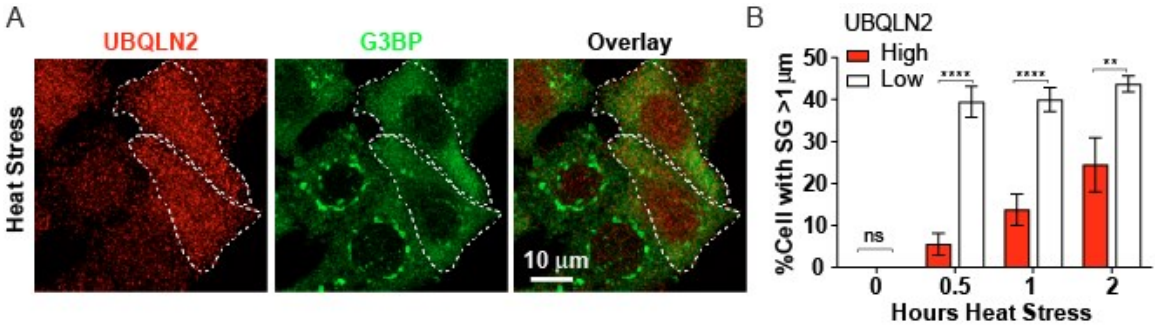

Figure 2-13 UBQLN2 affects SG size among UBQLN2 shRNA treated cells

(A) A representative confocal immunofluorescence image of UBQLN2 shRNA transfected HeLa cells after 30 min of heat stress (43.7°C). Dotted lines outline cells with a higher UBQLN2 expression level.

(B) Quantitation of (A). Cell numbers were quantitated from four fields totaling more than 400 cells at each time point. The experiment was repeated twice. A standard two-way ANOVA. P value for the effect of brightness was 0.0006. The results of Sidak's multiple comparisons are shown as **** $p<0.0001$, ** $p<0.01$, ns=not significant. Error bars are SEM. In cells with higher UBQLN2 levels, SG formation is significantly suppressed.

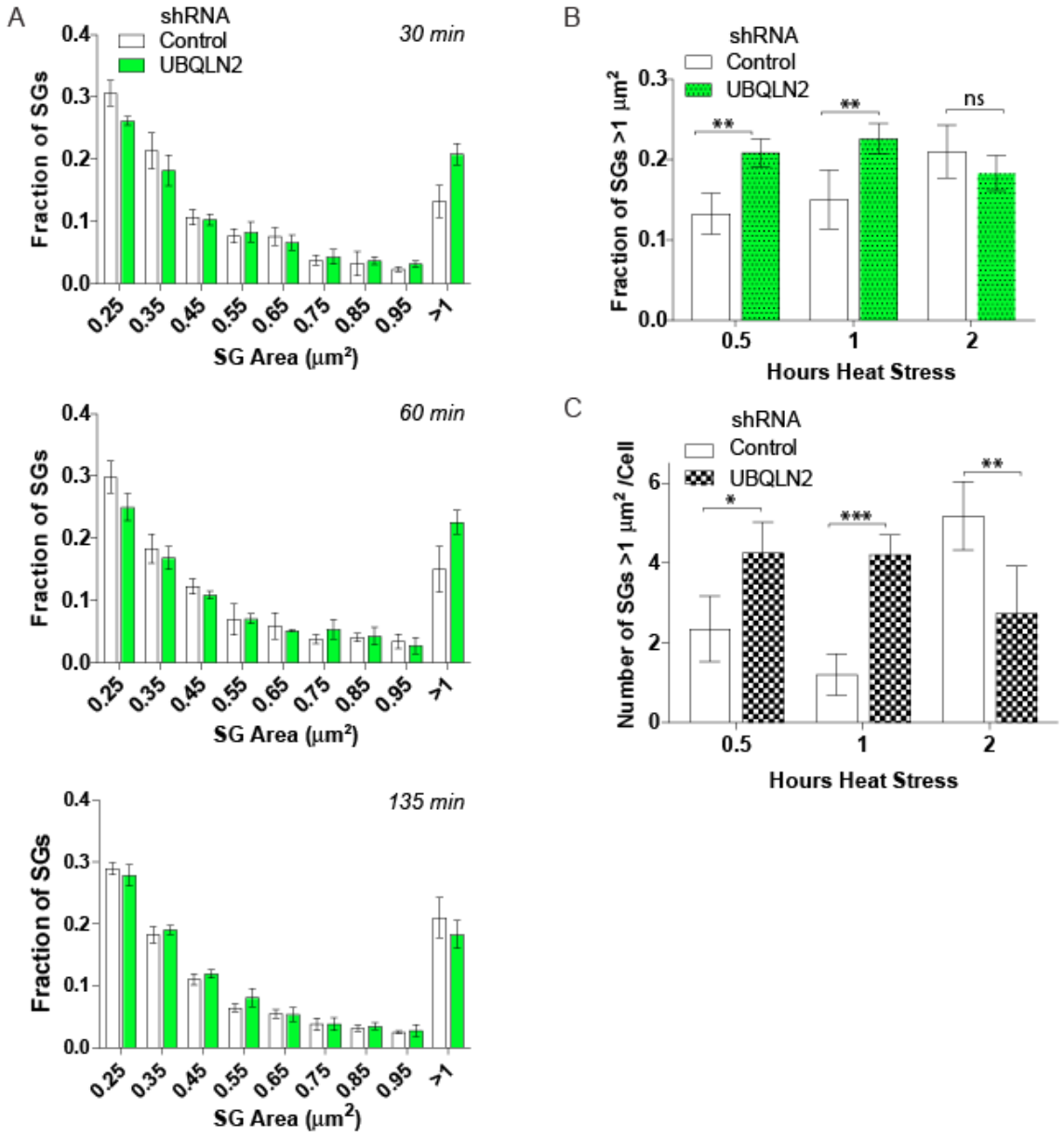

Figure 2-14 UBQLN2 depletion leads to an increase in SG size and number

(A) Histogram of SG particle size.

(B) Graph of fraction of large SGs >1μm².

(C) Graph of number of SGs per cell.

This data represents further analysis of data presented in Fig. 2-8 (D)-(F). Four fields with more than 400 fixed HeLa cells were imaged for each condition. A representative data set is shown. A standard

two-way ANOVA was performed for (B) $p=0.0012$ and (C) $p=0.0221$ for the effect of UBQLN2 level respectively. All error bars are SD. ***$p<0.001$, **$p<0.01$, *$p<0.05$, ns not significant ($p>0.05$) for Sidak's multiple comparison tests. The experiment was repeated twice.

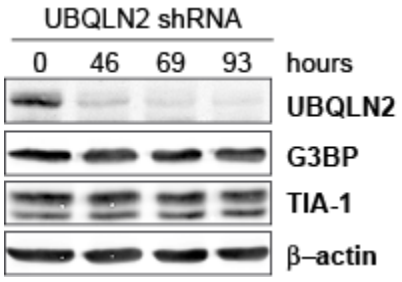

Figure 2-15 G3BP and TIA-1 levels are not perturbed by UBQLN2 depletion

Western blot showing levels of G3BP and TIA-1 46, 69 and 93 hrs post-transfection of HeLa cells. After 46 hrs post-transfection, the majority of UBQLN2 has already been depleted. Levels of G3BP or TIA-1 do not appear to be altered under these nonstress conditions.

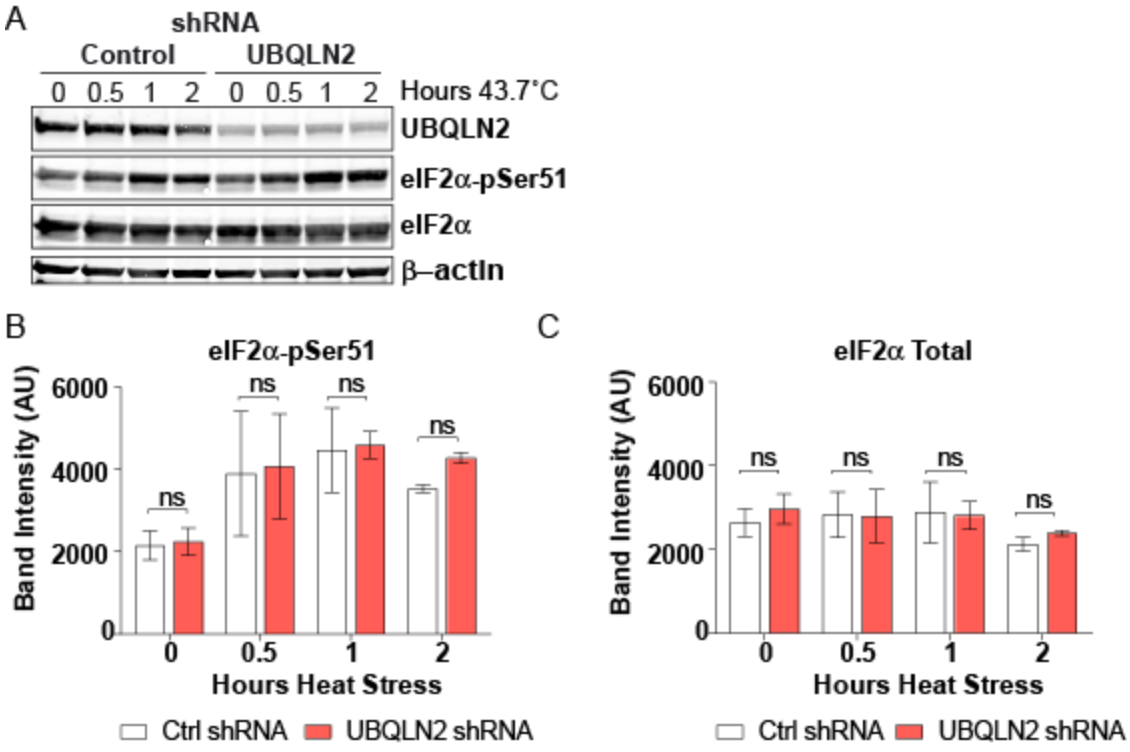

Figure 2-16 eIF2α phosphorylation is unaltered by UBQLN2 depletion

Representative Western blot showing Ser51 phosphorylated and total eIF2α levels during heat stress as indicated relative to UBQLN2 level. Results from at least three independent experiments are quantitated in (B) and (C). Error bars are SD. ns = not significant for Sidak's multiple comparison tests, significance level was set at 0.05. Results were analyzed by 2-way ANOVA with P=0.1692 for the effect of shRNA, which is not significant.

Table 2-1 Fixation/permeabilization techniques used for immunofluorescence staining

		Step 1		Step 2	
#	Method	Fix/Perm	Time,Temp	Fix/Perm	Time,Temp
1	PFA+TX100, PFA	2% PFA/0.25% TX-100	10 min, r.t.	2% PFA	20 min, r.t.
2	PFA+TX100, PFA	4% PFA/0.5% TX-100	5 min, r.t.	4% PFA	10 min, r.t.
3	PFA, TX100	4% PFA	15 min, r.t.	0.25% TX-100	5 min, r.t.
4	PFA, MeOH	4% PFA	15 min, r.t.	MeOH	10 min, ice cold
5	MeOH	MeOH	20 min ice cold	--	--

Time and temperature for each condition is listed. Each step was performed sequentially from left to right. In Methods 1 and 2 fixation and permeabilization were performed simultaneously. Method 2 is a harsher variation of Method 1. In Method 3, cells were fixed with PFA, then permeabilized with TX100 sequentially. In Method 4, cells were sequentially fixed with PFA then proteins were precipitated with MeOH. In Method 5 cells were permeabilized and proteins were precipitated simultaneously with MeOH. Method 1 was adapted from (Guzzo et al., 2012) and Method 4 from (Kedersha and Anderson, 2007). All fix/perm solutions were buffered with PBS. TX100=Triton X-100, PFA=Paraformaldehyde, MeOH=Methanol, r.t.=room temperature, ice cold=4°C to -20°C. UBQLN2 was seen most clearly in SGs using Method 1.

Chapter 3 UBQLN2 modulates ALS/FTD-linked FUS-RNA complex dynamics and SG formation

INTRODUCTION

Based on the localization and negative regulatory function of UBQLN2 at stress granules (SGs), I reasoned that UBQLN2 may physically interfere with the process of SG formation. To investigate the molecular mechanism of UBQLN2's function, I thus focused on UBQLN2's interaction with the highest ranked heterogenous ribonucleoprotein (hnRNP) from our proteomic analysis, FUS, which also has a well-established link to ALS/FTD (Table 3-1) and is present in inclusions in a large subset of ALS/FTD patients (Mackenzie et al., 2010). Over 40 mutations in FUS have been linked to ALS/FTD cases, including some of the most aggressive, juvenile-onset forms of the disease, in both familial and sporadic patients (Kwiatkowski et al., 2009; Vance et al., 2009). At the cellular level, FUS is an RNA binding protein (RBP) involved in the maintenance of genomic integrity, transcription, pre-mRNA splicing, and microRNA regulation (Ishigaki and Sobue, 2018). It contains two amino terminal intrinsically disordered regions (QGSY-rich and Gly-rich) (Figure 3-2A) that allow it to form biologically functional complexes in the cell such as SGs, but also make it prone to aggregate. ALS-linked mutations in FUS accelerate its recruitment to SGs in the absence of stress and the rate of formation of patient-associated inclusions (Patel et al., 2015). How FUS solubility is maintained in the cell and FUS functions in ALS/FTD pathology is still unclear.

Here, I report a direct role for UBQLN2 in modulating FUS solubility during SG formation. Mechanistically, UBQLN2 increased the fluidity of ALS-linked mutant FUS-RNA complexes leading to an increase in the dispersion of FUS liquid droplets and suppression of FUS-seeded SGs. ALS-linked mutations impaired the function of UBQLN2 in regulating RNP dynamics and SG formation. These results reveal a previously unrecognized role for UBQLN2 in directly modulating the early stage dynamics of liquid-liquid phase separation (LLPS) and SG formation associated with RBP solubility in SGs.

Note: The results presented here are given with minor modifications to fit the thesis format from the published manuscript: Alexander EJ, Niaki AG, Zhang T, Sarkar J, Liu Y, Nirogi RS, Pandey A, Myong S, and Wang J (2018) Ubiquilin 2 Modulates ALS/FTD-linked FUS-RNA Complex Dynamics and Stress Granule Formation. *PNAS* 115(49): E11485-E11494.

RESULTS

UBQLN2 forms a complex with FUS and suppresses its recruitment to SGs

To confirm the interaction between UBQLN2 and FUS detected in our SILAC analysis (Figure 2-1), with help from postdoc Tao Zhang, I performed co-immunoprecipitation experiments with FLAG-tagged UBQLN2 and V5-tagged FUS. FUS immunoprecipitated with FLAG-tagged UBQLN2 but not FLAG-tagged GUS control protein (Figure 3-1A). The introduction of an ALS-linked UBQLN2 mutation, P497H or P506T, significantly decreased the interaction between UBQLN2 and FUS despite similar FUS protein expression level (Figure 3-1A, B).

I then tested if UBQLN2 regulates the recruitment of FUS to SGs. I first developed a system in HeLa cells to monitor SG formation with a FUS-GFP construct which spontaneously forms SGs in a small percentage of cells in the absence of stress. I designed this C-terminally tagged FUS construct with a long linker (13 amino acids) between FUS and GFP to limit GFP interference with the FUS QGSY-rich/Gly-rich intrinsically disordered region (Figure 3-2A). The carboxy-terminally tagged FUS-GFP spontaneously formed SGs in the absence of stress in a small percentage of cells (Figure 3-2B). UBQLN2 was co-transfected with FUS-GFP and its effects on SG formation were monitored. Under heat stress, FUS-GFP positive SGs robustly formed in cells with endogenous UBQLN2 levels (Figure 3-1C, D). However, in cells in which UBQLN2 levels were elevated, there were significantly fewer large SGs present (Figure 3-1C, D), indicating that UBQLN2 interferes with FUS-GFP recruitment to SGs. These data are consistent with the observation that UBQLN2 negatively modulates large SG formation (Chapter 2).

Next, in collaboration with the Myong lab, I asked if UBQLN2 affects the formation of FUS-RNA complexes in an electromobility shift assay (EMSA). Monomer FUS formed a discreet complex with polyurdine-50 (polyU50) RNA (Figure 3-1E). Increasing the FUS protein concentration from 5 nM to 500 nM caused the probe signal to shift to a higher molecular weight position corresponding to FUS multimer. The Myong lab then added native purified UBQLN2 protein (Figure B-4) to test the effect of UBQLN2 on FUS-RNA complex formation. At a 500 nM concentration of FUS, UBQLN2 supershifted the FUS-RNA complex. Since UBQLN2 does not bind the RNA probe (Myong lab, personal communication), this result indicates that UBQLN2 can form a complex with FUS protein in the presence of RNA. Furthermore, increasing concentrations of UBQLN2 protein freed RNA from the FUS-RNA monomer complex and FUS monomer from the FUS-RNA multimer complex (Figure 3-1E), suggesting that by binding to FUS, UBQLN2 can disrupt FUS-RNA complex formation. Because FUS-RNA complex formation mediates the partitioning of FUS into and out of stress granules, these observations also suggest that UBQLN2 could mediate FUS SG formation by modulating FUS-RNA complex formation.

UBQLN2 promotes ALS-linked FUS-RNA complex dynamics

Next, we asked if UBQLN2 could affect the dynamics of individual FUS-RNA complexes. Based on our observation that UBQLN2 freed RNA from the FUS-RNA monomer complex and FUS-RNA monomer from the FUS-RNA multimer complex, we expected that UBQLN2 would decrease the stability of FUS-RNA complexes formed. To test this hypothesis, we employed a single molecule fluorescence resonance energy transfer (smFRET) assay to measure the dynamics of FUS-RNA complex assembly by tracking the RNA conformation. FUS binding to single stranded RNA perturbs RNA conformation in a concentration dependent manner (Figure 3-3B, panel 1-3). The Förster resonance energy between a Cy3 and Cy5 tag on opposite ends of a stretch of single stranded polyuridine (polyU) RNA was measured using a total internal reflection (TIRF) microscope (100 msec resolution). Addition of FUS to the RNA changes the distance between the Cy3 and Cy5 tags reflected by the FRET ratio change and alters the stability of the RNA conformation reflected by the FRET

fluctuation (Sarkar and Myong, 2018). We expected that addition of UBQLN2 protein would increase the static interaction of FUS Gly-rich region mutant R244C with RNA. In the absence of FUS, the RNA probe exhibited a steady low FRET signal due to the Cy3-Cy5 dye separation by polyuridine 50 (pU50) (Figure 3-3B, C panel 1). The addition of FUS R244C at high concentration (1 μM) resulted in a nearly static FUS-RNA interaction (Figure 3-3B, C, panel 3) in greater than 85% of molecules (Figure 3-3D, 0 min). Addition of wild type UBQLN2 to this complex, consistently shifted its dynamics from static to dynamic. Within 5 min of UBQLN2 addition, the proportion of dynamic molecules increased from 18% to 55% (Figure 3-3D, 5 min). After 40 min, nearly 65% of molecules were classified as dynamic (Figure 3-3D, 40 min). However, not only did the number of dynamic molecules increase but also the frequency of the FRET fluctuation among those dynamic molecules. Analysis of 300 time intervals between FRET peaks from over 100 single molecules revealed that between 5 and 20 min the time constant, τ, for the exponential decay fit decreased from approximately 10 sec down to 1 sec (Figure 3-3E). This change in dynamics indicates that UBQLN2 is able to increase the dynamics of FUS mutant interaction with RNA over time decreasing complex stability consistent with our EMSA results showing that UBQLN2 frees RNA bound FUS from soluble FUS complexes.

The FUS-bound RNA FRET ratio reflecting the conformation of the complex was also altered by addition of UBQLN2. At this high FUS concentration (1 μM), two populations of high and intermediate FRET signal molecules exist. The intermediate FRET signal represents RNA bound to soluble multimerized FUS, whereas the high FRET signal represents RNA bound to higher order insoluble FUS. Addition of UBQLN2 to this complex lead to a decrease in the intermediate FRET signal, between 5 and 20 min (Figure 3-3C, panel 3-6) on the same time scale that we saw an increase in FUS dynamics (Figure 3-3B, panel 3-6). The high FRET signal was unaltered by UBQLN2 addition. This shift suggests that UBQLN2 dissociates soluble FUS-RNA complexes. UBQLN2 was unable to alter the insoluble FUS-RNA complex composition. These data are consistent with the conclusion that UBQLN2 alters the dynamics of FUS-RNA complex formation during the early stages of liquid-liquid

phase separation, shifting the equilibrium of FUS into the soluble rather than the granular phase of the cytoplasm.

Furthermore, in contrast to WT UBQLN2, P497H and P506T mutant UBQLN2 failed to restore mutant FUS dynamics, with only 10%, 30% of molecules showing dynamic single molecule FRET signals, respectively (Figure 3-3B panel 7,8, D). This failure to affect FUS-RNA complex assembly dynamics indicates a partial compromise of UBQLN2 function conferred by these ALS-linked mutations.

UBQLN2 suppresses FUS liquid-liquid phase separation

The dynamics of RBP-RNA complex formation directly impact the liquid-liquid phase separation of RBPs into liquid droplets (Sarkar and Myong, 2018). The dynamic interaction of WT FUS with RNA leads to the formation of smaller liquid droplets. In contrast, the static interaction of FUS^{R244C} with RNA leads to the formation of large liquid droplets. Based on the finding that UBQLN2 increased FUS-RNA complex dynamics, we hypothesized that UBQLN2 addition would result in a decrease in FUS residence time in phase separated droplets and thus a decrease in the effective size of those droplets. To study the function of UBQLN2, we performed a FUS liquid droplet assay by mixing FUS^{R244C} protein and partially Cy3-labelled pdU40 RNAs with or without UBQLN2. TEV protease was added to cleave off the MBP solubility tag from FUS to trigger the formation of liquid droplets and fluorescent images were taken at regular time intervals after protease digestion to monitor the size and number of the droplets. Within a period of 20 hrs, FUS^{R244C}-RNA droplets formed and increased in both quantity and size. When UBQLN2 was present, the FUS^{R244C}-RNA droplets formed were smaller in size but more numerous compared to those formed in the absence of UBQLN2 (Figure 3-4A, B quantitated in (Figure 3-4C, D). Notably, the FUS^{R244C}-RNA droplets in the absence of UBQLN2 displayed non-spherical irregular patterns whereas those in the presence of UBQLN2 remained highly spherical over the entire time course. These non-spherical irregular droplets may represent the transition from the reversible liquid-like phase separated state of FUS to a more stable solid state of FUS. Taken together, these results suggest that UBQLN2 is able to prevent this liquid to

solid transition by increasing the FUS-RNA complex formation dynamics that underly FUS phase separation. This activity is consistent with the negative regulatory role that UBQLN2 plays in SG formation in suppressing large stress granule formation by increasing the dynamics of FUS recruitment into and out of SGs.

DISCUSSION

In this chapter, I demonstrate a previously unrecognized role for UBQLN2 in modulating the dynamics of SG formation. In the case of FUS highlighted here, UBQLN2 complexes with FUS, directly acts to promote the dynamics of FUS-RNA complexes and decrease the effective rate of FUS phase separation into liquid droplets thereby suppressing FUS SG formation. Mutations in UBQLN2 impair FUS binding, resulting in loss of UBQLN2's ability to regulate the dynamics of FUS-RNA complexes and SG formation. These results expand understanding of UBQLN2 function and provide a direct link between protein and RNA homeostasis in normal stress responses and the pathogenesis of ALS/FTD.

These findings reveal that UBQLN2 has the capacity to chaperone RBPs independently of its previously established roles in mediating protein clearance. UBQLN2 promotes the dynamics of FUS-RNA complexes with the effect of maintaining FUS solubility. This solubilizing effect results in the suppression FUS liquid droplet growth consistent with the role of UBQLN2 in negatively regulating SG formation and presumably the transition from a fluid to a solid, stable state. This function is reminiscent of the chaperone function of UBQLN2 in maintaining the solubility of transmembrane mitochondrial precursor proteins (Itakura et al., 2016) except that instead of interacting with the hydrophobic transmembrane domain of the mitochondrial precursor proteins, UBQLN2 may interact with the hydrophobic low complexity region of FUS that mediates its oligomerization. UBQLN2's effect on FUS phase separation most resembles the recently described role of the small molecule ATP acting as a biological hydrotrope (Patel et al., 2017). Like the recently described karyopherin Transportin 1/Karyopherin β2 UBQLN2 also phase separates itself, which has been attributed to the

second set of Sti1-like repeats in UBQLN2 (Dao et al., 2018). However, as I have shown (Chapter 2), UBQLN2 itself does not drive SG formation like other proteins with PrD domains, but rather acts as a factor that antagonizes the recruitment of SG components to SGs. These observations represent a potentially unrecognized mode of action for low complexity PrD-like proteins in SG formation. Previously described SG regulation has focused on regulation of levels of individual SG components, posttranslational modifications of SG components, and SG disaggregation through PQC mechanisms (Buchan et al., 2013; Ganassi et al., 2016; Goulet et al., 2008; Jain et al., 2016; Jayabalan et al., 2016; Kedersha et al., 2016; Ohn et al., 2008; Seguin et al., 2014). Our proteomic analysis shows that UBQLN2 associates with many of the PQC factors including Ubiquitin, Hsp70, VCP, and TriC (Table S1), suggesting that UBQLN2 may cooperate with other PQC factors in SG regulation. However, in a mechanism that is not mutually exclusive, our present study has demonstrated a distinct way that UBQLN2 directly influences the dynamics of protein-RNA complexes in the early stages of SG formation (Figure 3-5). Together, these findings expand our understanding of different modes of SG regulation.

The results indicating that ALS/FTD-linked mutations in UBQLN2 (P497H and P506T) dampen UBQLN2's association with FUS and thus impair the ability of UBQLN2 to regulate FUS-RNA interaction dynamics and SG formation, suggest that these processes may underlie the pathogenesis of ALS/FTD. FUS is one of a number of heterogenous ribonucleoproteins (hnRNPs) including EWS, hnRNPA1 and hnRNPA2/B1 associated with ALS/FTD that I isolated in my proteomic screen that contain low complexity flexible regions which impart the ability to phase separate, but also to aggregate. FUS have been reported to increase the propensity of these hnRNPs to collect in SGs, disrupting SG function as an adaptive stress response (Patel et al., 2015). Increased residence of hnRNPs in SGs may be directly linked to formation of abnormal SGs prone to form the pathological inclusions found in ALS/FTD patients. UBQLN2's function to maintain the fluidity of FUS-RNA interactions suggests that UBQLN2 is an intrinsic factor that protects against aberrant SG formation and subsequent disease pathology. I have shown that the relative level of UBQLN2 to SG components directly impacts the

rate of growth of large cytoplasmic SGs. Because ALS-linked mutations in UBQLN2 impair its interaction with hnRNPs or its function in maintaining hnRNP-RNA complex fluidity, the mutations could compromise the intrinsic ability of UBQLN2 to protect against aberrant SG formation and subsequent disease pathology.

This protective effect is consistent with previous reports that increasing the expression of UBQLN2 or its family members protects against the toxicity of a variety of neurodegeneration-related proteins, including amyloid-β, polyQ repeats, and TDP-43 (Adegoke et al., 2017; Hanson et al., 2010; Safren et al., 2015). Collectively, the present study results reveal that UBQLN2 directly regulates the early stages of SG formation and suggest it has a critical cytoprotective role at the junction of protein and RNA homeostasis underlying neurodegenerative diseases.

METHODS

DNA vectors

UBQLN2 wild type, mutants, and fragments along with GUS, and FUS wild type and mutant were cloned into pENTR221 to introduce UBQLN2 into pcDNA3.1-CMV/TO-n3xFLAG-UBQLN2-TetR-IRES-PuroR DEST, GUS into pcDNA3.1-CMV/TO-n3xFLAG and FUS into pcDNA6.2-emGFP and pcDNA3.1_CMV_cV5 via Gateway cloning (ThermoFisher, Waltham, MA). For *E. coli* expression, UBQLN2 was cloned into the *Sap*I cut pET-6xHis-GFP-LIC from Addgene via Gibson assembly.

Cell Culture

HeLa cells were cultured in DMEM with 10% Fetal Bovine Serum (FBS). at 37°C in an atmosphere of 5% CO_2 in standard circular tissue culture dishes. Cells were transfected with lipofectamine 2000 (Thermo-Fisher) in Opti-MEM reduced serum media, halving the manufacturers recommended volumes and following the manufacturer's protocol. Opti-MEM was replaced with DMEM with 10% FBS 5 hrs after transfection.

Antibodies for Western blotting and Immunocytochemistry

Rabbit anti-UBQLN2 (Sigma HPA0006431) was used to specifically detect UBQLN2 via immunofluorescence (Figure B-1). Goat anti-TIA-1 (Santa Cruz, C-20) was used to detect SGs. Mouse anti- DYKDDDDK (Sigma F3165) was used to detect FLAG constructs by Western blot. FUS-V5 was detected by mouse anti-GKPIPNPLLGLDST (Invitrogen R960-25) by Western blot and FUS-GFP by mouse anti-GFP (Invitrogen A11120) by ICC. Mouse anti-β-actin (Santa Cruz, C4) was used as a loading control for Western blots. Secondary antibodies Donkey anti-goat IgG-Alexa fluor 647 nm, Donkey anti-mouse IgG-Alexa flour 488 nm, and Donkey anti-rabbit IgG-Alexa fluor 555 nm (Invitrogen) were used for 3 color immunofluorescence staining. Secondary antibodies Goat/Donkey anti-mouse IgG and anti-rabbit IgG-800CW and 680LT pair were used for two color Odyssey Western blots (Licor).

SDS-PAGE and Immunoblotting

Cell lysates were collected in 1% CHAPSO [3-([3-Cholamidopropyl]dimethylammonio)-2-hydroxy-1-propanesulfonate], 50 mM HEPES pH 7.9, 150 mM NaCl, 2 mM EDTA supplemented with 1x Protease Inhibitor Cocktail (Sigma P8340) and 0.2 mM Na_3VO_4 and sonicated using a Diagenode Bioruptor 5 min (high setting, 30 sec pulse, 5 min) prior to spinning at 20,000 x g at 4°C. In our experience, ubiquilin protein separated well on an 8% isocratic Tris-Gly SDS-PAGE gel with 4% stacking gel at 65V or TGX Criterion 4-20% gradient gel at 85V (Bio-rad). Protein was transferred to 0.2 μm nitrocellulose membrane via Bio-rad Turboblot transfer (25V, 1.3 Amp, 12-15 min), the membrane was blocked with 5% Milk/TBS-T (20 mM Tris pH 7.6 ± 0.1, 150 mM NaCl, 0.1% Tween 20), and then incubated with primary antibody in 5% BSA, TBS-T, 0.03% sodium azide solution at 4°C. Secondary antibodies Donkey anti-Mouse IgG-680LT or 800CW and Donkey anti-Rabbit IgG-680LT or 800CW (Licor Biosciences, Nebraska, USA) at 1:10,000-1:20,000 in milk were used to detect primary antibody. An Odyssey scanner (Licor Biosciences, Nebraska, USA) equipped with 700 nm and 800 nm laser channels was used to image the blot.

Immunofluorescence microscopy

Cells grown on glass coverslips were simultaneously fixed and permeabilized to visualize UBQLN2 in SGs (Figure 2-5., Table S2). Coverslips were washed with PBS prior to blocking with 5% Donkey/Horse serum in 0.25% Triton X-100 for 1 hr at room temperature or overnight at 4°C. Primary antibody was incubated 3 hrs at room temperature or overnight at 4°C and secondary antibody, 2 hrs at room temperature in the dark. DAPI (4',6-diamidino-2-phenylindole) was diluted to 1 μg/mL with secondary antibody to label cell nuclei. Primary and secondary antibodies were diluted in a 3% BSA, 0.25% Triton X-100 solution. Three washes for 5 min each were performed after primary and secondary antibody incubations at room temperature on an orbital shaker. Coverslips were mounted with Prolong Gold mounting media and allowed to cure 24 hrs at room temperature in the dark prior to imaging on a Leica SP8 scanning confocal microscope. All solutions were buffered with Phosphate buffered saline (PBS) (8 mM Na_2HPO_4, and 2 mM KH_2PO_4, 137 mM NaCl, 2.7 mM KCl, pH 7.4 ± 0.1). Live cell images of FUS-GFP were taken on a Nikon fluorescent microscope.

FUS-UBQLN2 Coimmunoprecipitation

A doxycycline-inducible FLAG-UBQLN2 and a FUS-V5 construct were co-transfected into HEK293T cells at a molar ration 1:1. 24 hrs later, cells were harvested in lysis buffer (50 mM Tris-HCl (pH 7.5), 150 mM NaCl, 0.4 mM EDTA, 1% NP-40, 0.05% sodium deoxycholate, and complete protease inhibitor cocktail (Roche 11836153001)) and 200 μL of the cell pellet was sonicated 5 min on high power in 30 second intervals in a Diagenode Bioruptor on ice. Cell debris was pelleted at 20000 x g, 10 min at 4°C and the supernatant was loaded onto anti-Protein A/G magnetic beads pre-equilibrated with anti-FLAG (M2) antibody (Sigma F3165) and incubated overnight at 4°C. The beads were washed five times with lysis buffer and protein eluted via low pH buffer (Pierce IgG Elution Buffer 21208 pH 2.0) neutralized with 1/10th volume 1 M Tris pH 8.0 buffer.

Protein Purification

Native UBQLN2 Purification: UBQLN2 wild type and P497H, P506T mutants were purified from *E. coli* as 6xHis-GFP-TEV-UBQLN2 by NiNTA chromatography. TEV protease cleavage of the fusion protein resulted in two amino acid residues upstream of the initiator methionine residue (Ser-Ile). This product was further purified by collecting and concentrating the flow through passed back over freshly cleaned NiNTA beads. This product was injected into a size exclusion column then spin concentrated in a 50 MWCO centrifugation column (Amicon) before flash freezing aliquots in liquid nitrogen. This optimized purification method is described in detail in Appendix B (Figure B-4).

FUS Purification: GST-FUS and GST-FUS^{R244C} were purified for the EMSA assay as described in (Zhang et al., 2018b). FUS^{R244C} was purified for the smFRET assay as a 6x-His-FUS monomer from *E. coli* [BL21DE3] also described in (Zhang et al., 2018b). Briefly, the His tagged protein was purified by NiNTA affinity chromatography (HisTrap) followed by size exclusion chromatography and stored in buffer containing 1 M KCl and 1 M urea to prevent aggregation. MBP-TEV-FUS was purified for the liquid droplet assay as described in (Burke et al., 2015).

Electromobility Shift Assay (EMSA)

Sample was prepared by mixing 0.5-1 nM of Cy3-Cy5 dual-labelled RNA probe (used in smFRET experiments) with varying concentrations of proteins in a binding buffer containing 50 mM Tris-HCl pH 7.5, 150 mM KCl, 2 mM $MgCl_2$, 100 mM β-mercaptoethanol, and 0.1 mg/mL BSA. Samples were mixed with loading dye and run on a 6% DNA retardation polyacrylamide gel (Invitrogen). RNA mobility was visualized using a Typhoon scanner in fluorescent mode.

Single Molecule Fluorescence Resonance Energy Transfer (smFRET) via TIRF microscopy

A biotinylated RNA probe was immobilized on the surface of a PEG-coated quartz slide pretreated with 0.05 mg/mL Neutravidin. Purified FUS and UBQLN2 were added to the slide in imaging buffer (100 mM KCl, 20 mM Tris-HCl pH 7.5 with an oxygen scavenging system containing 1 mg/mL glucose oxidase, 0.5% glucose, and 88 U/mL catalase in 10 mM Trolox). Single molecule FRET signals were then measured using a home-built Total Internal Reflection Fluorescent (TIRF) microscope equipped with an EMCC Andor camera. Cy3 (donor) and Cy5 (acceptor) dyes were used as FRET pairs excited

by a solid state 532 nm laser (Coherent CUBE, 75mW). Quantification of individual fluorescent spots in multiple imaging fields was then performed using custom IDL and MATLAB codes. Codes can be found at the Center for Physics of Living Cells website (https://cplc.illinois.edu/software).

Liquid Droplet Assay

1 μM MBP-FUS, 1 μM unlabeled 40 nucleotide long polyU RNA (U40), 4 μM UBQLN2, and 10 nM Cy3-labeled U40 were prepared in 50mM Tris-HCl pH 7.4, 100mM NaCl, 1mM EDTA, 1mM DTT buffer. TEV protease was added to cleave the MBP tag off of FUS. To visualize droplets, this mixture was added to the surface of an 8-well chambered coverglass (Nunc Lab-Tek) and imaged using a Nikon Ti Eclipse microscope equipped with a 100x oil immersive objective, 555 nM laser, a Cy3 emission filter and an EMCCD Andor camera in a 133 μm^2 field. Myong lab used intensity thresholding in order to mask and quantify the number and shape of the droplets by ImageJ.

RNA probe preparation

The following pairs of RNA oligos were annealed to prepare the RNA probes for the EMSA and smFRET experiments (1 and 2), and the liquid droplet experiments (1 and 3):

1) 18-mer: 5'-biotin-UGG CGA CGG CAG CGA GGC-3'-amino modified;

2) U50-18mer: 5'-amino modified-polyU(50)-GCC UCG CUG CCG UCG CCA-3';

3) U40: 5'-polyU(40)- UGG CGA CGG CAG CGA GGC-3'-amino modified.

Amino modified RNA strands were end-labeled with Cy5 or Cy3 via NHS-ester-amine chemistry.

Statistical analysis

All statistical analysis for cell data was performed in GraphPad Prism. Column data was analyzed by a standard one-way ANOVA with Dunnett's method of correction for multiple paired comparisons. Grouped data was analyzed via a standard two-way ANOVA with Sidak's correction method for multiple comparisons.

Acknowledgements

Many thanks to Jaya Sarkar and Amirhossein Ghanbari Niaki from Sua Myong's lab with whom I collaborated to perform the single molecule fluorescence resonance energy transfer (smFRET), electromobility shift assay (EMSA), and droplet assays using our purified UBQLN2 protein. Dr. Tao Zhang helped with the FUS-UBQLN2 IP and Yang Liu aided in quantitation of UBQLN2 suppression of FUS SG formation while I was preparing the manuscript.

Table 3-1 Table of hnRNPs in the SG proteome that immunoprecipitate with UBQLN2

Gene symbol	Accession	Peptides	Intensity	SILAC Ratio
FUS	**NP_001164408.1**	**3**	**21,808,551**	**1.6**
HNRNPA2B1	NP_002128.1	22	21,405,728	1.9
HNRNPA3	NP_919223.1	6	20,659,907	1.8
KHDRBS1	NP_006550.1	3	19,275,127	1.7
HNRNPK	NP_112552.1	3	15,379,763	1.8
HNRNPE2	NP_001122386.1	8	13,417,898	1.9
IGF2BP1	NP_006537.3	5	11,938,355	1.7
EWSR1	NP_001156758.1	2	5,309,022	*
FAM120A	NP_055427.2	1	914,165	1.7

Protein and peptide false discovery rates were set at 1% for the Proteome Discoverer database search. Identified proteins were cross-referenced with the SG proteome using the vlookup function in Excel and sorted by intensity. This list contains 9 hnRNPs. FUS had the highest total precursor ion intensity. **Peptides** are the peptide spectrum matched hits. **Intensity** is the total integrated precursor ion intensity. **SILAC Ratio** is the average HEAVY (UBQLN2)/LIGHT (Control) peptide ratio. * indicates a corresponding light peptide was not automatically identified by the search software.

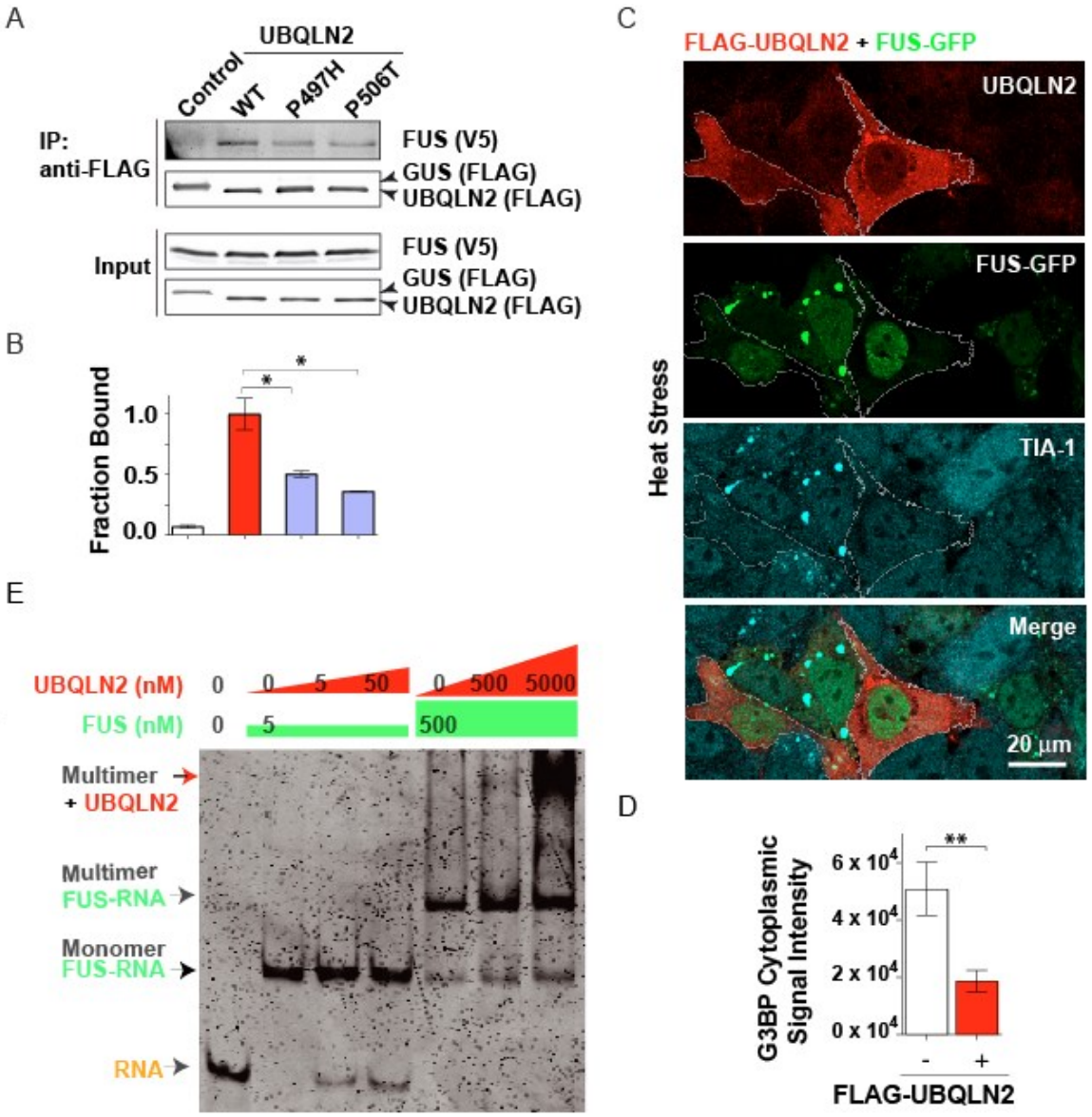

Figure 3-1 UBQLN2 forms a complex with FUS and suppresses its SG formation

(A) FUS-V5 immunoprecipitates with FLAG-UBQLN2 in HEK293T cells. UBQLN2 ALS-linked missense mutations P497H and P506T partially disrupt UBQLN2's interaction with FUS. The FLAG-tagged plant reporter protein β-Glucuronidase (GUS) was used as a control.

(B) Quantitation of WB shown in (A). The experiment was repeated twice and the average results are presented here. Error bars represent SD. **p<0.01 by Dunnett's multiple comparison test.

(C) IF images of fixed HeLa cells cotransfected with FLAG-UBQLN2 and FUS-GFP. Cells overexpressing FLAG-UBQLN2 are outlined. UBQLN2 overexpression suppresses FUS-GFP SG formation in response to heat stress. TIA-1 marks SGs.

(D) Quantitation of G3BP cytoplasmic signal in 13 pairs of cells expressing just FUS-GFP or FUS-GFP in the presence of FLAG-UBQLN2. **$p<0.01$ by a two-tailed student's t-test. FLAG-UBQLN2 overexpression suppresses FUS-GFP SG formation (marked by TIA-1) in response to heat stress (30 min, 43.7°C).

(E) Coomassie blue stained native PAGE gel of FUS-RNA and FUS-RNA-UBQLN2 electromobility shift. The RNA probe is Cy3 labelled polyU40. 5 nM FUS results in monomer FUS-RNA complex. whereas 500 nM FUS results in a shifted mobility multimer FUS-RNA complex. Addition of UBQLN2 to this preformed complex supershifts the multimer, but not monomer FUS-RNA complex.

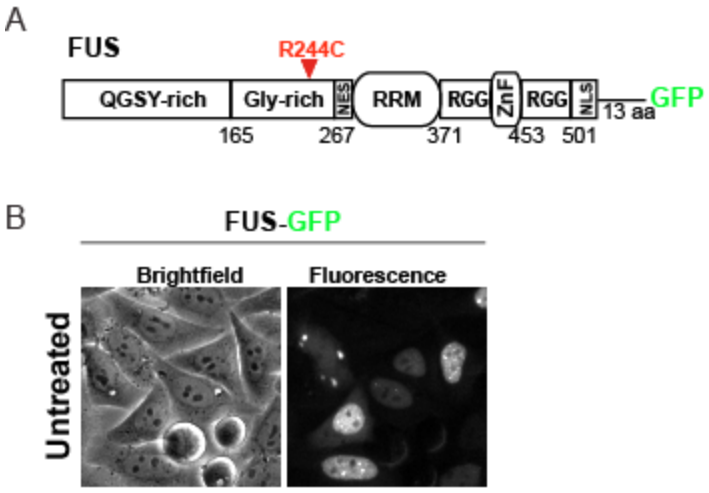

Figure 3-2 C-terminal FUS-GFP Construct forms SGs spontaneously

(A) FUS domain structure showing the position of the GFP tag placed on the C-terminus separated by a 13 amino acid (aa) linker to avoid interfering with the oligomerization of low complexity QGSY-rich and Gly-rich regions that drive SG formation.

(B) Live brightfield and widefield fluorescence images of HeLa cells transfected with FUS-GFP 24 hrs post-transfection. FUS-GFP spontaneously forms SGs in a small percentage of cells as expected.

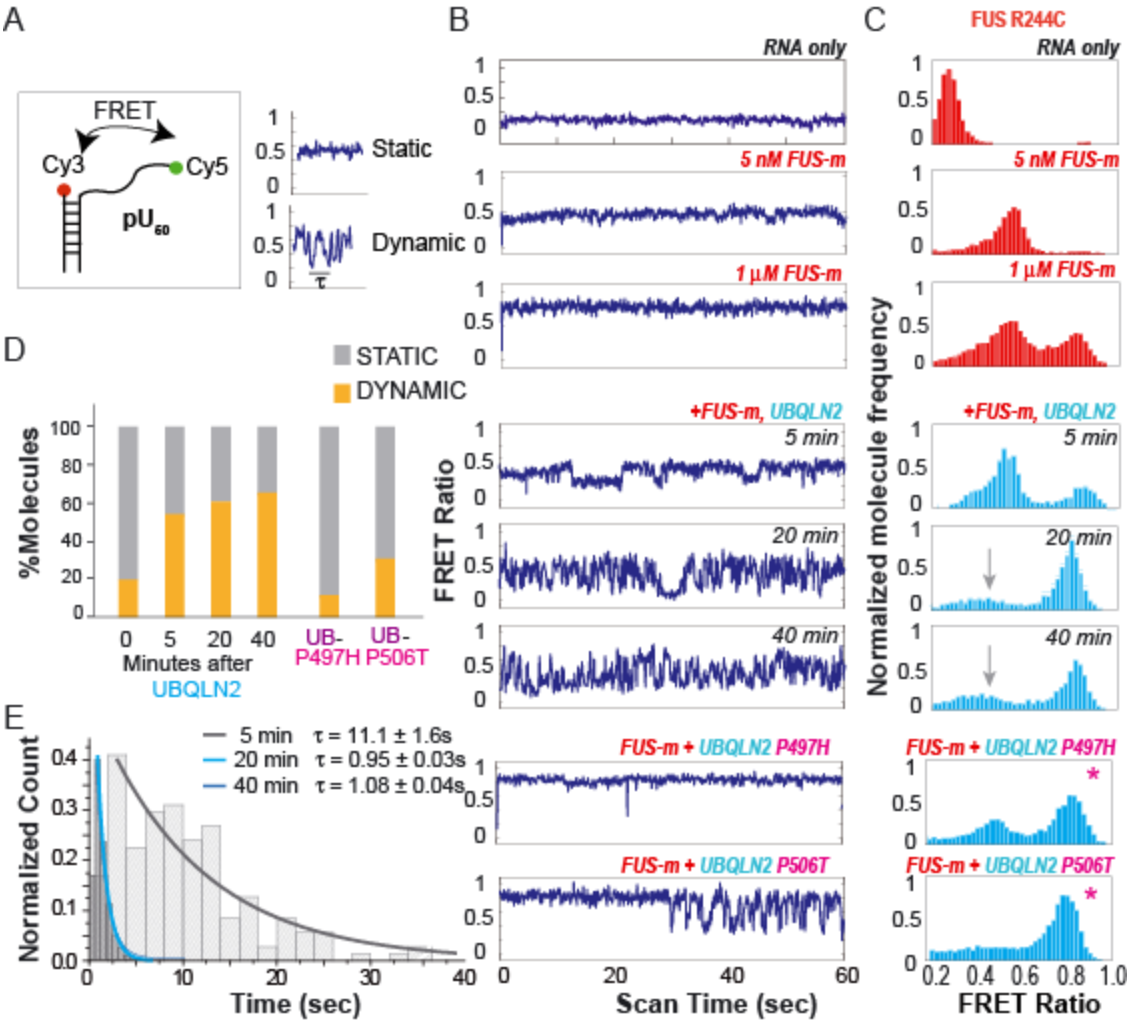

Figure 3-3 UBQLN2 increases FUS^{R244C} RNA Interaction Dynamics

(A) Polyuridine 50 RNA probe design and sample static and dynamic single molecule (sm) traces showing the dwell time constant τ.

(B) Representative traces showing the fluctuation of the FRET ratio for single molecules over time (Panel 1-8). FUS-m is the FUS mutant FUS^{R244C}.

(C) Histograms of single molecule FRET ratios for FUS-m mixed with pdU50 RNA (red) (Panel 1-3), FUS-m mixed with PdU50 in the presence of wild type UBQLN2 (Panel 4-6), and mutant UBQLN2 P497H and P506T (cyan) (Panel 7, 8). The grey arrow points to the FRET peak broadened and flattened by UBQLN2 addition.

(D) Percentage of single molecules with dynamic vs. static smFRET ratios. More than 1000 traces were surveyed for this analysis. UBQLN2 mutant traces were collected between 20 and 40 min. Wild type UBQLN2 addition alters FUS^{R244C}-RNA complex dynamics, while mutant UBQLN2 does to a lesser extent.

(E) Dwell time (τ) of FRET fluctuation taken at 5, 20 and 40 min after addition of wild type UBQLN2 to FUS^{R244C}. 5 to 20 min after UBQLN2 addition the FRET fluctuation rate dramatically increases for single molecules that are dynamic.

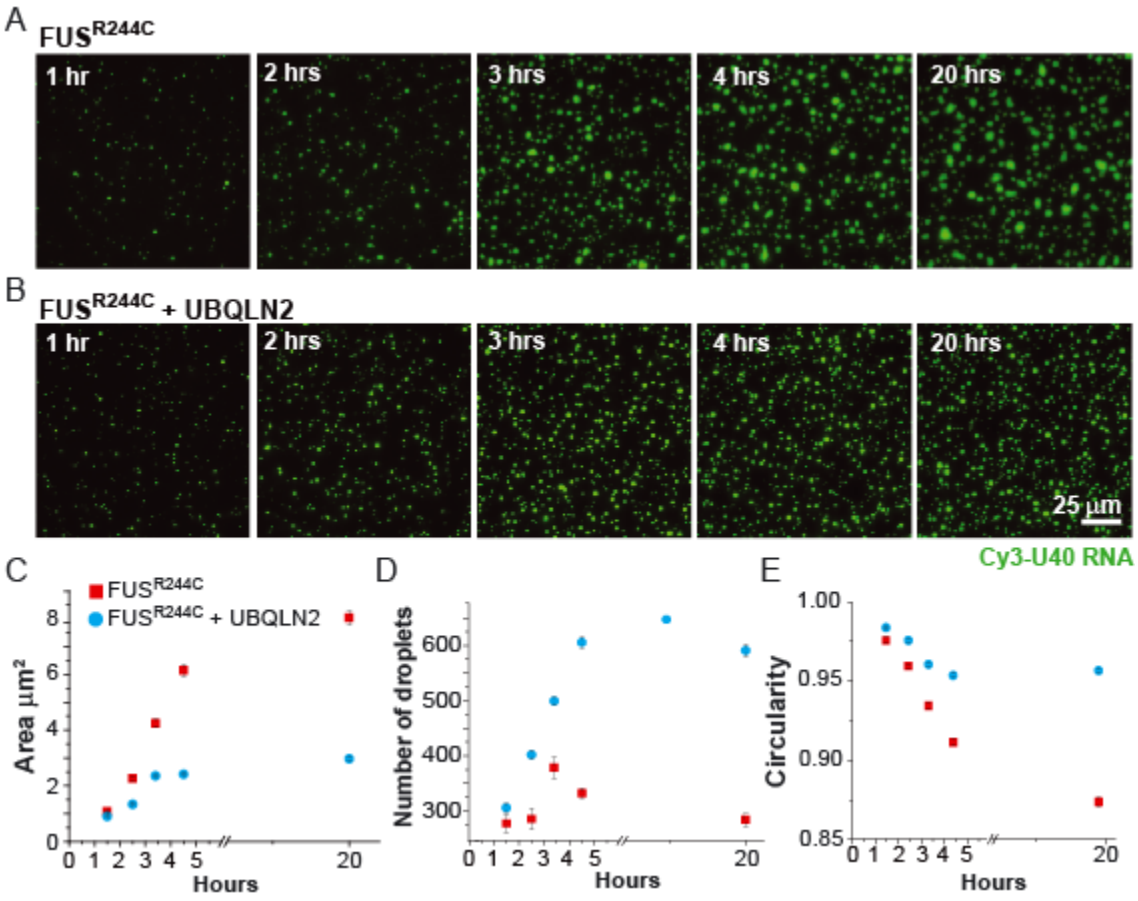

Figure 3-4 UBQLN2 suppresses mutant FUS recruitment into phase separated droplets.

(A) Phase separated droplets of FUS^{R244C} mutants formed over 20 hrs.

(B) Droplets of FUS^{R244C} with UBQLN2 formed over 20 hrs.

(C) Area of droplets taken over 20 hrs. Red and light blue indicate FUS^{R244C} without and with UBQLN2 added respectively. UBQLN2 addition leads to an increase in liquid droplet area.

(D) Number of droplets per imaging area. UBQLN2 addition leads to a decrease in droplet number.

(E) Circularity of droplets over 20 hrs. UBQLN2 addition leads to an increase in droplet circularity.

(F) More than 400 droplets in 3-4 fields of view were used for this analysis. All error bars shown are SEM. The experiment was repeated twice.

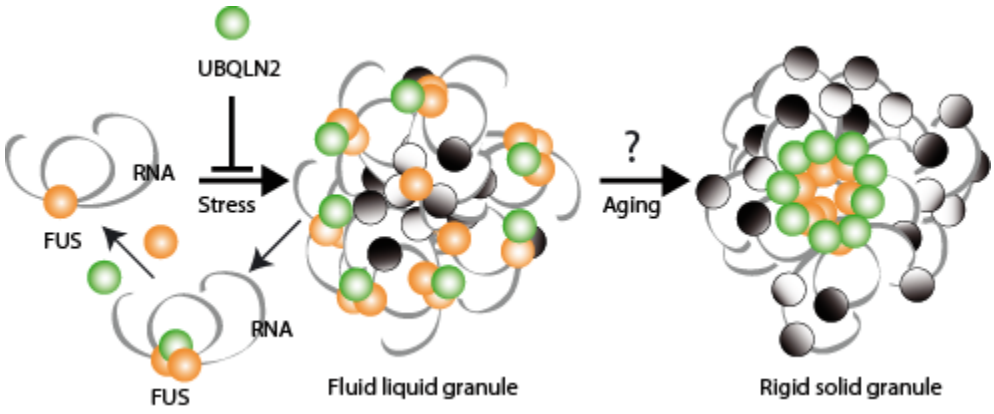

Figure 3-5 Model of UBQLN2 function in SG formation

Illustration of UBQLN2's negative regulatory role in the early stages of SG formation. Orange spheres represent hnRNPs including FUS that can be recruited to SGs. Black and white spheres represent other SG components as shown in Fig. 1E. Grey ribbons are RNA. The fluid liquid granule and rigid solid granule forms of SG assemblies represent different levels of complex fluidity that may exist within a single SG. I show UBQLN2 in both the liquid and solid forms, because both WT and ALS-linked mutant UBQLN2 collect in patient inclusions, for which solid forms may serve as precursors. Our in vitro and cell data show that UBQLN2 may promote exchange of FUS-RNA complex out of SGs to maintain FUS-RNA solubility.

Chapter 4 Conclusions & Future Directions

In this study, I have shown a cytoprotective role of the ubiquilin 2 (UBQLN2) protein in regulating the cell's adaptation to stress at stress granules (SGs). From a proteomic screen for UBQLN2 interactors I identified an enrichment of SG components. Staining of fixed cells using an unconventional staining technique revealed that UBQLN2 is universally recruited to SGs and the Sti1-like linker region of UBQLN2 is sufficient for this recruitment. This recruitment however was transient, and mediated by UBQLN2's association with soluble hnRNP-RNA complexes. Effectively, UBQLN2 limited the growth of SGs in the cytoplasm by increasing the dynamics of hnRNP-RNA interactions. I focused on FUS as an ALS-linked hnRNP known to localize to SGs, but I expect that this regulatory function will broadly apply to other RNA binding proteins (RBPs) that I isolated in my proteomic study that rely on low complexity intrinsically disordered regions to phase separate into SGs. This mode of regulating SG assembly at the level of liquid-liquid phase separation has not previously been described. Further investigation into UBQLN2's mechanism of action in SG formation might be addressed by answering the following questions:

- Does UBQLN2 function with other PQC components in SG assembly?
- Does UBQLN2 mediate phase separation of other membraneless compartments in the cell?
- Is UBQLN's function in SG formation applicable to motor and/or hippocampal neurons?

Other potential partners and functions of UBQLN2 in SG formation?

The mechanism by which UBQLN2 regulates hnRNP incorporation into SGs is distinct among PQC factors described, but does not preclude its cooperation with other known PQC factors in SG homeostasis. The two major protein degradation systems in the cell: the proteasome and autophagosome/lysosome machinery both reportedly disassemble SG components (Buchan et al., 2013; Ganassi et al., 2016). Both the proteasome inhibitor MG132 and ubiquilin 2 depletion lead to a build-up of polyubiquitinated proteins in the cells, but MG132 alone is sufficient to induce SG formation (Mazroui et al., 2007), whereas UBQLN2 only sensitizes cells to stress induced granule

formation. Inhibition of autophagy both inhibits SG assembly and disassembly, although one report estimated that only 30% of SGs are degraded by autophagy (Ganassi et al., 2016), indicating that proteasomal degradation may be the dominant means of SG protein degradation.

SGs are dynamic particles whose rapid dissolution following stress ensures that the cell can resume normal homeostasis. Protein disaggregases play an important role in this process. The Hsp70 HSPA1A with the small heat shock protein HSPB8 and nucleotide exchange cofactor BAG3 is able to extract prematurely terminated transcripts (termed defective ribosomal products or DRiPs) from SGs (Ganassi et al., 2016) to sequester them away from SGs. However, Hsp70 only colocalizes with abnormal SGs anchored by HSPB8 once DRiPs have accumulated or SGs have simply morphed into aggresomes. UBQLN2's exclusion from perinuclear aggregates and universal recruitment to large cytoplasmic aggregates suggests that UBQLN2 and Hsp70 may be present in separate SG related compartments at least upon the initial onset of an acute stress. VCP with its cofactors Ufd1 and Npl4 reportedly functions in SG disassembly (Buchan et al., 2013). However, inhibiting or knocking down VCP inhibits SG assembly (Seguin et al., 2014) counter to UBQLN2 depletion enhancing SG assembly. The deubiquitinating enzyme USP10 reportedly competes with caprin 1 to inhibit G3BP incorporation into SGs (Kedersha et al., 2016). This negative regulatory role is consistent with ubiquilin 2's role, but UBQLN2 in contrast to USP10 is recruited to SGs and binds hnRNPs. I did find evidence that UBQLN2's close homolog UBQLN1 may associate with G3BP (Table A-2), but I did not investigate this further. Jain et. al. also suggested that the actin/tubulin TriC complex may negatively regulate SG formation (Jain et al., 2016), but this functional role is yet to be investigated. Both ubiquitin and the E3 ubiquitin ligases Roquin or MNAB (membrane-associated nucleic acid binding protein) (Athanasopoulos et al., 2010) and TRAF2 (Kim et al., 2005), and the unconjugated autophagy marker LC3B (Seguin et al., 2014) have also been seen at SGs, but their role is as yet uncharacterized (Athanasopoulos et al., 2010; Kim et al., 2005; Seguin et al., 2014). Notably UBQLN2 precipitated all of these factors except the G3BP complex. I decidedly focused here on the function of UBQLN2

alone, but this study does not preclude that UBQLN2 could work in concert with any of these PQC factors.

In all other contexts in the cell in which UBQLN2 has been identified, ubiquitin and/or ubiquitin receptors containing UIM domains are important to its function. The role for UBQLN2 in modulating hnRNP fluidity might thus also be explored in the context Ubl and Uba domain function. It will be important to determine if the Ubl and Uba domains alone can localize to SGs. The Ubl alone is highly stable. The Uba domain is rarely visible by Western blot. Tagging the Uba domain with a larger tag or its own Ubl domain with a short linker might actively stabilize it. It will also be interesting to see if the linker from UBQLN1 and UBQLN4 which lacks the unique PXX repeats in UBQLN2 is also able to localize to SGs. I saw that UBQLN1 and 4 are able to localize to SGs, but not under all of the same conditions as UBQLN2. UBQLN1 and 4 depletion, unlike UBQLN2 also strongly induced eIF2α phosphorylation, a marker for stalled translation initiation complexes indicating that they may have a distinct function in SG formation. Recently it was shown that the second set of mammalian specific Sti1-like repeats in UBQLN2, which contain the predicted PrD are sufficient for UBQLN2's own phase separation required for its SG recruitment. The PXX repeat in UBQLN2 was not essential for this oligomerization, but ALS/FTD-linked proline missense mutations did promote aggregation of UBQLN2 in cells and in model organisms in response to stress (Sharkey et al., 2018) suggesting that the PXX repeats play a role in tuning UBQLN2's solubility within SGs. *In vitro* droplet aging experiments could be performed to assess whether prolonged residence of UBQLN2 in liquid droplets leads to its aggregation as previously observed for hnRNPA1 and A2/B1 mutants (Kim et al., 2013). FRAP measurements of fluorescently labeled UBQLN2 and/or hnRNP could be performed in cells to assess UBQLN2's mobility.

The fact that both mono- and polyubiquitin chains dispersed UBQLN2 liquid droplets in trans suggests that ubiquitin-binding may play an important role in UBQLN2 dissociation from SGs that I observed in our heat stress time course analysis. Expression of a ubiquitin-binding mutant could be used to test this hypothesis coupled with ubiquitin staining during the timecourse. It would also be informative to

test if the large cytoplasmic SGs with which UBQLN2 stably associates differ in their ubiquitin content because SGs that misincorporate misfolded ubiquitinated proteins may be inherently more prone to contain protein aggregates. These experiments would address whether UBQLN2's association with ubiquitin in SGs is important to its regulatory function or stable integration into SGs.

ILVBL: a promising UBQLN2 interactor at SGs

Other, unexplored UBQLN2 interactors may also play a role in UBQLN2's function at SGs. Among the strong interactors that I validated from our SILAC nLC-MS/MS analysis, the protein ILVBL showed a clear localization to SGs (Figure 4-1 B, C, D). ILVBL is a single-pass transmembrane protein of unknown function, most similar to the bacterial acetolactate synthase-like gene. ILVBL contains 3 predicted TPP binding domains preceded by a signal peptide (Figure 4-1A). Interestingly, acetolactate synthase is a thiamine pyrophosphate (TPP) dependent enzyme that catalyzes the first step in branched chain amino-acid synthesis. These enzymes have been characterized as potential evolutionary precursors of the E1/E2 ubiquitin activating and conjugating enzymes because they also use activation of their substrates by formation of a thioester bond (Hochstrasser, 2009). Whether this association is relevant to ILVBL's strong interaction with UBQLN2 remains to be determined.

ILVBL immunoprecipitated with UBQLN1 and 2 equally well (Figure 4-1C) but appeared to require the UBQLN Ubl domain for its interaction with UBQLN1. Unlike UBQLN2, ILVBL SG staining was not sensitive to the fixation and permeabilization method used similar to core SG components TIA-1 and G3BP, and was visible with heat and sodium arsenite stress in HeLa and U2OS cells (Figure 4-1D, E). This preliminary data suggests that ILVBL and UBQLN2 could function together at SGs.

UBQLN2 function in the LLPS of other membraneless compartments?

Liquid-liquid phase separation has recently been recognized as a critical step in the formation of membraneless organelles in the cell. This work focuses on the association and regulatory function of UBQLN2 in SG formation. However, other phase separated compartments in the cell such as nucleoli, Cajal bodies, gems, paraspeckles, and promyelocytic leukemia (PML) bodies in the nucleus, and processing bodies (P-bodies) in the cytoplasm also contain phase separated RBPs bound to RNA

(Brangwynne et al., 2011). Our preliminary data shows at least one instance in which UBQLN2 localizes to another phase separated compartment, the nucleolus (Figure 4-2A, B). In response to prolonged puromycin treatment UBQLN2 concentrated in large nuclear granules that colocalized with the nucleolar marker fibrillarin. I also saw the concentration of UBQLN2 in the nucleolus, another phase separated nuclear compartment (Brangwynne et al., 2011), following prolonged, low dose puromycin treatment. Puromycin, an aminoglycoside antibiotic leads to the accumulation of prematurely terminated translation products. Seguin *et. al.* also saw a similar concentration of puromycin-labelled prematurely terminated transcript in these large circular nuclear structures. The 60S ribosomal subunit Rpl19 in large round nuclear structures also concentrated here in Atg5$^{-/-}$ MEFs. Both are components of DRiPs (Defective Ribosomal Products). This effect might be linked to a nuclear to cytoplasmic trafficking defect (Mahboubi and Stochaj, 2014) because both compartments contain ribosomal components, although the functional consequences of this effect are as yet unknown. It will be interesting to investigate if UBQLN2's effect on the LLPS of SG components can be generalized to other compartments in the cell.

UBQLN2's effect on SG formation in neurons?

While the major part of this study focused on the cell biology of UBQLN2 function in SG formation, the partial loss of function of the ALS/FTD linked mutants suggests that the UBQLN2 mutants might function in a dominant negative manner in SGs in neurons by interacting with hnRNPs but failing to efficiently modulate complex formation. To assess the biological relevance of UBQLN2's action in SG formation, experiments might be done both in induced pluripotent stem cells that have been differentiated into motor neurons and in a worm model of ALS pathology. Unfortunately, I was unable to obtain patient cells and/or use CRISPR to alter the gene sequence in the time scale of this study. However, study of UBQLN2 mutants expressed at endogenous levels might help to better dissect the mechanism of the UBQLN2 mutant pathology.

A

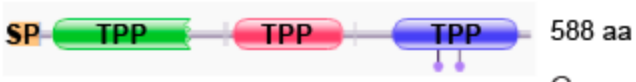

B

Gene symbol	SILAC Ratio	Peptides	Intensity
UBQLN2	33.3	73	159,943,535
UBQLN1	*	59	1,331,669,710
ILVBL	*51.6*	*23*	*61,191,206*

Gene symbol	SILAC Ratio	Peptides	Intensity
UBQLN1	34.5	171	14,721,415,075
UBQLN2	33.4	49	2,658,591,558
ILVBL	*42.3*	*58*	*398,193,490*

C

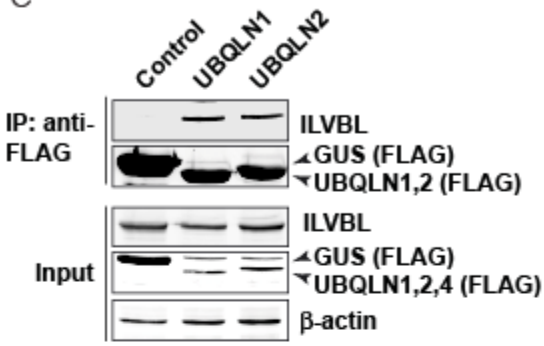

D

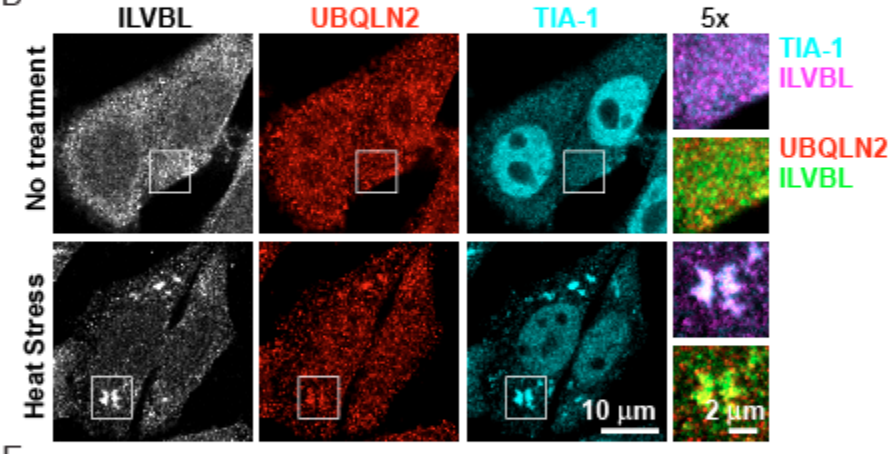

E

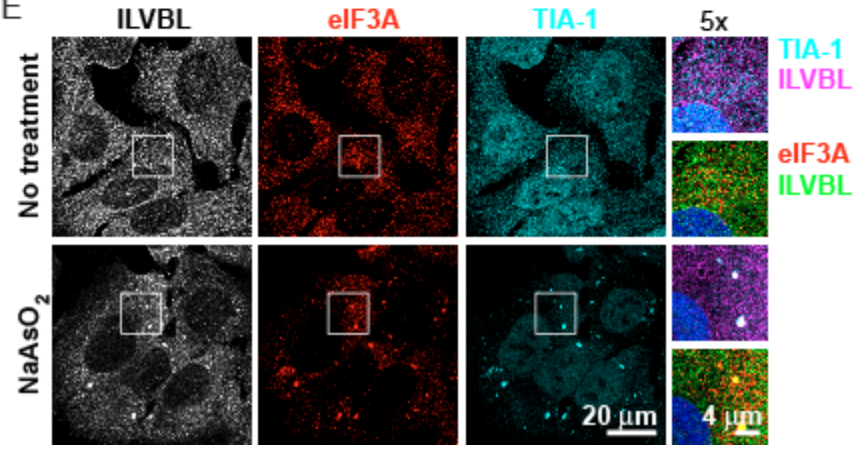

Figure 4-1 ILVBL is a strong interactor for UBQLN2 that localizes to SGs

(A) Pfam generated domain map of ILVBL drawn to scale. Human ILVBL is a 632 amino acid protein. SP=signal peptide. TPP=thiamine pyrophosphate binding domain. Blue dots represent sites of Mg ion binding. ILVBL was recently renamed 2-hydroxyacyl-CoA lyase 2 (HACL2) for its function in a novel fatty acid oxidation pathway in the ER.

(B) SILAC nLC-MS/MS data for ILBVL bound to UBQLN2 relative to UBQLN1 (top box) and UBQLN1 relative to UBQLN2

(C) Western blot validation of endogenous ILVBL immunoprecipitation (IP) with FLAG-UBQLN1 and FLAG-UBQLN2. FLAG-β-glucuronidase was used as a control. Β-actin was used as a loading control.

(D) Confocal immunofluorescence (IF) images of HeLa cells under normal conditions or exposed to 45 min heat stress (43.7°C). ILVBL colocalization with UBQLN2 and SG marker TIA-1 in response to heat stress is clearly visible. Cells were simultaneously fixed and permeabilized as described in Chapter 2. Antibodies used were mouse anti-ILVBL (Sigma, A262) 1:1000, rabbit anti-UBQLN2 (Sigma, HPA006431) 1:250, and goat anti-TIA-1 (Santa Cruz, C-20) 1:50.

(E) IF images of U2OS cells under normal and sodium arsenite stress (1 hr 0.5 mM $NaAsO_2$). Rabbit anti-eIF3A (CST, D51F4) is shown. ILVBL clearly colocalizes with SGs costained by TIA-1 and eIF3A.

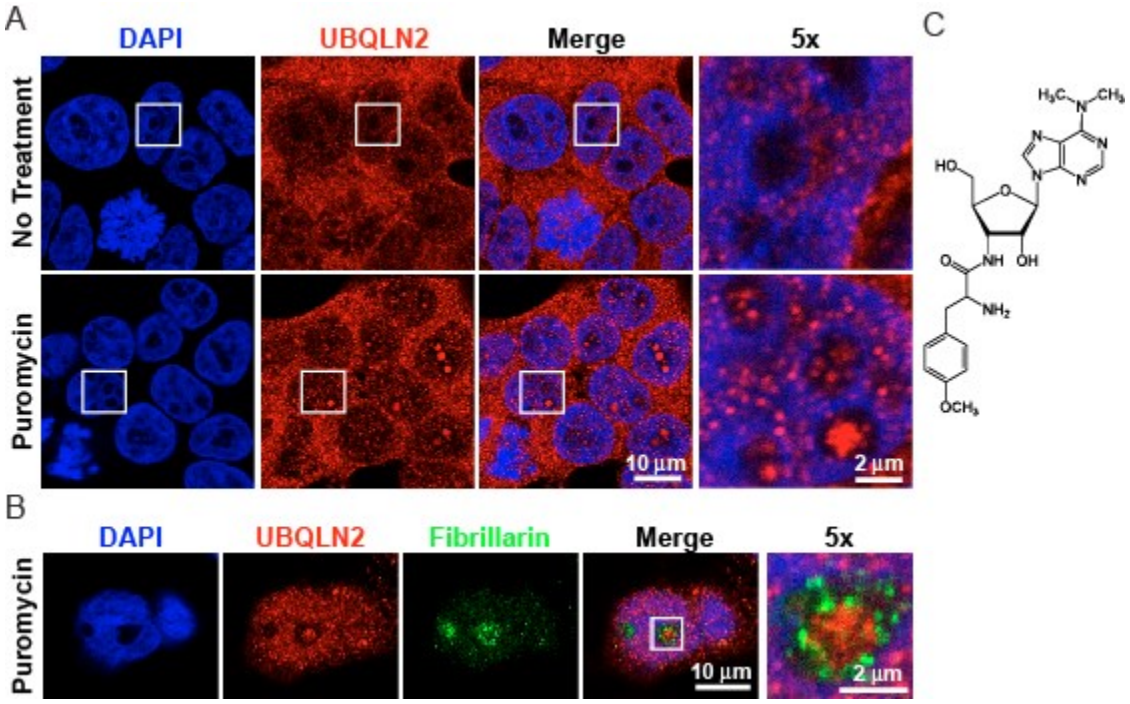

Figure 4-2 UBQLN2 localizes to nucleoli with prolonged puromycin treatment

(A) Immunofluorescence (IF) images of UBQLN2 localization relative to nuclei stained with DAPI before and after puromycin treatment in HEK293T cells. Cells were plated directly on glass coverslips and fixative was applied directly to retain cell structure. Rabbit anti-UBQLN2 (Sigma, HPA006431) marks the endogenous protein.

(B) IF image of HEK293T cells expressing PuroR treated with 3 µg/mL puromycin for more than 72 hr and stained with mouse anti-fibrillarin (Abcam, ab4566), a nucleolar marker.

(C) Chemical structure of puromycin, an aminonucleoside antibiotic from *Streptomyces alboniger* that results in premature chain termination on translating ribosomes. The resulting protein is puromycylated. This structure mimics aminoacyl-tRNA.

Appendix A: Building a UBQLN interactome via quantitative proteomic analysis

INTRODUCTION

ubiquilin 2 (UBQLN2) is one of 4 conserved UBQLNs in mammals. To identify interactors for the UBQLN proteins UBQLN1, 2 and 4, I optimized a FLAG-UBQLN immunoprecipitation protocol and analyzed the interactors by nano-liquid chromatography tandem mass spectrometry (nLC-MS/MS). This work was performed in collaboration with Akhilesh Pandey's lab. From this analysis I identified a number of common and unique interactors for the UBQLNs (Figure A-2B). Analysis of these interactors with respect to their interaction with individual UBQLN homologs was in part confounded by the strong interaction of UBQLN1, 2, and 4 with one another. However, several unique interactors were identified for UBQLN2. For example, I immunoprecipitated the Hsp70 HSPA1A with UBQLN1, 2, and 4, but only detected it by FLAG IP of UBQLN2 by Western blot. This observation is consistent with reports that UBQLNs homo- and heterodimerize. I was surprised to find that UBQLN2, but not UBQLN1 or 4 immunoprecipitated SG components, especially hnRNPs.

Interestingly, UBQLN2 itself has never been identified as a component of SGs in any of the SG proteome studies. The first reason for this absence may be related to the amino acid sequence and structure of UBQLN2. UBQLN2 contains no cysteines and its lysines are all clustered in its amino-terminal Ubl domain and may be buried in the interface between Ubl and Uba domain or Ubl and UIM domain of an interacting partner. iTRAQ tagging requires the presence of cysteine residues and both bioID and apex tagging strategies rely on the conjugation of biotin to protein lysine residues. Based on our staining results, I also might predict that UBQLN2 resides in the SG "shell" rather than the "core" unless its clients irreversibly integrate into the SG core.

A

Lysis/IP Buffer	Lysis Buffer Components	IP Dil
IGEPAL	1% IGEPAL, 50 mM Tris-HCl pH 7.4±0.1, 150 mM NaCl, 2mM EDTA	1:3
Triton X100	1% Triton X100, 50 mM Tris-HCl pH 7.4±0.1, 139 mM NaCl, 2mM EDTA, 10% glycerol	1:3
CHAPSO	1% CHAPSO, 50 mM HEPES, pH 7.4±0.1, 150 mM NaCl, 2mM EDTA	1:3
Triton X100 + CHAPSO	1:1 volume/volume mixture of Triton X100 + CHAPSO buffers	1:3
All lysis buffers were supplemented with 2x Protease Inhibitor Cocktail (Sigma P8430) and 0.2 mM Na_2VO_3.		

B

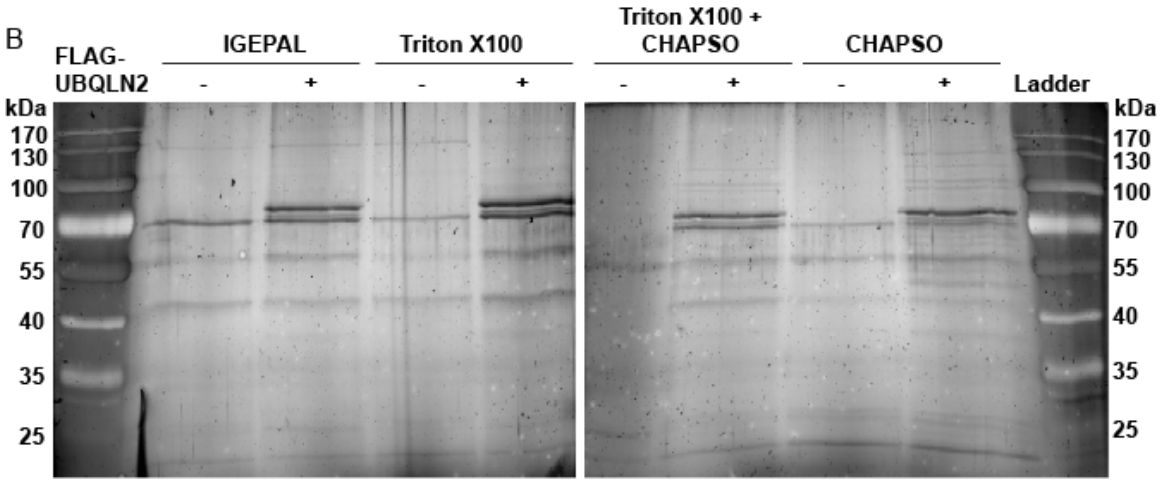

Figure A-1 CHAPSO enhances coimmunoprecipitation of UBQLN2 binding partners

(A) Table of lysis buffer compositions for each of the test immunoprecipitations (IP).

(B) Silver stained SDS-PAGE gel of proteins that coimmunoprecipitate with FLAG-UBQLN2 under different lysis/IP conditions. The zwitterionic detergent CHAPSO enhanced FLAG-UBQLN2 immunoprecipitation of unique interactors.

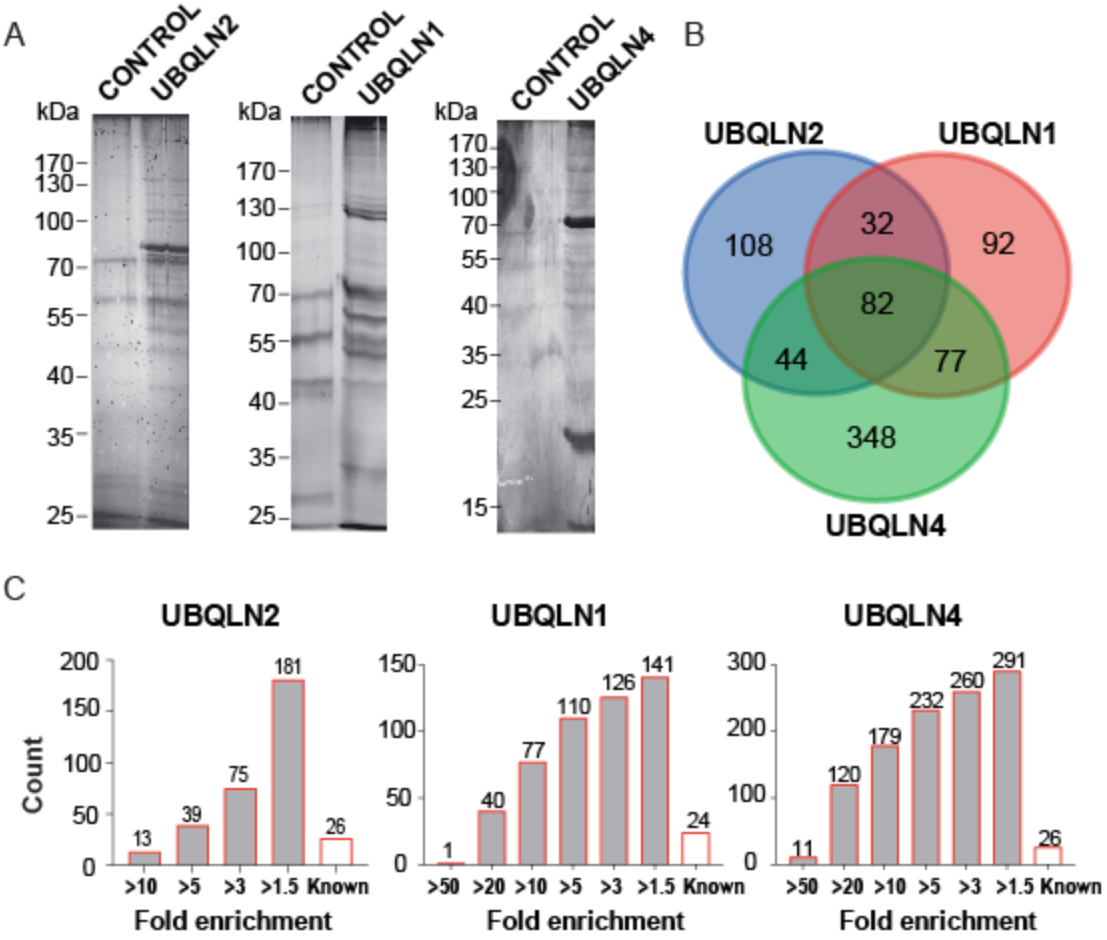

Figure A-2 UBQLN2 binds a set of unique and common UBQLN interactors

(A) Silver stained Tris-Gly SDS-PAGE gels of FLAG-UBQLN immunoprecipitation (IP) eluant.

(B) Venn diagram showing numbers of unique and common UBQLN1, 2 and 4 interactors

(C) Cumulative frequency distribution histograms for UBQLN interactors. Fold enrichment indicates the average SILAC HEAVY/LIGHT peptide ratio.

Table A-1 Table of UBQLN2 associated proteins identified by SILAC nLC-MS/MS

Gene	Accession	Protein name	Peptides	Intensity	Ratio
UBQLN1	NP_444295.1	ubiquilin-1 isoform 2	59	1,331,669,710	*
HSPA1A	NP_005336.3	heat shock 70 kDa protein 1A/1B	120	440,917,747	20.3
HSPA8	NP_006588.1	heat shock cognate 71 kDa protein isoform 1	138	369,392,192	13.8
CEP170	NP_001035864.1	centrosomal protein of 170 kDa isoform gamma	6	327,327,700	*
ALDH3A2	NP_000373.1	fatty aldehyde dehydrogenase isoform 2	40	275,359,967	32.0
TRIM5	NP_149084.2	tripartite motif-containing protein 5 isoform delta	14	190,548,370	*
LAMP1	NP_005552.3	lysosome-associated membrane glycoprotein 1 precursor	6	186,577,980	1.5
UBB	NP_061828.1	polyubiquitin-B precursor	23	168,367,867	20.6
UBQLN2	NP_038472.2	ubiquilin-2	73	159,943,535	33.3
UBQLN4	NP_064516.2	ubiquilin-4	36	159,813,723	*
ATP5B	NP_001677.2	ATP synthase subunit beta, mitochondrial precursor	89	158,634,225	1.8
TUBB4B	NP_006079.1	tubulin beta-4B chain	188	127,885,308	3.0
TUBA1B	NP_006073.2	tubulin alpha-1B chain	81	122,016,582	2.8
CDKN2C	NP_001253.1	cyclin-dependent kinase 4 inhibitor C	2	106,978,486	30.3
PPM1B	NP_002697.1	protein phosphatase 1B isoform 1	94	101,227,769	2.8
HNRNPC	NP_004491.2	heterogeneous nuclear ribonucleoproteins C1/C2 isoform b	12	74,603,245	1.7
ATP5A1	NP_001001937.1	ATP synthase subunit alpha, mitochondrial isoform a precursor	38	66,095,125	3.6
HNRNPH1	NP_005511.1	heterogeneous nuclear ribonucleoprotein H	51	64,510,490	1.5
ILVBL	NP_006835.2	acetolactate synthase-like protein	23	61,191,206	51.6
C10orf68	NP_078964.2	uncharacterized protein C10orf68	2	53,256,061	*
CCT3	NP_001008800.1	T-complex protein 1 subunit gamma isoform c	6	53,172,495	5.3
HSPA9	NP_004125.3	stress-70 protein, mitochondrial precursor	16	52,853,822	3.0
TUBB6	NP_115914.1	tubulin beta-6 chain	61	50,165,913	2.2
CANX	NP_001737.1	calnexin precursor	12	47,415,913	9.6
CCT4	NP_006421.2	T-complex protein 1 subunit delta isoform a	18	47,194,615	4.3
HSPD1	NP_002147.2	60 kDa heat shock protein, mitochondrial	15	46,600,293	3.2
ENO1	NP_001419.1	alpha-enolase isoform 1	38	46,116,335	3.7
NPM1	NP_001032827.1	nucleophosmin isoform 3	11	45,876,610	1.5
PRKDC	NP_001075109.1	DNA-dependent protein kinase catalytic subunit isoform 2	46	41,265,443	1.5

	Gene	Accession	Protein name	Peptides	Intensity	Ratio
	TRAP1	NP_001258978.1	heat shock protein 75 kDa, mitochondrial isoform 2	2	39,861,870	1.6
	HNRNPU	NP_004492.2	heterogeneous nuclear ribonucleoprotein U isoform b	58	38,523,831	2.1
	PHGDH	NP_006614.2	D-3-phosphoglycerate dehydrogenase	19	37,493,615	3.6
	KIF11	NP_004514.2	kinesin-like protein KIF11	69	33,048,167	1.5
	PSMD4	NP_002801.1	26S proteasome non-ATPase regulatory subunit 4	2	32,753,364	5.1
	RTN4	NP_722550.1	reticulon-4 isoform B	6	32,516,827	13.8
	PABPC1	NP_002559.2	polyadenylate-binding protein 1	31	31,570,195	1.5
	XRCC6	NP_001460.1	X-ray repair cross-complementing protein 6	13	28,749,508	2.5
	LSM14A	NP_056393.2	protein LSM14 homolog A isoform b	10	27,758,521	1.7
	VKORC1	NP_996560.1	vitamin K epoxide reductase complex subunit 1 isoform 2 precursor	2	26,859,753	*
	ESYT1	NP_056107.1	extended synaptotagmin-1 isoform 2	3	26,026,293	19.0
	ESYT2	NP_065779.1	extended synaptotagmin-2	17	25,724,668	21.4
	RIOK1	NP_113668.2	serine/threonine-protein kinase RIO1 isoform 1	26	25,666,483	1.6
	PABPC4	NP_001129126.1	polyadenylate-binding protein 4 isoform 3	9	24,977,593	1.6
	DDX3X	NP_001180346.1	ATP-dependent RNA helicase DDX3X isoform 3	65	24,238,144	2.0
	EEF1D	NP_001123528.1	elongation factor 1-delta isoform 4	4	23,443,019	3.2
	VIM	NP_003371.2	vimentin	22	21,906,105	1.6
	FUS	**NP_001164408.1**	**RNA-binding protein FUS isoform 3**	**3**	**21,808,551**	**1.6**
	HNRNPA2B1	NP_002128.1	heterogeneous nuclear ribonucleoproteins A2/B1 isoform A2	22	21,405,728	1.9
	HNRNPA3	NP_919223.1	heterogeneous nuclear ribonucleoprotein A3	6	20,659,907	1.8
	ATP1B3	NP_001670.1	sodium/potassium-transporting ATPase subunit beta-3	3	20,258,257	6.7
	ATAD2	NP_054828.2	ATPase family AAA domain-containing protein 2	1	19,295,978	*
	KHDRBS1	NP_006550.1	KH domain-containing, RNA-binding, signal transduction-associated protein 1 isoform 1	3	19,275,127	1.7
	BSG	NP_940991.1	basigin isoform 2	17	19,042,000	11.6
	RUVBL2	NP_006657.1	ruvB-like 2	19	18,526,328	2.9
	IMPDH2	NP_000875.2	inosine-5'-monophosphate dehydrogenase 2	4	18,378,716	1.5
	HSPA13	NP_008879.3	heat shock 70 kDa protein 13 precursor	3	18,248,766	30.0
	TGM3	NP_003236.3	protein-glutamine gamma-glutamyltransferase E	4	18,235,616	*
	DDX1	NP_004930.1	ATP-dependent RNA helicase DDX1.	10	18,066,203	2.6

	Gene	Accession	Protein name	Peptides	Intensity	Ratio
	DDOST	NP_005207.2	dolichyl-diphosphooligosaccharide--protein glycosyltransferase 48 kDa subunit precursor	13	18,065,095	2.2
	GLUL	NP_002056.2	glutamine synthetase	3	17,989,823	1.6
	ACSL3	NP_004448.2	long-chain-fatty-acid--CoA ligase 3	3	17,963,774	7.5
	H2AFV	NP_619541.1	histone H2A.V isoform 2	2	17,897,943	*
	CCT5	NP_036205.1	T-complex protein 1 subunit epsilon	2	17,212,181	3.1
	KPNB1	NP_002256.2	importin subunit beta-1 isoform 1	7	17,187,882	1.9
	HIST1H2BD	NP_066407.1	histone H2B type 1-D	4	16,972,105	2.0
	NSDHL	NP_001123237.1	sterol-4-alpha-carboxylate 3-dehydrogenase, decarboxylating	7	16,955,511	6.7
	PREX1	NP_065871.2	phosphatidylinositol 3,4,5-trisphosphate-dependent Rac exchanger 1 protein	2	15,630,087	2.2
	SGK196	NP_115613.1	probable inactive protein kinase-like protein SgK196	4	15,502,103	30.2
	HSP90AB1	NP_001258901.1	heat shock protein HSP 90-beta isoform c	12	15,481,520	1.7
	HNRNPK	NP_112552.1	heterogeneous nuclear ribonucleoprotein K isoform b	3	15,379,763	1.8
	VRK3	NP_001020949.1	inactive serine/threonine-protein kinase VRK3 isoform 2	4	15,111,551	1.6
	TUFM	NP_003312.3	elongation factor Tu, mitochondrial precursor	10	15,046,192	2.5
	LETM1	NP_036450.1	LETM1 and EF-hand domain-containing protein 1, mitochondrial precursor	3	14,751,288	10.7
	CCT7	NP_001159756.1	T-complex protein 1 subunit eta isoform c	11	14,473,214	5.0
	MCM3	NP_001257401.1	DNA replication licensing factor MCM3 isoform 2 (putative replicative helicase essential for 'once per cell cycle' DNA replication initiation and elongation in eukaryotic cells. O-glycosylated (O-GlcNAcylated), in a cell cycle-dependent manner.)	6	14,293,457	2.5
	PSMD2	NP_002799.3	26S proteasome non-ATPase regulatory subunit 2=RPN1	4	14,121,080	5.6
	HNRNPM	NP_112480.2	heterogeneous nuclear ribonucleoprotein M isoform b	7	13,986,205	1.5
	CCT6A	NP_001009186.1	T-complex protein 1 subunit zeta isoform b	4	13,753,259	3.7
	PCBP2	NP_001122386.1	poly(rC)-binding protein 2 isoform g	8	13,417,898	1.9
	HSPA5	NP_005338.1	78 kDa glucose-regulated protein precursor	8	13,336,933	*
	PFKFB3	NP_001138915.1	6-phosphofructo-2-kinase/fructose-2, 6-bisphosphatase 3 isoform 2	7	13,236,204	1.9
	CKM	NP_001815.2	creatine kinase M-type	2	12,880,168	*

UBQLN2…

Gene	Accession	Protein name	Peptides	Intensity	Ratio
PAICS	NP_006443.1	multifunctional protein ADE2 isoform 2	6	12,859,321	2.8
HIST1H1C	NP_005310.1	histone H1.2	5	12,730,924	1.6
TMPO	NP_003267.1	thymopoietin isoform alpha=LAP2a	10	12,554,996	3.8
CSE1L	NP_001243064.1	exportin-2 isoform 2	3	12,493,809	4.3
IDH2	NP_002159.2	isocitrate dehydrogenase [NADP], mitochondrial precursor	4	12,468,623	3.4
IGF2BP1	NP_006537.3	insulin-like growth factor 2 mRNA-binding protein 1 isoform 1	5	11,938,355	1.7
CCT8	NP_006576.2	T-complex protein 1 subunit theta	2	11,924,921	3.1
RBMX	NP_002130.2	RNA-binding motif protein, X chromosome isoform 1	4	11,898,714	1.9
HSPA1L	NP_005518.3	heat shock 70 kDa protein 1-like	12	11,767,756	*
PDHB	NP_001166939.1	pyruvate dehydrogenase E1 component subunit beta, mitochondrial isoform 2 precursor	2	11,633,152	7.0
CCT2	NP_001185771.1	T-complex protein 1 subunit beta isoform 2	4	11,546,933	1.8
EIF3G	NP_003746.2	eukaryotic translation initiation factor 3 subunit G	6	11,416,464	2.1
PSMD13	NP_002808.3	26S proteasome non-ATPase regulatory subunit 13 isoform 1	2	11,415,492	5.1
EEF2	NP_001952.1	elongation factor 2	6	11,378,907	2.4
RPN1	NP_002941.1	dolichyl-diphosphooligosaccharide--protein glycosyltransferase subunit 1 precursor	3	11,333,358	1.5
MOGS	NP_001139630.1	mannosyl-oligosaccharide glucosidase isoform 2	5	11,305,935	7.9
RUVBL1	NP_003698.1	ruvB-like 1	11	11,114,101	3.8
BAG6	NP_001186626.1	large proline-rich protein BAG6 isoform c (Bat3)	5	11,031,790	4.9
TIMM50	NP_001001563.1	mitochondrial import inner membrane translocase subunit TIM50	4	10,911,366	2.9
ENPP1	NP_006199.2	ectonucleotide pyrophosphatase/phosphodiesterase family member 1	2	10,793,518	*
PSMD7	NP_002802.2	26S proteasome non-ATPase regulatory subunit 7	5	10,736,805	5.2
DDX39A	NP_005795.2	ATP-dependent RNA helicase DDX39A	2	10,559,015	3.1
RPS9	NP_001004.2	40S ribosomal protein S9	3	10,518,235	1.6
EPRS	NP_004437.2	bifunctional glutamate/proline--tRNA ligase	5	10,447,513	2.0
XRCC5	NP_066964.1	X-ray repair cross-complementing protein 5=Ku80	13	10,399,345	2.8
COPRS	NP_060875.2	coordinator of PRMT5 and differentiation stimulator	8	10,379,302	1.6
LMNA	NP_005563.1	lamin isoform C	3	10,297,551	*

UBQLN2…

	Gene	Accession	Protein name	Peptides	Intensity	Ratio
	TIMM44	NP_006342.2	mitochondrial import inner membrane translocase subunit TIM44	7	10,155,998	9.4
	SRPR	NP_001171313.1	signal recognition particle receptor subunit alpha isoform 2	2	9,891,992	*
	PTBP1	NP_114368.1	polypyrimidine tract-binding protein 1 isoform c	5	9,888,787	2.0
	SF3B1	NP_036565.2	splicing factor 3B subunit 1 isoform 1	4	9,664,201	1.9
	PSMC4	NP_694546.1	26S protease regulatory subunit 6B isoform 2	6	9,564,581	5.9
	PSMD12	NP_002807.1	26S proteasome non-ATPase regulatory subunit 12 isoform 1	6	9,551,526	5.9
	RNF126	NP_919442.1	RING finger protein 126	3	9,467,761	7.7
	PRSS3	NP_001184027.1	trypsin-3 isoform 4 preproprotein	4	9,400,564	*
	SF3B2	NP_006833.2	splicing factor 3B subunit 2	4	9,391,733	1.9
	ACADM	NP_000007.1	medium-chain specific acyl-CoA dehydrogenase, mitochondrial isoform a precursor	8	8,996,741	5.7
	HIST1H4A	NP_003529.1	histone H4	22	8,900,738	1.7
	PSMC3	NP_002795.2	26S protease regulatory subunit 6A	5	8,848,862	5.9
	PSMD11	NP_001257411.1	26S proteasome non-ATPase regulatory subunit 11	7	8,728,764	5.9
	EIF3E	NP_001559.1	eukaryotic translation initiation factor 3 subunit E	3	8,673,657	2.1
	TUBA1A	NP_001257329.1	tubulin alpha-1A chain isoform 2	12	8,673,036	3.5
	B3GNT1	NP_006867.1	N-acetyllactosaminide beta-1,3-N-acetylglucosaminyltransferase	4	8,672,567	8.0
	RBM10	NP_001191396.1	RNA-binding protein 10 isoform 4	4	8,672,140	2.2
	VCP	NP_009057.1	transitional endoplasmic reticulum ATPase=VCP	5	8,607,121	3.5
	CERS2	NP_071358.1	ceramide synthase 2	3	8,600,777	5.9
	RPL3	NP_001029025.1	60S ribosomal protein L3 isoform b	2	8,418,979	2.0
	EIF3F	NP_003745.1	eukaryotic translation initiation factor 3 subunit F	16	8,270,952	2.5
	DDX6	NP_004388.2	probable ATP-dependent RNA helicase DDX6	3	8,270,045	1.7
	VAT1	NP_006364.2	synaptic vesicle membrane protein VAT-1 homolog	4	8,201,372	*
	DHX9	NP_001348.2	ATP-dependent RNA helicase A	14	8,151,662	1.8
	SPTLC1	NP_006406.1	serine palmitoyltransferase 1 isoform a	2	8,076,527	*
	DCTN2	NP_001248342.1	dynactin subunit 2 isoform 3	2	8,074,018	1.6
	MTHFD1	NP_005947.3	C-1-tetrahydrofolate synthase, cytoplasmic	5	8,041,608	2.5
	ST13	NP_003923.2	hsc70-interacting protein	2	8,013,742	4.0
	PSMC6	NP_002797.3	26S protease regulatory subunit 10B	3	7,915,075	5.8
	COPB1	NP_057535.1	coatomer subunit beta	3	7,911,623	3.1
	LRPPRC	NP_573566.2	leucine-rich PPR motif-containing protein, mitochondrial precursor	4	7,844,995	1.8

UBQLN2…

Gene	Accession	Protein name	Peptides	Intensity	Ratio
MYH9	NP_002464.1	myosin-9	4	7,801,507	2.1
PDZ8	NP_776152.1	PDZ domain-containing protein 8	4	7,794,565	*
CD63	NP_001244329.1	CD63 antigen isoform D precursor	2	7,726,939	5.6
MCM5	NP_006730.2	DNA replication licensing factor MCM5	4	7,695,032	2.5
POR	NP_000932.3	NADPH--cytochrome P450 reductase	9	7,489,233	7.7
APMAP	NP_065392.1	adipocyte plasma membrane-associated protein	6	7,315,428	*
MCM4	NP_877423.1	DNA replication licensing factor MCM4	1	7,275,650	**3.41**
BLMH	NP_000377.1	bleomycin hydrolase	2	7,123,152	*
RPL18	NP_001257419.1	60S ribosomal protein L18 isoform 2	3	7,061,769	1.5
SGTA	NP_003012.1	small glutamine-rich tetratricopeptide repeat-containing protein alpha	9	6,889,927	6.9
SLC25A6	NP_001627.2	ADP/ATP translocase 3	8	6,664,595	*
GNB4	NP_067642.1	guanine nucleotide-binding protein subunit beta-4	2	6,613,539	2.8
ALDH1L2	NP_001029345.2	mitochondrial 10-formyltetrahydrofolate dehydrogenase precursor	2	6,438,496	*
TMX4	NP_066979.2	thioredoxin-related transmembrane protein 4 precursor	2	6,433,585	8.5
ATP1A1	NP_001153706.1	sodium/potassium-transporting ATPase subunit alpha-1 isoform d	12	6,410,775	5.4
MARCKS	NP_002347.5	myristoylated alanine-rich C-kinase substrate	3	6,375,584	1.8
AP2M1	NP_001020376.1	AP-2 complex subunit mu isoform b	2	6,321,212	2.2
INSR	NP_001073285.1	insulin receptor isoform Short preproprotein	6	6,285,701	10.2
MARS	NP_004981.2	methionine--tRNA ligase, cytoplasmic	2	6,250,868	5.0
GAPDH	NP_002037.2	glyceraldehyde-3-phosphate dehydrogenase isoform 1	8	6,188,879	*
ERGIC3	NP_057050.1	endoplasmic reticulum-Golgi intermediate compartment protein 3 isoform b	4	6,164,440	5.5
ATP2A2	NP_001672.1	sarcoplasmic/endoplasmic reticulum calcium ATPase 2 isoform a	3	6,083,691	5.5
SLC3A2	NP_001013269.1	4F2 cell-surface antigen heavy chain isoform f	7	5,970,870	2.8
FAF2	NP_055428.1	FAS-associated factor 2	4	5,911,616	*
IDH3A	NP_005521.1	isocitrate dehydrogenase [NAD] subunit alpha, mitochondrial precursor	3	5,903,767	*
EEF1G	NP_001395.1	elongation factor 1-gamma	7	5,835,359	1.6

	Gene	Accession	Protein name	Peptides	Intensity	Ratio
	EIF3A	NP_003741.1	eukaryotic translation initiation factor 3 subunit A	12	5,825,481	3.4
	PSMC5	NP_001186092.1	26S protease regulatory subunit 8 isoform 2	14	5,692,381	5.9
	SAFB	NP_001188269.1	scaffold attachment factor B1 isoform 4	2	5,504,130	3.8
	B3GAT3	NP_036332.2	galactosylgalactosylxylosylprotein 3-beta-glucuronosyltransferase 3	2	5,501,462	3.6
	KPNA2	NP_002257.1	importin subunit alpha-2	2	5,482,660	2.1
	NDUFS2	NP_001159631.1	NADH dehydrogenase [ubiquinone] iron-sulfur protein 2, mitochondrial isoform 2 precursor	5	5,359,528	1.6
	CASP14	NP_036246.1	caspase-14 precursor	3	5,339,378	*
	SLC25A5	NP_001143.2	ADP/ATP translocase 2	10	5,337,110	2.2
	PSMD6	NP_001258710.1	26S proteasome non-ATPase regulatory subunit 6 isoform 4	3	5,323,490	4.2
	EWSR1	NP_001156758.1	RNA-binding protein EWS isoform 4 (Ewing sarcoma breakpoint region 1)	2	5,309,022	*
	RPLP0	NP_444505.1	60S acidic ribosomal protein P0	6	5,258,556	2.0
	CYP20A1	NP_803882.1	cytochrome P450 20A1	5	5,223,075	31.5
	GNAS	NP_001070957.1	protein GNAS isoform g	2	5,195,619	3.9
	MCM7	NP_005907.3	DNA replication licensing factor MCM7 isoform 1	4	5,141,775	3.0
	PCYT1B	NP_001156737.1	choline-phosphate cytidylyltransferase B isoform 3	2	5,095,267	*
	ANXA2	NP_001129487.1	annexin A2 isoform 2	8	5,026,577	*
	RAD50	NP_005723.2	DNA repair protein RAD50	2	4,971,819	2.7
	SRP54	NP_003127.1	signal recognition particle 54 kDa protein isoform 1	2	4,929,038	4.4
	CTSD	NP_001900.1	cathepsin D preproprotein	3	4,916,716	*
	HNRNPR	NP_001095867.1	heterogeneous nuclear ribonucleoprotein R isoform 4	3	4,914,800	1.6
	PSMC2	NP_002794.1	26S protease regulatory subunit 7 isoform 1	7	4,886,364	5.7
	HSP90AA1	NP_005339.3	heat shock protein HSP 90-alpha isoform 2	3	4,846,809	1.5
	SEC62	NP_003253.1	translocation protein SEC62	4	4,838,024	2.4
	AZGP1	NP_001176.1	zinc-alpha-2-glycoprotein precursor	2	4,836,685	*
	TXN	NP_001231867.1	thioredoxin isoform 2	5	4,835,216	*
	TCP1	NP_001008897.1	T-complex protein 1 subunit alpha isoform b	1	4,817,514	*
	DHODH	NP_001352.2	dihydroorotate dehydrogenase (quinone), mitochondrial	4	4,817,013	6.6
	MARCKSL1	NP_075385.1	MARCKS-related protein	7	4,813,216	1.7
	GCN1L1	NP_006827.1	translational activator GCN1	2	4,796,380	1.7
	OAT	NP_000265.1	ornithine aminotransferase, mitochondrial isoform 1 precursor	2	4,745,463	*
	FAR1	NP_115604.1	fatty acyl-CoA reductase 1	2	4,666,047	4.4

UBQLN2…

	Gene	Accession	Protein name	Peptides	Intensity	Ratio
	PSMC1	NP_002793.2	26S protease regulatory subunit 4	5	4,616,331	5.8
	KCTD5	NP_061865.1	BTB/POZ domain-containing protein KCTD5	9	4,610,457	1.9
	HNRNPUL2	NP_001073027.1	heterogeneous nuclear ribonucleoprotein U-like protein 2	4	4,589,802	1.8
	BUB3	NP_001007794.1	mitotic checkpoint protein BUB3 isoform b	4	4,568,556	1.6
	GTF2I	NP_001509.3	general transcription factor II-I isoform 4	8	4,562,355	2.3
	COPG2	NP_036265.3	coatomer subunit gamma-2	3	4,549,606	2.1
	SERBP1	NP_056455.3	plasminogen activator inhibitor 1 RNA-binding protein isoform 4	11	4,549,331	1.8
	ALDH1L1	NP_001257294.1	cytosolic 10-formyltetrahydrofolate dehydrogenase isoform 3	2	4,544,022	*
	PDHA1	NP_001166927.1	pyruvate dehydrogenase E1 component subunit alpha, somatic form, mitochondrial isoform 4 precursor	2	4,511,293	4.5
	PFKFB1	NP_001258734.1	6-phosphofructo-2-kinase/fructose-2, 6-bisphosphatase 1 isoform 3	2	4,504,574	1.5
	MCM6	NP_005906.2	DNA replication licensing factor MCM6	2	4,470,070	1.9
	NSF	NP_006169.2	vesicle-fusing ATPase=NSF	2	4,414,065	3.2
	TUBB	NP_821133.1	tubulin beta chain	3	4,338,050	6.8
	NUP205	NP_055950.1	nuclear pore complex protein Nup205	1	4,312,302	**4.31**
	KCTD17	NP_078957.2	BTB/POZ domain-containing protein KCTD17	5	4,151,795	1.8
	PRDX2	NP_005800.3	peroxiredoxin-2	2	4,127,660	*
	HADHB	NP_000174.1	trifunctional enzyme subunit beta, mitochondrial precursor	4	4,126,117	*
	IARS	NP_002152.2	isoleucine--tRNA ligase, cytoplasmic	5	4,049,162	1.8
	RPL27A	NP_000981.1	60S ribosomal protein L27a	5	4,031,316	1.6
	AFG3L2	NP_006787.2	AFG3-like protein 2= AAA ATPase	7	4,007,768	2.3
	STX12	NP_803173.1	syntaxin-12	2	3,933,053	1.9
	GSDMA	NP_835465.2	gasdermin-A	2	3,925,754	*
	THOC3	NP_115737.1	THO complex subunit 3	2	3,905,055	1.5
	DSC1	NP_004939.1	desmocollin-1 isoform Dsc1b preproprotein	2	3,839,581	*
	FAM162A	NP_055182.3	protein FAM162A	2	3,816,340	*
	DHRS7	NP_057113.1	dehydrogenase/reductase SDR family member 7 precursor	4	3,750,267	9.7
	RFC4	NP_002907.1	replication factor C subunit 4	2	3,725,522	2.9
	TOR1AIP1	NP_056417.2	torsin-1A-interacting protein 1 isoform 2	4	3,632,993	6.8
	MMS19	NP_071757.4	MMS19 nucleotide excision repair protein homolog	2	3,593,040	*
	SERPINB12	NP_536722.1	serpin B12	2	3,577,939	*

UBQLN2…

Gene	Accession	Protein name	Peptides	Intensity	Ratio
COL1A2	NP_000080.2	collagen alpha-2(I) chain precursor	2	3,569,111	*
CD320	NP_057663.1	CD320 antigen isoform 1 precursor	2	3,506,057	5.0
EIF2S2	NP_003899.2	eukaryotic translation initiation factor 2 subunit 2	2	3,436,968	2.0
TFRC	NP_003225.2	transferrin receptor protein 1	3	3,402,082	2.6
PRRC2B	NP_037450.2	proline-rich and coiled coil-containing protein 1	2	3,395,652	2.1
AMY2B	NP_066188.1	alpha-amylase 2B precursor	2	3,306,609	*
MRE11A	NP_005581.2	double-strand break repair protein MRE11A isoform 2	2	3,182,981	2.3
EIF4G1	NP_004944.3	eukaryotic translation initiation factor 4 gamma 1 isoform 4	1	2,982,537	**3.12**
CHD4	NP_001264.2	chromodomain-helicase-DNA-binding protein 4 (RING-type Zn-finger)	2	2,963,874	*
IDH1	NP_005887.2	isocitrate dehydrogenase [NADP] cytoplasmic	5	2,865,597	1.5
ARG1	NP_000036.2	arginase-1 isoform 2	4	2,860,871	2.7
EIF4G2	NP_001036024.3	eukaryotic translation initiation factor 4 gamma 2 isoform 2	1	2,777,127	1.55
TMX1	NP_110382.3	thioredoxin-related transmembrane protein 1 precursor	2	2,709,795	7.7
CREM	NP_874392.1	cAMP-responsive element modulator isoform 10	2	2,697,191	1.7
CXADR	NP_001329.1	coxsackievirus and adenovirus receptor isoform 1 precursor	3	2,617,719	*
MATR3	NP_954659.1	matrin-3 isoform a	3	2,613,955	1.5
ADPGK	NP_112574.3	ADP-dependent glucokinase precursor	2	2,611,902	*
ARMC6	NP_219483.1	armadillo repeat-containing protein 6 isoform 2	3	2,539,466	2.5
PLIN3	NP_001157666.1	perilipin-3 isoform 3	5	2,479,809	4.3
DNAJA1	NP_001530.1	dnaJ homolog subfamily A member 1	4	2,435,478	3.0
ANXA1	NP_000691.1	annexin A1	2	2,397,085	*
HERPUD1	NP_001259032.1	homocysteine-responsive endoplasmic reticulum-resident ubiquitin-like domain member 1 protein isoform 4	2	2,299,287	15.7
APOL2	NP_663612.1	apolipoprotein L2	2	2,206,650	9.3
NACA	NP_001106673.1	nascent polypeptide-associated complex subunit alpha isoform b	2	2,127,874	*
RPS3	NP_001243731.1	40S ribosomal protein S3 isoform 1	6	2,113,738	1.9
SLC25A11	NP_001158890.1	mitochondrial 2-oxoglutarate/malate carrier protein isoform 3	2	2,089,062	1.8
MDC1	NP_055456.2	mediator of DNA damage checkpoint protein 1	2	2,005,412	*
LDHB	NP_002291.1	L-lactate dehydrogenase B chain	3	1,722,938	1.5
TPD52L2	NP_001230821.1	tumor protein D54 isoform h	4	1,506,928	12.6

UBQLN2…

	Gene	Accession	Protein name	Peptides	Intensity	Ratio
	GNAQ	NP_002063.2	guanine nucleotide-binding protein G(q) subunit alpha	4	1,468,824	10.1
	ALDH18A1	NP_001017423.1	delta-1-pyrroline-5-carboxylate synthase isoform 2	2	1,368,128	2.6
	MTHFD2	NP_006627.2	bifunctional methylenetetrahydrofolate dehydrogenase/cyclohydrolase, mitochondrial precursor	2	1,266,779	*
	CDK1	NP_203698.1	cyclin-dependent kinase 1 isoform 2	1	1,153,981	3.05
	SAE1	NP_001139186.1	SUMO-activating enzyme subunit 1 isoform c	2	976,832	2.8
	FAM120A	NP_055427.2	constitutive coactivator of PPAR-gamma-like protein 1	1	914,165	1.72
	RPS3A	NP_000997.1	40S ribosomal protein S3a isoform 1	4	898,373	1.5
	LRRC59	NP_060979.2	leucine-rich repeat-containing protein 59	2	695,178	1.8
	PELO	NP_057030.3	protein pelota homolog	2	643,773	2.7
	HSD17B12	NP_057226.1	estradiol 17-beta-dehydrogenase 12	2	594,787	18.2

Only proteins with more than 1 peptide were included unless the protein was clearly part of a marked complex. Protein and peptide false discovery rates were set at 1% for the Proteome Discoverer database search. Proteins were sorted by intensity. Gene is the gene name. Blue text indicates proteins identified in the SG proteome. Orange text indicates SG proteome proteins that are hnRNPs. Peptides are the peptide spectrum matched hits. Intensity is the total integrated precursor ion peak density. SILAC ratio is the average HEAVY (UBQLN2)/LIGHT (Control) peptide ratio. * indicates a corresponding light peptide was not automatically identified by the search software. Red bars indicate proteins identified in this study. Orange bars indicate proteins identified in previous studies. A total of 266 proteins were identified in this analysis.

Table A-2 Table of UBQLN1 associated proteins identified by SILAC nLC-MS/MS

Gene	Accession	Protein name	Peptides	Intensity	SILAC Ratio
UBQLN1	NP_444295.1	ubiquilin-1 isoform 2	171	14,721,415,075	34.5
UBQLN4	NP_064516.2	ubiquilin-4	44	13,267,180,406	58.7
UBQLN2	NP_038472.2	ubiquilin-2	49	2,658,591,558	33.4
PDE4D	NP_001184147.1	cAMP-specific 3',5'-cyclic phosphodiesterase 4D	8	1,132,278,447	*
HSPA1A	NP_005336.3	heat shock 70 kDa protein 1A/1B	67	972,807,788	25.1
HSPA8	NP_006588.1	heat shock cognate 71 kDa protein isoform 1	81	921,427,447	20.8
ILVBL	NP_006835.2	acetolactate synthase-like protein	58	398,193,490	42.3
HSPA5	NP_005338.1	78 kDa glucose-regulated protein precursor	15	390,324,054	8.3
PRMT5	NP_006100.2	protein arginine N-methyltransferase 5	51	337,541,450	1.5
HSD17B12	NP_057226.1	estradiol 17-beta-dehydrogenase 12	4	290,551,062	34.7
ALDH3A2	NP_000373.1	fatty aldehyde dehydrogenase isoform 2	75	285,584,192	37.9
UBB	NP_061828.1	polyubiquitin-B precursor	206	197,312,983	27.6
FAM162A	NP_055182.3	protein FAM162A	6	131,914,564	42.3
XRCC6	NP_001460.1	X-ray repair cross-complementing protein 6	24	129,200,022	14.5
TUBA1A	NP_001257329.1	tubulin alpha-1A chain isoform 2	48	89,199,661	20.9
HIST1H2BD	NP_066407.1	histone H2B type 1-D	20	80,182,497	13.6
TUBB	NP_821133.1	tubulin beta chain	49	75,036,885	17.1
UBXN4	NP_055422.1	UBX domain-containing protein 4 (erasin)	12	73,457,198	46.5
ESYT2	NP_065779.1	extended synaptotagmin-2	30	71,257,770	36.4
NGLY1	NP_001138765.1	peptide-N(4)-(N-acetyl-beta-glucosaminyl)asparagine amidase	23	68,154,000	40.2
TMEM209	NP_116231.2	transmembrane protein 209	21	56,992,809	39.3
RTN4	NP_722550.1	reticulon-4 isoform B	9	52,343,609	41.9
BSG	NP_940991.1	basigin isoform 2	23	51,938,257	34.8
ACSL3	NP_004448.2	long-chain-fatty-acid--CoA ligase 3	3	50,284,689	*
LMNB1	NP_005564.1	lamin-B1 isoform 1	18	46,275,504	4.2
TUBB4B	NP_006079.1	tubulin beta-4B chain	38	45,393,234	14.5
ACTB	NP_001092.1	actin, cytoplasmic 1	18	43,282,173	14.2
RPN2	NP_001129243.1	dolichyl-diphosphooligosaccharide--protein glycosyltransferase subunit 2 isoform 2 precursor	10	43,276,689	*
GPX8	NP_001008398.2	probable glutathione peroxidase 8	11	41,911,870	35.7
HSPA9	NP_004125.3	stress-70 protein, mitochondrial precursor	10	39,047,336	19.8
SYNGR1	NP_663783.1	synaptogyrin-1 isoform 1b	5	27,295,445	35.6
XRCC5	NP_066964.1	X-ray repair cross-complementing protein 5	21	26,712,302	18.8

UBQLN1…

	Gene	Accession	Protein name	Peptides	Intensity	SILAC Ratio
	MOGS	NP_006293.2	mannosyl-oligosaccharide glucosidase isoform 1	24	26,658,414	23.3
	C9orf72	NP_060795.1	protein C9orf72 isoform a	50	24,985,100	*
	COL14A1	NP_066933.1	collagen alpha-1(XIV) chain precursor	3	21,264,540	*
	PRKDC	NP_001075109.1	DNA-dependent protein kinase catalytic subunit isoform 2	93	21,140,063	15.0
	HSPA13	NP_008879.3	heat shock 70 kDa protein 13 precursor	14	21,083,267	39.4
	MAN1A1	NP_005898.2	mannosyl-oligosaccharide 1,2-alpha-mannosidase IA	5	20,620,511	*
	LMAN1	NP_005561.1	protein ERGIC-53 precursor	4	19,648,002	19.8
	PPM1B	NP_002697.1	protein phosphatase 1B isoform 1	38	19,162,929	2.9
	SRPR	NP_001171313.1	signal recognition particle receptor subunit alpha isoform 2	2	18,990,472	*
	CD320	NP_001159367.1	CD320 antigen isoform 2 precursor	9	18,077,655	14.1
	TMPO	NP_001027454.1	thymopoietin isoform beta	19	17,651,183	12.1
	ADAM9	NP_003807.1	disintegrin and metalloproteinase domain-containing protein 9 precursor	9	17,424,092	*
	NBAS	NP_056993.2	neuroblastoma-amplified sequence	13	16,558,854	*
	HNRNPU	NP_004492.2	heterogeneous nuclear ribonucleoprotein U isoform b	33	16,235,839	12.5
	SEC22B	NP_004883.3	vesicle-trafficking protein SEC22b precursor	10	15,807,353	34.1
	PARP1	NP_001609.2	poly [ADP-ribose] polymerase 1	25	15,472,135	18.8
	PLD3	NP_001026866.1	phospholipase D3	8	15,187,458	*
	SUPT16H	NP_009123.1	FACT complex subunit SPT16	10	14,465,756	18.9
	DDX1	NP_004930.1	ATP-dependent RNA helicase DDX1	15	13,982,498	12.9
	COX4I1	NP_001852.1	cytochrome c oxidase subunit 4 isoform 1, mitochondrial precursor	2	13,954,344	*
	LMNB2	NP_116126.3	lamin-B2	12	13,412,652	*
	PSMB6	NP_001257410.1	proteasome subunit beta type-6 isoform 2 proprotein	2	13,207,610	4.6
	RAB1B	NP_112243.1	ras-related protein Rab-1B	4	12,866,705	11.6
	LBR	NP_919424.1	lamin-B receptor	7	12,815,332	9.7
	SCFD1	NP_057190.2	sec1 family domain-containing protein 1 isoform a	3	12,574,665	*
	FAF2	NP_055428.1	FAS-associated factor 2	4	12,488,410	26.7
	EMD	NP_000108.1	emerin	6	12,337,194	9.0
	PSMD3	NP_002800.2	26S proteasome non-ATPase regulatory subunit 3	9	11,866,075	14.8
	HSPD1	NP_002147.2	60 kDa heat shock protein, mitochondrial	21	11,828,104	4.1
	PUF60	NP_001258029.1	poly(U)-binding-splicing factor PUF60 isoform h	3	11,656,364	5.1
	XRCC1	NP_006288.2	DNA repair protein XRCC1	16	11,634,185	19.8

UBQLN1…

	Gene	Accession	Protein name	Peptides	Intensity	SILAC Ratio
	RTCB	NP_055121.1	tRNA-splicing ligase RtcB homolog	2	11,535,357	16.3
	BCLAF1	NP_001070908.1	bcl-2-associated transcription factor 1 isoform 2	14	11,089,899	2.8
	RAB5C	NP_958842.1	ras-related protein Rab-5C isoform a	2	11,069,816	17.1
	TCP1	NP_110379.2	T-complex protein 1 subunit alpha isoform a	13	10,960,022	11.2
	TOR1AIP2	NP_659471.1	torsin-1A-interacting protein 2 isoform b	3	10,864,164	*
	SLC25A5	NP_001143.2	ADP/ATP translocase 2	9	10,730,095	11.6
	LAMP1	NP_005552.3	lysosome-associated membrane glycoprotein 1 precursor	6	10,367,247	23.7
	SGK196	NP_115613.1	probable inactive protein kinase-like protein SgK196	4	10,309,237	30.5
	RBMX	NP_002130.2	RNA-binding motif protein, X chromosome isoform 1	13	10,129,200	10.7
	VKORC1	NP_076869.1	complex subunit 1 isoform 1	6	9,893,978	*
	FDFT1	NP_004453.3	squalene synthase	9	9,669,719	29.8
	KPNB1	NP_002256.2	importin subunit beta-1 isoform 1	5	9,624,470	12.8
	CCT3	NP_001008800.1	T-complex protein 1 subunit gamma isoform c	7	9,572,790	11.1
	SSR3	NP_009038.1	translocon-associated protein subunit gamma	7	9,272,382	7.9
	BAK1	NP_001179.1	bcl-2 homologous antagonist/killer	6	9,255,646	60.8
	RAB21	NP_055814.1	ras-related protein Rab-21	2	9,235,926	27.7
	DHCR24	NP_055577.1	delta(24)-sterol reductase precursor	11	9,121,103	27.4
	HERPUD1	NP_001259032.1	homocysteine-responsive endoplasmic reticulum-resident ubiquitin-like domain member 1 protein isoform 4	4	9,104,671	32.9
	VIM	NP_003371.2	vimentin	24	9,089,854	6.8
	RTN3	NP_001252520.1	reticulon-3 isoform g	2	8,764,348	32.9
	FAM3C	NP_055703.1	protein FAM3C precursor	4	8,704,339	12.7
	CDK1	NP_203698.1	cyclin-dependent kinase 1 isoform 2	2	8,691,291	6.5
	IMMT	NP_001093640.1	mitochondrial inner membrane protein isoform 3	21	8,541,705	8.8
	PHB2	NP_001138303.1	prohibitin-2 isoform 1	7	7,829,977	6.7
	RTN2	NP_996784.1	reticulon-2 isoform C	2	7,744,218	24.3
	PABPC1L2A	NP_001012995.1	polyadenylate-binding protein 1-like 2	2	7,522,217	*
	RPS18	NP_072045.1	40S ribosomal protein S18	16	7,478,679	6.0
	PSMC5	NP_001186092.1	26S protease regulatory subunit 8 isoform 2	2	7,358,341	24.2
	TIMM21	NP_054896.2	mitochondrial import inner membrane translocase subunit Tim21 precursor	9	7,311,279	39.6

UBQLN1…

Gene	Accession	Protein name	Peptides	Intensity	SILAC Ratio
MCM7	NP_877577.1	DNA replication licensing factor MCM7 isoform 2	6	7,192,703	19.6
LSM14A	NP_056393.2	protein LSM14 homolog A isoform b	7	6,770,277	4.0
ABCE1	NP_002931.2	ATP-binding cassette sub-family E member 1	7	6,742,306	36.1
LPCAT1	NP_079106.3	lysophosphatidylcholine acyltransferase 1	4	6,700,632	24.7
ATP1A1	NP_001153706.1	sodium/potassium-transporting ATPase subunit alpha-1 isoform d	19	6,252,723	11.9
SNRPD3	NP_004166.1	small nuclear ribonucleoprotein Sm D3	4	6,109,595	1.9
CCT5	NP_036205.1	T-complex protein 1 subunit epsilon	6	6,103,297	8.0
ARL6IP1	NP_055976.1	ADP-ribosylation factor-like protein 6-interacting protein 1	2	6,030,608	*
NDUFB11	NP_001129470.1	NADH dehydrogenase [ubiquinone] 1 beta subcomplex subunit 11, mitochondrial isoform 2	2	5,956,941	*
SSR4	NP_006271.1	translocon-associated protein subunit delta isoform 2 precursor	4	5,842,621	*
RAB11A	NP_001193765.1	ras-related protein Rab-11A isoform 2	2	5,787,289	21.7
HDAC1	NP_004955.2	histone deacetylase 1	3	5,568,393	7.6
POR	NP_000932.3	NADPH--cytochrome P450 reductase	8	5,252,538	22.3
LOC402160	NP_001180211.1	uncharacterized protein LOC402160	2	5,125,185	*
NDUFS2	NP_001159631.1	NADH dehydrogenase [ubiquinone] iron-sulfur protein 2, mitochondrial isoform 2 precursor	2	4,982,818	*
RNF139	NP_009149.2	E3 ubiquitin-protein ligase RNF139	2	4,845,334	*
PARP2	NP_001036083.1	poly [ADP-ribose] polymerase 2 isoform 2	12	4,779,634	*
CHPT1	NP_064629.2	cholinephosphotransferase 1	2	4,705,410	*
EXT2	NP_997005.1	exostosin-2 isoform 2	4	4,692,735	*
BZW1	NP_055485.2	basic leucine zipper and W2 domain-containing protein 1 isoform 4	3	4,684,238	*
NOMO2	NP_775885.1	nodal modulator 2 isoform 2 precursor	7	4,659,817	4.5
UQCRC2	NP_003357.2	cytochrome b-c1 complex subunit 2, mitochondrial precursor	7	4,563,833	6.5
BAG6	NP_001186626.1	large proline-rich protein BAG6 isoform c	4	4,530,726	*
LIG3	NP_002302.2	DNA ligase 3 isoform beta precursor	3	4,529,935	22.1
INSR	NP_001073285.1	insulin receptor isoform Short preproprotein	7	4,505,199	38.5

UBQLN1…

Gene	Accession	Protein name	Peptides	Intensity	SILAC Ratio
ENPP1	NP_006199.2	ectonucleotide pyrophosphatase/phosphodiesterase family member 1	2	4,497,209	*
LETM1	NP_036450.1	LETM1 and EF-hand domain-containing protein 1, mitochondrial precursor	10	4,483,550	9.3
RPS5	NP_001000.2	40S ribosomal protein S5	4	4,470,749	6.2
SPNS1	NP_001135921.1	protein spinster homolog 1 isoform 4	2	4,458,979	*
TMX1	NP_110382.3	thioredoxin-related transmembrane protein 1 precursor	2	4,454,310	*
PRDX1	NP_859048.1	peroxiredoxin-1	5	4,432,328	4.4
HNRNPK	NP_112552.1	heterogeneous nuclear ribonucleoprotein K isoform b	4	4,422,722	3.0
STK38	NP_009202.1	serine/threonine-protein kinase 38	8	4,377,778	4.3
ATL2	NP_001129145.1	atlastin-2 isoform 2	3	4,357,875	*
CLPTM1	NP_001285.1	cleft lip and palate transmembrane protein 1	2	4,319,688	20.4
LEMD2	NP_851853.1	LEM domain-containing protein 2 isoform 1	9	4,236,496	*
SLC3A2	NP_001013269.1	4F2 cell-surface antigen heavy chain isoform f	4	4,088,435	11.4
RPS3	NP_001243731.1	40S ribosomal protein S3 isoform 1	6	4,061,068	5.4
GBA	NP_001165282.1	glucosylceramidase isoform 2	6	4,024,721	*
RAB3D	NP_004274.1	ras-related protein Rab-3D	4	3,893,542	8.9
ROBO1	NP_001139317.1	roundabout homolog 1 isoform d	6	3,887,633	14.5
ERGIC3	NP_057050.1	endoplasmic reticulum-Golgi intermediate compartment protein 3 isoform b	3	3,868,735	*
ATP5B	NP_001677.2	ATP synthase subunit beta, mitochondrial precursor	3	3,771,714	8.7
RHOT2	NP_620124.1	mitochondrial Rho GTPase 2	2	3,724,280	35.5
PSMC1	NP_002793.2	26S protease regulatory subunit 4	8	3,647,153	20.7
IMPDH1	NP_001136047.1	inosine-5'-monophosphate dehydrogenase 1 isoform g	2	3,626,984	*
NCLN	NP_064555.2	nicalin precursor	4	3,624,052	24.2
CCT6A	NP_001009186.1	T-complex protein 1 subunit zeta isoform b	7	3,624,001	1.7
THRAP3	NP_005110.2	thyroid hormone receptor-associated protein 3	6	3,613,884	2.0
CASP14	NP_036246.1	caspase-14 precursor	2	3,602,790	*
STT3A	NP_001265433.1	dolichyl-diphosphooligosaccharide--protein glycosyltransferase subunit STT3A isoform b	2	3,580,514	*
LMNA	NP_005563.1	lamin isoform C	11	3,553,884	14.0

UBQLN1…

Gene	Accession	Protein name	Peptides	Intensity	SILAC Ratio
ADRM1	NP_008933.2	proteasomal ubiquitin receptor ADRM1 precursor	4	3,535,221	23.3
ENO1	NP_001188412.1	c-myc promoter-binding protein-1 isoform MBP-1	4	3,522,824	*
YWHAQ	NP_006817.1	14-3-3 protein theta	2	3,522,785	*
TMX2	NP_001137484.1	thioredoxin-related transmembrane protein 2 isoform 2	4	3,476,529	*
CANX	NP_001737.1	calnexin precursor	6	3,459,558	20.1
HIST1H1C	NP_005310.1	histone H1.2	25	3,422,421	20.2
ATP5A1	NP_001001935.1	ATP synthase subunit alpha, mitochondrial isoform c	7	3,420,303	10.9
PRKCA	NP_002728.1	protein kinase C alpha type	2	3,382,576	*
VIMP	NP_060915.2	selenoprotein S	6	3,330,068	4.6
CYP20A1	NP_803882.1	cytochrome P450 20A1	4	3,275,417	*
DHX9	NP_001348.2	ATP-dependent RNA helicase A	2	3,250,180	3.7
HNRNPM	NP_112480.2	heterogeneous nuclear ribonucleoprotein M isoform b	4	3,225,375	7.0
ATL3	NP_056274.3	atlastin-3	3	3,178,275	*
SIRPA	NP_001035111.1	tyrosine-protein phosphatase non-receptor type substrate 1 precursor	6	3,125,140	*
PFKM	NP_000280.1	6-phosphofructokinase, muscle type isoform 2	2	3,095,423	3.7
SEC62	NP_003253.1	translocation protein SEC62	2	3,092,926	8.6
SSRP1	NP_003137.1	FACT complex subunit SSRP1	3	3,053,331	28.7
VDAC1	NP_003365.1	voltage-dependent anion-selective channel protein 1	2	2,964,632	5.8
CLCC1	NP_001041675.1	chloride channel CLIC-like protein 1 isoform 1 precursor	4	2,929,227	*
AIFM1	NP_001124318.1	apoptosis-inducing factor 1, mitochondrial isoform 4	2	2,877,486	*
TUFM	NP_003312.3	elongation factor Tu, mitochondrial precursor	2	2,872,347	16.6
VRK3	NP_001020949.1	inactive serine/threonine-protein kinase VRK3 isoform 2	2	2,871,228	*
AAAS	NP_001166937.1	aladin isoform 2	2	2,866,466	*
PSMC4	NP_694546.1	26S protease regulatory subunit 6B isoform 2	2	2,795,461	*
ATP2A2	NP_001672.1	sarcoplasmic/endoplasmic reticulum calcium ATPase 2 isoform a	5	2,792,595	9.5
RPS9	NP_001004.2	40S ribosomal protein S9	5	2,762,188	6.9
CCT7	NP_001159757.1	T-complex protein 1 subunit eta isoform d	16	2,752,959	7.4
SLC25A24	NP_998816.1	calcium-binding mitochondrial carrier protein SCaMC-1 isoform 2	8	2,716,012	11.3
PVRL1	NP_976031.1	poliovirus receptor-related protein 1 isoform 3 precursor	4	2,714,888	*
WNK1	NP_055638.2	serine/threonine-protein kinase WNK1 isoform 2	3	2,683,209	*
CTSD	NP_001900.1	cathepsin D preproprotein	4	2,627,348	1.8

UBQLN1…

	Gene	Accession	Protein name	Peptides	Intensity	SILAC Ratio
	RPA1	NP_002936.1	replication protein A 70 kDa DNA-binding subunit	3	2,578,917	*
	PSMB5	NP_002788.1	proteasome subunit beta type-5 isoform 1	6	2,567,246	*
	PNKP	NP_009185.2	bifunctional polynucleotide phosphatase/kinase	2	2,496,633	*
	CCT8	NP_006576.2	T-complex protein 1 subunit theta	5	2,481,252	9.1
	ATP6AP1	NP_001174.2	V-type proton ATPase subunit S1 precursor	2	2,463,018	*
	CACHD1	NP_065976.2	VWFA and cache domain-containing protein 1	3	2,458,657	*
	RUVBL1	NP_003698.1	ruvB-like 1	2	2,443,132	*
	CYP51A1	NP_001139624.1	lanosterol 14-alpha demethylase isoform 2	2	2,438,310	*
	VCP	NP_009057.1	transitional endoplasmic reticulum ATPase	3	2,434,812	12.8
	PRPF31	NP_056444.3	U4/U6 small nuclear ribonucleoprotein Prp31	4	2,415,665	2.2
	ANXA2	NP_001129487.1	annexin A2 isoform 2	7	2,357,481	*
	CREM	NP_874392.1	cAMP-responsive element modulator isoform 10	2	2,307,291	14.6
	BTRC	NP_003930.1	F-box/WD repeat-containing protein 1A isoform 2	4	2,292,494	*
	ITPRIP	NP_001258941.1	inositol 1,4,5-trisphosphate receptor-interacting protein precursor	2	2,289,136	*
	SATB2	NP_056080.1	DNA-binding protein SATB2	4	2,272,279	8.0
	B3GNT1	NP_006867.1	N-acetyllactosaminide beta-1,3-N-acetylglucosaminyltransferase	8	2,217,659	*
	MRE11A	NP_005581.2	double-strand break repair protein MRE11A isoform 2	4	2,200,252	*
	ATAD3A	NP_001164007.1	ATPase family AAA domain-containing protein 3A isoform 3	5	2,165,529	5.1
	RHOT1	NP_060777.3	mitochondrial Rho GTPase 1 isoform 3	3	2,142,103	*
	RAP1B	NP_001238851.1	ras-related protein Rap-1b isoform 4	7	2,138,538	12.0
	ESYT1	NP_056107.1	extended synaptotagmin-1 isoform 2	6	2,105,947	*
	NUP210	NP_079199.2	nuclear pore membrane glycoprotein 210 precursor	11	2,095,570	18.1
	CUX1	NP_853530.2	protein CASP isoform a	6	2,081,198	*
	L2HGDH	NP_079160.1	L-2-hydroxyglutarate dehydrogenase, mitochondrial precursor	2	2,051,363	22.4
	TIMM17B	NP_005825.1	mitochondrial import inner membrane translocase subunit Tim17-B isoform 2	2	1,970,908	3.3
	OAT	NP_001165285.1	ornithine aminotransferase, mitochondrial isoform 2	2	1,928,706	30.9
	BAZ1A	NP_872589.1	bromodomain adjacent to zinc finger domain protein 1A isoform b	2	1,905,742	9.7

UBQLN1…

Gene	Accession	Protein name	Peptides	Intensity	SILAC Ratio
G3BP1	NP_005745.1	ras GTPase-activating protein-binding protein 1	2	1,888,348	*
ALDH18A1	NP_001017423.1	delta-1-pyrroline-5-carboxylate synthase isoform 2	4	1,884,114	11.2
EPRS	NP_004437.2	bifunctional glutamate/proline--tRNA ligase	4	1,868,883	5.8
DNAJB2	NP_001034639.1	dnaJ homolog subfamily B member 2 isoform a	2	1,842,418	*
HEATR2	NP_060272.3	HEAT repeat-containing protein 2	6	1,813,741	22.4
PHGDH	NP_006614.2	D-3-phosphoglycerate dehydrogenase	2	1,810,417	2.8
FBXW11	NP_387449.2	F-box/WD repeat-containing protein 11 isoform A	8	1,795,805	*
EIF3L	NP_057175.1	eukaryotic translation initiation factor 3 subunit L isoform 1	8	1,787,067	2.3
COL1A2	NP_000080.2	collagen alpha-2(I) chain precursor	11	1,758,989	*
DDX3X	NP_001180346.1	ATP-dependent RNA helicase DDX3X isoform 3	4	1,687,881	4.6
CCT4	NP_001243650.1	T-complex protein 1 subunit delta isoform b	7	1,658,264	5.0
ITGB1	NP_596867.1	integrin beta-1 isoform 1A precursor	3	1,584,995	*
ACTR1B	NP_005726.1	beta-centractin	2	1,573,546	6.3
RAD50	NP_005723.2	DNA repair protein RAD50	2	1,560,071	3.8
NONO	NP_001138882.1	non-POU domain-containing octamer-binding protein isoform 2	2	1,472,456	4.0
TIMM44	NP_006342.2	mitochondrial import inner membrane translocase subunit TIM44	2	1,452,132	3.1
EIF4B	NP_001408.2	eukaryotic translation initiation factor 4B	2	1,379,524	1.7
ACADM	NP_000007.1	medium-chain specific acyl-CoA dehydrogenase, mitochondrial isoform a precursor	6	1,359,632	32.2
DDX5	NP_004387.1	probable ATP-dependent RNA helicase DDX5	3	1,358,560	4.2
ATP1B3	NP_001670.1	sodium/potassium-transporting ATPase subunit beta-3	2	1,289,924	8.0
HNRNPC	NP_004491.2	heterogeneous nuclear ribonucleoproteins C1/C2 isoform b	2	1,286,731	*
PFKFB3	NP_001138915.1	6-phosphofructo-2-kinase/fructose-2, 6-bisphosphatase 3 isoform 2	4	1,282,344	1.9
MFN1	NP_284941.2	mitofusin-1	2	1,249,701	*
PSMD2	NP_002799.3	26S proteasome non-ATPase regulatory subunit 2	2	1,082,536	*
GCN1L1	NP_006827.1	translational activator GCN1	10	1,068,272	14.2
FAM127B	NP_001071640.1	protein FAM127B isoform 1	2	976,285	*
MDC1	NP_055456.2	mediator of DNA damage checkpoint protein 1	2	971,976	7.8

UBQLN1…

Gene	Accession	Protein name	Peptides	Intensity	SILAC Ratio
EIF3G	NP_003746.2	eukaryotic translation initiation factor 3 subunit G	2	950,124	7.8
SERBP1	NP_056455.3	plasminogen activator inhibitor 1 RNA-binding protein isoform 4	2	904,494	*
MCM6	NP_005906.2	DNA replication licensing factor MCM6	2	884,125	*
DNAJA1	NP_001530.1	dnaJ homolog subfamily A member 1	3	708,480	*
ZMYM4	NP_005086.2	zinc finger MYM-type protein 4	2	669,707	*
CDC5L	NP_001244.1	cell division cycle 5-like protein	2	741,057	*
IGF2R	NP_000867.2	cation-independent mannose-6-phosphate receptor precursor	2	693,877	*
AGPAT2	NP_001012745.1	1-acyl-sn-glycerol-3-phosphate acyltransferase beta isoform b precursor	2	637,216	*
IBTK	NP_056340.2	inhibitor of Bruton tyrosine kinase	2	555,839	*
NCL	NP_005372.2	nucleolin	2	405,056	*
ACIN1	NP_001158289.1	apoptotic chromatin condensation inducer in the nucleus isoform 5	2	346,494	*
MARS	NP_004981.2	methionine--tRNA ligase, cytoplasmic	2	272,846	*
CXADR	NP_001329.1	coxsackievirus and adenovirus receptor isoform 1 precursor	2	262,475	*
RPL31	NP_001093163.1	60S ribosomal protein L31 isoform 3	2	230,987	*
PLXNA1	NP_115618.3	plexin-A1 precursor	2	797,911	*
FASN	NP_004095.4	fatty acid synthase	2	794,076	1.9
PIGR	NP_002635.2	polymeric immunoglobulin receptor precursor	2	1,034,165	*
TMEM132A	NP_821174.1	transmembrane protein 132A isoform b precursor	2	1,019,924	*
TGFBR1	NP_001124388.1	TGF-beta receptor type-1 isoform 2 precursor	3	1,236,160	*
LOC100287515	XP_003846501.1	zinc finger protein 26-like	2	1,234,118	*
BBC3	NP_001120713.1	bcl-2-binding component 3 isoform 2	2	1,178,025	*
CHST14	NP_569735.1	carbohydrate sulfotransferase 14	2	1,163,866	*
SLC30A7	NP_598003.2	zinc transporter 7	2	1,153,897	*
GMPS	NP_003866.1	GMP synthase [glutamine-hydrolyzing]	2	1,790,316	*
RPL18A	NP_000971.1	60S ribosomal protein L18a	2	1,738,743	*
PTPLAD1	NP_057479.2	very-long-chain (3R)-3-hydroxyacyl-[acyl-carrier protein] dehydratase 3	2	1,698,420	*
CDKAL1	NP_060244.2	threonylcarbamoyladenosine tRNA methylthiotransferase	2	1,695,050	*
SERPINE2	NP_001130000.1	glia-derived nexin isoform b precursor	5	1,689,542	*
MAGOH	NP_002361.1	protein mago nashi homolog	2	1,684,867	*
CTNNA1	NP_001894.2	catenin alpha-1	5	1,680,443	1.5

UBQLN1…

Gene	Accession	Protein name	Peptides	Intensity	SILAC Ratio
SPTLC1	NP_847894.1	serine palmitoyltransferase 1 isoform b	2	1,677,314	*
TOP2A	NP_001058.2	DNA topoisomerase 2-alpha	2	1,650,326	*
HRAS	NP_789765.1	GTPase HRas isoform 2	2	1,616,774	*
SAAL1	NP_612430.2	protein SAAL1	2	1,615,444	*
GPAA1	NP_003792.1	glycosylphosphatidylinositol anchor attachment 1 protein	2	1,613,078	*
BPIFB1	NP_149974.2	BPI fold-containing family B member 1 precursor	4	1,605,502	*
FANCD2	NP_001018125.1	Fanconi anemia group D2 protein isoform b	2	1,602,002	*
ETFDH	NP_004444.2	electron transfer flavoprotein-ubiquinone oxidoreductase, mitochondrial precursor	2	1,526,835	*
ADPGK	NP_112574.3	ADP-dependent glucokinase precursor	2	1,511,138	*
PPP2R1A	NP_055040.2	serine/threonine-protein phosphatase 2A 65 kDa regulatory subunit A alpha isoform	2	1,501,161	*
RIOK1	NP_694550.1	serine/threonine-protein kinase RIO1 isoform 2	2	1,484,595	*
CLMN	NP_079010.2	calmin	2	1,475,600	*
BAZ1B	NP_115784.1	tyrosine-protein kinase BAZ1B	2	1,993,228	*
COL1A1	NP_000079.2	collagen alpha-1(I) chain preproprotein	2	1,968,663	*
FNDC3A	NP_055738.3	fibronectin type-III domain-containing protein 3A isoform 2	2	1,945,676	*
POLR2B	NP_000929.1	DNA-directed RNA polymerase II subunit RPB2	2	1,350,490	*
THEM6	NP_057731.1	protein THEM6 precursor	3	1,346,081	*
RPL27	NP_000979.1	60S ribosomal protein L27	2	1,334,148	*
TOR1AIP1	NP_056417.2	torsin-1A-interacting protein 1 isoform 2	2	1,298,814	*
H1F0	NP_005309.1	histone H1.0	2	1,293,987	*
CCDC47	NP_064583.2	coiled-coil domain-containing protein 47 precursor	4	1,447,419	*
TBX2	NP_005985.3	T-box transcription factor TBX2	4	1,419,992	*
KTN1	NP_004977.2	kinectin isoform c	3	1,406,440	*
UBAC2	NP_808882.1	ubiquitin-associated domain-containing protein 2 isoform 2	2	1,398,200	*

Only proteins with more than 1 peptide were included unless the protein was clearly part of a marked complex. Protein and peptide false discovery rates were set at 1% for the Proteome Discoverer database search. Proteins were sorted by intensity. Gene is the gene name. Blue text indicates proteins identified in the SG proteome. Orange text indicates SG proteome proteins that are hnRNPs. Peptides are the peptide spectrum matched hits. Intensity is the total integrated precursor ion peak density. SILAC ratio is the average HEAVY (UBQLN2)/LIGHT (Control) peptide ratio. * indicates a corresponding light peptide was not automatically identified by the search software. Red bars indicate proteins identified in this study. Orange bars indicate proteins identified in previous studies. A total of 289 proteins were identified in this analysis.

Table A-3 Table of UBQLN4 associated proteins identified by SILAC nLC-MS/MS

Gene	Accession	Protein name	Peptides	Intensity	Ratio
UBQLN4	NP_064516.2	ubiquilin-4	999	12,265,099,179	33.8
UBQLN1	NP_444295.1	ubiquilin-1 isoform 2	249	9,236,254,576	*
ALDH3A2	NP_000373.1	fatty aldehyde dehydrogenase isoform 2	211	878,564,638	44.6
PRMT5	NP_006100.2	protein arginine N-methyltransferase 5 isoform a	261	696,653,112	2.3
TUBA1A	NP_001257329.1	tubulin alpha-1A chain isoform 2	124	600,033,598	29.9
TUBB	NP_821133.1	tubulin beta chain	249	510,530,537	12.4
TUBB4B	NP_006079.1	tubulin beta-4B chain	221	427,364,998	24.0
TUBB4A	NP_006078.2	tubulin beta-4A chain	173	410,949,268	*
TUBB2A	NP_001060.1	tubulin beta-2A chain	193	348,209,029	*
TUBB2B	NP_821080.1	tubulin beta-2B chain	193	348,209,029	*
HSPA8	NP_006588.1	heat shock cognate 71 kDa protein isoform 1	184	253,487,412	22.8
ATP5B	NP_001677.2	ATP synthase subunit beta, mitochondrial precursor	112	244,634,339	20.6
EEF1A1	NP_001393.1	elongation factor 1-alpha 1	106	240,822,394	12.0
BSG	NP_940991.1	basigin isoform 2	27	224,158,719	33.0
SLC25A5	NP_001143.2	ADP/ATP translocase 2	103	203,386,835	21.2
SGK196	NP_115613.1	probable inactive protein kinase-like protein SgK196	54	195,969,868	42.3
TUBB6	NP_115914.1	tubulin beta-6 chain	92	187,617,808	36.4
HSPA1A	NP_005336.3	heat shock 70 kDa protein 1A/1B	110	180,826,337	17.9
SLC25A6	NP_001627.2	ADP/ATP translocase 3	79	165,436,666	17.7
ATP5A1	NP_001001937.1	ATP synthase subunit alpha, mitochondrial isoform a precursor	109	161,845,193	24.2
SLC25A4	NP_001142.2	ADP/ATP translocase 1	70	159,781,335	*
ILVBL	NP_006835.2	acetolactate synthase-like protein	80	130,893,848	42.0
RTN4	NP_722550.1	reticulon-4 isoform B	15	104,776,292	27.4
RPS27A	NP_001129064.1	ubiquitin-40S ribosomal protein S27a precursor=UBA52	320	97,095,355	25.1
SSBP1	NP_001243439.1	single-stranded DNA-binding protein, mitochondrial precursor	30	93,832,311	17.6
DDOST	NP_005207.2	dolichyl-diphosphooligosaccharide--protein glycosyltransferase 48 kDa subunit precursor	38	85,088,366	26.0
CROCC	NP_055490.3	rootletin	3	77,784,882	*
COX5A	NP_004246.2	cytochrome c oxidase subunit 5A, mitochondrial precursor	32	74,552,837	34.2
PGRMC2	NP_006311.2	membrane-associated progesterone receptor component 2	66	70,071,223	37.3
PSMD4	NP_002801.1	26S proteasome non-ATPase regulatory subunit 4	35	62,518,723	35.0
RPS18	NP_072045.1	40S ribosomal protein S18	48	57,117,491	6.1
CANX	NP_001737.1	calnexin precursor	45	55,936,078	32.0
PPM1B	NP_002697.1	protein phosphatase 1B isoform 1	62	54,786,810	14.4

UBQLN4…

	Gene	Accession	Protein name	Peptides	Intensity	Ratio
	VIM	NP_003371.2	vimentin	149	51,228,342	9.2
	SRPRB	NP_067026.3	signal recognition particle receptor subunit beta	32	50,600,885	34.3
	RUVBL1	NP_003698.1	ruvB-like 1	41	49,426,661	22.3
	UBQLN2	NP_038472.2	ubiquilin-2	110	48,481,757	16.9
	LRP6	NP_002327.2	low-density lipoprotein receptor-related protein 6 precursor	2	47,660,212	*
	HSPA9	NP_004125.3	stress-70 protein, mitochondrial precursor	68	46,895,126	9.4
	RUVBL2	NP_006657.1	ruvB-like 2	69	43,992,314	23.8
	HADHA	NP_000173.2	trifunctional enzyme subunit alpha, mitochondrial precursor	6	40,555,041	*
	HSPA13	NP_008879.3	heat shock 70 kDa protein 13 precursor	32	38,638,833	36.7
	UBQLN3	NP_059509.1	ubiquilin-3	6	37,744,268	*
	XRCC6	NP_001460.1	X-ray repair cross-complementing protein 6	31	37,241,513	11.0
	PHB	NP_002625.1	prohibitin	60	36,626,028	8.7
	TMPO	NP_001027454.1	thymopoietin isoform beta	71	35,882,630	4.6
	HSPD1	NP_002147.2	60 kDa heat shock protein, mitochondrial	75	30,892,294	9.5
	LMAN1	NP_005561.1	protein ERGIC-53 precursor	22	30,598,064	28.2
	APMAP	NP_065392.1	adipocyte plasma membrane-associated protein	24	27,997,910	28.4
	DESI1	NP_056519.1	desumoylating isopeptidase 1	3	27,576,818	48.9
	HSD17B12	NP_057226.1	estradiol 17-beta-dehydrogenase 12	27	25,961,357	41.3
	HNRNPU	NP_114032.2	heterogeneous nuclear ribonucleoprotein U isoform a	137	25,961,062	11.7
	CCT7	NP_006420.1	T-complex protein 1 subunit eta isoform a	69	25,090,552	28.8
	PSMA5	NP_002781.2	proteasome subunit alpha type-5 isoform 1	23	24,936,883	6.5
	CYP51A1	NP_001139624.1	lanosterol 14-alpha demethylase isoform 2	22	24,315,419	33.9
	WDR77	NP_077007.1	methylosome protein 50	53	24,112,350	1.6
	B3GNT1	NP_006867.1	N-acetyllactosaminide beta-1,3-N-acetylglucosaminyltransferase	25	24,061,034	42.9
	GPX8	NP_001008398.2	probable glutathione peroxidase 8	26	23,446,373	40.9
	TMPO	NP_003267.1	thymopoietin isoform alpha	43	21,503,973	25.5
	JTB	NP_006685.1	protein JTB precursor	8	21,283,575	40.9
	ATL3	NP_056274.3	atlastin-3	27	20,957,768	41.3
	ATP5D	NP_001678.1	ATP synthase subunit delta, mitochondrial precursor	8	20,888,193	*
	KCTD5	NP_061865.1	BTB/POZ domain-containing protein KCTD5	11	20,558,071	8.1
	ACSL3	NP_004448.2	long-chain-fatty-acid--CoA ligase 3	26	20,112,711	*
	HNRNPH1	NP_005511.1	heterogeneous nuclear ribonucleoprotein H	15	19,896,168	5.5
	CYP2R1	NP_078790.2	vitamin D 25-hydroxylase	2	19,172,310	*

UBQLN4…

Gene	Accession	Protein name	Peptides	Intensity	Ratio
NIPSNAP1	NP_001189431.1	protein NipSnap homolog 1 isoform 2	22	18,935,926	14.7
ATP1A1	NP_001153706.1	sodium/potassium-transporting ATPase subunit alpha-1 isoform d	72	18,416,828	37.1
COL14A1	NP_066933.1	collagen alpha-1(XIV) chain precursor	10	18,344,261	*
ENPP1	NP_006199.2	ectonucleotide pyrophosphatase/phosphodiesterase family member 1	26	18,279,118	49.2
CYB5A	NP_001905.1	cytochrome b5 isoform 2	2	18,278,104	44.3
XRCC5	NP_066964.1	X-ray repair cross-complementing protein 5	47	17,797,045	19.9
GOLGA3	NP_001166028.1	Golgin subfamily A member 3 isoform 2	24	17,580,325	*
RPL10A	NP_009035.3	60S ribosomal protein L10a	5	17,054,620	3.2
COX4I1	NP_001852.1	cytochrome c oxidase subunit 4 isoform 1, mitochondrial precursor	14	16,740,282	25.2
MOGS	NP_006293.2	mannosyl-oligosaccharide glucosidase isoform 1	31	16,715,502	36.0
CENPE	NP_001804.2	centromere-associated protein E	4	16,415,994	*
CHPT1	NP_064629.2	cholinephosphotransferase 1	2	15,901,853	36.3
CD320	NP_001159367.1	CD320 antigen isoform 2 precursor	36	15,550,847	19.6
CCT4	NP_006421.2	T-complex protein 1 subunit delta isoform a	47	15,475,755	20.8
COMT	NP_009294.1	catechol O-methyltransferase isoform S-COMT	6	14,557,316	29.0
SIGMAR1	NP_671513.1	sigma non-opioid intracellular receptor 1 isoform 2	5	14,417,517	15.8
BNIP1	NP_001196.2	vesicle transport protein SEC20 isoform BNIP1	20	14,364,283	34.7
RPS5	NP_001000.2	40S ribosomal protein S5	24	14,329,949	7.3
GBAS	NP_001474.1	protein NipSnap homolog 2 isoform 1	19	14,006,533	9.7
MYH9	NP_002464.1	myosin-9	79	13,946,803	1.5
LOC101060453	XP_003960578.1	fatty acid-binding protein, epidermal-like	6	13,842,703	*
ESYT2	NP_065779.1	extended synaptotagmin-2	28	13,838,452	39.0
UBIAD1	NP_037451.1	ubiA prenyltransferase domain-containing protein 1	17	13,631,830	39.7
INSR	NP_001073285.1	insulin receptor isoform Short preproprotein	34	13,433,903	45.5
GET4	NP_057033.2	Golgi to ER traffic protein 4 homolog	3	13,159,561	38.4
SNRPD2	NP_004588.1	small nuclear ribonucleoprotein Sm D2 isoform 1	4	12,455,213	2.3
TMX1	NP_110382.3	thioredoxin-related transmembrane protein 1 precursor	16	12,419,587	27.8
UBL4A	NP_055050.1	ubiquitin-like protein 4A	12	12,071,042	*
ELANE	NP_001963.1	neutrophil elastase preproprotein	12	12,015,240	*

UBQLN4…

###	Gene	Accession	Protein name	Peptides	Intensity	Ratio
	TSPAN3	NP_001161884.1	tetraspanin-3 isoform 3	2	11,941,421	14.7
	PHGDH	NP_006614.2	D-3-phosphoglycerate dehydrogenase	38	11,933,629	24.6
	ZNF622	NP_219482.1	zinc finger protein 622	2	11,619,221	3.2
	RPS19	NP_001013.1	40S ribosomal protein S19	11	11,511,914	5.6
	STK38	NP_009202.1	serine/threonine-protein kinase 38	17	11,393,473	6.0
	VKORC1L1	NP_775788.2	vitamin K epoxide reductase complex subunit 1-like protein 1	4	11,164,414	42.2
	PSMA6	NP_002782.1	proteasome subunit alpha type-6	28	11,120,482	4.4
	CFL1	NP_005498.1	cofilin-1	14	10,802,909	2.3
	PSMA3	NP_687033.1	proteasome subunit alpha type-3 isoform 2	23	10,622,791	3.7
	PSMC4	NP_694546.1	26S protease regulatory subunit 6B isoform 2	12	10,591,618	24.9
	NAP1L1	NP_004528.1	nucleosome assembly protein 1-like 1	6	10,163,414	*
	PCYOX1	NP_057381.3	prenylcysteine oxidase 1 precursor	12	9,949,536	27.1
	NUP210	NP_079199.2	nuclear pore membrane glycoprotein 210 precursor	34	9,943,088	35.8
	TMEM9	NP_057540.1	transmembrane protein 9 precursor	20	9,937,456	41.2
	ERH	NP_004441.1	enhancer of rudimentary homolog	15	9,888,875	2.1
	SURF4	NP_149351.1	surfeit locus protein 4	16	9,711,653	57.3
	PSMC2	NP_002794.1	26S protease regulatory subunit 7 isoform 1	17	9,693,260	34.3
	ERGIC3	NP_057050.1	endoplasmic reticulum-Golgi intermediate compartment protein 3 isoform b	12	9,649,457	31.6
	KIAA1467	NP_065904.1	uncharacterized protein KIAA1467	20	9,593,174	52.9
	DMBT1	NP_060049.2	deleted in malignant brain tumors 1 protein isoform c precursor	4	9,473,327	*
	CDSN	NP_001255.3	corneodesmosin precursor	4	9,460,397	*
	NGLY1	NP_001138767.1	peptide-N(4)-(N-acetyl-beta-glucosaminyl)asparagine amidase isoform 4	10	9,444,537	*
	BCLAF1	NP_001070908.1	bcl-2-associated transcription factor 1 isoform 2	58	9,373,942	7.7
	CCT5	NP_036205.1	T-complex protein 1 subunit epsilon	26	9,301,113	3.8
	S100A8	NP_002955.2	protein S100-A8	14	9,294,132	*
	PSMA4	NP_002780.1	proteasome subunit alpha type-4 isoform 1	19	9,185,475	3.3
	DHCR24	NP_055577.1	delta(24)-sterol reductase precursor	14	9,089,530	44.2
	CTNS	NP_004928.2	cystinosin isoform 2 precursor	5	9,086,485	*
	LMNB1	NP_005564.1	lamin-B1 isoform 1	19	8,962,864	5.9
	POLR2H	NP_006223.2	DNA-directed RNA polymerases I, II, and III subunit RPABC3	4	8,868,673	25.9

UBQLN4…

Gene	Accession	Protein name	Peptides	Intensity	Ratio
TMX3	NP_061895.3	protein disulfide-isomerase TMX3 precursor	8	8,838,083	42.7
SNRPB	NP_003082.1	small nuclear ribonucleoprotein-associated proteins B and B' isoform B	17	8,745,331	1.9
YWHAZ	NP_003397.1	14-3-3 protein zeta/delta	37	8,724,986	1.8
SYNGR1	NP_663783.1	synaptogyrin-1 isoform 1b	2	8,638,878	40.2
PSMA7	NP_002783.1	proteasome subunit alpha type-7	14	8,571,548	4.8
RPN1	NP_002941.1	dolichyl-diphosphooligosaccharide--protein glycosyltransferase subunit 1 precursor	28	8,483,175	11.3
SRP54	NP_003127.1	signal recognition particle 54 kDa protein isoform 1	11	8,306,498	22.2
SERBP1	NP_056455.3	plasminogen activator inhibitor 1 RNA-binding protein isoform 4	40	8,224,543	1.6
CCT3	NP_005989.3	T-complex protein 1 subunit gamma isoform a	29	8,168,658	2.8
PCCA	NP_001171475.1	propionyl-CoA carboxylase alpha chain, mitochondrial isoform c precursor	2	8,117,199	*
EEF2	NP_001952.1	elongation factor 2	38	8,063,770	5.0
RPS4X	NP_000998.1	40S ribosomal protein S4, X isoform X isoform	25	8,029,211	5.4
RAB10	NP_057215.3	ras-related protein Rab-10	9	7,942,720	33.3
RPS3	NP_001243731.1	40S ribosomal protein S3 isoform 1	27	7,858,748	8.8
SEC61B	NP_006799.1	protein transport protein Sec61 subunit beta	6	7,841,422	*
SPCS2	NP_055567.2	signal peptidase complex subunit 2	3	7,778,377	9.0
PGRMC1	NP_006658.1	membrane-associated progesterone receptor component 1	18	7,748,049	31.9
SLC25A11	NP_001158890.1	mitochondrial 2-oxoglutarate/malate carrier protein isoform 3	4	7,735,390	48.6
CCT2	NP_001185771.1	T-complex protein 1 subunit beta isoform 2	26	7,733,345	10.1
SRPR	NP_001171313.1	signal recognition particle receptor subunit alpha isoform 2	8	7,590,978	*
CLPTM1	NP_001285.1	cleft lip and palate transmembrane protein 1	12	7,502,274	33.2
C14orf166	NP_057123.1	UPF0568 protein C14orf166	19	7,501,554	10.2
PSMB7	NP_002790.1	proteasome subunit beta type-7 proprotein	12	7,500,380	5.2
RPS9	NP_001004.2	40S ribosomal protein S9	19	7,441,320	5.9
PSMC3	NP_002795.2	26S protease regulatory subunit 6A	10	7,428,274	*
SPTLC1	NP_006406.1	serine palmitoyltransferase 1 isoform a	14	7,337,668	23.0
PPHLN1	NP_001137260.1	periphilin-1 isoform 7	6	7,226,268	5.6
UQCRC1	NP_003356.2	cytochrome b-c1 complex subunit 1, mitochondrial precursor	16	7,049,039	12.0

UBQLN4…

###	Gene	Accession	Protein name	Peptides	Intensity	Ratio
	RTCB	NP_055121.1	tRNA-splicing ligase RtcB homolog	23	6,990,097	10.7
	HAL	NP_001245263.1	histidine ammonia-lyase isoform 3	5	6,953,413	*
	SYS1	NP_291020.1	protein SYS1 homolog isoform a	2	6,834,028	*
	LOR	NP_000418.2	loricrin	8	6,810,220	*
	IGF1R	NP_000866.1	insulin-like growth factor 1 receptor precursor	6	6,779,164	24.8
	PSMD2	NP_002799.3	26S proteasome non-ATPase regulatory subunit 2	21	6,715,617	3.4
	RPN2	NP_002942.2	dolichyl-diphosphooligosaccharide--protein glycosyltransferase subunit 2 isoform 1 precursor	16	6,700,806	36.6
	MTMR11	NP_870988.2	myotubularin-related protein 11 isoform b	2	6,698,175	*
	TOR1AIP2	NP_659471.1	torsin-1A-interacting protein 2 isoform b	8	6,375,276	36.5
	RTN3	NP_006045.1	reticulon-3 isoform a	9	6,373,949	30.1
	FAM20B	NP_055679.1	glycosaminoglycan xylosylkinase	14	6,360,198	84.6
	EMD	NP_000108.1	emerin	26	6,312,588	6.9
	RAB7A	NP_004628.4	ras-related protein Rab-7a	14	6,267,977	1.5
	CASP14	NP_036246.1	caspase-14 precursor	6	6,143,468	*
	PTPLB	NP_940684.1	very-long-chain (3R)-3-hydroxyacyl-[acyl-carrier protein] dehydratase 2	2	6,102,677	15.8
	SACM1L	NP_054735.3	phosphatidylinositide phosphatase SAC1	3	6,039,957	24.9
	INA	NP_116116.1	alpha-internexin	8	6,013,918	3.9
	TGM3	NP_003236.3	protein-glutamine gamma-glutamyltransferase E	24	5,861,565	*
	EIF3E	NP_001559.1	eukaryotic translation initiation factor 3 subunit E	18	5,606,517	9.5
	LPCAT1	NP_079106.3	lysophosphatidylcholine acyltransferase 1	7	5,580,369	*
	ADPGK	NP_112574.3	ADP-dependent glucokinase precursor	6	5,512,495	27.8
	NONO	NP_031389.3	non-POU domain-containing octamer-binding protein isoform 1	27	5,434,759	7.8
	TPD52	NP_005070.1	tumor protein D52 isoform 3	5	5,361,826	29.8
	TECR	NP_612510.1	very-long-chain enoyl-CoA reductase	15	5,342,189	15.8
	FBXW11	NP_387449.2	F-box/WD repeat-containing protein 11 isoform A	10	5,338,306	12.6
	HNRNPF	NP_004957.1	heterogeneous nuclear ribonucleoprotein F	10	5,322,380	10.7
	CYB5B	NP_085056.2	cytochrome b5 type B	2	5,303,989	63.8
	BPIFB1	NP_149974.2	BPI fold-containing family B member 1 precursor	8	5,302,573	*
	LAMP1	NP_005552.3	lysosome-associated membrane glycoprotein 1 precursor	8	5,293,087	*
	DEFA1B	NP_001035965.1	neutrophil defensin 1 precursor	4	5,265,455	*

UBQLN4…

Gene	Accession	Protein name	Peptides	Intensity	Ratio
COX5B	NP_001853.2	cytochrome c oxidase subunit 5B, mitochondrial precursor	4	5,240,323	*
LGALS7B	NP_001035972.1	galectin-7	28	5,217,975	*
RBBP4	NP_001128727.1	histone-binding protein RBBP4 isoform b	13	5,196,123	7.3
ARL6IP1	NP_055976.1	ADP-ribosylation factor-like protein 6-interacting protein 1	4	5,180,588	36.3
PHB2	NP_001138303.1	prohibitin-2 isoform 1	8	5,164,569	10.1
VAT1	NP_006364.2	synaptic vesicle membrane protein VAT-1 homolog	17	5,156,357	16.5
CPT2	NP_000089.1	carnitine O-palmitoyltransferase 2, mitochondrial precursor	11	5,105,239	*
YWHAQ	NP_006817.1	14-3-3 protein theta	42	5,100,992	15.2
VAPB	NP_004729.1	vesicle-associated membrane protein-associated protein B/C isoform 1	19	5,093,408	31.6
SLC25A3	NP_998776.1	phosphate carrier protein, mitochondrial isoform b precursor	22	4,992,073	22.7
SDHB	NP_002991.2	succinate dehydrogenase [ubiquinone] iron-sulfur subunit, mitochondrial precursor	9	4,962,431	33.7
DCTN2	NP_001248342.1	dynactin subunit 2 isoform 3	8	4,899,823	11.4
SDHA	NP_004159.2	succinate dehydrogenase [ubiquinone] flavoprotein subunit, mitochondrial	10	4,877,438	18.8
FAF2	NP_055428.1	FAS-associated factor 2	10	4,754,437	*
BCAP31	NP_001132913.1	B-cell receptor-associated protein 31 isoform b	26	4,728,528	8.1
RBBP7	NP_002884.1	histone-binding protein RBBP7 isoform 2	10	4,695,771	8.0
RHEB	NP_005605.1	GTP-binding protein Rheb	2	4,655,396	*
PSMC1	NP_002793.2	26S protease regulatory subunit 4	10	4,638,047	5.0
DPM1	NP_003850.1	dolichol-phosphate mannosyltransferase	9	4,633,730	17.8
PAM16	NP_057153.8	mitochondrial import inner membrane translocase subunit TIM16	2	4,613,469	13.8
SPRR2B	NP_001017418.1	small proline-rich protein 2B	33	4,608,791	*
EIF2B3	NP_001248347.1	translation initiation factor eIF-2B subunit gamma isoform 3	12	4,512,557	23.9
VRK3	NP_057524.3	inactive serine/threonine-protein kinase VRK3 isoform 1	9	4,510,949	24.9
NDUFS3	NP_004542.1	NADH dehydrogenase [ubiquinone] iron-sulfur protein 3, mitochondrial precursor	4	4,506,037	18.6
ARG1	NP_000036.2	arginase-1 isoform 2	4	4,470,771	*
MTAP	NP_002442.2	S-methyl-5'-thioadenosine phosphorylase	8	4,459,219	4.6
EFNB1	NP_004420.1	ephrin-B1 precursor	6	4,396,454	63.5
TBC1D15	NP_001139685.2	TBC1 domain family member 15 isoform 3	2	4,366,299	*
CD63	NP_001244329.1	CD63 antigen isoform D precursor	2	4,360,401	20.1

UBQLN4…

Gene	Accession	Protein name	Peptides	Intensity	Ratio
KPNB1	NP_002256.2	importin subunit beta-1 isoform 1	18	4,241,667	9.8
APOD	NP_001638.1	apolipoprotein D precursor	6	4,198,501	*
YKT6	NP_006546.1	synaptobrevin homolog YKT6	2	4,184,975	*
HSD17B10	NP_004484.1	3-hydroxyacyl-CoA dehydrogenase type-2 isoform 1	10	4,175,952	22.8
UBE2J2	NP_477515.2	ubiquitin-conjugating enzyme E2 J2 isoform 2	4	4,160,528	*
TPD52L2	NP_001230821.1	tumor protein D54 isoform h	4	4,151,320	*
ADAM9	NP_003807.1	disintegrin and metalloproteinase domain-containing protein 9 precursor	4	4,090,459	*
AIFM1	NP_665811.1	apoptosis-inducing factor 1, mitochondrial isoform 2 precursor	8	4,084,090	*
TGM1	NP_000350.1	protein-glutamine gamma-glutamyltransferase K	10	4,051,795	*
RPL17	NP_001186274.1	60S ribosomal protein L17 isoform b	8	3,992,606	2.4
LPCAT3	NP_005759.4	lysophospholipid acyltransferase 5	5	3,992,043	*
BLMH	NP_000377.1	bleomycin hydrolase	5	3,973,842	*
PGM3	NP_001186847.1	phosphoacetylglucosamine mutase isoform 3	6	3,954,877	46.2
KPNA2	NP_002257.1	importin subunit alpha-2	6	3,823,181	13.2
ABCB7	NP_001258626.1	ATP-binding cassette sub-family B member 7, mitochondrial isoform 3	2	3,822,709	*
EIF3F	NP_003745.1	eukaryotic translation initiation factor 3 subunit F	18	3,790,241	8.1
SLC25A10	NP_036272.2	mitochondrial dicarboxylate carrier isoform 2	6	3,785,996	17.6
UBXN4	NP_055422.1	UBX domain-containing protein 4	10	3,785,341	*
UMPS	NP_000364.1	uridine 5'-monophosphate synthase	9	3,785,090	10.5
PSMA1	NP_002777.1	proteasome subunit alpha type-1 isoform 2	10	3,777,622	5.0
CDK1	NP_203698.1	cyclin-dependent kinase 1 isoform 2	6	3,723,973	65.4
CALML5	NP_059118.2	calmodulin-like protein 5	2	3,709,612	*
PYCRL	NP_075566.2	pyrroline-5-carboxylate reductase 3	8	3,690,341	20.8
EIF4A3	NP_055555.1	eukaryotic initiation factor 4A-III	20	3,680,947	2.3
SLC3A2	NP_001013269.1	4F2 cell-surface antigen heavy chain isoform f	17	3,651,460	47.8
IGJ	NP_653247.1	immunoglobulin J chain precursor	9	3,644,293	*
LMNB2	NP_116126.3	lamin-B2	7	3,630,553	5.1
PSMB5	NP_001124197.1	proteasome subunit beta type-5 isoform 2	8	3,600,192	1.6
RPL30	NP_000980.1	60S ribosomal protein L30	2	3,559,107	6.2
PTPN1	NP_002818.1	tyrosine-protein phosphatase non-receptor type 1	15	3,513,788	*

UBQLN4…

Gene	Accession	Protein name	Peptides	Intensity	Ratio
PSMD12	NP_777360.1	26S proteasome non-ATPase regulatory subunit 12 isoform 2	12	3,498,070	24.7
PSMD8	NP_002803.2	26S proteasome non-ATPase regulatory subunit 8	8	3,487,743	25.5
LTF	NP_001186078.1	lactotransferrin isoform 2	13	3,464,281	*
PRDX6	NP_004896.1	peroxiredoxin-6	13	3,461,880	5.2
GTF2I	NP_001509.3	general transcription factor II-I isoform 4	20	3,434,610	12.8
LPCAT2	NP_060309.2	lysophosphatidylcholine acyltransferase 2	6	3,429,520	42.1
ALDH1B1	NP_000683.3	aldehyde dehydrogenase X, mitochondrial precursor	6	3,413,744	*
SERPINA12	NP_776249.1	serpin A12 precursor	2	3,405,400	*
CXADR	NP_001329.1	coxsackievirus and adenovirus receptor isoform 1 precursor	4	3,362,722	*
YBX1	NP_004550.2	nuclease-sensitive element-binding protein 1	14	3,360,612	1.7
AGK	NP_060708.1	acylglycerol kinase, mitochondrial precursor	2	3,357,970	22.4
COPB2	NP_004757.1	coatomer subunit beta'	10	3,356,402	35.1
NOMO2	NP_775885.1	nodal modulator 2 isoform 2 precursor	10	3,355,437	31.0
IGLL5	NP_001171597.1	immunoglobulin lambda-like polypeptide 5 isoform 1	6	3,324,964	*
NUBP2	NP_036357.1	cytosolic Fe-S cluster assembly factor NUBP2	5	3,290,008	*
ME1	NP_002386.1	NADP-dependent malic enzyme	2	3,270,656	*
MT1G	NP_005941.1	metallothionein-1G	4	3,225,870	*
SNRPB2	NP_937863.1	U2 small nuclear ribonucleoprotein B"	12	3,169,809	2.6
GEMIN4	NP_056536.2	gem-associated protein 4	2	3,160,408	*
SFN	NP_006133.1	14-3-3 protein sigma	16	3,154,492	*
CHCHD3	NP_060282.1	coiled-coil-helix-coiled-coil-helix domain-containing protein 3, mitochondrial precursor	13	3,150,449	9.9
KIF11	NP_004514.2	kinesin-like protein KIF11	21	3,131,237	8.2
TUFM	NP_003312.3	elongation factor Tu, mitochondrial precursor	4	3,060,744	4.0
CADM1	NP_001091987.1	cell adhesion molecule 1 isoform 2 precursor	6	3,046,328	44.3
PIGR	NP_002635.2	polymeric immunoglobulin receptor precursor	14	3,040,489	*
GAA	NP_000143.2	lysosomal alpha-glucosidase preproprotein	2	3,003,548	*
GLUD2	NP_036216.2	glutamate dehydrogenase 2, mitochondrial precursor	2	2,997,476	*
PFKFB3	NP_001138915.1	6-phosphofructo-2-kinase/fructose-2, 6-bisphosphatase 3 isoform 2	8	2,997,199	9.8
XRCC1	NP_006288.2	DNA repair protein XRCC1	4	2,993,191	12.7
DDX1	NP_004930.1	ATP-dependent RNA helicase DDX1	16	2,969,709	3.6
ACSL1	NP_001986.2	long-chain-fatty-acid--CoA ligase 1	2	2,961,544	*

UBQLN4…

Gene	Accession	Protein name	Peptides	Intensity	Ratio
GNB4	NP_067642.1	guanine nucleotide-binding protein subunit beta-4	2	2,955,743	32.5
CASP6	NP_116787.1	caspase-6 isoform beta	2	2,929,913	1.8
CMBL	NP_620164.1	carboxymethylenebutenolidase homolog	4	2,925,413	3.9
SFXN1	NP_073591.2	sideroflexin-1	4	2,915,349	48.8
VIMP	NP_060915.2	selenoprotein S	2	2,864,976	*
SEC61A2	NP_001136099.1	protein transport protein Sec61 subunit alpha isoform 2 isoform c	7	2,850,968	12.4
MARS	NP_004981.2	methionine--tRNA ligase, cytoplasmic	8	2,832,721	33.7
THRAP3	NP_005110.2	thyroid hormone receptor-associated protein 3	21	2,828,342	4.3
PRPF19	NP_055317.1	pre-mRNA-processing factor 19	6	2,825,671	2.2
DNAJA2	NP_005871.1	dnaJ homolog subfamily A member 2	6	2,801,144	17.5
TMX2	NP_001137484.1	thioredoxin-related transmembrane protein 2 isoform 2	4	2,763,227	*
BAG6	NP_001186626.1	large proline-rich protein BAG6 isoform c	7	2,748,888	35.4
RPL7	NP_000962.2	60S ribosomal protein L7	10	2,745,159	6.8
CLCC1	NP_001265132.1	chloride channel CLIC-like protein 1 isoform 4 precursor	10	2,743,653	*
NCLN	NP_064555.2	nicalin precursor	10	2,739,175	11.1
NDUFAF3	NP_951033.1	NADH dehydrogenase [ubiquinone] 1 alpha subcomplex assembly factor 3 isoform b	2	2,708,423	9.7
FDFT1	NP_004453.3	squalene synthase	6	2,700,627	*
OXNAD1	NP_612390.1	oxidoreductase NAD-binding domain-containing protein 1 precursor	4	2,695,366	*
RPL31	NP_001093163.1	60S ribosomal protein L31 isoform 3	2	2,690,805	*
ARL6IP5	NP_006398.1	PRA1 family protein 3	2	2,653,974	*
HERPUD1	NP_001259032.1	homocysteine-responsive endoplasmic reticulum-resident ubiquitin-like domain member 1 protein isoform 4	6	2,618,938	76.6
TRIM21	NP_003132.2	E3 ubiquitin-protein ligase TRIM21	10	2,605,038	7.1
UFSP2	NP_060829.2	ufm1-specific protease 2	2	2,596,652	*
TFRC	NP_003225.2	transferrin receptor protein 1	10	2,596,089	28.7
FUS	NP_001164408.1	RNA-binding protein FUS isoform 3	7	2,578,978	4.3
SSB	NP_003133.1	lupus La protein	8	2,575,790	4.5
HSPA4L	NP_055093.2	heat shock 70 kDa protein 4L	3	2,570,329	*
ATRAID	NP_057169.2	all-trans retinoic acid-induced differentiation factor isoform a	2	2,550,591	*
DNAJB6	NP_005485.1	dnaJ homolog subfamily B member 6 isoform b	8	2,536,719	*
RAB14	NP_057406.2	ras-related protein Rab-14	4	2,527,152	35.2

UBQLN4…

Gene	Accession	Protein name	Peptides	Intensity	Ratio
RPA1	NP_002936.1	replication protein A 70 kDa DNA-binding subunit	5	2,527,025	18.8
DDX3X	NP_001180346.1	ATP-dependent RNA helicase DDX3X isoform 3	8	2,516,157	11.6
ATP5H	NP_006347.1	ATP synthase subunit d, mitochondrial isoform a	6	2,473,466	26.4
EDF1	NP_694880.1	endothelial differentiation-related factor 1 isoform beta	2	2,468,841	3.8
SCO2	NP_001162580.1	protein SCO2 homolog, mitochondrial precursor	8	2,448,974	15.1
CDH2	NP_001783.2	cadherin-2 preproprotein	2	2,441,173	*
SNRPA	NP_004587.1	U1 small nuclear ribonucleoprotein A	10	2,439,989	6.2
RAB32	NP_006825.1	ras-related protein Rab-32	6	2,411,307	3.7
SEC62	NP_003253.1	translocation protein SEC62	2	2,392,672	*
COPG2	NP_036265.3	coatomer subunit gamma-2	8	2,384,936	*
LOC101060541	XP_003960226.1	RNA-binding protein 8A-like isoform 1	3	2,382,919	2.2
HEATR2	NP_060272.3	HEAT repeat-containing protein 2	10	2,374,657	7.5
IDI2	NP_150286.1	isopentenyl-diphosphate Delta-isomerase 2	2	2,365,235	*
SMPDL3B	NP_055289.2	acid sphingomyelinase-like phosphodiesterase 3b isoform 1 precursor	2	2,360,323	33.9
MAGT1	NP_115497.4	magnesium transporter protein 1	6	2,358,292	*
PSMD1	NP_001177966.1	26S proteasome non-ATPase regulatory subunit 1 isoform 2	10	2,357,334	30.5
EIF3L	NP_057175.1	eukaryotic translation initiation factor 3 subunit L isoform 1	6	2,351,826	9.2
DDB1	NP_001914.3	DNA damage-binding protein 1	12	2,349,674	6.4
TMEM33	NP_060596.2	transmembrane protein 33	2	2,347,001	94.6
SERPINB8	NP_001027018.1	serpin B8 isoform b	2	2,318,941	*
LOC101060578	XP_003960503.1	COBW domain-containing protein 5-like	2	2,318,397	*
RPL35	NP_009140.1	60S ribosomal protein L35	2	2,314,143	6.2
CYC1	NP_001907.2	cytochrome c1, heme protein, mitochondrial	2	2,311,201	58.6
PRDX2	NP_005800.3	peroxiredoxin-2	8	2,311,195	1.8
TMEM209	NP_116231.2	transmembrane protein 209	3	2,304,225	*
PRDX1	NP_859048.1	peroxiredoxin-1	14	2,290,139	3.2
ALG1	NP_061982.3	chitobiosyldiphosphodolichol beta-mannosyltransferase	4	2,282,316	10.2
DLD	NP_000099.2	dihydrolipoyl dehydrogenase, mitochondrial precursor	4	2,253,354	*
NDUFB11	NP_001129470.1	NADH dehydrogenase [ubiquinone] 1 beta subcomplex subunit 11, mitochondrial isoform 2	4	2,244,452	14.2
CPVL	NP_112601.3	probable serine carboxypeptidase CPVL precursor	2	2,241,983	*
COL1A2	NP_000080.2	collagen alpha-2(I) chain precursor	9	2,237,493	*

UBQLN4…

Gene	Accession	Protein name	Peptides	Intensity	Ratio
FKBP8	NP_036313.3	peptidyl-prolyl cis-trans isomerase FKBP8	12	2,229,131	10.8
TOR1AIP1	NP_056417.2	torsin-1A-interacting protein 1 isoform 2	14	2,228,679	*
ATP2A2	NP_001672.1	sarcoplasmic/endoplasmic reticulum calcium ATPase 2 isoform a	28	2,218,552	36.0
GPR107	NP_066011.2	protein GPR107 isoform 3	5	2,211,005	17.1
FAR1	NP_115604.1	fatty acyl-CoA reductase 1	6	2,207,563	*
NAMPT	NP_005737.1	nicotinamide phosphoribosyltransferase precursor	2	2,202,659	18.5
EIF4E	NP_001959.1	eukaryotic translation initiation factor 4E isoform 1	2	2,154,096	*
A2ML1	NP_653271.2	alpha-2-macroglobulin-like protein 1 precursor	2	2,148,219	*
FARSA	NP_004452.1	phenylalanine--tRNA ligase alpha subunit	5	2,137,145	18.0
TRIM28	NP_005753.1	transcription intermediary factor 1-beta	2	2,126,812	*
SLC25A15	NP_055067.1	mitochondrial ornithine transporter 1	4	2,117,641	23.9
C1orf68	NP_001019850.1	skin-specific protein 32	8	2,096,818	*
PLIN3	NP_001157661.1	perilipin-3 isoform 2	6	2,094,439	*
PDCD10	NP_665858.1	programmed cell death protein 10	2	2,084,178	*
MMGT1	NP_775741.1	membrane magnesium transporter 1 precursor	2	2,074,075	*
NUP93	NP_055484.3	nuclear pore complex protein Nup93 isoform 1	6	2,052,141	89.4
RPS7	NP_001002.1	40S ribosomal protein S7	6	2,042,348	2.4
TP53	NP_001263625.1	cellular tumor antigen p53 isoform i	4	2,033,638	6.5
PSMD3	NP_002800.2	26S proteasome non-ATPase regulatory subunit 3	8	2,023,599	25.3
CTNNB1	NP_001895.1	catenin beta-1	9	2,021,507	14.0
RAB5C	NP_958842.1	ras-related protein Rab-5C isoform a	2	2,020,646	*
COQ7	NP_001177912.1	ubiquinone biosynthesis protein COQ7 homolog isoform 2	2	2,018,133	*
TMEM164	NP_115603.2	transmembrane protein 164 isoform b	4	2,015,190	*
PFKP	NP_002618.1	6-phosphofructokinase type C isoform 1	3	1,993,617	*
LSM14A	NP_056393.2	protein LSM14 homolog A isoform b	5	1,987,975	*
RABL3	NP_776186.2	rab-like protein 3	7	1,966,061	19.4
VAMP3	NP_004772.1	vesicle-associated membrane protein 3	2	1,965,718	25.0
TM9SF3	NP_064508.3	transmembrane 9 superfamily member 3 precursor	6	1,920,456	*
POLR2E	NP_002686.2	DNA-directed RNA polymerases I, II, and III subunit RPABC1	2	1,913,497	20.6
ZFYVE27	NP_001167592.1	protrudin isoform f	2	1,905,870	*
MPO	NP_000241.1	myeloperoxidase precursor	4	1,876,290	*

UBQLN4…

Gene	Accession	Protein name	Peptides	Intensity	Ratio
PRKAR2A	NP_004148.1	cAMP-dependent protein kinase type II-alpha regulatory subunit	3	1,873,493	1.7
HNRNPUL2	NP_001073027.1	heterogeneous nuclear ribonucleoprotein U-like protein 2	6	1,867,407	6.3
PARP1	NP_001609.2	poly [ADP-ribose] polymerase 1	7	1,862,809	28.5
TMED7	NP_861974.1	transmembrane emp24 domain-containing protein 7 precursor	4	1,852,988	*
TIPIN	NP_060328.2	TIMELESS-interacting protein	2	1,844,619	2.6
CYP20A1	NP_803882.1	cytochrome P450 20A1	11	1,839,933	44.1
RAB34	NP_001138414.1	ras-related protein Rab-34 isoform 4	5	1,838,845	*
RAB12	NP_001020471.2	ras-related protein Rab-12	6	1,832,949	*
TBRG4	NP_112162.1	protein TBRG4 isoform 2	2	1,832,864	*
RPS3A	NP_000997.1	40S ribosomal protein S3a isoform 1	8	1,819,025	18.3
MCM7	NP_877577.1	DNA replication licensing factor MCM7 isoform 2	4	1,814,536	*
NDUFC2-KCTD14	NP_001190191.1	NDUFC2-KCTD14 protein isoform 3	2	1,799,464	*
ATP1B3	NP_001670.1	sodium/potassium-transporting ATPase subunit beta-3	5	1,785,430	*
TMEM230	NP_054864.3	transmembrane protein 230 isoform 2	2	1,782,227	*
AHNAK	NP_001611.1	neuroblast differentiation-associated protein AHNAK isoform 1	22	1,762,291	*
LYPLAL1	NP_620149.1	lysophospholipase-like protein 1	5	1,762,001	*
LEMD2	NP_851853.1	LEM domain-containing protein 2 isoform 1	4	1,756,739	*
ACTL6A	NP_817126.1	actin-like protein 6A isoform 2	2	1,753,009	4.6
PTDSS2	NP_110410.1	phosphatidylserine synthase 2	4	1,751,657	*
SDF4	NP_057260.2	45 kDa calcium-binding protein isoform 2 precursor	2	1,732,595	*
GNA13	NP_006563.2	guanine nucleotide-binding protein subunit alpha-13	2	1,732,095	*
NBAS	NP_056993.2	neuroblastoma-amplified sequence	2	1,731,572	*
EPHX1	NP_001129490.1	epoxide hydrolase 1 precursor	8	1,729,617	*
GBA	NP_001165282.1	glucosylceramidase isoform 2	2	1,720,060	6.4
REEP6	NP_612402.1	receptor expression-enhancing protein 6	4	1,688,926	*
OAT	NP_000265.1	ornithine aminotransferase, mitochondrial isoform 1 precursor	4	1,666,924	*
PPIL1	NP_057143.1	peptidyl-prolyl cis-trans isomerase-like 1	2	1,664,061	2.0
TXNDC15	NP_078991.3	thioredoxin domain-containing protein 15 precursor	2	1,659,630	*
COX15	NP_004367.2	cytochrome c oxidase assembly protein COX15 homolog isoform 2	2	1,648,392	*
CD151	NP_004348.2	CD151 antigen	2	1,648,349	*

UBQLN4…

	Gene	Accession	Protein name	Peptides	Intensity	Ratio
	PHF5A	NP_116147.1	PHD finger-like domain-containing protein 5A	6	1,640,308	1.6
	ZMYM3	NP_001164633.1	zinc finger MYM-type protein 3 isoform 2	2	1,607,789	*
	LSS	NP_001138909.1	lanosterol synthase isoform 3	2	1,601,908	*
	RPA2	NP_002937.1	replication protein A 32 kDa subunit	4	1,587,505	*
	GHDC	NP_001136095.1	GH3 domain-containing protein isoform 3 precursor	4	1,583,764	*
	NDUFV1	NP_001159574.1	NADH dehydrogenase [ubiquinone] flavoprotein 1, mitochondrial isoform 2 precursor	4	1,578,549	*
	PRPF31	NP_056444.3	U4/U6 small nuclear ribonucleoprotein Prp31	5	1,573,405	7.2
	LBR	NP_919424.1	lamin-B receptor	10	1,570,800	2.2
	MPDU1	NP_004861.2	mannose-P-dolichol utilization defect 1 protein	3	1,560,907	5.6
	SLC25A1	NP_005975.1	tricarboxylate transport protein, mitochondrial isoform a precursor	4	1,551,847	17.9
	RPL11	NP_000966.2	60S ribosomal protein L11 isoform 1	3	1,546,305	2.8
	LIG3	NP_002302.2	DNA ligase 3 isoform beta precursor	6	1,544,634	32.0
	PTK7	NP_690620.1	inactive tyrosine-protein kinase 7 isoform c precursor	2	1,542,499	*
	FYTTD1	NP_001011537.2	UAP56-interacting factor isoform 2	5	1,539,580	4.6
	MRPL10	NP_660298.2	39S ribosomal protein L10, mitochondrial isoform a precursor	2	1,538,966	*
	THEM6	NP_057731.1	protein THEM6 precursor	2	1,525,427	*
	HYOU1	NP_006380.1	hypoxia up-regulated protein 1 precursor	2	1,525,107	23.0
	LACRT	NP_150593.1	extracellular glycoprotein lacritin precursor	2	1,522,653	*
	NUP85	NP_079120.1	nuclear pore complex protein Nup85	2	1,509,585	*
	JAGN1	NP_115881.3	protein jagunal homolog 1	2	1,490,872	21.3
	ITGB1	NP_596867.1	integrin beta-1 isoform 1A precursor	2	1,478,618	*
	CALU	NP_001124146.1	calumenin isoform b precursor	3	1,464,837	*
	POR	NP_000932.3	NADPH--cytochrome P450 reductase	8	1,463,492	45.3
	SEC22B	NP_004883.3	vesicle-trafficking protein SEC22b precursor	12	1,455,997	7.5
	RAP2C	NP_001258115.1	ras-related protein Rap-2c isoform 1 precursor	3	1,453,325	*
	CBS	NP_000062.1	cystathionine beta-synthase	6	1,451,850	*
	RAB18	NP_001243341.1	ras-related protein Rab-18 isoform 5	3	1,444,550	26.1
	CUL3	NP_003581.1	cullin-3 isoform 1	2	1,407,604	*
	CD2BP2	NP_001230575.1	CD2 antigen cytoplasmic tail-binding protein 2	2	1,399,915	*

UBQLN4…

Gene	Accession	Protein name	Peptides	Intensity	Ratio
UGT8	NP_003351.2	2-hydroxyacylsphingosine 1-beta-galactosyltransferase precursor	2	1,398,777	*
MTA2	NP_004730.2	metastasis-associated protein MTA2	2	1,394,406	*
STARD3NL	NP_114405.1	MLN64 N-terminal domain homolog	2	1,392,639	*
LRPPRC	NP_573566.2	leucine-rich PPR motif-containing protein, mitochondrial precursor	3	1,382,791	30.3
EIF4A1	NP_001191439.1	eukaryotic initiation factor 4A-I isoform 2	4	1,371,642	15.3
ATXN10	NP_001161093.1	ataxin-10 isoform 2	4	1,371,192	*
GAR1	NP_061856.1	H/ACA ribonucleoprotein complex subunit 1	2	1,366,101	4.5
CCDC167	NP_612502.1	coiled-coil domain-containing protein 167	2	1,356,647	*
SCD	NP_005054.3	acyl-CoA desaturase	2	1,351,057	*
VPS4A	NP_037377.1	vacuolar protein sorting-associated protein 4A	2	1,329,382	37.7
TUBG1	NP_001061.2	tubulin gamma-1 chain	4	1,326,233	40.5
MAT2A	NP_005902.1	S-adenosylmethionine synthase isoform type-2	4	1,324,268	*
TMEM30A	NP_001137430.1	cell cycle control protein 50A isoform 2	2	1,318,756	*
PANK4	NP_060686.1	pantothenate kinase 4	2	1,316,739	*
CLPX	NP_006651.2	ATP-dependent Clp protease ATP-binding subunit clpX-like, mitochondrial precursor	2	1,308,891	*
EPRS	NP_004437.2	bifunctional glutamate/proline--tRNA ligase	2	1,306,204	8.6
SLC33A1	NP_004724.1	acetyl-coenzyme A transporter 1	2	1,286,248	*
CKAP4	NP_006816.2	cytoskeleton-associated protein 4	5	1,282,681	7.6
SPTLC2	NP_004854.1	serine palmitoyltransferase 2	2	1,280,886	*
ZMYM4	NP_005086.2	zinc finger MYM-type protein 4	11	1,279,354	10.6
HAT1	NP_003633.1	histone acetyltransferase type B catalytic subunit	2	1,256,903	*
DCTPP1	NP_077001.1	dCTP pyrophosphatase 1	2	1,251,824	*
PRKDC	NP_008835.5	DNA-dependent protein kinase catalytic subunit isoform 1	7	1,250,546	*
NTPCR	NP_115700.1	cancer-related nucleoside-triphosphatase	2	1,250,471	*
NDUFS7	NP_077718.3	NADH dehydrogenase [ubiquinone] iron-sulfur protein 7, mitochondrial	4	1,246,136	20.8
CDC42EP1	NP_689449.1	cdc42 effector protein 1	2	1,244,618	*
DRAP1	NP_006433.2	dr1-associated corepressor	4	1,238,665	*
RPL19	NP_000972.1	60S ribosomal protein L19	4	1,222,981	4.9
MAN1A1	NP_005898.2	mannosyl-oligosaccharide 1,2-alpha-mannosidase IA	8	1,222,367	*
SLC35A1	NP_001161870.1	CMP-sialic acid transporter isoform b	2	1,217,098	*
SAMM50	NP_056195.3	sorting and assembly machinery component 50 homolog	2	1,215,272	*
H1F0	NP_005309.1	histone H1.0	2	1,210,477	*

UBQLN4…

Gene	Accession	Protein name	Peptides	Intensity	Ratio
VAPA	NP_919415.2	vesicle-associated membrane protein-associated protein A isoform 2	2	1,204,874	10.9
CAMP	NP_004336.3	cathelicidin antimicrobial peptide preproprotein	2	1,198,281	*
ETFDH	NP_004444.2	electron transfer flavoprotein-ubiquinone oxidoreductase, mitochondrial precursor	6	1,192,015	*
SYNGR2	NP_004701.1	synaptogyrin-2	7	1,190,482	17.7
GART	NP_001129477.1	trifunctional purine biosynthetic protein adenosine-3 isoform 1	6	1,181,277	14.5
PPID	NP_005029.1	peptidyl-prolyl cis-trans isomerase D	4	1,166,983	*
RAB8A	NP_005361.2	ras-related protein Rab-8A	4	1,165,323	*
SMCR7L	NP_061881.2	mitochondrial dynamic protein MID51	4	1,162,188	*
RHOA	NP_001655.1	transforming protein RhoA precursor	4	1,156,165	*
SLC25A18	NP_113669.1	mitochondrial glutamate carrier 2	2	1,151,077	*
TADA2B	NP_689506.2	transcriptional adapter 2-beta	2	1,150,299	*
MSH2	NP_001245210.1	DNA mismatch repair protein Msh2 isoform 2	4	1,148,678	*
RAB2A	NP_001229573.1	ras-related protein Rab-2A isoform b	7	1,137,126	66.2
CHTOP	NP_001231593.1	chromatin target of PRMT1 protein isoform 3	2	1,131,060	4.4
ATP2C1	NP_001186114.1	calcium-transporting ATPase type 2C member 1 isoform 1c	2	1,125,665	*
ZMYM3	NP_963893.1	zinc finger MYM-type protein 3 isoform 1	2	1,123,749	4.0
MGAT2	NP_002399.1	alpha-1,6-mannosyl-glycoprotein 2-beta-N-acetylglucosaminyltransferase	2	1,119,565	22.2
PEPD	NP_001159529.1	xaa-Pro dipeptidase isoform 3	4	1,109,390	2.4
MMS19	NP_071757.4	MMS19 nucleotide excision repair protein homolog	2	1,096,266	*
SAAL1	NP_612430.2	protein SAAL1	4	1,090,963	25.9
SH3GL1	NP_001186873.1	endophilin-A2 isoform 3	2	1,089,768	*
RTN2	NP_996784.1	reticulon-2 isoform C	2	1,089,575	*
NXT1	NP_037380.1	NTF2-related export protein 1	2	1,089,361	*
ACLY	NP_942127.1	ATP-citrate synthase isoform 2	4	1,086,407	1.9
PI4K2A	NP_060895.1	phosphatidylinositol 4-kinase type 2-alpha	2	1,086,154	*
ELOVL4	NP_073563.1	elongation of very long chain fatty acids protein 4	2	1,083,413	*
TELO2	NP_057195.2	telomere length regulation protein TEL2 homolog	5	1,080,764	*
SPIN3	NP_001010862.2	spindlin-3	2	1,079,819	1.8
RAB6A	NP_001230647.1	ras-related protein Rab-6A isoform d	4	1,079,766	*
GM2A	NP_000396.2	ganglioside GM2 activator isoform 1 precursor	2	1,076,485	*
CSNK2B	NP_001311.3	casein kinase II subunit beta	3	1,069,248	8.8

Gene	Accession	Protein name	Peptides	Intensity	Ratio
NLGN4Y	NP_001193779.1	neuroligin-4, Y-linked isoform 3	2	1,061,612	*
NSUN2	NP_001180384.1	tRNA (cytosine(34)-C(5))-methyltransferase isoform 2	4	1,051,526	*
CD59	NP_001120695.1	CD59 glycoprotein preproprotein	2	1,048,284	7.4
ARMC6	NP_219483.1	armadillo repeat-containing protein 6 isoform 2	2	1,047,630	*
POLR2B	NP_000929.1	DNA-directed RNA polymerase II subunit RPB2	2	1,039,508	11.4
DLST	NP_001924.2	dihydrolipoyllysine-residue succinyltransferase component of 2-oxoglutarate dehydrogenase complex, mitochondrial isoform 1 precursor	4	1,027,928	4.7
VKORC1	NP_996560.1	vitamin K epoxide reductase complex subunit 1 isoform 2 precursor	6	1,023,425	*
RPS2	NP_002943.2	40S ribosomal protein S2	2	1,022,369	*
COX18	NP_776188.1	mitochondrial inner membrane protein COX18	4	1,020,943	*
MAPRE1	NP_036457.1	microtubule-associated protein RP/EB family member 1	2	1,014,788	*
SNAP23	NP_570710.1	synaptosomal-associated protein 23 isoform SNAP23B	2	1,005,053	*
ECE1	NP_001106819.1	endothelin-converting enzyme 1 isoform 4	2	1,000,531	17.5
PLXNA1	NP_115618.3	plexin-A1 precursor	2	1,000,384	*
GIGYF2	NP_001096618.1	PERQ amino acid-rich with GYF domain-containing protein 2 isoform c	2	1,000,110	3.9
GOSR1	NP_001007025.1	Golgi SNAP receptor complex member 1 isoform 3	2	999,968	*
LPCAT4	NP_705841.2	lysophospholipid acyltransferase LPCAT4	2	998,164	*
BZW1	NP_055485.2	basic leucine zipper and W2 domain-containing protein 1 isoform 4	2	994,100	*
VTI1B	NP_006361.1	vesicle transport through interaction with t-SNAREs homolog 1B	2	983,057	*
TTC27	NP_001180438.1	tetratricopeptide repeat protein 27 isoform 2	6	980,613	26.6
RAB1A	NP_004152.1	ras-related protein Rab-1A isoform 1	4	974,988	*
CDIPT	NP_006310.1	CDP-diacylglycerol--inositol 3-phosphatidyltransferase	2	971,299	*
MCM4	NP_877423.1	DNA replication licensing factor MCM4	2	969,246	*
ESYT1	NP_056107.1	extended synaptotagmin-1 isoform 2	6	965,899	*
RPS8	NP_001003.1	40S ribosomal protein S8	6	965,546	4.5
NDUFAF4	NP_054884.1	NADH dehydrogenase [ubiquinone] 1 alpha subcomplex assembly factor 4	2	964,176	*
ITGA2	NP_002194.2	integrin alpha-2 precursor	2	962,540	*

UBQLN4…

Gene	Accession	Protein name	Peptides	Intensity	Ratio
MRPL46	NP_071446.2	39S ribosomal protein L46, mitochondrial	2	961,358	3.6
ATP11B	NP_055431.1	probable phospholipid-transporting ATPase IF	2	960,629	*
ATP5F1	NP_001679.2	ATP synthase subunit b, mitochondrial precursor	2	951,956	1.5
GRWD1	NP_113673.3	glutamate-rich WD repeat-containing protein 1	2	949,705	3.6
PCDH7	NP_002580.2	protocadherin-7 isoform a precursor	4	944,895	*
CAPRIN1	NP_976240.1	caprin-1 isoform 2	2	943,613	*
ITGA6	NP_000201.2	integrin alpha-6 isoform b precursor	4	935,356	*
APLP2	NP_001135750.1	amyloid-like protein 2 isoform 4 precursor	2	931,606	54.2
TIMMDC1	NP_057673.2	translocase of inner mitochondrial membrane domain-containing protein 1 precursor	4	929,921	5.8
ROBO1	NP_001139317.1	roundabout homolog 1 isoform d	2	924,016	*
GGT7	NP_821158.2	gamma-glutamyltransferase 7	2	909,035	*
OS9	NP_001248352.1	protein OS-9 isoform 8 precursor	2	902,460	*
TMEM245	NP_114401.2	transmembrane protein 245	2	901,646	*
LMNA	NP_005563.1	lamin isoform C	2	894,311	*
OPA1	NP_570844.1	dynamin-like 120 kDa protein, mitochondrial isoform 2	2	889,767	*
MRPL43	NP_115488.2	39S ribosomal protein L43, mitochondrial isoform a	2	883,994	*
AMY2B	NP_066188.1	alpha-amylase 2B precursor	2	882,937	*
NCSTN	NP_056146.1	nicastrin precursor	2	878,916	19.4
C1orf112	NP_060656.2	uncharacterized protein C1orf112	2	874,913	*
IMMT	NP_001093640.1	mitochondrial inner membrane protein isoform 3	4	873,169	8.1
NAA16	NP_078837.3	N-alpha-acetyltransferase 16, NatA auxiliary subunit isoform 1	2	872,826	*
VTI1A	NP_660207.2	vesicle transport through interaction with t-SNAREs homolog 1A	4	870,848	32.8
IGF2R	NP_000867.2	cation-independent mannose-6-phosphate receptor precursor	2	867,620	*
ARMC10	NP_001154485.1	armadillo repeat-containing protein 10 isoform f	2	843,341	*
NDUFA8	NP_055037.1	NADH dehydrogenase [ubiquinone] 1 alpha subcomplex subunit 8	2	826,043	*
MST4	NP_001035918.1	serine/threonine-protein kinase MST4 isoform 2	6	826,040	*
CLGN	NP_004353.1	calmegin precursor	2	825,371	*
SCO1	NP_004580.1	protein SCO1 homolog, mitochondrial	2	795,512	2.0
SPIN1	NP_006708.2	spindlin-1	2	792,518	3.6
CERS1	NP_937850.1	ceramide synthase 1 isoform 2	2	785,026	*
SF3B1	NP_036565.2	splicing factor 3B subunit 1 isoform 1	2	779,793	2.7

UBQLN4…

Gene	Accession	Protein name	Peptides	Intensity	Ratio
SDR39U1	NP_064580.2	epimerase family protein SDR39U1	4	778,893	*
PARP2	NP_001036083.1	poly [ADP-ribose] polymerase 2 isoform 2	2	773,721	*
SEL1L	NP_005056.3	protein sel-1 homolog 1 isoform 1 precursor	2	752,030	*
HELLS	NP_060533.2	lymphoid-specific helicase	2	747,226	*
GSTM2	NP_001135840.1	glutathione S-transferase Mu 2 isoform 2	2	733,154	6.7
OSBPL8	NP_001003712.1	oxysterol-binding protein-related protein 8 isoform b	3	730,303	*
SATB2	NP_056080.1	DNA-binding protein SATB2	2	720,166	7.1
DCTN3	NP_077324.1	dynactin subunit 3 isoform 2	2	718,119	15.6
PTPRF	NP_569707.2	receptor-type tyrosine-protein phosphatase F isoform 2 precursor	2	700,692	46.4

Only proteins with more than 1 peptide were included unless the protein was clearly part of a marked complex. Protein and peptide false discovery rates were set at 1% for the Proteome Discoverer database search. Proteins were sorted by intensity. Gene is the gene name. Blue text indicates proteins identified in the SG proteome. Orange text indicates SG proteome proteins that are hnRNPs. Peptides are the peptide spectrum matched hits. Intensity is the total integrated precursor ion peak density. SILAC ratio is the average HEAVY (UBQLN2)/LIGHT (Control) peptide ratio. * indicates a corresponding light peptide was not automatically identified by the search software. Red bars indicate proteins identified in this study. Orange bars indicate proteins identified in previous studies. A total of 571 proteins were identified in this analysis.

Appendix B: Ubiquilin specific tools developed

INTRODUCTION

The human ubiquilin paralogs UBQLN1, 2, and 4 are highly similar with UBQLN4 most closely related to the single yeast homolog Dsk2. The original studies on the ubiquilins proteins grouped them together functionally due to the lack of paralog-specific reagents. In the course of completing this work, I characterized a number of paralog specific antibodies and shRNA's, generated a number of mammalian expression plasmids, cell lines, and worm lines and optimized purification of the UBQLN2 protein from *E. coli*. These tools are presented here to supplement the methods in the previous chapters and as a reference for future lab members.

RESULTS

Characterization of UBQLN specific antibodies and shRNAs

Previous efforts to characterize the unique functional roles of the ubiquilin paralogs UBQLN1, 2 and 4 in humans were hampered by the high degree of similarity between the ubiquilin proteins. For example, ubiquilin paralogs UBQLN2 and UBQLN1 are 75% identical and 87% similar, while UBQLN2 and UBQLN4 are 58% identical and 77% similar (Lalign). UBQLN2 however, contains a unique 12x PXX repeat region and all the ubiquilins have unique amino-termini. Commercially available peptide and monoclonal antibodies that recognize this central variable region of UBQLN1, 2, and 4 were chosen to uniquely recognize UBQLN1, 2, and 4 (Table B-1, Figure B-1). Notably, early lots of the Sigma Prestige rabbit anti-UBQLN2 antibody raised against a 149 amino acid peptide containing this PXX repeat region (Cat. No. HPA006431 Lot#A08472) were highly specific for the 67 kDa UBQLN2 band. Based on this specificity, the majority of Western blot and immunofluorescence assays were performed with this antibody. However, later lots of HPA006431 (especially lot #A89939) showed considerably more background bands by Western blot. The Novus 6H9 mouse anti-UBQLN2 monoclonal antibody made against the full-length recombinant protein is highly specific for UBQLN2 and may be a suitable alternative for the less reliable Sigma peptide rabbit antibody. This antibody does

however require the presence of the amino-terminal Ubl domain of UBQLN2 to detect UBQLN2 by Western blot, which could be a limitation for studying the native UBQLN2 fragments (Figure B-3B). Overall, these tools provided the basis for studying the role of UBQLN2 in SG formation in cells described.

Cell lines that inducibly express or constitutively suppress UBQLN expression

To investigate specific cellular functions of the UBQLN2 protein, I constructed four sets of stable cell lines using two different strategies: selection of random integration events, and flippase-short flippase recognition target site (FLP-FRT) recombination.

First, to quantitatively analyze proteins that coimmunoprecipitate with the UBQLN2 protein, I selected HEK293T cells that spontaneously integrated FLAG-UBQLN2 under control of a tetracycline inducible CMV promoter in a vector carrying the puromycin resistance gene. Despite artifacts potentially introduced by treating cells with the tetracycline analog doxycycline, I reasoned that the Tet repressor would minimize selection for suppressors of toxicity associated with overexpressing UBQLN2 protein (Huang et al., 2016). Following lipofectamine 2000 transfection with linearized vector, cells were continuously selected with 3 μg/mL puromycin until individual colonies appeared (after approximately 2 weeks). Individual clones were characterized by Western blot and clones that expressed UBQLN2, 1, and 4 at levels close to endogenous expression were selected for the SILAC IP (Figure B-3 A). HEK293T cells were selected for this analysis due to their ease of transfection and the broad range of proteins that they express, including some neuronal markers (Stepanenko and Dmitrenko, 2015).

HEK293T cells, however are not ideal for imaging due to their irregular shape and weak adherence to glass coverslips. To study the localization of UBQLN2 to SGs microscopically, I thus turned to HeLa cells, a commonly used cell line to study SG formation. The same strategy of selecting for the random integration of both tetracycline inducible expression constructs and constitutive shRNA knockdown constructs was performed. The highest concentration of puromycin under which integrant clones carrying constitutively expressed shRNA's appeared was 2 μg/mL puromycin. These clones were not

used for the UBQLN2 depletion time course experiments because transient transfection proved to be a more efficient method to effectively deplete UBQLN2. By selecting for random integration of regulatable FLAG-UBQLN2 in HeLa cells I also tried to generate stable cell lines for imaging. Unfortunately, no HeLa clones that inducibly express the UBQLN proteins were selected under these conditions.

To study the effects of UBQLN overexpression on SG formation in HeLa cells, I integrated UBQLN2 into the FRT site in a HeLa Flp-In cell line with the Flp recombinase. Stable integrants were selected by treatment with Hygromycin B (400 μg/mL) over a period of 2 weeks and were pooled to avoid a founder effect. A relatively low level of UBQLN expression was visible by treating cells in this tetracycline inducible system (Figure B-3 B) which was optimal for looking at UBQLN2 fragment localization. I observed that UBQLN2 fragment expression level varied greatly due to the loss of fragment stability in the absence of the Ubl domain (Figure B-3 B). I also introduced these UBQLN fragments into a HEK293T Flp-In cell line in which all three UBQLN proteins have been removed via CRISPR-Cas9 (Itakura et al., 2016) (Table B-3), but did not make use of this cell line in the current studies due to time constraints. This Flp-In system allows the rapid generation of isogenic clones for expression studies relatively quickly (within 2-3 weeks). Some consideration should be given to the site at which the Tet-repressor is integrated for tetracycline inducible expression from a tetracycline operator. I did see that HeLa cells with the Tet-repressor integrated, more rapidly formed SGs than our lab HeLa strain, indicating a difference in sensitivity.

Worm lines for studying ubiquilin function in *C. elegans*

Transgenic Worm Line Generation

To characterize the function of the human UBQLN2 protein in neurons *in vivo* I generated transgenic *Caenorhabditis elegans* worm lines that constitutively express the human UBQLN2 wild type or mutant (P497H, P506T) protein under control of the synaptobrevin neuronal promoter (*psnb-1*). With help from Jiou and the talented postdoc Tao Zhang I began by generating an extrachromosomal array, then screened for array integrants generated by UV/TMP mutagenesis. To generate worm lines carrying an

extrachromosomal array, Jiou coinjected a 20 ng/µL *psnb-1*::hUBQLN2 in pPD30_38 (Fire Lab Vector, Addgene) with 2.5 ng/µL *pmyo-2*::RFP into the gonad of hermaphrodite worms. Progeny carrying the red fluorescent protein (RFP) marker were moved to new plates and inspected daily for lines that had stable extrachromosomal arrays (Mello et al., 1991). These worm lines were expanded and frozen (Table B-5).

Worms carrying an extrachromosomal array were used to generate worm lines with stably integrated copies of the human *UBQLN2* gene, L4 hermaphrodite extrachromosomal array worms were treated with 30 µg/mL trimethylpsoralen and 300 µJ 365 nm UV light. Progeny were moved to new plates and screened for stable integration of the extrachromosomal array. Expression of the hUBQLN2 transgene was assessed by Western blot of whole worm lysate. Select integrated lines were then backcrossed with the Bristol N2 strain at least four times prior to freezing using standard methods (TableB-5).

Endogenous worm ubiquilin, *ubql-1* null worm lines

To characterize the function of the endogenous worm ubiquilin, ubql-1, I used two uncharacterized worm ubiquilin null strains from the *Caenorhabditis* Genetics Center *ubql-1* (tm1574) and *ubql-1* (ok997) previously obtained by the lab. These strains were backcrossed six times to the Bristol N2 strain. Neither strain appeared to show a movement defect (Table B-6).

Worm crosses

To characterize the phenotype of worms deficient in endogenous ubql-1 or overexpressing wild type or mutant UBQLN2, I performed preliminary worm movement assays and crossed worms to strain carrying fluorescently labelled autophagy markers, other ALS/FTD-linked proteins prone to aggregate and a daf-2 insulin receptor mutant strain. RFP, expressed in the pharyngeal muscle was used to trace segregation of transgenic ubiquilin alleles (Table B-7).

Optimization of native UBQLN2 purification from *E. coli*

To perform in vitro studies on the UBQLN2 protein, I optimized its purification from *E. coli*. I started with a protocol shared by a lab member from Dr. Mervin Monteiro's lab (University of Maryland) to

purify 6xHis-UBQLN2 and adapted it to a 6xHis-GFP-TEV-UBQLN2 construct. 6xHis-GFP-UBQLN2 expression was induced overnight at 16°C with 1 mM IPTG in pRosettaII BL21DE3 *E. coli* cells. Cell were pelleted at 4000 x g, 4°C, 20 min and resuspended in 50 mM Tris-Cl, pH 8.0, 300 mM NaCl, 10% glycerol, 10 mM imidazole with a Roche EDTA-free Complete protease inhibitor cocktail at a ratio of 2 mL of Lysis/Resuspension buffer per gram of wet cell pellet. Cells were lysed via French Press and cell debrís/unlysed cells were removed by pelleting at 20000 x g, 4°C, 20 min twice. 6xHisGFP-UBQLN2 was then batch purified via NiNTA affinity chromatography as follows: the supernatant was incubated overnight with NiNTA beads. Beads were washed with 350 mM salt buffer, 175 mM salt buffer, 0 mM salt buffer, then 150 mM NaCl buffer containing 50 mM Tris-Cl, pH 8.0, 10% glycerol and 30 mM imidazole buffer. The majority of the protein was eluted with 250 mM imidazole. The affinity purified protein was then simultaneously dialyzed against 50 mM Tris-Cl, pH 8.0, 10% glycerol and 10 mM imidazole buffer and cleaved with TEV protease to remove the 6xHis-GFP tag overnight at 4°C in Snakeskin 3.5 MWCO dialysis tubing spiked with sodium chloride. Cleaved protein was then passed back over the cleaned and recharged Ni-NTA beads and the flow-through was collected. This flow-through was spin concentrated in an Amicon-Ultra 10 MWCO spin filter to an appropriate volume to inject into a Superdex 200 size exclusion column at a flow rate of 0.5 mL/min. Fractions were checked via Coomassie gel for molecular weight and Western blot. The second size exclusion peak contained purified UBQLN2 protein (Figure B-4). Protein fractions were then pooled and again spin concentrated in a 50 MWCO Amicon spin filter to approximately 10 mg/mL before the protein was flash frozen in liquid nitrogen.

At concentrations above 10 mg/mL the protein appeared to precipitate out of solution. When warmed to room temperature the solution became cloudy and phase separated as previously described (Dao et al., 2018), so all steps were performed on ice. Highly concentrated fractions were thawed on ice and spun 10,000 x g, 4°C, 10 min and absorbance was measured prior to use in the FUS-UBQLN2 interaction assays described (ε=11460 M-1cm-1 (Protparam), and MW= 65896.32 Da) (Chapter 3).

The 6xHis-GFP-UBQLN2 protein itself was stable in a 10% buffered glycerol solution at 4°C for more than 2 years. UBQLN2 P497H and P506T mutants were purified as described for the wild type protein. The purified protein has a Serine, Isoleucine residue upstream of the initiator methionine in the consensus human sequence (RefSeq NP_038472.2). This protein was sufficiently pure to set up crystal trays to test for UBQLN2 crystallization in collaboration with Jurgen Bosch's lab. Unfortunately, I did not see the formation of crystals under any of the conditions that we tested. I was later, however able to use this optimized purification protocol to purify sufficient protein for the *in vitro* FUS-RNA smFRET studies performed in collaboration with the Myong lab that form the basis of our current mechanistic understanding of UBQLN2's function in SG formation.

DISCUSSION

Here I have highlighted several tools that I developed to investigate UBQLN2 function.

Identifying UBQLN2 specific antibodies and shRNA's was critical to differentiating UBQLN2 from UBQLN1 and 4 by Western Blot and immunocytochemistry. The pan-ubiquilin antibody was also useful for staining all forms of UBQLN2 simultaneously. Although to clearly separate UBQLN2 and 4 a gradient or 8% isocratic Tris-Gly SDS-PAGE gel worked best. Previous efforts to characterize the functions of UBQLN1 and 2 were hampered by the lack of ubiquilin specific tools, so I hope this brief characterization is helpful to future studies and evaluating past studies despite the fact that new antibodies continue to be commercially developed.

Some cell lines such as the Flp-In HeLa cell line and the HEK293T stable cells lines that inducibly express UBQLN2 were critical to the experiments described. The stable HEK293T stable cell line that inducibly expresses the UBQLN proteins was important for the SILAC experiments to ensure reproducibility. The Flp-In HeLa cell line was critical for imaging FLAG-UBQLN2 fragments at near endogenous levels.

Other cell lines, such as the HEK293T UBQLN2 knockout cell lines and HeLa UBQLN constitutive knockdown cell were not employed in the experiments described here, but may be useful to the lab in the future. Originally, I constructed the UBQLN 1, 2, 4 CRISPR knockout cell lines that inducibly express UBQLN2 and its fragments to perform SG fluorescence recovery after photobleaching experiments in collaboration with the Myong lab to show that UBQLN2 increases the dynamics of FUS exchange in and out of SGs. However due to technical problems with FUS-GFP bleaching and time constraints, I was unable to complete these experiments. The constitutive knockdown HeLa cells were also constructed to optimize reproducibility in SG timecourse experiments, but the knockdown failed to be as efficient as that obtained from a 72-96 hr transient transfection.

The worm lines that I made may be useful to future lab members in characterizing UBQLN2 neuronal function in SGs *in vivo*. Hopefully the optimized UBQLN2 purification protocol will prove useful for future *in vitro* experiments to study UBQLN2 function. I still, of course, dream of a full-length structure of UBQLN2 in complex with its functional interactors.

All the best luck to future Wang Lab members!

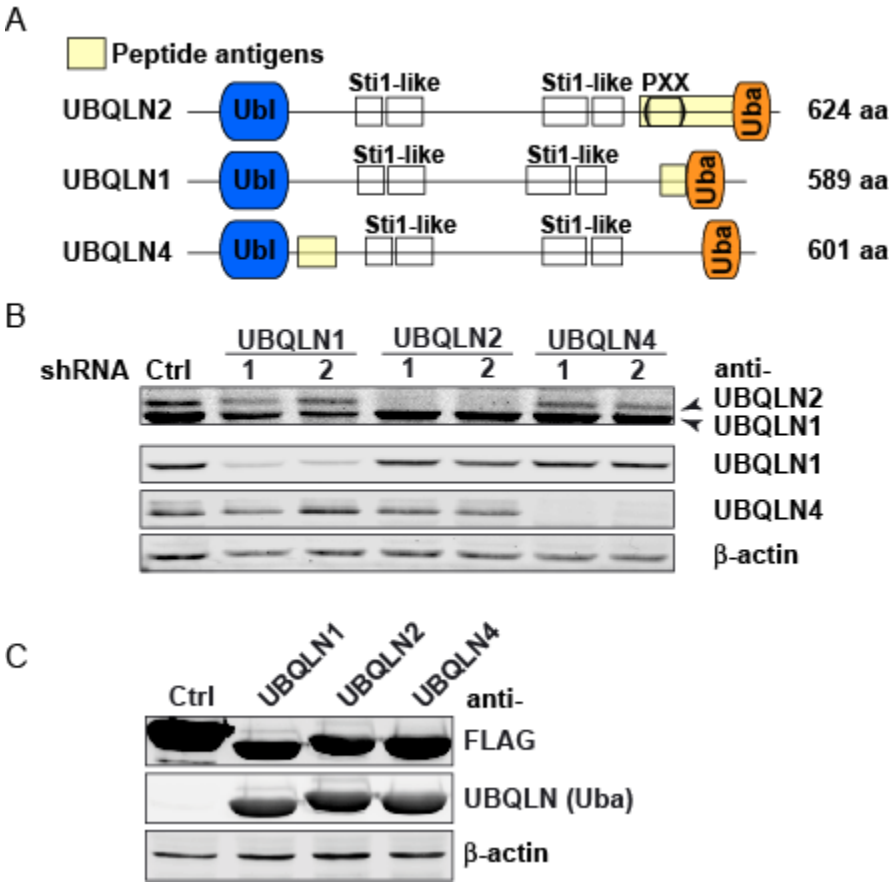

Figure B-1 UBQLN1, 2, 4 specific antibodies reveal specific shRNA depletion

(A) Domain maps of UBQLN2, 1, and 4 showing the position of the unique peptide antigens targeted by the antibodies used in (B). The antigen positions correspond to amino acid residues 502-519 in UBQLN1, 443-591 in UBQLN2, and 100-116 in UBQLN4.

(B) Western blot (WB) of SDS-PAGE separated HEK293T cell lysate, 72 hrs post-transfection with the specified shRNA's. Two shRNA's specific to UBQLN1, UBQLN2, and UBQLN4 are shown. Mouse anti-UBQLN4 (Santa Cruz H-2) and rabbit anti-UBQLN1 (Sigma U7258) distinguished UBQLN1 and UBQLN4 from UBQLN2 recognized by rabbit anti-UBQLN2 (Sigma Prestige HPA0006431). Mouse anti-β-actin was used as a loading control. UBQLN2 migrates more slowly than UBQLN1, consistent with its larger molecular weight (65.7 kDa vs. 62.5 kDa).

(C) WB of overexpressed FLAG-UBQLN1, 2, and 4. FLAG-GUS (β-glucuronidase) a plant protein with a similar molecular weight was used as a control. The mouse monoclonal anti-UBQLN2 (Uba) (Sigma, 5F5), antibody recognizes all three ubiquilins which have nearly identical Uba domains.

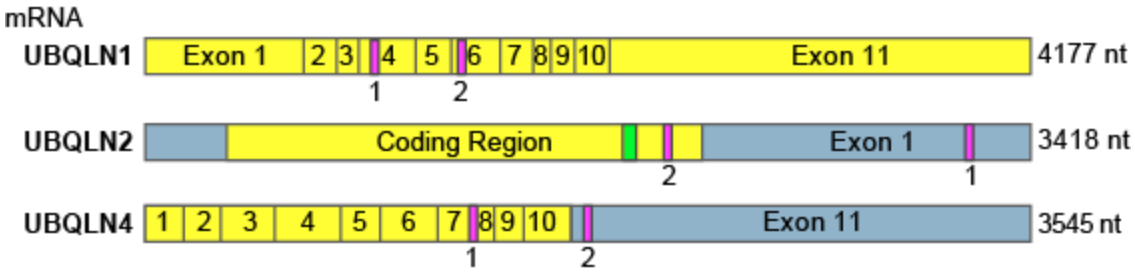

Figure B-2. UBQLN shRNA target sites

Diagrams of UBQLN1, 2, and 4 mRNA with numbered exons and specific shRNA target sites shown in magenta. UBQLN2 is encoded by a single exon on the X-chromosome. The unique PXX repeat in UBQLN2 is marked with a green box. mRNA is shown in the 5'-3' direction. The UBQLN2 specific shRNA in the 3' UTR was used to deplete endogenous UBQLN2 levels while exogenously expressing UBQLN2 fragments to attain near endogenous UBQLN2 levels in the Flp-In HeLa cells (Figure 2-11).

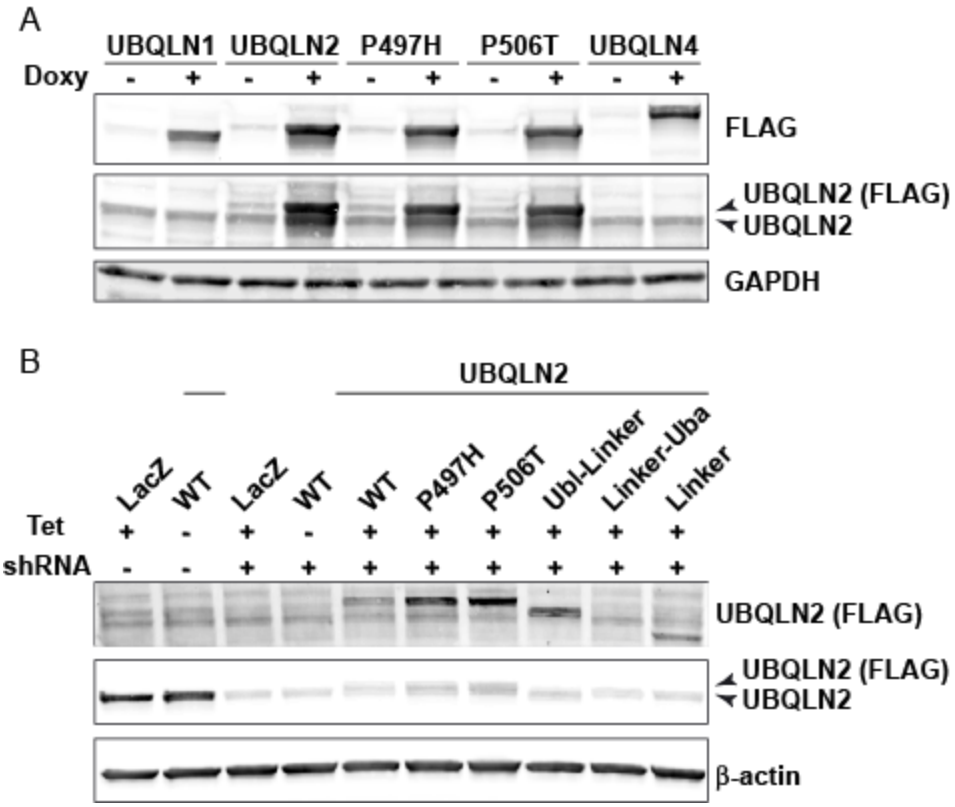

Figure B-3. UBQLN integrated cell line expression

(A) Western blot (WB) of tetracycline-inducible FLAG-UBQLN expression before and after 1 μg/mL doxycycline treatment in stable HEK293T cells used for proteomic analysis of UBQLN interacting partners. The anti-UBQLN2 blot shows less than two-fold overexpression of the UBQLN2 protein after 24 hrs of induction. GAPDH was used as a loading control.

(B) WB of FLAG-UBQLN2 expression induced by Flp-In HeLa cell treatment with 1 μg/mL tetracycline for 24 hrs following 72 hrs exposure to UBQLN2 specific shRNA to deplete endogenous UBQLN2 protein. The UBQLN2 protein expression level is less than endogenous levels. The cell line LacZ/Zeo (LacZ) was used as a negative control. β-actin was used as a loading control.

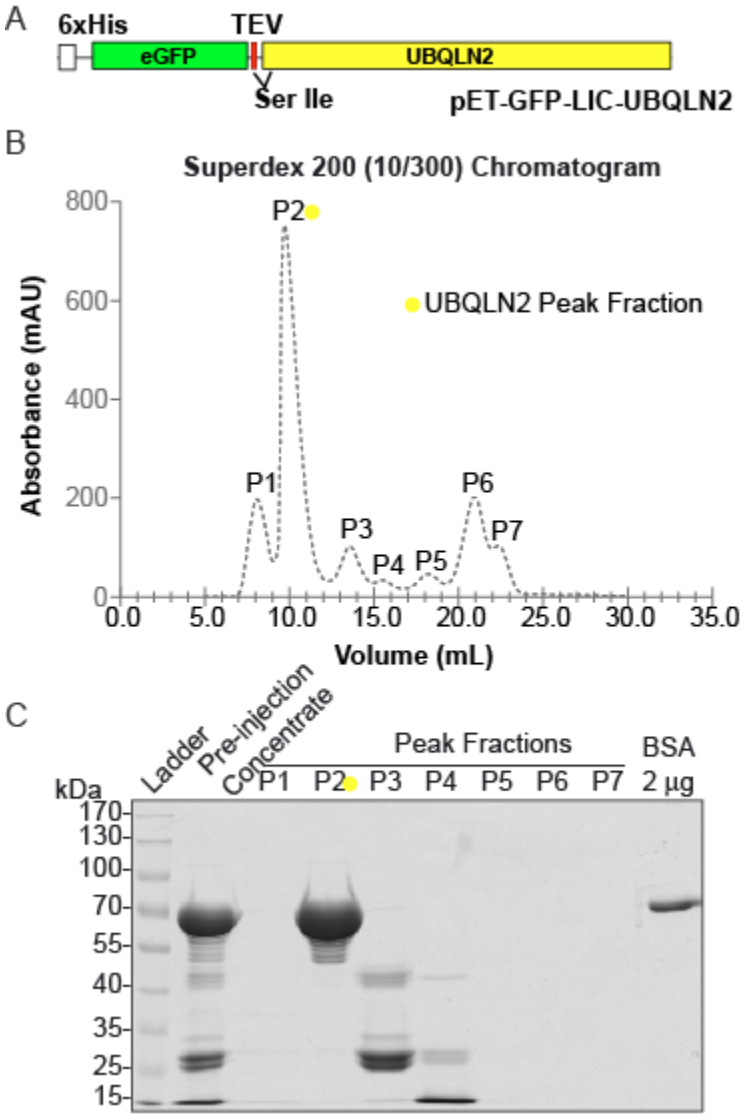

Figure B-4. Native UBQLN2 purification from *E. coli*

(A) Diagram of the pET-6xHis-GFP-UBQLN2 construct showing the location of the TEV site and Ser, Ile residues left upstream of the Met start site after the TEV cleavage site.

(B) Size exclusion chromatogram, showing elution of pure UBQLN2 protein in P2 (yellow dot).

(C) Western blot analysis of size exclusion peak fractions. Size exclusion removed the majority of lower molecular weight bands from the purified protein. P2 is marked with a yellow dot.

Table B-1. UBQLN antibodies tested

UBQLN specific antibodies

Target	Epitope	Host	Isotype	Source	Cat. No.
UBQLN1	502-519	Rabbit	Polyclonal	Sigma	U7258
UBQLN2	443-591	Rabbit	Polyclonal	Sigma Prestige	HPA006431
UBQLN4	100-116	Mouse	Monoclonal (H-2)	Santa Cruz	sc-515250

Alternative UBQLN specific antibodies

UBQLN1	1-19	Rabbit	Polyclonal	Sigma	U7383
UBQLN2	Ubl	Mouse	Monoclonal (6H9)	Novus	NBP2-25164
UBQLN4	Central	Rabbit	Polyclonal	Aviva Biosystems	ARP57355
UBQLN4	Central	Mouse	Monoclonal (M398)	Santa Cruz	sc-136146

pan-UBQLN antibody

UBQLN2	555-624	Mouse	Monoclonal (5F5)	Sigma	WH0029978M3

Table B-2. UBQLN shRNA target sequences

shRNA target sequences

Gene	shRNA plasmid	Target sequence
non-targetting	shCTRL-RFP-C-RS	gcactaccagagctaactcagatagtact
UBQLN2	shUBQLN2-RFP-C-RS #54	tgtatatgaccttaatctttgtgcagcct
UBQLN2	shUBQLN2-RFP-C-RS #55	aaccacgagtcctacatcagaatctggac
UBQLN1	shUBQLN1-RFP-C-RS #31	ctgaactacagagtcagatgcagcgacaa
UBQLN1	shUBQLN1-RFP-C-RS #32	tacatcctctggtgaaggtagtcaacctt
UBQLN4	shUBQLN2-RFP-C-RS #21	gctgctcagatgatggtgaatgtgccgct
UBQLN4	shUBQLN2-RFP-C-RS #22	ggcttcatcaatcgtgaggctaacctgca

siRNA targeting sequences were from Origene. The hairpin loop introduced was TCAAGAG followed by the reverse complement of the target sequence. All shRNA's were cloned into the BamHI/BglII-HindIII sites in the pRFP-C-RS vector from Origene. RFP was removed by *Mlu*I, *Bgl*II digestion followed by blunting and religation.

Table B-3. UBQLN integrated mammalian cell lines

SILAC

Host	cDNA	Vector backbone	Integration	Resistance	Drug selection
HEK293T	UBQLN2	pcDNA3.1*	Random	PuroR	3 µg/mL Puromycin
HEK293T	UBQLN2 P497H	pcDNA3.1*	Random	PuroR	3 µg/mL Puromycin
HEK293T	UBQLN2 P506T	pcDNA3.1*	Random	PuroR	3 µg/mL Puromycin
HEK293T	UBQLN1	pcDNA3.1*	Random	PuroR	3 µg/mL Puromycin
HEK293T	UBQLN4	pcDNA3.1*	Random	PuroR	3 µg/mL Puromycin
HEK293T	GFP	pcDNA3.1*	Random	PuroR	3 µg/mL Puromycin
Endogenous level expression					
Flp-In HeLa	UBQLN2	pcDNA5_DEST	FRT site	HygR	400 µg/mL Hygromycin B
Flp-In HeLa	UBQLN2 P497H	pcDNA5_DEST	FRT site	HygR	400 µg/mL Hygromycin B
Flp-In HeLa	UBQLN2 P506T	pcDNA5_DEST	FRT site	HygR	400 µg/mL Hygromycin B
Flp-In HeLa	UBQLN2 Ubl-Sti1	pcDNA5_DEST	FRT site	HygR	400 µg/mL Hygromycin B
Flp-In HeLa	UBQLN2 Sti1-Uba	pcDNA5_DEST	FRT site	HygR	400 µg/mL Hygromycin B
Flp-In HeLa	UBQLN2 Sti1	pcDNA5_DEST	FRT site	HygR	400 µg/mL Hygromycin B
Flp-In HeLa	eGFP	pcDNA5_DEST	FRT site	HygR	400 µg/mL Hygromycin B
Unused HEK293T Triple UBQLN Knockout Cell Lines					
TKO UBQLN HEK293T	UBQLN2	pcDNA5_DEST	FRT site	HygR	400 µg/mL Hygromycin B
TKO UBQLN HEK293T	UBQLN2 P497H	pcDNA5_DEST	FRT site	HygR	400 µg/mL Hygromycin B
TKO UBQLN HEK293T	UBQLN2 P506T	pcDNA5_DEST	FRT site	HygR	400 µg/mL Hygromycin B
TKO UBQLN HEK293T	UBQLN2 Ubl-Sti1	pcDNA5_DEST	FRT site	HygR	400 µg/mL Hygromycin B
TKO UBQLN HEK293T	UBQLN2 Sti1-Uba	pcDNA5_DEST	FRT site	HygR	400 µg/mL Hygromycin B
TKO UBQLN HEK293T	UBQLN2 Sti1	pcDNA5_DEST	FRT site	HygR	400 µg/mL Hygromycin B
TKO UBQLN HEK293T	eGFP	pcDNA5_DEST	FRT site	HygR	400 µg/mL Hygromycin B
Unused HeLa Constituitive Knockdown Cell Lines					
HeLa	UBQLN2 shRNA 1	pRFP-C-RS**	Random	PuroR	2 µg/mL Puromycin
HeLa	UBQLN2 shRNA 2	pRFP-C-RS**	Random	PuroR	2 µg/mL Puromycin
HeLa	UBQLN1 shRNA 1	pRFP-C-RS**	Random	PuroR	2 µg/mL Puromycin
HeLa	UBQLN1 shRNA 2	pRFP-C-RS**	Random	PuroR	2 µg/mL Puromycin
HeLa	UBQLN4 shRNA 1	pRFP-C-RS**	Random	PuroR	2 µg/mL Puromycin
HeLa	UBQLN4 shRNA 2	pRFP-C-RS**	Random	PuroR	2 µg/mL Puromycin
HeLa	Ctrl shRNA	pRFP-C-RS**	Random	PuroR	2 µg/mL Puromycin

*CMV/TO_Nt-3xFLAG_DEST_TetR-IRES-PuroR

**pRFP *MluI*/*BglII* digested and religated to remove RFP

Table B-4. UBQLN cDNA constructs for mammalian and *E. coli* expression

SILAC IP HEK293T Stable Cell Line Construction

cDNA	Insertion site	Vector backbone
UBQLN2	attR1-attR2	pcDNA3.1*_TetR_IRES_PuroR_DEST
UBQLN2 P497H	attR1-attR2	pcDNA3.1*_TetR_IRES_PuroR_DEST
UBQLN2 P506T	attR1-attR2	pcDNA3.1*_TetR_IRES_PuroR_DEST
UBQLN1	attR1-attR2	pcDNA3.1*_TetR_IRES_PuroR_DEST
UBQLN4	attR1-attR2	pcDNA3.1*_TetR_IRES_PuroR_DEST
GFP	attR1-attR2	pcDNA3.1*_TetR_IRES_PuroR_DEST
RFP	attR1-attR2	pcDNA3.1*_TetR_IRES_PuroR_DEST

FLAG IP Interaction Validation

cDNA	Insertion site	Vector backbone
UBQLN2	attR1-attR2	pcDNA3.1*
UBQLN2 P497H	attR1-attR2	pcDNA3.1*
UBQLN2 P506T	attR1-attR2	pcDNA3.1*
UBQLN2 UBL	attR1-attR2	pcDNA3.1*
UBQLN2 UBA	attR1-attR2	pcDNA3.1*
UBQLN2 STI1	attR1-attR2	pcDNA3.1*
UBQLN2 STCH BD	attR1-attR3	pcDNA3.1*
UBQLN2 UBL-STI1	attR1-attR2	pcDNA3.1*
UBQLN2 STI1-UBA	attR1-attR2	pcDNA3.1*
UBQLN1	attR1-attR2	pcDNA3.1*
UBQLN1 UBL	attR1-attR2	pcDNA3.1*
UBQLN1 UBA	attR1-attR2	pcDNA3.1*
UBQLN1 STI1	attR1-attR2	pcDNA3.1*
UBQLN1 UBL-STI1	attR1-attR2	pcDNA3.1*
UBQLN1 STI1-UBA	attR1-attR2	pcDNA3.1*
UBQLN4	attR1-attR2	pcDNA3.1*
UBQLN4 UBL	attR1-attR2	pcDNA3.1*
UBQLN4 UBA	attR1-attR2	pcDNA3.1*
UBQLN4 STI1	attR1-attR2	pcDNA3.1*
UBQLN4 UBL-STI1	attR1-attR2	pcDNA3.1*
UBQLN4 STI1-UBA	attR1-attR2	pcDNA3.1*
GUS	attR1-attR2	pcDNA3.1*

Flp-In HeLa and HEK293T cell line construction

cDNA	Insertion site	Vector backbone
UBQLN2	attR1-attR2	pcDNA5-FRT_DEST
UBQLN2 P497H	attR1-attR2	pcDNA5-FRT_DEST
UBQLN2 P506T	attR1-attR2	pcDNA5-FRT_DEST
UBQLN2 UBL	attR1-attR2	pcDNA5-FRT_DEST
UBQLN2 UBA	attR1-attR2	pcDNA5-FRT_DEST
UBQLN2 STI1	attR1-attR2	pcDNA5-FRT_DEST
UBQLN2 STCH BD	attR1-attR2	pcDNA5-FRT_DEST
UBQLN2 UBL-STI1	attR1-attR2	pcDNA5-FRT_DEST
UBQLN2 STI1-UBA	attR1-attR2	pcDNA5-FRT_DEST
UBQLN1	attR1-attR2	pcDNA5-FRT_DEST
UBQLN1 STI1	attR1-attR2	pcDNA5-FRT_DEST
UBQLN4	attR1-attR2	pcDNA5-FRT_DEST
eGFP	attR1-attR2	pcDNA5-FRT_DEST

UBQLN myc expression vectors

cDNA	Insertion site	Vector backbone
UBQLN2	*XhoI/XhoI*	pRK5-myc (Wang Lab)
UBQLN2 P497H	*XhoI/XhoI*	pRK5-myc (Wang Lab)
UBQLN2 P506T	*XhoI/XhoI*	pRK5-myc (Wang Lab)
UBQLN1	*SalI/SalI*	pRK5-myc (Wang Lab)
UBQLN4	*SalI/SalI*	pRK5-myc (Wang Lab)
UBQLN2	*XhoI/XhoI*	pRK5-myc**
UBQLN2 P497H	*XhoI/XhoI*	pRK5-myc**
UBQLN2 P506T	*XhoI/XhoI*	pRK5-myc**
UBQLN1	*SalI/SalI*	pRK5-myc**
UBQLN4	*SalI/SalI*	pRK5-myc**

shRNA target vectors

cDNA	Insertion site	Vector backbone
UBQLN2 shRNA 2.54	*BamHI/HindIII*	pRFP-C-RS
UBQLN2 shRNA 2.55	*BamHI/HindIII*	pRFP-C-RS
UBQLN1 shRNA 1.31	*BamHI/HindIII*	pRFP-C-RS
UBQLN1 shRNA 1.32	*BamHI/HindIII*	pRFP-C-RS
UBQLN4 shRNA 4.21	*BamHI/HindIII*	pRFP-C-RS
UBQLN4 shRNA 4.22	*BamHI/HindIII*	pRFP-C-RS
Ctrl shRNA	*BamHI/HindIII*	pRFP-C-RS
UBQLN2 shRNA 2.54	*BamHI/HindIII*	pRFP-C-RS***
UBQLN2 shRNA 2.55	*BamHI/HindIII*	pRFP-C-RS***
UBQLN1 shRNA 1.31	*BamHI/HindIII*	pRFP-C-RS***
UBQLN1 shRNA 1.32	*BamHI/HindIII*	pRFP-C-RS***
UBQLN4 shRNA 4.21	*BamHI/HindIII*	pRFP-C-RS***
UBQLN4 shRNA 4.22	*BamHI/HindIII*	pRFP-C-RS***
Ctrl shRNA	*BamHI/HindIII*	pRFP-C-RS***

E. coli expression vectors

cDNA	Insertion site	Vector backbone
UBQLN2	*SspI*	pET-6xHis-GFP-LIC
UBQLN2 P497H	*SspI*	pET-6xHis-GFP-LIC
UBQLN2 P506T	*SspI*	pET-6xHis-GFP-LIC
UBQLN2	*NdeI/XhoI*	pET28a-6xHis
UBQLN2 P497H	*NdeI/XhoI*	pET28a-6xHis
UBQLN2 P506T	*NdeI/XhoI*	pET28a-6xHis

*pcDNA3.1_CMV/TO-n3xFLAG

***MluI/AgeI* digested and religated to remove foreign long 3'UTR.

****MluI/BglII* digested and religated to remove RFP.

Table B-5. Transgenic hUBQLN2 *C. elegans* lines

Transgenic extrachromosomal arrays

strain	allele [genotype]
IW180	*iwEx69 [psnb-1::hUBQLN2; pmyo-2::RFP]*
IW203	*iwEx68 [psnb-1::hUBQLN2 P497H; pmyo-2::RFP]*
IW278	*iwEx67 [psnb-1::hUBQLN2 P506T; pmyo-2::RFP]*

Integrated arrays

IW200	*iwIs52 [psnb-1::hUBQLN2 WT int; pmyo-2::RFP]*
IW301	*iwIs40 [psnb-1::hUBQLN2 P497H int; pmyo-2::RFP]*
IW302	*iwIs41 [psnb-1::hUBQLN2 P497H int; pmyo-2::RFP]*
IW303	*iwIs42 [psnb-1::hUBQLN2 P497H int; pmyo-2::RFP]*
IW304	*iwIs43 [psnb-1::hUBQLN2 P497H int; pmyo-2::RFP]*
IW305	*iwIs44 [psnb-1::hUBQLN2 P497H int; pmyo-2::RFP]*
IW306	*iwIs45 [psnb-1::hUBQLN2 P497H int; pmyo-2::RFP]*
IW307	*iwIs46 [psnb-1::hUBQLN2 P497H int; pmyo-2::RFP]*
IW309	*iwIs47 [psnb-1::hUBQLN2 P497H int; pmyo-2::RFP]*
IW316	*iwIs48 [psnb-1::hUBQLN2 P497H int; pmyo-2::RFP]*
IW319	*iwIs50 [psnb-1::hUBQLN2 P497H int; pmyo-2::RFP]*
IW320	*iwIs51 [psnb-1::hUBQLN2 P497H int; pmyo-2::RFP]*

Outcrossed strains

IW295	*iwIs52 [psnb-1::hUBQLN2; pmyo-2::RFP]*
IW318	*iwIs43 [psnb-1::hUBQLN2 P497H int; pmyo-2::RFP]*
IW321	*iwIs46 [psnb-1::hUBQLN2 P497H int; pmyo-2::RFP]*
IW323	*iwIs45 [psnb-1::hUBQLN2 P497H int; pmyo-2::RFP]*

Table B-6. *ubql-1* mutant *C. elegans* lines

Null allele strains

tm1574	*ubql-1(tm1574)*
ok997	*ubql-1(ok997)*

Outcrossed null allele strains

IW296	*ubql-1(tm1574)*
IW298	*ubql-1(ok997)*

Null allele; Transgenic hUBQLN2

IW310	*ubql-1(tm1574)*; *iwIs52* [*psnb-1*::*hUBQLN2*; *pmyo-2*::RFP]
IW341	*ubql-1(tm1574); iwIs43 [psnb-1::hUBQLN2 P497H int; pMyo-2::RFP]*
IW340	*ubql-1(ok997); iwIs43 [psnb-1::hUBQLN2 P497H int; pMyo-2::RFP]*

Table B-7 Transgenic hUBQLN2 and null *ubql-1 C. elegans* strains

Lgg1::GFP

IW328	*ubql-1(tm1574); adIs2122 [lgg-1::GFP; rol-6(su1006)]*
IW343	*ubql-1(tm1574); iwIs43 [psnb-1::hUBQLN2 P497H int; pmyo-2::RFP]; adIs2122*
IW311	*iwIs52 [psnb-1::hUBQLN2; pMyo-2::RFP]; adIs2122 [GFP::Lgg-1; rol-6(su1006)]*
IW342	*iwIs43 [psnb-1::hUBQLN2 P497H int; pmyo-2::RFP]; adIs2122 [lgg-1::GFP + rol-6(su1006)]*
IW355	*iwIs45 [psnb-1::hUBQLN2 P497H int; pmyo-2::RFP]; adIs2122[lgg-1::GFP + rol-6(su1006)]*

SOD1G85::YFP

IW337	*ubql-1(ok997); iwIs8 [psnb-1::hSOD1 G85R::YFP]*
IW338	*ubql-1(tm1574); iwIs8 [psnb-1::hSOD1 G85R::YFP]*
IW339	*iwIs52 [psnb-1::hUBQLN2; pmyo-2::RFP]; iwIs8 [psnb-1::hSOD1 G85R::YFP]*

TDP43::YFP

IW365	*ubql-1(tm1574); IwIs22 [psnb-1::hTDP43::YFP]*

polyQ67::YFP

IW333	*ubql-1(ok997); rmIs284 [pF25B3.3::Q(67)::YFP]*
IW334	*ubql-1(tm1574); rmIs284 [pF25B3.3::Q(67)::YFP]*
IW335	*iwIs52 [psnb-1::hUBQLN2; pmyo-2::RFP]; rmIs284 [pF25B3.3::Q(67)::YFP]*

daf-2(e1370)

IW414	*adIs2122[lgg-1::GFP + rol-6(su1006)]; daf-2(e1370)*
IW415	*ubql-1(tm1574); adIs2122[lgg-1::GFP + rol-6(su1006)]; daf-2(e1370)*

Bibliography

Adegoke, O.O., Qiao, F., Liu, Y., Longley, K., Feng, S., and Wang, H. (2017). Overexpression of ubiquilin-1 alleviates Alzheimer's disease-caused cognitive and motor deficits and reduces amyloid-β accumulation in mice. J Alzheimers Dis *59*, 575–590.

Alberti, S., Halfmann, R., King, O., Kapila, A., and Lindquist, S. (2009). A systematic survey identifies prions and illuminates sequence features of prionogenic proteins. Cell *137*, 146–158.

Alexander, E.J., Niaki, A.G., Zhang, T., Sarkar, J., Liu, Y., Nirujogi, R.S., Pandey, A., Myong, S., and Wang, J. (2018). Ubiquilin 2 modulates ALS/FTD-linked FUS–RNA complex dynamics and stress granule formation. PNAS *115*, E11485–E11494.

Altmeyer, M., Neelsen, K.J., Teloni, F., Pozdnyakova, I., Pellegrino, S., Grøfte, M., Rask, M.-B.D., Streicher, W., Jungmichel, S., Nielsen, M.L., et al. (2015). Liquid demixing of intrinsically disordered proteins is seeded by poly(ADP-ribose). Nat Commun *6*, 8088.

Alzheimer, A. (1991). Über eigenartige Krankheitsfälle des späteren Alters: (On certain peculiar diseases of old age. Hist Psychiatry *2*, 74–101.

Anderson, P., and Kedersha, N. (2008). Stress granules: the Tao of RNA triage. Trends Biochem. Sci. *33*, 141–150.

Anderson, P., and Kedersha, N. (2009). RNA granules: post-transcriptional and epigenetic modulators of gene expression. Nat Rev Mol Cell Biol *10*, 430–436.

Arai, T., Hasegawa, M., Akiyama, H., Ikeda, K., Nonaka, T., Mori, H., Mann, D., Tsuchiya, K., Yoshida, M., Hashizume, Y., et al. (2006). TDP-43 is a component of ubiquitin-positive tau-negative inclusions in frontotemporal lobar degeneration and amyotrophic lateral sclerosis. Biochem. Biophys. Res. Commun. *351*, 602–611.

Arimoto, K., Fukuda, H., Imajoh-Ohmi, S., Saito, H., and Takekawa, M. (2008). Formation of stress granules inhibits apoptosis by suppressing stress-responsive MAPK pathways. Nat Cell Biol *10*, 1324–1332.

Athanasopoulos, V., Barker, A., Yu, D., Tan, A.H.-M., Srivastava, M., Contreras, N., Wang, J., Lam, K.-P., Brown, S.H.J., Goodnow, C.C., et al. (2010). The ROQUIN family of proteins localizes to stress granules via the ROQ domain and binds target mRNAs. FEBS Journal *277*, 2109–2127.

Aulas, A., and Vande Velde, C. (2015). Alterations in stress granule dynamics driven by TDP-43 and FUS: a link to pathological inclusions in ALS? Front. Cell. Neurosci. 423.

Aulas, A., Lyons, S.M., Fay, M.M., Anderson, P., and Ivanov, P. (2018). Nitric oxide triggers the assembly of "type II" stress granules linked to decreased cell viability. Cell Death Dis *9*.

Ayadi, A.E., Stieren, E.S., Barral, J.M., and Boehning, D. (2012). Ubiquilin-1 regulates amyloid precursor protein maturation and degradation by stimulating K63-linked polyubiquitination of lysine 688. PNAS.

Baker, M., Mackenzie, I.R., Pickering-Brown, S.M., Gass, J., Rademakers, R., Lindholm, C., Snowden, J., Adamson, J., Sadovnick, A.D., Rollinson, S., et al. (2006). Mutations in progranulin cause tau-negative frontotemporal dementia linked to chromosome 17. Nature *442*, 916–919.

Beal, R., Deveraux, Q., Xia, G., Rechsteiner, M., and Pickart, C. (1996). Surface hydrophobic residues of multiubiquitin chains essential for proteolytic targeting. PNAS *93*, 861–866.

Bedford, F.K., Kittler, J.T., Muller, E., Thomas, P., Uren, J.M., Merlo, D., Wisden, W., Triller, A., Smart, T.G., and Moss, S.J. (2001). GABAA receptor cell surface number and subunit stability are regulated by the ubiquitin-like protein Plic-1. Nature Neuroscience *4*, 908–916.

Beverly, L.J., Lockwood, W.W., Shah, P.P., Erdjument-Bromage, H., and Varmus, H. (2012). Ubiquitination, localization, and stability of an anti-apoptotic BCL2-like protein, BCL2L10/BCLb, are regulated by Ubiquilin1. PNAS *109*, E119–E126.

Biggins, S., Ivanovska, I., and Rose, M.D. (1996). Yeast ubiquitin-like genes are involved in duplication of the microtubule organizing center. J Cell Biol *133*, 1331–1346.

Boeynaems, S., Bogaert, E., Kovacs, D., Konijnenberg, A., Timmerman, E., Volkov, A., Guharoy, M., De Decker, M., Jaspers, T., Ryan, V.H., et al. (2017). Phase Separation of C9orf72 Dipeptide Repeats Perturbs Stress Granule Dynamics. Mol. Cell *65*, 1044-1055.e5.

Boeynaems, S., Alberti, S., Fawzi, N.L., Mittag, T., Polymenidou, M., Rousseau, F., Schymkowitz, J., Shorter, J., Wolozin, B., Van Den Bosch, L., et al. (2018). Protein Phase Separation: A New Phase in Cell Biology. Trends in Cell Biology *28*, 420–435.

Bosco, D.A., Lemay, N., Ko, H.K., Zhou, H., Burke, C., Kwiatkowski, T.J., Sapp, P., McKenna-Yasek, D., Brown, R.H., and Hayward, L.J. (2010). Mutant FUS proteins that cause amyotrophic lateral sclerosis incorporate into stress granules. Hum. Mol. Genet. *19*, 4160–4175.

Brangwynne, C.P., Eckmann, C.R., Courson, D.S., Rybarska, A., Hoege, C., Gharakhani, J., Jülicher, F., and Hyman, A.A. (2009). Germline P Granules Are Liquid Droplets That Localize by Controlled Dissolution/Condensation. Science *324*, 1729–1732.

Brangwynne, C.P., Mitchison, T.J., and Hyman, A.A. (2011). Active liquid-like behavior of nucleoli determines their size and shape in Xenopus laevis oocytes. PNAS *108*, 4334–4339.

Brettschneider, J., Van Deerlin, V.M., Robinson, J.L., Kwong, L., Lee, E.B., Ali, Y.O., Safren, N., Monteiro, M.J., Toledo, J.B., Elman, L., et al. (2012). Pattern of ubiquilin pathology in ALS and FTLD indicates presence of C9ORF72 hexanucleotide expansion. Acta Neuropathol. *123*, 825–839.

Buchan, J.R., and Parker, R. (2009). Eukaryotic Stress Granules: The Ins and Out of Translation. Mol Cell *36*, 932.

Buchan, J.R., Kolaitis, R.-M., Taylor, J.P., and Parker, R. (2013). Eukaryotic Stress Granules Are Cleared by Autophagy and Cdc48/VCP Function. Cell *153*, 1461–1474.

Burke, K.A., Janke, A.M., Rhine, C.L., and Fawzi, N.L. (2015). Residue-by-Residue View of In Vitro FUS Granules that Bind the C-Terminal Domain of RNA Polymerase II. Mol. Cell *60*, 231–241.

Cai, H., Lin, X., Xie, C., Laird, F.M., Lai, C., Wen, H., Chiang, H.-C., Shim, H., Farah, M.H., Hoke, A., et al. (2005). Loss of ALS2 function is insufficient to trigger motor neuron degeneration in knock-out mice but predisposes neurons to oxidative stress. J. Neurosci. *25*, 7567–7574.

Cai, H., Shim, H., Lai, C., Xie, C., Lin, X., Yang, W.J., and Chandran, J. (2008). ALS2/Alsin Knockout Mice and Motor Neuron Diseases. Neurodegener Dis *5*, 359–366.

Ceballos-Diaz, C., Rosario, A.M., Park, H.-J., Chakrabarty, P., Sacino, A., Cruz, P.E., Siemienski, Z., Lara, N., Moran, C., Ravelo, N., et al. (2015). Viral expression of ALS-linked ubiquilin-2 mutants causes inclusion pathology and behavioral deficits in mice. Molecular Neurodegeneration *10*, 25.

Chang, L., and Monteiro, M.J. (2015). Defective Proteasome Delivery of Polyubiquitinated Proteins by Ubiquilin-2 Proteins Containing ALS Mutations. PLoS ONE *10*, e0130162.

Charcot, J.-M., and Joffroy, A. (1869). Deux cas d'atrophie musculaire progressive: avec lésions de la substance grise et des faisceaux antérolatéraux de la moelle épinière (Paris: Masson).

Chen, X., Randles, L., Shi, K., Tarasov, S.G., Aihara, H., and Walters, K.J. (2016). Structures of Rpn1 T1:Rad23 and hRpn13:hPLIC2 Reveal Distinct Binding Mechanisms between Substrate Receptors and Shuttle Factors of the Proteasome. Structure *24*, 1257–1270.

Conklin, D., Holderman, S., Whitmore, T.E., Maurer, M., and Feldhaus, A.L. (2000). Molecular cloning, chromosome mapping and characterization of UBQLN3 a testis-specific gene that contains an ubiquitin-like domain. Gene *249*, 91–98.

Cougot, N., Bhattacharyya, S.N., Tapia-Arancibia, L., Bordonné, R., Filipowicz, W., Bertrand, E., and Rage, F. (2008). Dendrites of Mammalian Neurons Contain Specialized P-Body-Like Structures That Respond to Neuronal Activation. J. Neurosci. *28*, 13793–13804.

Couthouis, J., Hart, M.P., Shorter, J., DeJesus-Hernandez, M., Erion, R., Oristano, R., Liu, A.X., Ramos, D., Jethava, N., Hosangadi, D., et al. (2011). A yeast functional screen predicts new candidate ALS disease genes. Proc. Natl. Acad. Sci. U.S.A. *108*, 20881–20890.

Couthouis, J., Hart, M.P., Erion, R., King, O.D., Diaz, Z., Nakaya, T., Ibrahim, F., Kim, H.-J., Mojsilovic-Petrovic, J., Panossian, S., et al. (2012). Evaluating the role of the FUS/TLS-related gene EWSR1 in amyotrophic lateral sclerosis. Hum. Mol. Genet. *21*, 2899–2911.

Cruts, M., Gijselinck, I., van der Zee, J., Engelborghs, S., Wils, H., Pirici, D., Rademakers, R., Vandenberghe, R., Dermaut, B., Martin, J.-J., et al. (2006). Null mutations in progranulin cause ubiquitin-positive frontotemporal dementia linked to chromosome 17q21. Nature *442*, 920–924.

Dang, Y., Kedersha, N., Low, W.-K., Romo, D., Gorospe, M., Kaufman, R., Anderson, P., and Liu, J.O. (2006). Eukaryotic Initiation Factor 2α-independent Pathway of Stress Granule Induction by the Natural Product Pateamine A. J. Biol. Chem. *281*, 32870–32878.

Dao, T.P., Kolaitis, R.-M., Kim, H.J., O'Donovan, K., Martyniak, B., Colicino, E., Hehnly, H., Taylor, J.P., and Castañeda, C.A. (2018). Ubiquitin Modulates Liquid-Liquid Phase Separation of UBQLN2 via Disruption of Multivalent Interactions. Molecular Cell *69*, 965-978.e6.

Daoud, H., Suhail, H., Szuto, A., Camu, W., Salachas, F., Meininger, V., Bouchard, J.-P., Dupré, N., Dion, P.A., and Rouleau, G.A. (2012). UBQLN2 mutations are rare in French and French–Canadian amyotrophic lateral sclerosis. Neurobiology of Aging *33*, 2230.e1-2230.e5.

Davidson, J.D., Riley, B., Burright, E.N., Duvick, L.A., Zoghbi, H.Y., and Orr, H.T. (2000). Identification and characterization of an ataxin-1-interacting protein: A1Up, a ubiquitin-like nuclear protein. Hum. Mol. Genet. *9*, 2305–2312.

DeJesus-Hernandez, M., Mackenzie, I.R., Boeve, B.F., Boxer, A.L., Baker, M., Rutherford, N.J., Nicholson, A.M., Finch, N.A., Gilmer, H.F., Adamson, J., et al. (2011). Expanded GGGGCC

hexanucleotide repeat in non-coding region of C9ORF72 causes chromosome 9p-linked frontotemporal dementia and amyotrophic lateral sclerosis. Neuron *72*, 245–256.

Deng, H.-X., Zhai, H., Fu, R., Shi, Y., Gorrie, G.H., Yang, Y., Liu, E., Dal Canto, M.C., Mugnaini, E., and Siddique, T. (2007). Distal axonopathy in an alsin-deficient mouse model. Hum. Mol. Genet. *16*, 2911–2920.

Deng, H.-X., Chen, W., Hong, S.-T., Boycott, K.M., Gorrie, G.H., Siddique, N., Yang, Y., Fecto, F., Shi, Y., Zhai, H., et al. (2011). Mutations in UBQLN2 cause dominant X-linked juvenile and adult-onset ALS and ALS/dementia. Nature *477*, 211–215.

Devon, R.S., Orban, P.C., Gerrow, K., Barbieri, M.A., Schwab, C., Cao, L.P., Helm, J.R., Bissada, N., Cruz-Aguado, R., Davidson, T.-L., et al. (2006). Als2-deficient mice exhibit disturbances in endosome trafficking associated with motor behavioral abnormalities. Proc. Natl. Acad. Sci. U.S.A. *103*, 9595–9600.

Dewey, C.M., Cenik, B., Sephton, C.F., Dries, D.R., Mayer, P., Good, S.K., Johnson, B.A., Herz, J., and Yu, G. (2011). TDP-43 is directed to stress granules by sorbitol, a novel physiological osmotic and oxidative stressor. Mol. Cell. Biol. *31*, 1098–1108.

Eisinger-Mathason, T.S.K., Andrade, J., Groehler, A.L., Clark, D.E., Muratore-Schroeder, T.L., Pasic, L., Smith, J.A., Shabanowitz, J., Hunt, D.F., Macara, I.G., et al. (2008). Codependent Functions of RSK2 and the Apoptosis-Promoting Factor TIA-1 in Stress Granule Assembly and Cell Survival. Molecular Cell *31*, 722–736.

Elbaum-Garfinkle, S., Kim, Y., Szczepaniak, K., Chen, C.C.-H., Eckmann, C.R., Myong, S., and Brangwynne, C.P. (2015). The disordered P granule protein LAF-1 drives phase separation into droplets with tunable viscosity and dynamics. Proc. Natl. Acad. Sci. U.S.A. *112*, 7189–7194.

Emara, M.M., Ivanov, P., Hickman, T., Dawra, N., Tisdale, S., Kedersha, N., Hu, G.-F., and Anderson, P. (2010). Angiogenin-induced tRNA-derived Stress-induced RNAs Promote Stress-induced Stress Granule Assembly. J. Biol. Chem. *285*, 10959–10968.

Emara, M.M., Fujimura, K., Sciaranghella, D., Ivanova, V., Ivanov, P., and Anderson, P. (2012). Hydrogen peroxide induces stress granule formation independent of eIF2α phosphorylation. Biochemical and Biophysical Research Communications *423*, 763–769.

Esler, W.P., Kimberly, W.T., Ostaszewski, B.L., Ye, W., Diehl, T.S., Selkoe, D.J., and Wolfe, M.S. (2002). Activity-dependent isolation of the presenilin– γ-secretase complex reveals nicastrin and a γ substrate. PNAS *99*, 2720–2725.

Fahed, A.C., McDonough, B., Gouvion, C.M., Newell, K.L., Dure, L.S., Bebin, M., Bick, A.G., Seidman, J.G., Harter, D.H., and Seidman, C.E. (2014). UBQLN2 mutation causing heterogeneous X-linked dominant neurodegeneration. Ann Neurol. *75*, 793–798.

Fey, E.G., Krochmalnic, G., and Penman, S. (1986). The nonchromatin substructures of the nucleus: the ribonucleoprotein (RNP)-containing and RNP-depleted matrices analyzed by sequential fractionation and resinless section electron microscopy. J. Cell Biol. *102*, 1654–1665.

Ficklin, M.B., Zhao, S., and Feng, G. (2005). Ubiquilin-1 Regulates Nicotine-induced Up-regulation of Neuronal Nicotinic Acetylcholine Receptors. J. Biol. Chem. *280*, 34088–34095.

Figley, M.D., Bieri, G., Kolaitis, R.-M., Taylor, J.P., and Gitler, A.D. (2014). Profilin 1 Associates with Stress Granules and ALS-Linked Mutations Alter Stress Granule Dynamics. J. Neurosci. *34*, 8083–8097.

Ford, D.L., and Monteiro, M.J. (2006). Dimerization of ubiquilin is dependent upon the central region of the protein: evidence that the monomer, but not the dimer, is involved in binding presenilins. Biochemical Journal *399*, 397.

Fujimura, K., Sasaki, A.T., and Anderson, P. (2012). Selenite targets eIF4E-binding protein-1 to inhibit translation initiation and induce the assembly of non-canonical stress granules. Nucleic Acids Res. *40*, 8099–8110.

Funakoshi, M., Geley, S., Hunt, T., Nishimoto, T., and Kobayashi, H. (1999). Identification of XDRP1; a Xenopus protein related to yeast Dsk2p binds to the N-terminus of cyclin A and inhibits its degradation. The EMBO Journal *18*, 5009–5018.

Fushman, D., and Wilkinson, K.D. (2011). Structure and recognition of polyubiquitin chains of different lengths and linkage. F1000 Biol Rep *3*.

Gal, J., Kuang, L., Barnett, K.R., Zhu, B.Z., Shissler, S.C., Korotkov, K.V., Hayward, L.J., Kasarskis, E.J., and Zhu, H. (2016). ALS mutant SOD1 interacts with G3BP1 and affects stress granule dynamics. Acta Neuropathol *132*, 563–576.

Ganassi, M., Mateju, D., Bigi, I., Mediani, L., Poser, I., Lee, H.O., Seguin, S.J., Morelli, F.F., Vinet, J., Leo, G., et al. (2016). A Surveillance Function of the HSPB8-BAG3-HSP70 Chaperone Complex Ensures Stress Granule Integrity and Dynamism. Molecular Cell *63*, 796–810.

Gao, L., Tu, H., Shi, S.T., Lee, K.-J., Asanaka, M., Hwang, S.B., and Lai, M.M.C. (2003). Interaction with a Ubiquitin-Like Protein Enhances the Ubiquitination and Degradation of Hepatitis C Virus RNA-Dependent RNA Polymerase. J. Virol. *77*, 4149–4159.

Gao, Y., Li, Y., Zhang, C., Zhao, M., Deng, C., Lan, Q., Liu, Z., Su, N., Wang, J., Xu, F., et al. (2016). Enhanced Purification of Ubiquitinated Proteins by Engineered Tandem Hybrid Ubiquitin-binding Domains (ThUBDs). Mol. Cell Proteomics *15*, 1381–1396.

Gavriilidis, C., Laredj, L., Solinhac, R., Messaddeq, N., Viaud, J., Laporte, J., Sumara, I., and Hnia, K. (2018). The MTM1–UBQLN2–HSP complex mediates degradation of misfolded intermediate filaments in skeletal muscle. Nature Cell Biology *20*, 198–210.

Gellera, C., Tiloca, C., Bo, R.D., Corrado, L., Pensato, V., Agostini, J., Cereda, C., Ratti, A., Castellotti, B., Corti, S., et al. (2012). Ubiquilin 2 mutations in Italian patients with amyotrophic lateral sclerosis and frontotemporal dementia. J Neurol Neurosurg Psychiatry.

Gilks, N., Kedersha, N., Ayodele, M., Shen, L., Stoecklin, G., Dember, L.M., and Anderson, P. (2004). Stress granule assembly is mediated by prion-like aggregation of TIA-1. Mol. Biol. Cell *15*, 5383–5398.

Gilpin, K.M., Chang, L., and Monteiro, M.J. (2015). ALS-linked mutations in ubiquilin-2 or hnRNPA1 reduce interaction between ubiquilin-2 and hnRNPA1. Hum. Mol. Genet. *24*, 2565–2577.

Gorrie, G.H., Fecto, F., Radzicki, D., Weiss, C., Shi, Y., Dong, H., Zhai, H., Fu, R., Liu, E., Li, S., et al. (2014). Dendritic spinopathy in transgenic mice expressing ALS/dementia-linked mutant UBQLN2. PNAS *111*, 14524–14529.

Goulet, I., Boisvenue, S., Mokas, S., Mazroui, R., and Côté, J. (2008). TDRD3, a novel Tudor domain-containing protein, localizes to cytoplasmic stress granules. Hum Mol Genet *17*, 3055–3074.

Guo, L., Kim, H.J., Wang, H., Monaghan, J., Freyermuth, F., Sung, J.C., O'Donovan, K., Fare, C.M., Diaz, Z., Singh, N., et al. (2018). Nuclear-Import Receptors Reverse Aberrant Phase Transitions of RNA-Binding Proteins with Prion-like Domains. Cell *173*, 677-692.e20.

Gupta, R., Lan, M., Mojsilovic-Petrovic, J., Choi, W.H., Safren, N., Barmada, S., Lee, M.J., and Kalb, R. (2017). The Proline/Arginine Dipeptide from Hexanucleotide Repeat Expanded C9ORF72 Inhibits the Proteasome. ENeuro *4*.

Guzzo, C.M., Berndsen, C.E., Zhu, J., Gupta, V., Datta, A., Greenberg, R.A., Wolberger, C., and Matunis, M.J. (2012). RNF4-Dependent Hybrid SUMO-Ubiquitin Chains Are Signals for RAP80 and Thereby Mediate the Recruitment of BRCA1 to Sites of DNA Damage. Sci. Signal. *5*, ra88.

Hadano, S., Benn, S.C., Kakuta, S., Otomo, A., Sudo, K., Kunita, R., Suzuki-Utsunomiya, K., Mizumura, H., Shefner, J.M., Cox, G.A., et al. (2006). Mice deficient in the Rab5 guanine nucleotide exchange factor ALS2/alsin exhibit age-dependent neurological deficits and altered endosome trafficking. Hum. Mol. Genet. *15*, 233–250.

Haeusler, A.R., Donnelly, C.J., Periz, G., Simko, E.A.J., Shaw, P.G., Kim, M.-S., Maragakis, N.J., Troncoso, J.C., Pandey, A., Sattler, R., et al. (2014). C9orf72 nucleotide repeat structures initiate molecular cascades of disease. Nature *507*, 195–200.

Hanson, K.A., Kim, S.H., Wassarman, D.A., and Tibbetts, R.S. (2010). Ubiquilin Modifies TDP-43 Toxicity in a Drosophila Model of Amyotrophic Lateral Sclerosis (ALS). J. Biol. Chem. *285*, 11068–11072.

Hartmann-Petersen, R., Hendil, K.B., and Gordon, C. (2003). Ubiquitin binding proteins protect ubiquitin conjugates from disassembly. FEBS Letters *535*, 77–81.

Heir, R., Ablasou, C., Dumontier, E., Elliott, M., Fagotto-Kaufmann, C., and Bedford, F.K. (2006). The UBL domain of PLIC-1 regulates aggresome formation. EMBO Rep *7*, 1252–1258.

Higgins, R., Gendron, J.M., Rising, L., Mak, R., Webb, K., Kaiser, S.E., Zuzow, N., Riviere, P., Yang, B., Fenech, E., et al. (2015). The Unfolded Protein Response Triggers Site-Specific Regulatory Ubiquitylation of 40S Ribosomal Proteins. Molecular Cell *59*, 35–49.

Hiltunen, M., Lu, A., Thomas, A.V., Romano, D.M., Kim, M., Jones, P.B., Xie, Z., Kounnas, M.Z., Wagner, S.L., Berezovska, O., et al. (2006). Ubiquilin 1 modulates amyloid precursor protein trafficking and Abeta secretion. J. Biol. Chem. *281*, 32240–32253.

Hjerpe, R., Aillet, F., Lopitz-Otsoa, F., Lang, V., England, P., and Rodriguez, M.S. (2009). Efficient protection and isolation of ubiquitylated proteins using tandem ubiquitin-binding entities. EMBO Rep. *10*, 1250–1258.

Hjerpe, R., Bett, J.S., Keuss, M.J., Solovyova, A., McWilliams, T.G., Johnson, C., Sahu, I., Varghese, J., Wood, N., Wightman, M., et al. (2016). UBQLN2 Mediates Autophagy-Independent Protein Aggregate Clearance by the Proteasome. Cell *166*, 935–949.

Hochstrasser, M. (2009). Origin and function of ubiquitin-like proteins. Nature *458*, 422–429.

Hofmann, K., and Bucher, P. (1996). The UBA domain: a sequence motif present in multiple enzyme classes of the ubiquitination pathway. Trends in Biochemical Sciences *21*, 172–173.

Hofweber, M., Hutten, S., Bourgeois, B., Spreitzer, E., Niedner-Boblenz, A., Schifferer, M., Ruepp, M.-D., Simons, M., Niessing, D., Madl, T., et al. (2018). Phase Separation of FUS Is Suppressed by Its Nuclear Import Receptor and Arginine Methylation. Cell *173*, 706-719.e13.

Höhfeld, J., Minami, Y., and Hartl, F.U. (1995). Hip, a novel cochaperone involved in the eukaryotic Hsc70/Hsp40 reaction cycle. Cell *83*, 589–598.

Huang, B., Wu, Q., Zhou, H., Huang, C., and Xia, X.-G. (2016). Increased Ubqln2 expression causes neuron death in transgenic rats. J. Neurochem. *139*, 285–293.

Huang, X., Shen, S., and Fan, D. (2017). No Evidence for Pathogenic Role of UBQLN2 Mutations in Sporadic Amyotrophic Lateral Sclerosis in the Mainland Chinese Population. PLoS ONE *12*, e0170943.

Hubstenberger, A., Cameron, C., Noble, S.L., Keenan, S., and Evans, T.C. (2015). Modifiers of solid RNP granules control normal RNP dynamics and mRNA activity in early development. J Cell Biol *211*, 703–716.

Hurley, J.H., Lee, S., and Prag, G. (2006). Ubiquitin-binding domains. Biochemical Journal *399*, 361.

Hutton, M., Lendon, C.L., Rizzu, P., Baker, M., Froelich, S., Houlden, H., Pickering-Brown, S., Chakraverty, S., Isaacs, A., Grover, A., et al. (1998). Association of missense and 5'-splice-site mutations in tau with the inherited dementia FTDP-17. Nature *393*, 702–705.

Hyman, A.A., Weber, C.A., and Jülicher, F. (2014). Liquid-Liquid Phase Separation in Biology. Annual Review of Cell and Developmental Biology *30*, 39–58.

Ishigaki, S., and Sobue, G. (2018). Importance of Functional Loss of FUS in FTLD/ALS. Front Mol Biosci *5*.

Itakura, E., Zavodszky, E., Shao, S., Wohlever, M.L., Keenan, R.J., and Hegde, R.S. (2016). Ubiquilins Chaperone and Triage Mitochondrial Membrane Proteins for Degradation. Molecular Cell *63*, 21–33.

Ivanov, P., Emara, M.M., Villen, J., Gygi, S.P., and Anderson, P. (2011). Angiogenin-Induced tRNA Fragments Inhibit Translation Initiation. Molecular Cell *43*, 613–623.

Jain, A., and Vale, R.D. (2017). RNA phase transitions in repeat expansion disorders. Nature *546*, 243–247.

Jain, S., Wheeler, J.R., Walters, R.W., Agrawal, A., Barsic, A., and Parker, R. (2016). ATPase-Modulated Stress Granules Contain a Diverse Proteome and Substructure. Cell *164*, 487–498.

Jayabalan, A.K., Sanchez, A., Park, R.Y., Yoon, S.P., Kang, G.-Y., Baek, J.-H., Anderson, P., Kee, Y., and Ohn, T. (2016). NEDDylation promotes stress granule assembly. Nat Commun *7*, 12125.

Kang, Y., Zhang, N., Koepp, D.M., and Walters, K.J. (2007). Ubiquitin Receptor Proteins hHR23a and hPLIC2 Interact. Journal of Molecular Biology *365*, 1093–1101.

Katz, J.S., Dimachkie, M.M., and Barohn, R.J. (2015). Amyotrophic Lateral Sclerosis: A Historical Perspective. Neurol Clin *33*, 727–734.

Kaye, F.J., Modi, S., Ivanovska, I., Koonin, E.V., Thress, K., Kubo, A., Kornbluth, S., and Rose, M.D. (2000). A family of ubiquitin-like proteins binds the ATPase domain of Hsp70-like Stch. FEBS Letters *467*, 348–355.

Kedersha, N., and Anderson, P. (2007). Mammalian Stress Granules and Processing Bodies. B.-M. in Enzymology, ed. (Academic Press), pp. 61–81.

Kedersha, N., Cho, M.R., Li, W., Yacono, P.W., Chen, S., Gilks, N., Golan, D.E., and Anderson, P. (2000). Dynamic Shuttling of Tia-1 Accompanies the Recruitment of mRNA to Mammalian Stress Granules. The Journal of Cell Biology *151*, 1257–1268.

Kedersha, N., Panas, M.D., Achorn, C.A., Lyons, S., Tisdale, S., Hickman, T., Thomas, M., Lieberman, J., McInerney, G.M., Ivanov, P., et al. (2016). G3BP–Caprin1–USP10 complexes mediate stress granule condensation and associate with 40S subunits. J Cell Biol *212*, 845–860.

Kedersha, N.L., Gupta, M., Li, W., Miller, I., and Anderson, P. (1999). RNA-Binding Proteins Tia-1 and Tiar Link the Phosphorylation of Eif-2α to the Assembly of Mammalian Stress Granules. J Cell Biol *147*, 1431–1442.

Kessler, R., Tisserand, J., Font-Burgada, J., Reina, O., Coch, L., Attolini, C.S., Garcia-Bassets, I., and Azorín, F. (2015). dDsk2 regulates H2Bub1 and RNA polymerase II pausing at dHP1c complex target genes. Nat Commun *6*, 7049.

Kim, B., Cooke, H.J., and Rhee, K. (2012). DAZL is essential for stress granule formation implicated in germ cell survival upon heat stress. Development *139*, 568–578.

Kim, H.J., Kim, N.C., Wang, Y.-D., Scarborough, E.A., Moore, J., Diaz, Z., MacLea, K.S., Freibaum, B., Li, S., Molliex, A., et al. (2013). Mutations in prion-like domains in hnRNPA2B1 and hnRNPA1 cause multisystem proteinopathy and ALS. Nature *495*, 467–473.

Kim, H.-J., Kwon, M.-J., Choi, W.-J., Oh, K.-W., Oh, S.-I., Ki, C.-S., and Kim, S.H. (2014). Mutations in UBQLN2 and SIGMAR1 genes are rare in Korean patients with amyotrophic lateral sclerosis. Neurobiol. Aging *35*, 1957.e7-8.

Kim, S.H., Stiles, S.G., Feichtmeier, J.M., Ramesh, N., Zhan, L., Scalf, M.A., Smith, L.M., Pandey, U.B., and Tibbetts, R.S. (2018). Mutation-dependent aggregation and toxicity in a Drosophila model for UBQLN2-associated ALS. Hum Mol Genet *27*, 322–337.

Kim, T.-Y., Kim, E., Yoon, S.K., and Yoon, J.-B. (2008). Herp enhances ER-associated protein degradation by recruiting ubiquilins. Biochemical and Biophysical Research Communications *369*, 741–746.

Kim, W.J., Back, S.H., Kim, V., Ryu, I., and Jang, S.K. (2005). Sequestration of TRAF2 into Stress Granules Interrupts Tumor Necrosis Factor Signaling under Stress Conditions. Mol. Cell. Biol. *25*, 2450–2462.

Kleijnen, M.F., Shih, A.H., Zhou, P., Kumar, S., Soccio, R.E., Kedersha, N.L., Gill, G., and Howley, P.M. (2000). The hPLIC Proteins May Provide a Link between the Ubiquitination Machinery and the Proteasome. Molecular Cell *6*, 409–419.

Kleijnen, M.F., Alarcón, R.M., and Howley, P.M. (2003). The Ubiquitin-associated Domain of hPLIC-2 Interacts with the Proteasome. Mol. Biol. Cell *14*, 3868–3875.

Ko, H.S., Uehara, T., Tsuruma, K., and Nomura, Y. (2004). Ubiquilin interacts with ubiquitylated proteins and proteasome through its ubiquitin-associated and ubiquitin-like domains. FEBS Lett. *566*, 110–114.

Krichevsky, A.M., and Kosik, K.S. (2001). Neuronal RNA granules: a link between RNA localization and stimulation-dependent translation. Neuron *32*, 683–696.

Kroschwald, S., Maharana, S., Mateju, D., Malinovska, L., Nüske, E., Poser, I., Richter, D., and Alberti, S. (2015). Promiscuous interactions and protein disaggregases determine the material state of stress-inducible RNP granules. Elife *4*, e06807.

Kumar, D.R., Aslinia, F., Yale, S.H., and Mazza, J.J. (2011). Jean-Martin Charcot: The Father of Neurology. Clin Med Res *9*, 46–49.

Kurlawala, Z., Shah, P.P., Shah, C., and Beverly, L.J. (2017a). The STI and UBA Domains of UBQLN1 Are Critical Determinants of Substrate Interaction and Proteostasis. J. Cell. Biochem. *118*, 2261–2270.

Kurlawala, Z., Dunaway, R., Shah, P.P., Gosney, J.A., Siskind, L.J., Ceresa, B.P., and Beverly, L.J. (2017b). Regulation of insulin-like growth factor receptors by Ubiquilin1. Biochem. J. *474*, 4105–4118.

Kwiatkowski, T.J., Bosco, D.A., Leclerc, A.L., Tamrazian, E., Vanderburg, C.R., Russ, C., Davis, A., Gilchrist, J., Kasarskis, E.J., Munsat, T., et al. (2009). Mutations in the FUS/TLS gene on chromosome 16 cause familial amyotrophic lateral sclerosis. Science *323*, 1205–1208.

Kwon, S., Zhang, Y., and Matthias, P. (2007). The deacetylase HDAC6 is a novel critical component of stress granules involved in the stress response. Genes Dev. *21*, 3381–3394.

Lancaster, A.K., Nutter-Upham, A., Lindquist, S., and King, O.D. (2014). PLAAC: a web and command-line application to identify proteins with prion-like amino acid composition. Bioinformatics *30*, 2501–2502.

Langdon, E.M., Qiu, Y., Niaki, A.G., McLaughlin, G.A., Weidmann, C., Gerbich, T.M., Smith, J.A., Crutchley, J.M., Termini, C.M., Weeks, K.M., et al. (2018). mRNA structure determines specificity of a polyQ-driven phase separation. Science eaar7432.

Lässle, M., Blatch, G.L., Kundra, V., Takatori, T., and Zetter, B.R. (1997). Stress-inducible, murine protein mSTI1. Characterization of binding domains for heat shock proteins and in vitro phosphorylation by different kinases. J. Biol. Chem. *272*, 1876–1884.

Le, N.T.T., Chang, L., Kovlyagina, I., Georgiou, P., Safren, N., Braunstein, K.E., Kvarta, M.D., Dyke, A.M.V., LeGates, T.A., Philips, T., et al. (2016). Motor neuron disease, TDP-43 pathology, and memory deficits in mice expressing ALS–FTD-linked UBQLN2 mutations. PNAS *113*, E7580–E7589.

Lee, D.Y., Arnott, D., and Brown, E.J. (2013a). Ubiquilin4 is an adaptor protein that recruits Ubiquilin1 to the autophagy machinery. EMBO Rep *advance online publication*.

Lee, J.-E., Jeon, I.-S., Han, N.-E., Song, H.-J., Kim, E.-G., Choi, J.-W., Song, K.-D., Lee, H.-K., and Choi, J.-K. (2013b). Ubiquilin 1 interacts with Orai1 to regulate calcium mobilization. Mol Cells *35*, 41–46.

Lee, K.-H., Zhang, P., Kim, H.J., Mitrea, D.M., Sarkar, M., Freibaum, B.D., Cika, J., Coughlin, M., Messing, J., Molliex, A., et al. (2016). C9orf72 Dipeptide Repeats Impair the Assembly, Dynamics, and Function of Membrane-Less Organelles. Cell *167*, 774-788.e17.

Leung, A.K.L., Vyas, S., Rood, J.E., Bhutkar, A., Sharp, P.A., and Chang, P. (2011). Poly(ADP-Ribose) Regulates Stress Responses and MicroRNA Activity in the Cytoplasm. Molecular Cell *42*, 489–499.

Li, X., Su, V., Kurata, W.E., Jin, C., and Lau, A.F. (2008). A Novel Connexin43-interacting Protein, CIP75, Which Belongs to the UbL-UBA Protein Family, Regulates the Turnover of Connexin43. J. Biol. Chem. *283*, 5748–5759.

Li, Y.R., King, O.D., Shorter, J., and Gitler, A.D. (2013). Stress granules as crucibles of ALS pathogenesis. J Cell Biol *201*, 361–372.

Lim, P.J., Danner, R., Liang, J., Doong, H., Harman, C., Srinivasan, D., Rothenberg, C., Wang, H., Ye, Y., Fang, S., et al. (2009). Ubiquilin and p97/VCP bind erasin, forming a complex involved in ERAD. J Cell Biol *187*, 201–217.

Lin, Y., Protter, D.S.W., Rosen, M.K., and Parker, R. (2015). Formation and Maturation of Phase-Separated Liquid Droplets by RNA-Binding Proteins. Mol. Cell *60*, 208–219.

Lindquist, S. (1981). Regulation of protein synthesis during heat shock. Nature *293*, 311–314.

Ling, S.-C., Polymenidou, M., and Cleveland, D.W. (2013). Converging Mechanisms in ALS and FTD: Disrupted RNA and Protein Homeostasis. Neuron *79*, 416–438.

Lipinszki, Z., Pál, M., Nagy, O., Deák, P., Hunyadi-Gulyas, E., and Udvardy, A. (2011). Overexpression of Dsk2/dUbqln results in severe developmental defects and lethality in Drosophila melanogaster that can be rescued by overexpression of the p54/Rpn10/S5a proteasomal subunit. FEBS Journal *278*, 4833–4844.

Liu-Yesucevitz, L., Bilgutay, A., Zhang, Y.-J., Vanderweyde, T., Vanderwyde, T., Citro, A., Mehta, T., Zaarur, N., McKee, A., Bowser, R., et al. (2010). Tar DNA binding protein-43 (TDP-43) associates with stress granules: analysis of cultured cells and pathological brain tissue. PLoS ONE *5*, e13250.

Loschi, M., Leishman, C.C., Berardone, N., and Boccaccio, G.L. (2009). Dynein and kinesin regulate stress-granule and P-body dynamics. J Cell Sci *122*, 3973–3982.

Lowe, E.D., Hasan, N., Trempe, J.-F., Fonso, L., Noble, M.E.M., Endicott, J.A., Johnson, L.N., and Brown, N.R. (2006). Structures of the Dsk2 UBL and UBA domains and their complex. Acta Crystallographica Section D Biological Crystallography *62*, 177–188.

Lu, K., Brave, F. den, and Jentsch, S. (2017). Receptor oligomerization guides pathway choice between proteasomal and autophagic degradation. Nature Cell Biology *19*, 732–739.

Mackenzie, I.R., Rademakers, R., and Neumann, M. (2010). TDP-43 and FUS in amyotrophic lateral sclerosis and frontotemporal dementia. The Lancet Neurology *9*, 995–1007.

Mackenzie, I.R., Nicholson, A.M., Sarkar, M., Messing, J., Purice, M.D., Pottier, C., Annu, K., Baker, M., Perkerson, R.B., Kurti, A., et al. (2017). TIA1 Mutations in Amyotrophic Lateral Sclerosis and Frontotemporal Dementia Promote Phase Separation and Alter Stress Granule Dynamics. Neuron *95*, 808-816.e9.

Mah, A.L., Perry, G., Smith, M.A., and Monteiro, M.J. (2000). Identification of Ubiquilin, a Novel Presenilin Interactor That Increases Presenilin Protein Accumulation. J Cell Biol *151*, 847–862.

Mahboubi, H., and Stochaj, U. (2014). Nucleoli and Stress Granules: Connecting Distant Relatives. Traffic *15*, 1179–1193.

Mao, Y.S., Sunwoo, H., Zhang, B., and Spector, D.L. (2011). Direct visualization of the co-transcriptional assembly of a nuclear body by noncoding RNAs. Nat. Cell Biol. *13*, 95–101.

March, Z.M., King, O.D., and Shorter, J. (2016). Prion-like domains as epigenetic regulators, scaffolds for subcellular organization, and drivers of neurodegenerative disease. Brain Research *1647*, 9–18.

Marín, I. (2014). The ubiquilin gene family: evolutionary patterns and functional insights. BMC Evolutionary Biology *14*, 63.

Markmiller, S., Soltanieh, S., Server, K.L., Mak, R., Jin, W., Fang, M.Y., Luo, E.-C., Krach, F., Yang, D., Sen, A., et al. (2018a). Context-Dependent and Disease-Specific Diversity in Protein Interactions within Stress Granules. Cell *172*, 590-604.e13.

Markmiller, S., Fulzele, A., Higgins, R., Yeo, G., and Bennett, E.J. (2018b). Active protein neddylation or ubiquitylation is dispensable for stress granule dynamics.

Massey, L.K., Mah, A.L., Ford, D.L., Miller, J., Liang, J., Doong, H., and Monteiro, M.J. (2004). Overexpression of ubiquilin decreases ubiquitination and degradation of presenilin proteins. J. Alzheimers Dis. *6*, 79–92.

Massey, L.K., Mah, A.L., and Monteiro, M.J. (2005). Ubiquilin regulates presenilin endoproteolysis and modulates γ-secretase components, Pen-2 and nicastrin. Biochemical Journal *391*, 513.

Mateju, D., Franzmann, T.M., Patel, A., Kopach, A., Boczek, E.E., Maharana, S., Lee, H.O., Carra, S., Hyman, A.A., and Alberti, S. (2017). An aberrant phase transition of stress granules triggered by misfolded protein and prevented by chaperone function. EMBO J *36*, 1669–1687.

Matsuda, M., Koide, T., Yorihuzi, T., Hosokawa, N., and Nagata, K. (2001). Molecular Cloning of a Novel Ubiquitin-like Protein, UBIN, That Binds to ER Targeting Signal Sequences. Biochemical and Biophysical Research Communications *280*, 535–540.

Mazroui, R., Sukarieh, R., Bordeleau, M.-E., Kaufman, R.J., Northcote, P., Tanaka, J., Gallouzi, I., and Pelletier, J. (2006). Inhibition of Ribosome Recruitment Induces Stress Granule Formation Independently of Eukaryotic Initiation Factor 2α Phosphorylation. MBoC *17*, 4212–4219.

Mazroui, R., Di Marco, S., Kaufman, R.J., and Gallouzi, I.-E. (2007). Inhibition of the Ubiquitin-Proteasome System Induces Stress Granule Formation. Mol Biol Cell *18*, 2603–2618.

McEwen, E., Kedersha, N., Song, B., Scheuner, D., Gilks, N., Han, A., Chen, J.-J., Anderson, P., and Kaufman, R.J. (2005). Heme-regulated Inhibitor Kinase-mediated Phosphorylation of Eukaryotic Translation Initiation Factor 2 Inhibits Translation, Induces Stress Granule Formation, and Mediates Survival upon Arsenite Exposure. J. Biol. Chem. *280*, 16925–16933.

Mehta, P. (2018). Prevalence of Amyotrophic Lateral Sclerosis — United States, 2014. MMWR Morb Mortal Wkly Rep *67*.

Mello, C.C., Kramer, J.M., Stinchcomb, D., and Ambros, V. (1991). Efficient gene transfer in C.elegans: extrachromosomal maintenance and integration of transforming sequences. EMBO J. *10*, 3959–3970.

Mittag, T., and Parker, R. (2018). Multiple Modes of Protein–Protein Interactions Promote RNP Granule Assembly. Journal of Molecular Biology.

Mollet, S., Cougot, N., Wilczynska, A., Dautry, F., Kress, M., Bertrand, E., and Weil, D. (2008). Translationally repressed mRNA transiently cycles through stress granules during stress. Mol. Biol. Cell *19*, 4469–4479.

Molliex, A., Temirov, J., Lee, J., Coughlin, M., Kanagaraj, A.P., Kim, H.J., Mittag, T., and Taylor, J.P. (2015). Phase Separation by Low Complexity Domains Promotes Stress Granule Assembly and Drives Pathological Fibrillization. Cell *163*, 123–133.

Morais, V.A., Verstreken, P., Roethig, A., Smet, J., Snellinx, A., Vanbrabant, M., Haddad, D., Frezza, C., Mandemakers, W., Vogt-Weisenhorn, D., et al. (2009). Parkinson's disease mutations in PINK1 result in decreased Complex I activity and deficient synaptic function. EMBO Mol Med *1*, 99–111.

Munoz, D.G., Neumann, M., Kusaka, H., Yokota, O., Ishihara, K., Terada, S., Kuroda, S., and Mackenzie, I.R. (2009). FUS pathology in basophilic inclusion body disease. Acta Neuropathol. *118*, 617–627.

Murakami, T., Qamar, S., Lin, J.Q., Schierle, G.S.K., Rees, E., Miyashita, A., Costa, A.R., Dodd, R.B., Chan, F.T.S., Michel, C.H., et al. (2015). ALS/FTD Mutation-Induced Phase Transition of FUS Liquid Droplets and Reversible Hydrogels into Irreversible Hydrogels Impairs RNP Granule Function. Neuron *88*, 678–690.

Murray, D.T., Kato, M., Lin, Y., Thurber, K.R., Hung, I., McKnight, S.L., and Tycko, R. (2017). Structure of FUS Protein Fibrils and Its Relevance to Self-Assembly and Phase Separation of Low-Complexity Domains. Cell *171*, 615-627.e16.

N'Diaye, E.-N., and Brown, E.J. (2003). The ubiquitin-related protein PLIC-1 regulates heterotrimeric G protein function through association with Gβγ. J Cell Biol *163*, 1157–1165.

N'Diaye, E.-N., Hanyaloglu, A.C., Kajihara, K.K., Puthenveedu, M.A., Wu, P., Zastrow, M. von, and Brown, E.J. (2008). The Ubiquitin-like Protein PLIC-2 Is a Negative Regulator of G Protein-coupled Receptor Endocytosis. Mol. Biol. Cell *19*, 1252–1260.

Neumann, M., Sampathu, D.M., Kwong, L.K., Truax, A.C., Micsenyi, M.C., Chou, T.T., Bruce, J., Schuck, T., Grossman, M., Clark, C.M., et al. (2006). Ubiquitinated TDP-43 in frontotemporal lobar degeneration and amyotrophic lateral sclerosis. Science *314*, 130–133.

Neumann, M., Rademakers, R., Roeber, S., Baker, M., Kretzschmar, H.A., and Mackenzie, I.R.A. (2009a). A new subtype of frontotemporal lobar degeneration with FUS pathology. Brain *132*, 2922–2931.

Neumann, M., Roeber, S., Kretzschmar, H.A., Rademakers, R., Baker, M., and Mackenzie, I.R.A. (2009b). Abundant FUS-immunoreactive pathology in neuronal intermediate filament inclusion disease. Acta Neuropathol. *118*, 605–616.

Nguyen, K., Puthenveetil, R., and Vinogradova, O. (2017). Investigation of the adaptor protein PLIC-2 in multiple pathways. Biochemistry and Biophysics Reports *9*, 341–348.

Nonhoff, U., Ralser, M., Welzel, F., Piccini, I., Balzereit, D., Yaspo, M.-L., Lehrach, H., and Krobitsch, S. (2007). Ataxin-2 interacts with the DEAD/H-box RNA helicase DDX6 and interferes with P-bodies and stress granules. Mol. Biol. Cell *18*, 1385–1396.

Nott, T.J., Petsalaki, E., Farber, P., Jervis, D., Fussner, E., Plochowietz, A., Craggs, T.D., Bazett-Jones, D.P., Pawson, T., Forman-Kay, J.D., et al. (2015). Phase Transition of a Disordered Nuage Protein Generates Environmentally Responsive Membraneless Organelles. Molecular Cell *57*, 936–947.

Nover, L., Scharf, K.D., and Neumann, D. (1983). Formation of cytoplasmic heat shock granules in tomato cell cultures and leaves. Molecular and Cellular Biology *3*, 1648–1655.

Nover, L., Scharf, K.D., and Neumann, D. (1989). Cytoplasmic heat shock granules are formed from precursor particles and are associated with a specific set of mRNAs. Molecular and Cellular Biology *9*, 1298–1308.

Ohn, T., Kedersha, N., Hickman, T., Tisdale, S., and Anderson, P. (2008). A functional RNAi screen links O-GlcNAc modification of ribosomal proteins to stress granule and processing body assembly. Nat. Cell Biol. *10*, 1224–1231.

Ong, S.-E., Blagoev, B., Kratchmarova, I., Kristensen, D.B., Steen, H., Pandey, A., and Mann, M. (2002). Stable isotope labeling by amino acids in cell culture, SILAC, as a simple and accurate approach to expression proteomics. Mol. Cell Proteomics *1*, 376–386.

Ozaki, T., Kondo, K., Nakamura, Y., Ichimiya, S., Nakagawara, A., and Sakiyama, S. (1997). Interaction of DA41, a DAN-Binding Protein, with the Epidermal Growth Factor-like Protein, S(1–5). Biochemical and Biophysical Research Communications *237*, 245–250.

Özoğuz, A., Uyan, Ö., Birdal, G., Iskender, C., Kartal, E., Lahut, S., Ömür, Ö., Agim, Z.S., Eken, A.G., Sen, N.E., et al. (2015). The distinct genetic pattern of ALS in Turkey and novel mutations. Neurobiol. Aging *36*, 1764.e9-1764.e18.

Panas, M.D., Ivanov, P., and Anderson, P. (2016). Mechanistic insights into mammalian stress granule dynamics. J Cell Biol *215*, 313–323.

Panniers, R., and Henshaw, E.C. (1984). Mechanism of inhibition of polypeptide chain initiation in heat-shocked Ehrlich ascites tumour cells. Eur. J. Biochem. *140*, 209–214.

Patel, A., Lee, H.O., Jawerth, L., Maharana, S., Jahnel, M., Hein, M.Y., Stoynov, S., Mahamid, J., Saha, S., Franzmann, T.M., et al. (2015). A Liquid-to-Solid Phase Transition of the ALS Protein FUS Accelerated by Disease Mutation. Cell *162*, 1066–1077.

Patel, A., Malinovska, L., Saha, S., Wang, J., Alberti, S., Krishnan, Y., and Hyman, A.A. (2017). ATP as a biological hydrotrope. Science *356*, 753–756.

Persson, P., Stockhausen, M.-T., Påhlman, S., and Axelson, H. (2004). Ubiquilin-1 is a novel HASH-1-complexing protein that regulates levels of neuronal bHLH transcription factors in human neuroblastoma cells. International Journal of Oncology *25*, 1213.

Pick, A. (1892). Uber die beziehungen der senilen hirnatrophie zur aphasie. Prager Medizinische Wochenschrift *17*, 165–167.

Protter, D.S.W., and Parker, R. (2016). Principles and Properties of Stress Granules. Trends in Cell Biology *26*, 668–679.

Qamar, S., Wang, G., Randle, S.J., Ruggeri, F.S., Varela, J.A., Lin, J.Q., Phillips, E.C., Miyashita, A., Williams, D., Ströhl, F., et al. (2018). FUS Phase Separation Is Modulated by a Molecular Chaperone and Methylation of Arginine Cation-π Interactions. Cell *173*, 720-734.e15.

Raasi, S., Varadan, R., Fushman, D., and Pickart, C.M. (2005). Diverse polyubiquitin interaction properties of ubiquitin-associated domains. Nat Struct Mol Biol *12*, 708–714.

Rademakers, R., Neumann, M., and Mackenzie, I.R. (2012). Advances in understanding the molecular basis of frontotemporal dementia. Nat Rev Neurol *8*, 423–434.

Ratnavalli, E., Brayne, C., Dawson, K., and Hodges, J.R. (2002). The prevalence of frontotemporal dementia. Neurology *58*, 1615–1621.

Regan-Klapisz, E., Sorokina, I., Voortman, J., Keizer, P. de, Roovers, R.C., Verheesen, P., Urbé, S., Fallon, L., Fon, E.A., Verkleij, A., et al. (2005). Ubiquilin recruits Eps15 into ubiquitin-rich cytoplasmic aggregates via a UIM-UBL interaction. J Cell Sci *118*, 4437–4450.

Reineke, L.C., Dougherty, J.D., Pierre, P., and Lloyd, R.E. (2012). Large G3BP-induced granules trigger eIF2α phosphorylation. Mol. Biol. Cell *23*, 3499–3510.

Robberecht, W., and Philips, T. (2013). The changing scene of amyotrophic lateral sclerosis. Nat. Rev. Neurosci. *14*, 248–264.

Rosen, D.R., Siddique, T., Patterson, D., Figlewicz, D.A., Sapp, P., Hentati, A., Donaldson, D., Goto, J., O'Regan, J.P., Deng, H.-X., et al. (1993). Mutations in Cu/Zn superoxide dismutase gene are associated with familial amyotrophic lateral sclerosis. , Published Online: 04 March 1993; | Doi:10.1038/362059a0 *362*, 59–62.

Rothenberg, C., Srinivasan, D., Mah, L., Kaushik, S., Peterhoff, C.M., Ugolino, J., Fang, S., Cuervo, A.M., Nixon, R.A., and Monteiro, M.J. (2010). Ubiquilin functions in autophagy and is degraded by chaperone-mediated autophagy. Hum. Mol. Genet. *19*, 3219–3232.

Safren, N., Chang, L., Dziki, K.M., and Monteiro, M.J. (2015). Signature changes in ubiquilin expression in the R6/2 mouse model of Huntington's disease. Brain Research *1597*, 37–46.

Saliba, R.S., Pangalos, M., and Moss, S.J. (2008). The Ubiquitin-like Protein Plic-1 Enhances the Membrane Insertion of GABAA Receptors by Increasing Their Stability within the Endoplasmic Reticulum. J. Biol. Chem. *283*, 18538–18544.

Sama, R.R.K., Ward, C.L., Kaushansky, L.J., Lemay, N., Ishigaki, S., Urano, F., and Bosco, D.A. (2013). FUS/TLS assembles into stress granules and is a prosurvival factor during hyperosmolar stress. J. Cell. Physiol. *228*, 2222–2231.

Sarkar, J., and Myong, S. (2018). Single-Molecule and Ensemble Methods to Probe Initial Stages of RNP Granule Assembly. In Nanoscale Imaging, (Humana Press, New York, NY), pp. 325–338.

Scharf, K.-D., Heider, H., Höhfeld, I., Lyck, R., Schmidt, E., and Nover, L. (1998). The Tomato Hsf System: HsfA2 Needs Interaction with HsfA1 for Efficient Nuclear Import and May Be Localized in Cytoplasmic Heat Stress Granules. Molecular and Cellular Biology *18*, 2240–2251.

Schultz, J., Milpetz, F., Bork, P., and Ponting, C.P. (1998). SMART, a simple modular architecture research tool: Identification of signaling domains. PNAS *95*, 5857–5864.

Scotter, E.L., Smyth, L., Bailey, J.A.W.T., Wong, C.-H., de Majo, M., Vance, C.A., Synek, B.J., Turner, C., Pereira, J., Charleston, A., et al. (2017). C9ORF72 and UBQLN2 mutations are causes of amyotrophic lateral sclerosis in New Zealand: a genetic and pathologic study using banked human brain tissue. Neurobiol. Aging *49*, 214.e1-214.e5.

Seguin, S.J., Morelli, F.F., Vinet, J., Amore, D., De Biasi, S., Poletti, A., Rubinsztein, D.C., and Carra, S. (2014). Inhibition of autophagy, lysosome and VCP function impairs stress granule assembly. Cell Death Differ *21*, 1838–1851.

Sharkey, L.M., Safren, N., Pithadia, A.S., Gerson, J.E., Dulchavsky, M., Fischer, S., Patel, R., Lantis, G., Ashraf, N., Kim, J.H., et al. (2018). Mutant UBQLN2 promotes toxicity by modulating intrinsic self-assembly. PNAS *115*, E10495–E10504.

Shen, T.H., Lin, H.-K., Scaglioni, P.P., Yung, T.M., and Pandolfi, P.P. (2006). The Mechanisms of PML-Nuclear Body Formation. Mol. Cell *24*, 805.

Souquere, S., Mollet, S., Kress, M., Dautry, F., Pierron, G., and Weil, D. (2009). Unravelling the ultrastructure of stress granules and associated P-bodies in human cells. Journal of Cell Science *122*, 3619–3626.

Spector, D.L. (2001). Nuclear domains. Journal of Cell Science *114*, 2891–2893.

Stepanenko, A.A., and Dmitrenko, V.V. (2015). HEK293 in cell biology and cancer research: phenotype, karyotype, tumorigenicity, and stress-induced genome-phenotype evolution. Gene *569*, 182–190.

Storti, R.V., Scott, M.P., Rich, A., and Pardue, M.L. (1980). Translational control of protein synthesis in response to heat shock in D. melanogaster cells. Cell *22*, 825–834.

Su, V., and Lau, A.F. (2009). Ubiquitin-like and ubiquitin-associated domain proteins: significance in proteasomal degradation. Cell. Mol. Life Sci. *66*, 2819–2833.

Su, V., Nakagawa, R., Koval, M., and Lau, A.F. (2010). Ubiquitin-independent Proteasomal Degradation of Endoplasmic Reticulum-localized Connexin43 Mediated by CIP75. J. Biol. Chem. *285*, 40979–40990.

Suzuki, R., and Kawahara, H. (2016). UBQLN4 recognizes mislocalized transmembrane domain proteins and targets these to proteasomal degradation. EMBO Rep *17*, 842–857.

Synofzik, M., Maetzler, W., Grehl, T., Prudlo, J., vom Hagen, J.M., Haack, T., Rebassoo, P., Munz, M., Schöls, L., and Biskup, S. (2012). Screening in ALS and FTD patients reveals 3 novel UBQLN2 mutations outside the PXX domain and a pure FTD phenotype. Neurobiology of Aging *33*, 2949.e13-2949.e17.

Szklarczyk, D., Franceschini, A., Wyder, S., Forslund, K., Heller, D., Huerta-Cepas, J., Simonovic, M., Roth, A., Santos, A., Tsafou, K.P., et al. (2015). STRING v10: protein-protein interaction networks, integrated over the tree of life. Nucleic Acids Res. *43*, D447-452.

Taylor, J.P., Brown, R.H., and Cleveland, D.W. (2016). Decoding ALS: from genes to mechanism. Nature *539*, 197–206.

Thedieck, K., Holzwarth, B., Prentzell, M.T., Boehlke, C., Kläsener, K., Ruf, S., Sonntag, A.G., Maerz, L., Grellscheid, S.-N., Kremmer, E., et al. (2013). Inhibition of mTORC1 by Astrin and Stress Granules Prevents Apoptosis in Cancer Cells. Cell *154*, 859–874.

Ticozzi, N., Vance, C., LeClerc, A.L., Keagle, P., Glass, J.D., McKenna-Yasek, D., Sapp, P.C., Silani, V., Bosco, D.A., Shaw, C.E., et al. (2011). Mutational analysis reveals the FUS homolog TAF15 as a candidate gene for familial amyotrophic lateral sclerosis. American Journal of Medical Genetics Part B: Neuropsychiatric Genetics *156*, 285–290.

Tourrière, H., Chebli, K., Zekri, L., Courselaud, B., Blanchard, J.M., Bertrand, E., and Tazi, J. (2003). The RasGAP-associated endoribonuclease G3BP assembles stress granules. J. Cell Biol. *160*, 823–831.

Treeck, B.V., Protter, D.S.W., Matheny, T., Khong, A., Link, C.D., and Parker, R. (2018). RNA self-assembly contributes to stress granule formation and defining the stress granule transcriptome. PNAS *115*, 2734–2739.

Tsukamoto, S., Shimada, K., Honoki, K., Kido, A., Akahane, M., Tanaka, Y., and Konishi, N. (2015). Ubiquilin 2 enhances osteosarcoma progression through resistance to hypoxic stress. Oncology Reports.

Turakhiya, A., Meyer, S.R., Marincola, G., Böhm, S., Vanselow, J.T., Schlosser, A., Hofmann, K., and Buchberger, A. (2018). ZFAND1 Recruits p97 and the 26S Proteasome to Promote the Clearance of Arsenite-Induced Stress Granules. Molecular Cell *70*, 906-919.e7.

Ugolino, J., Ji, Y.J., Conchina, K., Chu, J., Nirujogi, R.S., Pandey, A., Brady, N.R., Hamacher-Brady, A., and Wang, J. (2016). Loss of C9orf72 Enhances Autophagic Activity via Deregulated mTOR and TFEB Signaling. PLOS Genetics *12*, e1006443.

Vallen, E.A., Ho, W., Winey, M., and Rose, M.D. (1994). Genetic interactions between CDC31 and KAR1, two genes required for duplication of the microtubule organizing center in Saccharomyces cerevisiae. Genetics *137*, 407–422.

Van Langenhove, T., van der Zee, J., and Van Broeckhoven, C. (2012). The molecular basis of the frontotemporal lobar degeneration-amyotrophic lateral sclerosis spectrum. Ann. Med. *44*, 817–828.

Vance, C., Rogelj, B., Hortobágyi, T., De Vos, K.J., Nishimura, A.L., Sreedharan, J., Hu, X., Smith, B., Ruddy, D., Wright, P., et al. (2009). Mutations in FUS, an RNA processing protein, cause familial amyotrophic lateral sclerosis type 6. Science *323*, 1208–1211.

Walters, K.J., Kleijnen, M.F., Goh, A.M., Wagner, G., and Howley, P.M. (2002). Structural Studies of the Interaction between Ubiquitin Family Proteins and Proteasome Subunit S5a†. Biochemistry *41*, 1767–1777.

Wang, H., and Monteiro, M.J. (2007a). Ubiquilin interacts and enhances the degradation of expanded-polyglutamine proteins. Biochemical and Biophysical Research Communications *360*, 423–427.

Wang, H., and Monteiro, M.J. (2007b). Ubiquilin overexpression reduces GFP-polyalanine-induced protein aggregates and toxicity. Experimental Cell Research *313*, 2810–2820.

Wang, J., Choi, J.-M., Holehouse, A.S., Lee, H.O., Zhang, X., Jahnel, M., Maharana, S., Lemaitre, R., Pozniakovsky, A., Drechsel, D., et al. (2018). A Molecular Grammar Governing the Driving Forces for Phase Separation of Prion-like RNA Binding Proteins. Cell *174*, 688-699.e16.

Williams, K.L., Warraich, S.T., Yang, S., Solski, J.A., Fernando, R., Rouleau, G.A., Nicholson, G.A., and Blair, I.P. (2012). UBQLN2/ubiquilin 2 mutation and pathology in familial amyotrophic lateral sclerosis. Neurobiology of Aging *33*, 2527.e3-2527.e10.

Wu, Q., Liu, M., Huang, C., Liu, X., Huang, B., Li, N., Zhou, H., and Xia, X.-G. (2015). Pathogenic Ubqln2 gains toxic properties to induce neuron death. Acta Neuropathol. *129*, 417–428.

Wu, S., Mikhailov, A., Kallo-Hosein, H., Hara, K., Yonezawa, K., and Avruch, J. (2002). Characterization of ubiquilin 1, an mTOR-interacting protein. Biochimica et Biophysica Acta (BBA) - Molecular Cell Research *1542*, 41–56.

Xia, Y., Yan, L.H., Huang, B., Liu, M., Liu, X., and Huang, C. (2013). Pathogenic Mutation of UBQLN2 Impairs its Interaction with UBXD8 and Disrupts Endoplasmic Reticulum-Associated Protein Degradation. J. Neurochem.

Xia, Y., Yan, L.H., Huang, B., Liu, M., Liu, X., and Huang, C. (2014). Pathogenic mutation of UBQLN2 impairs its interaction with UBXD8 and disrupts endoplasmic reticulum-associated protein degradation. J. Neurochem. *129*, 99–106.

Xie, X., Matsumoto, S., Endo, A., Fukushima, T., Kawahara, H., Saeki, Y., and Komada, M. (2018). Deubiquitylases USP5 and USP13 are recruited to and regulate heat-induced stress granules through their deubiquitylating activities. J Cell Sci *131*, jcs210856.

Yamanaka, K., Miller, T.M., McAlonis-Downes, M., Chun, S.J., and Cleveland, D.W. (2006). Progressive spinal axonal degeneration and slowness in ALS2-deficient mice. Ann. Neurol. *60*, 95–104.

Yoshizawa, T., Ali, R., Jiou, J., Fung, H.Y.J., Burke, K.A., Kim, S.J., Lin, Y., Peeples, W.B., Saltzberg, D., Soniat, M., et al. (2018). Nuclear Import Receptor Inhibits Phase Separation of FUS through Binding to Multiple Sites. Cell *173*, 693-705.e22.

Youn, J.-Y., Dunham, W.H., Hong, S.J., Knight, J.D.R., Bashkurov, M., Chen, G.I., Bagci, H., Rathod, B., MacLeod, G., Eng, S.W.M., et al. (2018). High-Density Proximity Mapping Reveals the Subcellular Organization of mRNA-Associated Granules and Bodies. Molecular Cell *69*, 517-532.e11.

Yuan, S., Mcswiggin, H., Zheng, H., and Yan1,2*, A.W. (2015). A Testis-specific Gene, Ubqlnl, Is Dispensable for Mouse Embryonic Development and Spermatogenesis. Mol Reprod Dev *82*, 408–409.

Zhang, D., Raasi, S., and Fushman, D. (2008). Affinity Makes the Difference: Nonselective Interaction of the UBA Domain of Ubiquilin-1 with Monomeric Ubiquitin and Polyubiquitin Chains. Journal of Molecular Biology *377*, 162–180.

Zhang, H., Elbaum-Garfinkle, S., Langdon, E.M., Taylor, N., Occhipinti, P., Bridges, A.A., Brangwynne, C.P., and Gladfelter, A.S. (2015). RNA Controls PolyQ Protein Phase Transitions. Molecular Cell *60*, 220–230.

Zhang, K., Daigle, J.G., Cunningham, K.M., Coyne, A.N., Ruan, K., Grima, J.C., Bowen, K.E., Wadhwa, H., Yang, P., Rigo, F., et al. (2018a). Stress Granule Assembly Disrupts Nucleocytoplasmic Transport. Cell *173*, 958-971.e17.

Zhang, T., Wu, Y.-C., Mullane, P., Ji, Y.J., Liu, H., He, L., Arora, A., Hwang, H.-Y., Alessi, A.F., Niaki, A.G., et al. (2018b). FUS Regulates Activity of MicroRNA-Mediated Gene Silencing. Molecular Cell *69*, 787-801.e8.

Zhang, Y.-J., Gendron, T.F., Ebbert, M.T.W., O'Raw, A.D., Yue, M., Jansen-West, K., Zhang, X., Prudencio, M., Chew, J., Cook, C.N., et al. (2018c). Poly(GR) impairs protein translation and stress granule dynamics in C9orf72 -associated frontotemporal dementia and amyotrophic lateral sclerosis. Nature Medicine *24*, 1136.

Zhu, D., Wang, C., Liu, B., Wu, Y., Zhong, L., and Wang, C. (2010). Interaction between nuclear localization signal-retinoic acid receptor alpha and Ubiquilin 1. Zhong Nan Da Xue Xue Bao Yi Xue Ban *35*, 649–654.

BIRTH

New Haven, CT *Dec. 15, 1980*

EDUCATION

Johns Hopkins Bloomberg School of Public Health, Baltimore, MD
PhD Candidate, *2011-Present*

Indiana University, Bloomington, IN
B.S. Microbiology, B.A. Biochemistry with Honors, *1999–2003*

LABORATORY EXPERIENCE

Johns Hopkins Bloomberg School of Public Health, Baltimore, MD *2011-2018*
Department of Biochemistry & Molecular Biology, Advisor: Dr. Jiou Wang
PhD Candidate
Project: Identified a novel role for the ALS-FTD linked protein ubiquilin 2 in maintaining stress granule fluidity by increasing the dynamics of protein-RNA interactions. Found that ALS/FTD-linked mutations partially impaired this function. Used proteomic, molecular biology, worm genetic, biochemical and confocal microscopy techniques.

Nektar Therapeutics, Huntsville, AL *2006-2011*
Quality Control Analytical Research & Development Group
Analytical Chemist I-III
Projects: Developed methods for determining average PEG polymer molecular weight, purity, and ion impurities by MALDI-TOF mass spectrometry, reverse phase HPLC, and ion exchange chromatography respectively. Performed routine H^1NMR, reverse phase HPLC, FTIR, UV/vis spectrometry, and basic wet chemistry analysis as per GMP standards.

University of Wisconsin, Madison, WI *2004-2006*
School of Veterinary Medicine, Supervisor: Dr. Susan West *2005-2006*
Research Assistant
Project: Adapted a serum-based enzyme linked immunoadsorbent (ELISA) assay to a saliva-based ELISA to detect the opportunistic pathogen *Pseudomonas aeruginosa* in cystic fibrosis patients. Enrolled participants, collected, tested and catalogued patient samples. Managed lab.

Department of Biochemistry, Supervisor: Dr. Betty Craig *2004-2005*
Research Assistant
Project: Began characterization of the interaction of budding yeast *Saccharomyces cerevisiae* chaperones Sis1 with RNA binding protein Sro9 and non-canonical Hsp70 Ssz with Hsp70 Ssb using yeast genetic, molecular biology and biochemical techniques.

Indiana University, Bloomington, IN *1999-2003*
STARS (Science Technology & Research Scholars) Program
Department of Biology, Mentor: Dr. Lingling Chen *2001-2003*
Undergraduate researcher
Project: Optimized affinity purification of the Alzheimer's associated amyloid peptide (Aβ-42) from *E. coli* to study its interaction with the chaperonin GroEL as a model substrate.

Department of Ecology, PhD Student Leader: Dr. Nancy Beecher *Summer 2003*
Field Project volunteer, Monteverde Cloud Forest Biological Reserve, Costa Rica
Project: Located, staked, and monitored water levels of temporary frog breeding ponds in a team to monitor the effects of faster metamorphosis of the tree frog *Hyla pseudopuma* under drier climate conditions on immunity. Collected eggs and weighed and staged tadpoles.

GRANTS AND AWARDS

2012-2015 **Ruth L. Kirschstein National Research Service Award (T32), NCI**
Johns Hopkins School of Public Health

1999-2003 **IU Faculty Scholarship**
Indiana University, Bloomington

2002 **Honors College Summer Grant**
Indiana University, Bloomington

2002, 2003 **HHMI Capstone Grants**
Indiana University, Bloomington

1999-2003 **IU Science Technology & Research Scholars Program Grant**
Indiana University, Bloomington

1996-1999 **Choate Scholar Award**-Full 4-year scholarship to attend private boarding school including tuition, room & board, educational testing, a stipend, 2 summer experiences: Cross cultural/service trips to Ghana 1997, Thailand 1998 and term abroad to Mexico 1998.
Choate Rosemary Hall, Wallingford, CT

PUBLICATIONS

"Ubiquilin 2 Modulates ALS/FTD-linked FUS-RNA Complex Dynamics and Stress Granule Formation"
Elizabeth J. Alexander, Amirhossein Ghanbari Niaki, Tao Zhang, Jaya Sarkar, Yang Liu, Raja Sekhar Nirujogi, Akhilesh Pandey, Sua Myong, Jiou Wang.
PNAS 115(49): E11485-E11494.
PMID: 30442662

"The duality of ubiquilin function as shuttle and chaperone"
Elizabeth J. Alexander and Jiou Wang
Manuscript in preparation

ORAL PRESENTATIONS

2018 "The ubiquitin-like protein, ubiquilin 2 modulates ALS-linked FUS-RNA complex dynamics and stress granule formation
Alexander EJ, Niaki AG, Zhang T, Sarkar J, Nirujogi RS, Pandey A, Myong S, Wang J
Hopkins Ubiquitin Club, Baltimore, MD

2017 "Ubiquilin 2, Hsp70 and Stress Granule Assembly"
Alexander EJ, Nirujogi RS, Pandey A, Wang J
Hopkins Ubiquitin Club, Baltimore, MD

2016 "Ubiquilin 2, Stress Granules, and ALS Pathology"
Alexander EJ, Nirujogi RS, Pandey A, Wang J
Annual Retreat- Department of Biochemistry & Molecular Biology
Shephard Pratt Conference Center, Towson, MD

2016 "Ubiquilin 2, Translation Inhibition, and Stress Granules"
Alexander EJ, Nirujogi RS, Pandey A, Wang J
Hopkins Ubiquitin Club, Baltimore, MD

2015 "Ubiquilin 2, RNA Binding Proteins, and ALS Pathology"
Alexander EJ, Nirujogi RS, Pandey A, Wang J
PhD Club – Department of Biochemistry & Molecular Biology, Baltimore, MD

2014, 2015 "Ubiquitin-like protein, Ubiquilin 2 Function and Role in ALS Pathology" presentation. *Alexander EJ, Nirujogi RS, Pandey A, Wang J*
Hopkins Ubiquitin Club, Baltimore, MD

POSTER PRESENTATIONS

2015 "Investigating a Novel Nuclear Role for ubiquilin Proteins"
Alexander EJ, Nirujogi RS, Pandey A, Wang J
Annual Retreat- Department of Biochemistry & Molecular Biology
Shephard Pratt Conference Center, Towson, MD

2014 "Ubiquitin-like protein, Ubiquilin 2 Function and Role in ALS Pathology"
Alexander EJ, Nirujogi RS, Pandey A, Wang J
Annual Retreat- Department of Biochemistry & Molecular Biology
Shephard Pratt Conference Center, Towson, MD

2003 "Amyloid β (1-42) Fusion Peptide Overexpression and Purification from Inclusion Bodies in *E. coli*"
Alexander EJ and Chen L
Annual STARS Symposium. Indiana University, Bloomington, IN

2002 "Amyloid β (40, 42) Interaction with the GroEL Chaperonin Complex"
Alexander EJ and Chen L
Annual STARS Symposium. Indiana University, Bloomington, IN

2001 "Bifurcation of Planar Conservative Systems & Its Application to a Biological System"
Alexander EJ and Wang S
Annual STARS Symposium. Indiana University, Bloomington, IN

TEACHING & MENTORING EXPERIENCE

Lab Mentoring:

2016 **Nathan Magalit (Undergraduate student)**: Stress granule ImageJ quantitation, confocal microscopy, cell culture techniques to track the role of ubiquilin 2 in stress granule formation

2015-2016 **Yajas Shah (MHS student)**: Isca1 cloning for in vivo magnetic manipulation

2014-2015 **Justin Chu (MHS student)**: Ubiquilin 2 mutant cloning

2013-2014 **Luis Rendon (Undergraduate student)**: Confocal microscopy, cell culture, cell fixation and staining to monitor the role of ubiquilin 2 in autophagy

Group/Individual tutoring: Molecular Biology (Fall 2014), Pola Olzak (2015), Shuo Li (2016)

Teaching:

Fall 2016 **Core Research Literature**
Lead a graduate level discussion class on protein quality control.

Springs 2013-2016 **Cellular Stress in Physiology & Disease**
Teaching assistant for graduate level course.
Lead a discussion on protein homeostasis in 2016.

Summers 2014-2016 **Introduction to Biological Sciences**
Graduate level course for non-majors entering the School of Public Health
Taught 15 min segments on the "Nervous System" and "Autonomic Nervous System" incorporating active learning activities.
Designed and participated in a 3 hr "Molecular Biology Session" with a team.
Gave a 1 hr lecture on Motor Neuron Disease in 2016.

Summer 2016 **JHU Teaching Institute Teaching Academy**
Participated in 3-day workshop on course planning, active learning, and assessment.

Summer 2016 **PhD Education Reform Focus Group**
Participated in focus groups to revise the School of Public Health's PhD program.

Fall 2005 **Hmong Refugee Volunteer Teacher**, Madison, WI.
Taught newly arrived refugees improvised lessons in English 1-4 hours/week.

Summer 2005 **Teaching English as a Foreign Language Certification**
Wisconsin English Language Institute.
Participated in a 5-week intensive teacher training program focusing on the using the communicative method to teach English as a foreign language.
Designed lesson plans for and taught 12 hours of English class.
Worked with Turkish and Korean conversation partners 1-4 hours/week.